

การสังเคราะห์และสมบัติเชิงแสงของพรีโรลิตินิลเพปไทด์นิวคลีอิกแอซิดที่มีนิวคลีโอเบสเรืองแสง



บทคัดย่อและแฟ้มข้อมูลฉบับเต็มของวิทยานิพนธ์ตั้งแต่ปีการศึกษา 2554 ที่ให้บริการในคลังปัญญาจุฬาฯ (CUIR)
เป็นแฟ้มข้อมูลของนิสิตเจ้าของวิทยานิพนธ์ ที่ส่งผ่านทางบัณฑิตวิทยาลัย

The abstract and full text of theses from the academic year 2011 in Chulalongkorn University Intellectual Repository (CUIR)
are the thesis authors' files submitted through the University Graduate School.

วิทยานิพนธ์นี้เป็นส่วนหนึ่งของการศึกษาตามหลักสูตรปริญญาวิทยาศาสตรดุษฎีบัณฑิต

สาขาวิชาเคมี ภาควิชาเคมี

คณะวิทยาศาสตร์ จุฬาลงกรณ์มหาวิทยาลัย

ปีการศึกษา 2560

ลิขสิทธิ์ของจุฬาลงกรณ์มหาวิทยาลัย

SYNTHESIS AND OPTICAL PROPERTIES OF PYRROLIDINYL PEPTIDE NUCLEIC ACID
CARRYING FLUORESCENCE NUCLEOBASES

Miss Duangrat Nim-anussornkul



A Dissertation Submitted in Partial Fulfillment of the Requirements
for the Degree of Doctor of Philosophy Program in Chemistry

Department of Chemistry

Faculty of Science

Chulalongkorn University

Academic Year 2017

Copyright of Chulalongkorn University

Thesis Title	SYNTHESIS AND OPTICAL PROPERTIES OF PYRROLIDINYL PEPTIDE NUCLEIC ACID CARRYING FLUORESCENCE NUCLEOBASES
By	Miss Duangrat Nim-anussornkul
Field of Study	Chemistry
Thesis Advisor	Professor Tirayut Vilaivan, D.Phil.

Accepted by the Faculty of Science, Chulalongkorn University in Partial
Fulfillment of the Requirements for the Doctoral Degree

.....Dean of the Faculty of Science
(Professor Polkit Sangvanich, Ph.D.)

THESIS COMMITTEE

.....Chairman
(Associate Professor Vudhichai Parasuk, Ph.D.)

.....Thesis Advisor
(Professor Tirayut Vilaivan, D.Phil.)

.....Examiner
(Assistant Professor Aroonsiri Shitangkoon, Ph.D.)

.....Examiner
(Assistant Professor Panuwat Padungros, Ph.D.)

.....External Examiner
(Associate Professor Tienthong Thongpanchang, Ph.D.)

CHULALONGKORN UNIVERSITY

ดวงรัตน์ นิมอนุสรณ์กุล : การสังเคราะห์และสมบัติเชิงแสงของไพร์โรลิดินิลเพปไทด์นิวคลีอิกแอซิดที่มีนิวคลีโอเบสเรืองแสง (SYNTHESIS AND OPTICAL PROPERTIES OF PYRROLIDINYL PEPTIDE NUCLEIC ACID CARRYING FLUORESCENCE NUCLEOBASES) อ.ที่ปรึกษาวิทยานิพนธ์หลัก: ศ. ดร.ธีรยุทธ วิไลวัลย์, 165 หน้า.

ไพร์โรลิดินิล เพปไทด์นิวคลีอิกแอซิดที่ประกอบด้วย ดี-โพรลีน-2-อะมิโนไซโคลเพนเทนคาร์บอกซิลิกแอซิด (เอซีพีซีพีเอ็นเอ) เป็นโครงสร้างหลัก เป็นสารเลียนแบบกรดนิวคลีอิกที่แสดงความแข็งแรงของการจับยึด ความเสถียร และความจำเพาะเจาะจงต่อดีเอ็นเอคู่สมได้ดีกว่าพีเอ็นเอต้นแบบ งานวิจัยนี้มุ่งเน้นการพัฒนาเอซีพีซีพีเอ็นเอโพรบเรืองแสงที่มีนิวคลีโอเบสเรืองแสง ซึ่งสามารถตอบสนองต่อการเกิดไฮบริดโดยการให้สัญญาณการเรืองแสงเพิ่มขึ้นเมื่อเกิดการเข้าคู่อย่างจำเพาะเจาะจงกับดีเอ็นเอเป้าหมาย เอซีพีซีพีเอ็นเอที่มีนิวคลีโอเบสเรืองแสงได้ถูกสังเคราะห์โดย 2 วิธีที่แตกต่างกัน ได้แก่ 1) การสังเคราะห์ผ่านมอนอเมอร์เรืองแสงของพีเอ็นเอ แล้วนำมอนอเมอร์ดังกล่าวไปติดบนสายพีเอ็นเอโดยการสังเคราะห์บนวัฏภาคของแข็ง และ 2) การสังเคราะห์ด้วยวิธีตัดแปรรูปโครงสร้างภายหลังการสังเคราะห์ของเอซีพีซีพีเอ็นเอที่มีหมู่ที่ว่องไว (ในการศึกษานี้ใช้ 5-ไอโอดิยูเรซิล) ด้วยปฏิกิริยาครอสส์ลิงคิงที่เร่งด้วยแพลเลเดียม งานในส่วนแรกได้สังเคราะห์ 8-(ไพรีน-1-อิล)เอไทนิลอะดีนีน (A^{PYE}) มอนอเมอร์โดยวิธีมาตรฐาน จากนั้นนำไปติดบนสายเอซีพีซีพีเอ็นเอด้วยวิธีสังเคราะห์บนวัฏภาคของแข็ง โดย A^{PYE} ในเอซีพีซีพีเอ็นเอมีความสามารถจับกับดีเอ็นเอเป้าหมายได้อย่างจำเพาะเจาะจง อีกทั้งการเข้าคู่เบสดังกล่าวทำให้สัญญาณการเรืองแสงเพิ่มขึ้น ซึ่งการแสดงออกดังกล่าวของ A^{PYE} ในเอซีพีซีพีเอ็นเอนั้นแตกต่างจากกรณีของดีเอ็นเอที่การเข้าคู่ของเบสและการเพิ่มขึ้นของสัญญาณการเรืองแสงนั้นไม่จำเพาะเจาะจงกับเฉพาะเบสดีเอ็นเอ นอกจากนี้การเกิดไฮบริดระหว่าง A^{PYE} ในเอซีพีซีพีเอ็นเอกับดีเอ็นเอที่มีลำดับเบสผิดไปหนึ่งตำแหน่งส่งผลให้สัญญาณการเรืองแสงลดลงซึ่งอธิบายได้โดยการซ้อนทับของไพรีนกับนิวคลีโอเบสในโมเลกุลสายคู่ของพีเอ็นเอกับดีเอ็นเอ จากนั้นจึงได้นำเอซีพีซีพีเอ็นเอที่ตัดแปรรูปด้วย A^{PYE} ไปประยุกต์ใช้เป็นโพรบเรืองแสงที่ตอบสนองต่อการเกิดไฮบริดสำหรับการตรวจสอบลำดับเบสของดีเอ็นเอ งานในส่วนที่สองเป็นการสังเคราะห์ด้วยวิธีตัดแปรรูปโครงสร้างภายหลังการสังเคราะห์ของเอซีพีซีพีเอ็นเอที่มี 5-ไอโอดิยูเรซิล ผ่านปฏิกิริยาครอสส์ลิงคิงแบบซุซูกิ-มียะฮาระ และโซโนกะชิระ ที่เร่งด้วยแพลเลเดียม เพื่อติดฉลากฟลูออโรฟอร์ในกลุ่มของ 5-เอริล หรือ 5-เอริลแอลคิลนึลยูเรซิล บนสายเอซีพีซีพีเอ็นเอ ในการสังเคราะห์เอซีพีซีพีเอ็นเอโพรบที่มี 5-(ไพรีน-1-อิล)เอไทนิลยูเรซิล (U^{PYE}) ผ่านปฏิกิริยาการตัดแปรรูปโครงสร้างภายหลังการสังเคราะห์สามารถเกิดได้อย่างมีประสิทธิภาพในสภาวะสารละลาย ซึ่งการตัดแปรรูปดังกล่าวไม่สามารถทำได้บนวัฏภาคของแข็งเนื่องจาก 5-แอลคิลนึลยูเรซิลสามารถเกิดการปดวไปเป็นอนุพันธ์ของฟิวแรนยูเรซิล โดย U^{PYE} ในเอซีพีซีพีเอ็นเอมีความจำเพาะกับอะดีนีนเบสในสายดีเอ็นเอและแสดงการเพิ่มของสัญญาณการเรืองแสงอย่างมากซึ่งสอดคล้องกับการศึกษาในดีเอ็นเอโพรบ ดังนั้นเอซีพีซีพีเอ็นเอที่ตัดแปรรูปด้วย U^{PYE} สามารถนำไปใช้เป็นโพรบเรืองแสงที่ตอบสนองต่อการเกิดไฮบริด นอกจากนี้การสังเคราะห์ด้วยการตัดแปรรูปโครงสร้างภายหลังการสังเคราะห์ของเอซีพีซีพีเอ็นเอที่มี 5-ไอโอดิยูเรซิลในสภาวะสารละลายผ่านปฏิกิริยาครอสส์ลิงคิงแบบซุซูกิ-มียะฮาระยังมีประสิทธิภาพอย่างมากในการเตรียมเอซีพีซีพีเอ็นเอโพรบเรืองแสงที่มีหมู่เฮเทอโรเอริล (ฟิวแรน, ไทโอฟิน, เบนโซฟิวแรน และเบนโซไทโอฟิน) แทนที่บนเบสยูเรซิล การวิเคราะห์ความเสถียรของสายพีเอ็นเอกับดีเอ็นเอต่อความร้อนแสดงให้เห็นว่าการติดฉลากด้วยหมู่แทนที่ขนาดเล็กดังกล่าวไม่ส่งผลกระทบต่อแข็งแรงและความจำเพาะเจาะจงของการเข้าคู่เบส อย่างไรก็ตาม พีเอ็นเอโพรบดังกล่าวให้สัญญาณการเรืองแสงที่เพิ่มขึ้นทั้งในสภาวะที่มีดีเอ็นเอคู่สมและดีเอ็นเอที่มีเบสผิดไปหนึ่งตำแหน่ง ซึ่งทำให้ไม่สามารถบอกความแตกต่างของดีเอ็นเอเป้าหมายได้ ทั้งนี้อาจเนื่องมาจากเสถียรภาพที่ค่อนข้างสูงของไฮบริดระหว่างพีเอ็นเอกับดีเอ็นเอที่มีเบสผิดไปหนึ่งตำแหน่ง การศึกษานี้แสดงให้เห็นว่าพฤติกรรมของนิวคลีโอเบสที่ถูกตัดแปรรูปโครงสร้างชนิดเดียวกันในเอซีพีซีพีเอ็นเออาจจะไม่สอดคล้องกับในดีเอ็นเอหรืออนุพันธ์ของดีเอ็นเออื่นๆ การสังเคราะห์เอซีพีซีพีเอ็นเอโพรบที่ถูกตัดแปรรูปอย่างหลากหลายผ่านการตัดแปรรูปโครงสร้างภายหลังการสังเคราะห์ยังเป็นวิธีใหม่ที่มีประสิทธิภาพมาก และสามารถนำไปสู่การพัฒนาโพรบชนิดใหม่ที่มีประสิทธิภาพสูงขึ้นได้ต่อไปในอนาคต

ภาควิชา เคมี

ลายมือชื่อนิสิต

สาขาวิชา เคมี

ลายมือชื่อ อ.ที่ปรึกษาหลัก

ปีการศึกษา 2560

5572814223 : MAJOR CHEMISTRY

KEYWORDS: MOLECULAR BEACON, HYBRIDIZATION PROBES, DNA, PNA, FLUORESCENCE

DUANGRAT NIM-ANUSSORNKUL: SYNTHESIS AND OPTICAL PROPERTIES OF PYRROLIDINYL PEPTIDE NUCLEIC ACID CARRYING FLUORESCENCE NUCLEOBASES. ADVISOR: PROF. TIRAYUT VILAIVAN, D.Phil., 165 pp.

Pyrrrolidinyl peptide nucleic acid bearing D-prolyl-2-aminocyclopentanecarboxylic acid backbone (acpcPNA) is a nucleic acid mimic that shows superior binding affinity, stability and specificity to complementary DNA than the original PNA. This research focuses on the development of hybridization responsive fluorescence acpcPNA probes bearing fluorescent nucleobases that exhibit fluorescence increase upon hybridization to a specific nucleobase in the DNA target. The acpcPNA carrying the fluorescent nucleobases were synthesized via two different approaches, namely 1) pre-synthesized fluorescence PNA monomer as a building block that was subsequently incorporated into the PNA by solid phase synthesis and 2) post-synthetic modification of acpcPNA carrying a reactive precursor (5-iodouridine in this case) by palladium-catalyzed cross-coupling reactions. In the first approach, the 8-(pyrene-1-yl)ethynyl-adenine (A^{PyE}) monomer was synthesized by conventional methods and then incorporated into the acpcPNA probe via solid phase peptide synthesis. The A^{PyE} in acpcPNA can specifically recognize thymine base in the DNA target, and the base pairing is accompanied by a strong fluorescence enhancement. The behavior of A^{PyE} in acpcPNA is quite different from the case of DNA whereby the base pairing and fluorescence enhancement was not quite specific for dT. Moreover, fluorescence quenching was observed in mismatched A^{PyE} -acpcPNA and DNA hybrids, which was explained by the stacking of the pyrene moiety inside the duplex. Applications of the A^{PyE} -acpcPNA as a hybridization-responsive fluorescence probe for DNA detection was demonstrated. In the second approach, a versatile post-synthetic modification of 5-iodouracil-containing acpcPNA via a palladium catalyzed Suzuki-Miyaura and Sonogashira cross couplings to introduce 5-aryl or 5-arylalkynyl fluorophores into acpcPNA. The post-synthetic Sonogashira cross coupling in the solution phase allows efficient synthesis of 5-(pyren-1-yl)ethynyl-uracil (U^{PyE}) acpcPNA probes that could not be obtained by solid phase synthesis due to the susceptibility of the 5-arylalkynyl uridine to cyclize to the corresponding furanouracil derivatives. The U^{PyE} in acpcPNA specifically recognized base A in the DNA strand and showed a strong fluorescence increase similar to the DNA case, and thus could be useful as a hybridization-responsive fluorescence probe. The highly efficient post-synthetic modification of 5-iodouracil-modified acpcPNA in solution phase allows easy access to a wide range of fluorescence acpcPNA probe bearing heteroaryl (furan, thiophene, benzofuran and benzothiophene) substituted uracil via post-synthetic Suzuki-Miyaura cross coupling. Attachment of such small substituents did not significantly alter the base pairing strength and specificity as shown by thermal denaturation analyses. Unfortunately, none of these probes could discriminate between complementary and mismatched DNA targets since fluorescence increase was consistently observed due to the high stability of the mismatched hybrid. This study revealed that the behavior of the same modified nucleobase in acpcPNA may not necessarily be the same with DNA or other DNA analogues. The post-synthetic modification approach developed also opens up a new and efficient way to rapidly generate various modified acpcPNA probes which could lead to other new probes with superior performance in the future.

Department: Chemistry

Student's Signature

Field of Study: Chemistry

Advisor's Signature

Academic Year: 2017

ACKNOWLEDGEMENTS

Firstly, I would like to express my sincere gratitude to my thesis advisor, Professor Dr. Tirayut Vilaivan, for his supervision, insightful guidance, and uplifting encouragement given to me during my study and writing this thesis. Apart from these, he also fosters me logical thinking skills needed for my Ph.D. life and my future career. Furthermore, I am also thankful to him for providing me with the valuable opportunity to have a research experience at Pohang University of Science and Technology (POSTECH) under the guidance of Professor Byeang Hyeon Kim. In addition, I would like to thank the thesis committees: Associate Professor Dr. Vudhichai Parasuk, Assistant Professor Dr. Aroonsiri Shitangkoon, Assistant Professor Dr. Panuwat Padungros and Associate Professor Dr. Tienthong Thongpanchang for their useful comments and suggestions which could be implemented to fulfill and improve my study. Besides, I would like to express my grateful to the Science Achievement Scholarship of Thailand (SAST) and the Distinguished Research Professor Grant (DPG578002) for affording me the opportunity to study from Master's degree to Doctoral degree. Moreover, I couldn't forget to thank members of the TV research group for their thought-provoking discussions, advice, and also friendship. Finally, I devoted this study to my mother who is my all-time superwoman and also my sister who never ceases to give supports and encouragement throughout my study. These two important persons are truly wind beneath my wings.

CONTENTS

	Page
THAI ABSTRACT	iv
ENGLISH ABSTRACT	v
ACKNOWLEDGEMENTS	vi
CONTENTS	vii
List of Figures.....	xi
List of Tables	xxi
List of Abbreviations and Symbols	xxiii
CHAPTER I INTRODUCTION.....	1
1.1 Fluorescence nucleic acid sensors.....	1
1.2 Hybridization probes carrying fluorescence nucleobases.....	6
1.3 Peptide nucleic acid (PNA).....	15
1.4 Fluorescence hybridization probes based on peptide nucleic acid	17
1.5 Fluorescent oligonucleotide labeling methods.....	20
1.6 Objectives of this research.....	22
CHAPTER II EXPERIMENTAL SECTION.....	24
2.1 Materials and instruments.....	24
2.2 Synthesis of pyrrolidinyl PNA monomers, ACPC spacer.....	25
2.3 Synthesis of A ^{PyE} -modified pyrrolidinyl PNA monomer	26
2.3.1 Synthesis of <i>N</i> -tert-Butoxycarbonyl- <i>cis</i> -(4' <i>R</i>)-(8-bromoadenine-9-yl)- (2' <i>R</i>)-proline diphenylmethyl ester (2)	26
2.3.2 Synthesis of <i>N</i> -tert-Butoxycarbonyl-(4' <i>R</i>)-[8-(pyrene-1- yl)ethynyladenine-9-yl]-(2' <i>R</i>)-proline diphenylmethyl ester (3).....	27

2.3.3 Synthesis of <i>N</i> -Fluoren-9-ylmethoxycarbonyl-(4' <i>R</i>)-[8-(pyrene-1-yl)ethynyl-adenine-9-yl]-(2' <i>R</i>)-proline (4)	28
2.4 Synthesis of IU ^{Bz} -modified pyrrolidinyl PNA monomer	30
2.4.1 Synthesis of <i>N</i> - <i>tert</i> -Butoxycarbonyl- <i>cis</i> -4-(<i>N</i> ³ -benzoyl-5-iodouracil-1-yl)-(2' <i>R</i>)-proline diphenylmethyl ester (6).....	30
2.4.2 Synthesis of <i>N</i> -Fluoren-9-ylmethoxycarbonyl- <i>cis</i> -(4' <i>R</i>)-(5-iodouracil-1-yl)-(2' <i>R</i>)-proline -proline (7).....	30
2.5 General procedure for post-synthetic modification of acpcPNA by Sonogashira reaction	32
2.5.1 Post-synthetic Sonogashira reaction in solution phase	32
2.5.2 Post-synthetic Sonogashira reaction on the solid phase.....	33
2.6 General procedure for post-synthetic modification of acpcPNA by Suzuki-Miyaura reaction in solution phase.....	35
2.7 General procedure for the synthesis of acpcPNA	39
2.7.1 Solid phase synthesis of acpcPNA.....	39
2.7.2 Purification and analysis of modified acpcPNA	40
2.7.3 Characterization of modified acpcPNA.....	41
2.7.4 Determination of PNA concentration.....	41
2.8 Investigation of PNA•DNA binding	42
2.8.1 Fluorescence experiments.....	42
2.8.2 UV-vis and thermal denaturation experiments	42
2.8.3 Circular dichroism experiments.....	43
2.8.4 Photographing.....	43
2.8.5 Polyacrylamide gel electrophoresis (PAGE).....	43

CHAPTER III RESULTS AND DISCUSSION.....	44
3.1 Fluorescence acpcPNA probes incorporating pre-synthesized fluorescence monomer: Pyrenylethynyladenine (A^{PyE}).....	46
3.1.1 Synthesis of A^{PyE} -pyrroldinyl PNA monomer.....	47
3.1.2 Synthesis of A^{PyE} -modified acpcPNA probes.....	49
3.2 Thermal stability of A^{PyE} -modified acpcPNA with DNA.....	50
3.2.1 Determination of thermal stability of A^{PyE} -modified acpcPNA.....	50
3.2.2 Thermal stability of homothymine acpcPNA bearing A^{PyE} base.....	52
3.2.3 Thermal stability of mix-base acpcPNA bearing A^{PyE}	53
3.3 Optical properties of A^{PyE} -modified acpcPNA with DNA.....	55
3.3.1 Optical properties of homothymine A^{PyE} acpcPNA.....	55
3.3.2 Effects of neighboring bases to base pairing and optical properties of A^{PyE}	56
3.3.3 Effects of position of A^{PyE} in the PNA strand (internal vs terminal).....	63
3.4 Improving the discrimination of A^{PyE} modified acpcPNA probes using graphene oxide.....	64
3.5 Applications of A^{PyE} modified acpcPNA as color-shifting probes.....	67
3.6 Fluorescence acpcPNA probes synthesized via post-synthetic modification.....	72
3.6.1 Synthesis of U^I -acpcPNA monomer.....	73
3.6.2 Synthesis of 5-iodouracil-containing acpcPNA.....	74
3.7 Post-synthetic modification of acpcPNA by Sonogashira reaction.....	75
3.8 Post-synthetic Sonogashira reaction of acpcPNA in the solution phase.....	76

	Page
3.8.1 Post-synthetic Sonogashira reaction of homothymine U ^{PyE} -modified acpcPNA.....	76
3.8.2 Post-synthetic Sonogashira reaction of mix-base U ^{PyE} -modified acpcPNA.....	81
3.9 Post-synthetic Sonogashira reaction on the solid phase	83
3.9.1 Attempted synthesis of 5-(pyrene-1-yl)ethynyl-uracil acpcPNA in solid phase via Rink amide (RAM) linker	83
3.9.2 Attempted synthesis of 5-(pyrene-1-yl)ethynyl-uracil acpcPNA in solid phase via hydroxymethylbenzoyl (HMBA) linker	85
3.10 Purification and characterization of pyrene-modified acpcPNA derived from post-synthetic modification	86
3.11 Thermal stability of DNA hybrids of pyrene-modified acpcPNA	87
3.12 Optical properties of pyrene-modified acpcPNA probes.....	89
3.13 Post-synthetic modification of acpcPNA by Suzuki-Miyaura reaction in solution phase.....	94
3.14 Purification and characterization of C5-aryl-modified uracil acpcPNA derived from post-synthetic modification	102
3.15 Thermal stability of DNA hybrids of C5-aryl-modified uracil acpcPNA probes	102
3.16 Optical properties of fluorescence C5-aryl-modified uracil acpcPNA probes with DNA.....	104
CHAPTER IV CONCLUSION	113
REFERENCES	118
APPENDIX.....	135
VITA.....	165

List of Figures

Figure 1.1 The illustration of fluorescence biosensor.....	1
Figure 1.2 Schematic illustration of hybridization probe concept	2
Figure 1.3 The working principle of the classical molecular beacon	3
Figure 1.4 Quencher-free molecular beacons ²² in the forms of (A) hairpin and (B) linear probes.....	4
Figure 1.5 Schematic representation of strand displacement probe	6
Figure 1.6 Numbering the typically modified sites of purines and pyrimidines state as arrows ⁴¹	6
Figure 1.7 Examples of purine and pyrimidine rings fusion modifications	8
Figure 1.8 Purine and pyrimidine rings substituents modification.....	9
Figure 1.9 Purines and pyrimidines ring extension by conjugated fluorophores....	10
Figure 1.10 The working principle of chromophore-guided DNA disassembly ⁶⁸	11
Figure 1.11 The structures of C ^{Py} and G ^{PyE} (A) and molecular modeling of B-DNA and Z-DNA bearing G ^{PyE} and C ^{Py} (B). (The molecular modeling pictures were taken from Ref. 73).....	13
Figure 1.12 The proposed structures of the hybridization of ^{Py} U probe with its (A) complementary base pair (^{Py} U/A) and (B) mismatch base pair (^{Py} U/G) ²³	14
Figure 1.13 The structures of the Py—C≡C—dX modified DNA where X is dA, dG, dU or dC ⁷⁴	15
Figure 1.14 The working principle of White-Light-Emitting DNA (WED) and the structures of ethynylpyrene and ethynyl Nile red functionalized deoxyuridine ⁷⁵ .	15
Figure 1.15 Basic structures of DNA and PNA. B = pyrimidine base (T or C) or purine bases (A or G).....	16

Figure 1.16 Comparison structures of aegPNA and acpcPNA. B = nucleobase (A, T, C or G).....	17
Figure 1.17 The structures of C5-modified with bicyclic heterocycles based PNA18	
Figure 1.18 Structure of boPhpC and proposed the hydrogen bonding interaction of boPhpC with guanine base ⁸⁹	19
Figure 1.19 Synthetic approaches to palladium-catalyzed nucleobase functionalization	21
Figure 1.20 Synthetic plan for fluorescence acpcPNA probes in this work.....	23
Figure 2.1 Structures of pyrrolidinyl PNA monomers and ACPC spacer for solid phase peptide synthesis.....	25
Figure 3.1 Schematic representation of the two approaches for incorporation of base discriminating fluorescence nucleobases into PNA probes.	46
Figure 3.2 The structure of base discriminating fluorescence nucleobases, A ^{PyE} , used in this work.....	47
Figure 3.3 A schematic diagram of the hypothesis of this work.....	47
Figure 3.4 Synthesis of Fmoc-protected A ^{PyE} PNA monomer	49
Figure 3.5 (A) UV-vis and (B) fluorescence spectra of T4(A ^{PyE})T4 and its DNA hybrids. Conditions: 1.0 μ M PNA, 1.2 μ M DNA, 10 mM sodium phosphate buffer pH 7.0, λ_{ex} 376 nm.....	56
Figure 3.6 UV-vis spectra of M12C(A ^{PyE})C and its DNA hybrids. Conditions: 1.0 μ M PNA, 1.2 μ M DNA, 10 mM sodium phosphate buffer pH 7.0	57
Figure 3.7 CD spectra of M12C(A ^{PyE})C with (A) dcompM12C (complementary), (B) dsmAM12C (single mismatch) and, (C) din4M12C (indirect single mismatch). Conditions: 1.0 μ M PNA, 1.2 μ M DNA in 10 mM phosphate buffer pH 7.0	58
Figure 3.8 Fluorescence spectra of M12C(A ^{PyE})C and its DNA hybrids. Conditions: 1.0 μ M PNA, 1.2 μ M DNA, 10 mM sodium phosphate buffer pH 7.0, λ_{ex} 376 nm.....	59

- Figure 3.9** (A) Fluorescence, (B) UV-vis and (C) CD spectra of **M10A(A^{PyE})C** and its DNA hybrids. Conditions: 1.0 μM PNA, 1.2 μM DNA, 10 mM sodium phosphate buffer pH 7.0, λ_{ex} 376 nm.....60
- Figure 3.10** The concept of using GO or rGO as nanoquenchers to improve the performance of fluorescence hybridization probe detection.....65
- Figure 3.11** Percentage fluorescence quenching of single-stranded PNA **M12T(A^{PyE})T** by GO (green) or rGO (blue). Conditions: 0.1 μM PNA, 0.1 μM DNA, 10 mM Tris HCl pH 7.4, λ_{ex} 376 nm. The fluorescence intensity was measured after incubating the ssPNA with GO/rGO for 1 h.....65
- Figure 3.12** (A) Fluorescence spectra of PNA **M12T(A^{PyE})T** before and after addition of GO or rGO, and after addition of GO/rGO and complementary DNA, (B) The discrimination graph compared between without/with rGO in the presence of DNA and (C) The discrimination graph defined as complementary divided by mismatched hybrid. Conditions: 0.1 μM PNA, 0.5 μM DNA, GO/rGO = 0.2 $\mu\text{g/mL}$, 10 mM Tris HCl pH 7.4, λ_{ex} 376 nm, λ_{em} 438 nm. The fluorescence intensity was measured after incubating the ssPNA with GO/rGO for 1 h.....66
- Figure 3.13** (A) Fluorescence spectra, (B) CD spectra, (C) photograph, and (D) gel electrophoresis of **CAG(A^{PyE})** and its DNA hybrids under UV light. Conditions: 1.0 μM PNA, 1.2 μM DNA, 10 mM phosphate buffer pH 7.0, λ_{ex} 376 nm.....69
- Figure 3.14** Fluorescence spectra of (A) **T8A^{PyE}2_0B** and (B) **T8A^{PyE}2_3B** with DNA. In set shows a photograph of **T8A^{PyE}2_3B** with DNA. Conditions: 1.0 μM PNA, 1.2 μM DNA, 10 mM phosphate buffer pH 7.0, λ_{ex} 376 nm.....71
- Figure 3.15** A schematic showing the post-synthetic modification of acpcPNA through palladium-catalyzed reactions73
- Figure 3.16** Synthesis of Fmoc-protect U^I monomer74
- Figure 3.17** The structures of base discriminating fluorescence nucleobase, U^{PyE} in this work.....75

- Figure 3.18** The post-synthetic approach for the introduction 5-(pyrene-1-yl)ethynyl-uracil (U^{PyE}) into acpcPNA76
- Figure 3.19** MALDI-TOF mass spectra of (A) starting material **TU^lT**, (B) and (C) post-synthetic Sonogashira reaction between **TU^lT** and alkynylfluorophores proceeded in the $Pd(OAc)_2 \cdot [DMADHP]_2$ complex. Arrows indicated the mass of the product peak. (Condition: 600 equiv. alkynylfluorophore, 4.0 equiv. $Pd(OAc)_2 \cdot [DMADHP]_2$, 700 equiv. $K_2HPO_4 \cdot 3H_2O$, 17.0 equiv., sodium ascorbate, 37 °C)77
- Figure 3.20** MALDI-TOF mass spectra of (A) starting material **T4U^lT4** and (B)-(D) post-synthetic Sonogashira reaction performed under the catalytic system of $Pd(PPh_3)_2Cl_2$, CuI and triethylamine. The product peak was indicated by an arrow. The entry number referred to the entry number in **Table 3.9**79
- Figure 3.21** MALDI-TOF mass spectra of (A) starting material **T4U^lT4**, (B) post-synthetic Sonogashira reaction between **T4U^lT4** and 1-ethynylpyrene and (C)-(D) the scale-up reactions between **T4U^lT4** and 1-ethynylpyrene performed under the catalytic system of $Pd(PPh_3)_2Cl_2$, CuI and triethylamine. The entry number referred to the entry number in **Table 3.9**80
- Figure 3.22** The mechanism of Sonogashira cross coupling reaction between **T4U^lT4** and 1-ethynylpyrene81
- Figure 3.23** MALDI-TOF mass spectra of (A) starting material **M10U^l** and (B) post-synthetic Sonogashira reaction between **M10U^l** and 1-ethynylpyrene. (Condition: 500 equiv. 1-ethynylpyrene, 2.5 equiv. $Pd(PPh_3)_2Cl_2$, 3.0 equiv., 16.3 equiv. triethylamine in DMF, 80 °C, 4 hours)82
- Figure 3.24** MALDI-TOF mass spectra of (A) starting material and (B) post-synthetic Sonogashira reaction between **T4U^lT4** and 1-ethynylpyrene using solid phase synthesis. (Condition: 500 equiv. 1-ethynylpyrene, 2.5 equiv. $Pd(PPh_3)_2Cl_2$, 3.0 equiv., 16.3 equiv. triethylamine in DMF, 80 °C, 6 hours)84

Figure 3.25 The possible mechanism of cyclization through 5-endo-dig annulation of 5-(pyrene-1-yl)ethynyl-uracil under acidic condition based on Agrofoglio's hypothesis.....	85
Figure 3.26 MALDI-TOF mass spectra of post-synthetic Sonogashira cross coupling reaction between Lys2M10U^I and 1-ethynylpyrene performing through HMBA linker.....	86
Figure 3.27 Hydrogen bonds formation of (A) fU ^{Py} •dA and (B) fU ^{Py} •dG ¹⁵⁶	89
Figure 3.28 (A) Fluorescence, (B) UV-vis and (C)–(D) CD spectra of T4U^{PyE}T4 and its DNA hybrids. Conditions: 1.0 μM PNA, 1.2 μM DNA, 10 mM sodium phosphate buffer pH 7.0, λ _{ex} 385 nm.....	92
Figure 3.29 (A) Fluorescence, (B) UV-vis and (C)–(D) CD spectra of T4fU^{Py}T4 and its DNA hybrids. Conditions: 1.0 μM PNA, 1.2 μM DNA, 10 mM sodium phosphate buffer pH 7.0, λ _{ex} 385 nm.....	93
Figure 3.30 A method to incorporate C5-heteroaromatic substituent into iodouracil-containing acpcPNA	94
Figure 3.31 The structures of C5-modified uracil-acpcPNA bearing heteroaromatic substituents proposed in this work.....	95
Figure 3.32 MALDI-TOF mass spectra of (A) starting material TU^IT and (B)–(E) post-synthetic Suzuki-Miyaura coupling of TU^IT with phenylboronic acid under buffer conditions. The entry number referred to the entry number in Table 3.13	96
Figure 3.33 MALDI-TOF mass spectra of (A) starting material and (B)–(D) post-synthetic Suzuki-Miyaura coupling of TU^IT with different organoboron compounds.....	98
Figure 3.34 MALDI-TOF mass spectra of T4U^{2Th}T4 from Suzuki-Miyaura coupling in the absence and presence of SiO ₂ . The product was indicated by an arrow. The entry number referred to the entry number in Table 3.14	100

- Figure 3.35** MALDI-TOF mass spectra of $\text{T4U}^{2\text{Th}}\text{T4}$ from Suzuki-Miyaura coupling in 250 nmol scale. The product was indicated by an arrow. The entry number referred to the entry number in **Table 3.14**. 101
- Figure 3.36** MALDI-TOF mass spectra of $\text{T4U}^{\text{Ar}}\text{T4}$ from Suzuki-Miyaura coupling in 250 nmol scale..... 101
- Figure 3.37** UV-vis spectra of (A) $\text{T4U}^{2\text{Th}}\text{T4}$, (B) $\text{T4U}^{3\text{-Th}}\text{T4}$, (C) $\text{T4U}^{2\text{Fu}}\text{T4}$, (D) $\text{T4U}^{3\text{Fu}}\text{T4}$, (E) $\text{T4U}^{2\text{BT}}\text{T4}$ and (F) $\text{T4U}^{2\text{BF}}\text{T4}$ and its DNA hybrids. Conditions: 1.0 μM PNA, 1.2 μM DNA, 10 mM sodium phosphate buffer pH 7.0 105
- Figure 3.38** (A) Fluorescence spectra and (B) normalized fluorescence of $\text{T4U}^{2\text{Th}}\text{T4}$ with its DNA hybrids. Conditions: 1.0 μM PNA, 1.2 μM DNA, 10 mM sodium phosphate buffer pH 7.0, λ_{ex} 330 nm..... 108
- Figure 3.39** (A) Fluorescence spectra and (B) normalized fluorescence spectra of $\text{T4U}^{3\text{Th}}\text{T4}$ with its DNA hybrids. Conditions: 1.0 μM PNA, 1.2 μM DNA, 10 mM sodium phosphate buffer pH 7.0, λ_{ex} 330 nm..... 108
- Figure 3.40** (A) Fluorescence spectra and (B) normalized fluorescence of $\text{T4U}^{2\text{Fu}}\text{T4}$ with its DNA hybrids. Conditions: 1.0 μM PNA, 1.2 μM DNA, 10 mM sodium phosphate buffer pH 7.0, λ_{ex} 330 nm..... 110
- Figure 3.41** (A) Fluorescence spectra and (B) normalized fluorescence of $\text{T4U}^{3\text{Fu}}\text{T4}$ with its DNA hybrids. Conditions: 1.0 μM PNA, 1.2 μM DNA, 10 mM sodium phosphate buffer pH 7.0, λ_{ex} 330 nm..... 110
- Figure 3.42** CD spectra of $\text{T4U}^{2\text{Fu}}\text{T4}$ with its DNA hybrids. Conditions: 1.0 μM PNA, 1.2 μM DNA, 10 mM sodium phosphate buffer pH 7.0. The sum spectra were obtained by combining the CD spectra of $\text{T4U}^{2\text{Fu}}\text{T4}$ and **dA9**, which should represent the spectrum to be observed if there were no interactions between the PNA and DNA..... 111
- Figure 3.43** (A) Fluorescence and (B) UV-vis of $\text{T4U}^{2\text{BT}}\text{T4}$ and its DNA hybrids. Conditions: 1.0 μM PNA, 1.2 μM DNA, 10 mM sodium phosphate buffer pH 7.0, λ_{ex} 330 nm..... 112

Figure 3.44 (A) Fluorescence and (B) UV-vis and of T4U^{2BF}T4 and its DNA hybrids. Conditions: 1.0 μM PNA, 1.2 μM DNA, 10 mM sodium phosphate buffer pH 7.0, λ_{ex} 330 nm.....	112
Figure A1. ¹ H NMR (CDCl ₃ , 400 MHz) of <i>N</i> -tert-Butoxycarbonyl- <i>trans</i> -(4' <i>R</i>)-(8-bromoadenine-9-yl)-(2' <i>R</i>)-proline diphenylmethyl ester (2).....	136
Figure A2. ¹³ C NMR (CDCl ₃ , 100 MHz) of <i>N</i> -tert-Butoxycarbonyl- <i>trans</i> -(4' <i>R</i>)-(8-bromoadenine-9-yl)-(2' <i>R</i>)-proline diethylmethyl ester (2).....	136
Figure A3. ¹ H NMR (CDCl ₃ , 400 MHz) of <i>N</i> -tert-Butoxycarbonyl-(4' <i>R</i>)-[8-(pyrene-1-yl)ethynyladenine-9-yl]-(2' <i>R</i>)-proline diphenylmethyl ester (3).....	137
Figure A4. ¹³ C NMR (CDCl ₃ , 100 MHz) of <i>N</i> -tert-Butoxycarbonyl-(4' <i>R</i>)-[8-(pyrene-1-yl)ethynyladenine-9-yl]-(2' <i>R</i>)-proline diphenylmethyl ester (3).....	137
Figure A5. ¹ H NMR (CDCl ₃ , 400 MHz) of <i>N</i> -Fluoren-9-ylmethoxycarbonyl-(4' <i>R</i>)-[8-(pyrene-1-yl)ethynyladenine-9-yl]-(2' <i>R</i>)-proline (4).....	138
Figure A6. ¹³ C NMR (DMSO- <i>d</i> ₆ , 100 MHz) of <i>N</i> -Fluoren-9-ylmethoxycarbonyl-(4' <i>R</i>)-[8-(pyrene-1-yl)ethynyladenine-9-yl]-(2' <i>R</i>)-proline (4).....	138
Figure A7. ¹ H NMR (CDCl ₃ , 400 MHz) of <i>N</i> -Fluoren-9-ylmethoxycarbonyl- <i>cis</i> -(4' <i>R</i>)-(5-iodouracil-1-yl)-(2' <i>R</i>)-proline (7).....	139
Figure A8. ¹³ C NMR (DMSO- <i>d</i> ₆ , 100 MHz) of <i>N</i> -Fluoren-9-ylmethoxycarbonyl- <i>cis</i> -(4' <i>R</i>)-(5-iodouracil-1-yl)-(2' <i>R</i>)-proline (7).....	139
Figure A9. Analytical HPLC chromatogram of T4(A^{PyE})T4	140
Figure A10. MALDI-TOF mass spectrum of T4(A^{PyE})T4 (calcd for [M•H] ⁺ = 3413.4).....	140
Figure A11. Analytical HPLC chromatogram of M12T(A^{PyE})T	141
Figure A12. MALDI-TOF mass spectrum of M12T(A^{PyE})T (calcd for [M•H] ⁺ = 4543.7).....	141
Figure A13. Analytical HPLC chromatogram of M12A(A^{PyE})A	142

Figure A14. MALDI-TOF mass spectrum of M12A(A^{PyE})A (calcd for [M•H] ⁺ = 4561.7).....	142
Figure A15. Analytical HPLC chromatogram of M12G(A^{PyE})G	143
Figure A16. MALDI-TOF mass spectrum of M12G(A^{PyE})G (calcd for [M•H] ⁺ = 4593.7).....	143
Figure A17. Analytical HPLC chromatogram of M12C(A^{PyE})C	144
Figure A18. MALDI-TOF mass spectrum of M12C(A^{PyE})C (calcd for [M•H] ⁺ = 4513.7).....	144
Figure A19. Analytical HPLC chromatogram of T8(A^{PyE})2_0B	145
Figure A20. MALDI-TOF mass spectrum of T8(A^{PyE})2_0B (calcd for [M•H] ⁺ = 4065.9).....	145
Figure A21. Analytical HPLC chromatogram of T8(A^{PyE})2_3B	146
Figure A22. MALDI-TOF mass spectrum of T8(A^{PyE})2_3B (calcd for [M•H] ⁺ = 4065.9).....	146
Figure A23. Analytical HPLC chromatogram of A^{PyE}M12	147
Figure A24. MALDI-TOF mass spectrum of A^{PyE}M12 (calcd for [M•H] ⁺ = 4543.7).....	147
Figure A25. Analytical HPLC chromatogram of M10A(A^{PyE})C	148
Figure A26. MALDI-TOF mass spectrum of M10A(A^{PyE})C (calcd for [M•H] ⁺ = 3792.8).....	148
Figure A27. Analytical HPLC chromatogram of M10G(A^{PyE})T	149
Figure A28. MALDI-TOF mass spectrum of M10G(A^{PyE})T (calcd for [M•H] ⁺ = 3779.0).....	149
Figure A29. Analytical HPLC chromatogram of CAG(A^{PyE})	150
Figure A30. MALDI-TOF mass spectrum of CAG(A^{PyE}) (calcd for [M•H] ⁺ = 4477.6).....	150

Figure A31. Analytical HPLC chromatogram of T4U^{PyE}T4	151
Figure A32. MALDI-TOF mass spectrum of T4U^{PyE}T4 (calcd for $[M \cdot H]^+ = 3389.7$).....	151
Figure A33. Analytical HPLC chromatogram of T4fU^{Py}T4	152
Figure A34. MALDI-TOF mass spectrum of T4fU^{Py}T4 (calcd for $[M \cdot H]^+ = 3390.7$).....	152
Figure A35. Analytical HPLC chromatogram of T4U^{2Th}T4	153
Figure A36. MALDI-TOF mass spectrum of T4U^{2Th}T4 (calcd for $[M \cdot H]^+ = 3247.4$).....	153
Figure A37. Analytical HPLC chromatogram of T4U^{3Th}T4	154
Figure A38. MALDI-TOF mass spectrum of T4U^{3Th}T4 (calcd for $[M \cdot H]^+ = 3247.4$).....	154
Figure A39. Analytical HPLC chromatogram of T4U^{2Fu}T4	155
Figure A40. MALDI-TOF mass spectrum of T4U^{2Fu}T4 (calcd for $[M \cdot H]^+ = 3231.4$).....	155
Figure A41. Analytical HPLC chromatogram of T4U^{3Fu}T4	156
Figure A42. MALDI-TOF mass spectrum of T4U^{3Fu}T4 (calcd for $[M \cdot H]^+ = 3231.4$).....	156
Figure A43. Analytical HPLC chromatogram of T4U^{2BT}T4	157
Figure A44. MALDI-TOF mass spectrum of T4U^{2BT}T4 (calcd for $[M \cdot H]^+ = 3297.4$).....	157
Figure A45. Analytical HPLC chromatogram of T4U^{2BF}T4	158
Figure A46. MALDI-TOF mass spectrum of T4U^{2BF}T4 (calcd for $[M \cdot H]^+ = 3281.4$).....	158

- Figure A47.** (A) UV-vis spectra, (B) fluorescence spectra of **M12T(A^{PyE})T** and its DNA hybrids; Conditions: 1.0 μM PNA, 1.2 μM DNA, 10 mM phosphate buffer pH 7.0, λ_{ex} 376 nm 159
- Figure A48.** (A) UV-vis spectra, (B) fluorescence spectra of **M12A(A^{PyE})A** and its DNA hybrids; Conditions: 1.0 μM PNA, 1.2 μM DNA, 10 mM phosphate buffer pH 7.0, λ_{ex} 376 nm 159
- Figure A49.** (A) UV-vis spectra, (B) Fluorescence spectra of **M12G(A^{PyE})G** and its DNA hybrids; Conditions: 1.0 μM PNA, 1.2 μM DNA, 10 mM phosphate buffer pH 7.0, λ_{ex} 376 nm 159
- Figure A50.** (A) UV-vis spectra, (B) Fluorescence spectra of **M10G(A^{PyE})T** and its DNA hybrids; Conditions: 1.0 μM PNA, 1.2 μM DNA, 10 mM phosphate buffer pH 7.0, λ_{ex} 376 nm 160
- Figure A51.** CD spectra of **M12C(A^{PyE})C** (A: double mismatched hybrid with dCAGTTTTTG ACT, B: single mismatched hybrid with dCAGTGAGTGACT); Conditions: 1.0 μM PNA, 1.2 μM DNA (A) or 2.0 μM PNA, 2.4 μM DNA (B) in 10 mM phosphate buffer pH 7.0..... 160
- Figure A52.** CD spectra of (A) **M12T(A^{PyE})T** (complementary hybrid with dCAGTATATGACT, single mismatched hybrid with dCAGTAAATGACT) and (B) **A^{PyE}M12** (complementary hybrid with dCAGTATATGACT, single mismatched hybrid with dCAGTATATGACA); Conditions: 1.0 μM PNA, 1.2 μM DNA, 10 mM phosphate buffer pH 7.0..... 161
- Figure A53.** Fluorescence spectra of **M12T(A^{PyE})T** (A) and **A^{PyE}M12** (B) and their DNA hybrids; Conditions: 1.0 μM PNA, 1.2 μM DNA, 10 mM phosphate buffer pH 7.0, λ_{ex} 376 nm 161
- Figure A54.** (A) UV-vis spectra, (B) gel electrophoresis (left, UV shadowing at 265 nm; right, viewed under transilluminator at 365 nm), (C) and (D) CD spectra of **CAG(A^{PyE})** and its DNA hybrids. Conditions: 1.0 μM PNA, 1.2 μM DNA, 10 mM phosphate buffer pH 7.0, λ_{ex} 376 nm..... 162

List of Tables

Table 2.1 Sequences of fluorescent modified-nucleobases acpcPNA by incorporating fluorescent monomers.....	29
Table 2.2 Sequences of fluorescence modified nucleobases acpcPNA by post-synthetic modification	38
Table 3.1 Sequences and characterization data of fluorescence-modified acpcPNA probes.....	50
Table 3.2 Thermal stability data of A ^{PyE} -modified acpcPNA probes and their DNA hybrids (Condition: 1.0 μM PNA, 1.2 μM DNA, 10 mM phosphate buffer pH 7.0)..	51
Table 3.3 Optical properties of A ^{PyE} -modified acpcPNA probes and their DNA hybrids (Condition: 1.0 μM PNA, 1.2 μM DNA, 10 mM phosphate buffer pH 7.0, λ_{ex} 376 nm).....	61
Table 3.4 Optical properties of A ^{PyE} -modified acpcPNA probes and their DNA hybrids (Condition: 1.0 μM PNA, 1.2 μM DNA, 10 mM phosphate buffer pH 7.0, λ_{ex} 376 nm).....	63
Table 3.5 Fluorescence emission ratio of the M12T(A ^{PyE})T-rGO complex in the presence of DNA. (Condition: 0.1 μM PNA, 0.5 μM DNA, 0.2 $\mu\text{g/mL}$ rGO, 10 mM Tris HCl pH 7.4, λ_{ex} 376 nm, λ_{em} 438 nm. The fluorescence intensity was measured after incubated ssPNA with rGO for 1 hour.)	67
Table 3.6 Optical properties of A ^{PyE} -modified acpcPNA probes and their DNA hybrids (Condition: 1.0 μM PNA, 1.2 μM DNA, 10 mM phosphate buffer pH 7.0, λ_{ex} 376 nm).....	69
Table 3.7 Optical properties of A ^{PyE} -modified acpcPNA probes and their DNA hybrids (Condition: 1.0 μM PNA, 1.2 μM DNA, 10 mM phosphate buffer pH 7.0, λ_{ex} 376 nm).....	70
Table 3.8 Sequences and characterization data of U ^I -acpcPNA.....	74

Table 3.9 Optimization of post-synthetic Sonogashira reaction of acpcPNA.....	78
Table 3.10 Sequences and characterization data of pyrene-modified acpcPNA probes obtained from post-synthetic Sonogashira reaction.	87
Table 3.11 Thermal stability data of pyrene-modified acpcPNA and their DNA hybrids. (Condition: 1.0 μM PNA, 1.2 μM DNA, 10 mM phosphate buffer pH 7.0).	88
Table 3.12 Optical properties of pyrene-modified acpcPNA probes and their DNA hybrids (Condition: 1.0 μM PNA, 1.2 μM DNA, 10 mM phosphate buffer pH 7.0, λ_{ex} 385 nm).....	90
Table 3.13 Optimization of post-synthetic Suzuki-Miyaura reaction of acpcPNA..	96
Table 3.14 Optimization of post-synthetic Suzuki-Miyaura reaction of acpcPNA containing 5-iodouracil	99
Table 3.15 Sequences and characterization data of C5-aryl-modified uracil acpcPNA probes.....	102
Table 3.16 Thermal stability data of C5-aryl-modified uracil acpcPNA and their DNA hybrids. (Condition: 1.0 μM PNA, 1.2 μM DNA, 10 mM phosphate buffer pH 7.0).....	103
Table 3.17 Optical properties of C5-aryl-modified uracil acpcPNA and their DNA hybrids (Condition: 1.0 μM PNA, 1.2 μM DNA, 10 mM phosphate buffer pH 7.0, λ_{ex} 330 nm).....	106
Table A1. UV absorption data of A ^{PyE} -modified acpcPNA probes (condition: 1.0 μM PNA, 1.2 μM DNA, 10 mM phosphate buffer pH 7.0).....	163
Table A2. UV absorption data of doubly A ^{PyE} -modified acpcPNA probes (condition: 1.0 μM PNA, 1.2 μM DNA, 10 mM phosphate buffer pH 7.0).....	164

List of Abbreviations and Symbols

2^{BF}	benzofuran-2-yl
2^{BT}	benzothiophene-2-yl
2^{Fu}	fur-2-yl
3^{Fu}	fur-3-yl
2^{Th}	thiophen-2-yl
3^{Th}	thiophen-3-yl
δ	chemical shift
μL	microliter
μmol	micromole
$[\alpha]_{\text{D}}$	specific rotation
A	adenine
A^{Bz}	<i>N</i> ⁶ -benzoyladenine
Ac	acetyl
Ac_2O	acetic anhydride
Boc	<i>tert</i> -butoxycarbonyl
Bz	benzoyl
c	concentration
C	cytosine
calcd	calculated
C^{Bz}	<i>N</i> ⁴ -benzoylcytosine
CCA	α -cyano-4-hydroxy cinnamic acid
CDCl_3	deuterated chloroform
DMSO-d_6	deuterated dimethyl sulfoxide
d	doublet
DBU	1,8-diazabicyclo[5.4.0]undec-7-ene
DCM	dichloromethane
DIEA	diisopropylethylamine
DMF	<i>N,N'</i> -dimethylformamide

DNA	deoxyribonucleic acid
Dpm	diphenylmethyl
ds	double strand
equiv	equivalent (s)
Fmoc	9 <i>H</i> -fluoren-9-ylmethoxycarbonyl
FmocCl	9 <i>H</i> -fluoren-9-ylmethyl chloroformate
FmocOSu	9 <i>H</i> -fluoren-9-ylmethyl succinimidyl carbonate
FRET	Förster (fluorescence) resonance energy transfer
g	gram
G	guanine
h	hour
HATU	<i>O</i> -(7-azabenzotriazol-1-yl)- <i>N,N,N',N'</i> -tetramethyluronium hexafluorophosphate
HOAt	1-hydroxy-7-azabenzotriazol
HPLC	high performance liquid chromatography
Hz	hertz
<i>J</i>	coupling constant
Lys	lysine
m	multiplet
M	molar
MALDI-TOF	matrix-assisted laser desorption/ionization-time of flight
MeCN	acetonitrile
MeOH	methanol
mg	milligram
MHz	megahertz
min	minute
mL	milliliter
mM	millimolar
mmol	millimole
MS	mass spectrometry
<i>m/z</i>	mass to charge ratio

nm	nanometer
NMR	nuclear magnetic resonance
°C	degree celsius
Pfp	pentafluorophenyl
Ph	phenyl
Py	pyrene
PyE	1-ethynylpyrene
PNA	peptide nucleic acid or polyamide nucleic acid
R _f	retention factor
RNA	ribonucleic acid
s	singlet
SPPS	Solid phase peptide synthesis
ss	single strand
t	triplet
T	thymine
TFA	trifluoroacetic acid
THF	tetrahydrofuran
TLC	thin layer chromatography
T _m	melting temperature
t _R	retention time
U	uracil or uridine
UV	ultraviolet

CHAPTER I

INTRODUCTION

1.1 Fluorescence nucleic acid sensors

The working principle of biosensors relies on the specific biological recognition between the bioanalyte of interest and an appropriate bioreceptor, which must be coupled with a signal transduction unit that can convert the molecular interaction into a measurable signal that is directly associated with the specific binding between the bioreceptor and its target bioanalyte (**Figure 1.1**).

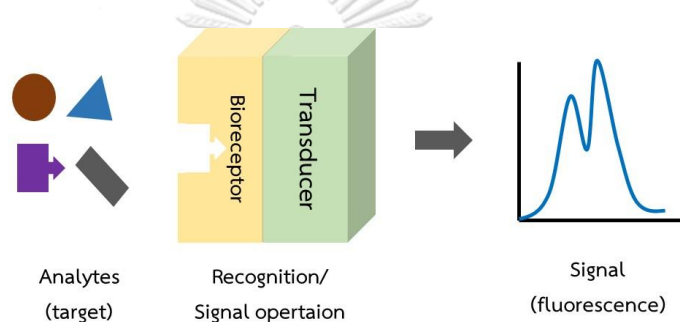


Figure 1.1 The illustration of fluorescence biosensor

Nucleic acids including DNA and RNA are present in all living organisms. The ability of the nucleobases to form specific Watson-Crick base pairing is the basis of their essential functions in the storage and transfer of genetic information. Based on the knowledge that nucleic acids can specifically bind to a specific complementary nucleic acid strand, oligonucleotides or analogues can be applied in a wide variety of applications in the areas of diagnostics and therapeutics.¹ Nucleic acid sensing can be carried out in many different ways.²⁻⁴ One of the most widely used platform is hybridization probe, which usually consists of a single-stranded oligonucleotide with predefined base sequence that can bind specifically to the correct nucleic acid targets through the noncovalent interaction between nucleobases in the probe and the target strands according to Watson-crick base pairing rules as the recognition element (**Figure 1.2**). To enable the detection, the probe must be chemically modified with one or more reporter groups that can transduce the probe-target binding into measurable

signals, which can be fluorescence,⁵⁻⁶ electrochemistry,⁷⁻⁹ surface plasmon resonance,¹⁰⁻¹² chemiluminescence,¹³⁻¹⁴ and colorimetry.¹⁵⁻¹⁷ In the most primitive design, the reporter group may simply act as a “dumb” label, and therefore it is necessary to separate the hybridized and unhybridized probes, usually by performing the hybridization on a solid-phase followed by washing, before measuring the signal. Alternatively, a “smart” probe may be designed to be directly responsive to the hybridization, which is more advantageous since the free and the hybridized probes exhibit different signals and can be directly detected without the need for separation.

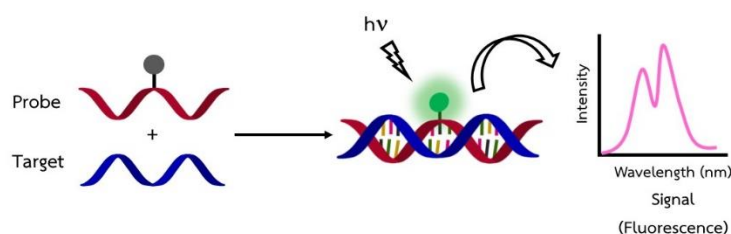


Figure 1.2 Schematic illustration of hybridization probe concept

Fluorescence spectroscopy is one of the most important techniques for studying nucleic acids both *in vivo* and *in vitro* in terms of sensitivity, versatility, accessibility, cost and speed. Oligonucleotide-based fluorescent hybridization probes that can generate distinct fluorescence signal upon specifically binding to the correct nucleic acid target, preferably in real time, have a wide variety of applications such as disease diagnosis, of nucleic acids and drug discovery.¹⁸

To introduce the mechanism of fluorescence change in to the hybridization probe, the presence of two dyes – a fluorophore and a quencher (or a second fluorophore) – is often required. The probe must be designed so that the interaction between the two dyes is dependent on the hybridization state of the probe in such a way that their optical properties are different between non-hybridized and hybridized states. Example of common designs include “classical” doubly-labeled molecular beacons, singly-labeled “quencher-free” molecular beacons, and strand displacement probes. The most well-known example of such probes are molecular beacon (MB),¹⁹ which is a doubly-labeled single stranded oligonucleotide designed to have 5-8 bases self-complementary ends. In the free state, it forms a hairpin structure comprising of

the loop that acts as a recognition site for binding with the DNA target and the stem part that acts as a signaling unit. In the hairpin conformation, the fluorophore and the quencher are brought into close proximity, resulting in fluorescence quenching and therefore no or only weak signals were observed. In the presence of complementary target, the binding of the DNA to the loop region rigidifies the DNA structure, leading to dissociation of the stem part. In this open conformation of molecular beacon, the fluorophore and quencher are separated thereby the fluorescence signal was restored (Figure 1.3).

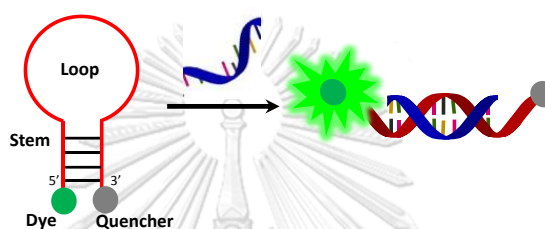


Figure 1.3 The working principle of the classical molecular beacon

However, there are some drawbacks of such design. The interactions between the two dyes must be carefully fine-tuned. This will depend on the relative stability of the stem part and the newly formed duplex at the loop region. Too low stability of the stem part will result in high background signal due to incomplete quenching, and too high stability will result in no signal change since the hybridization will fail to open the stem-loop structure.¹⁹⁻²⁰

In addition, since the unhybridized fluorophore-quencher molecular beacons remain dark, delivery of the molecular beacon into the cells cannot be easily monitored. To overcome this problem, another type of molecular beacon based on the Förster resonance energy transfer (FRET) mechanism employing two fluorophores that act as donor-acceptor pair instead of the fluorophore-quencher pair was developed. Upon excitation of the donor fluorophore in the hairpin form, the energy transfer from the donor fluorophore to the acceptor fluorophore occurs leading to the fluorescence of the acceptor while the fluorescence of the donor fluorophore is quenched. Upon hybridization to the DNA target, the fluorescence of the donor is enhanced and that of the acceptor is reduced due to the separation of the two

fluorophores.²¹ In this way, the FRET-based molecular beacons in the free and hybridized states exhibit different fluorescence emission wavelengths in addition to fluorescence intensities change. In the abovementioned designs, two labels are still required in the same probe which are expensive and difficult to synthesize. It is highly desirable to have a single-fluorophore-labeled probe that can change the fluorescence in response to the hybridization state without requiring the quencher or another fluorophore. These can be achieved in many different ways.

In a typical design, a single environment sensitive dye that can change the fluorescence emission without requiring a quencher has been employed to create the so-called “quencher-free” molecular beacon. The probe can have a hairpin structure (Figure 1.4A) or present as a linear probe (Figure 1.4B), with the former exhibiting higher specificity. The fluorophore can be an isolated label which could be attached to a specific position of the oligonucleotide probe (terminal, internal at sugar or at nucleobase).²² Alternatively, the fluorophore can be attached or incorporated into the nucleobase in such a way that they can communicate (e.g. through π -conjugation), the fluorescence change will be directly responsive to the formation of base pair or base stack. Such fluorescent nucleobase are known as base discriminating fluorescent nucleobase (BDF)²³⁻²⁴ (Figure 1.4B) and will be discussed in more details in the next section.²⁵⁻²⁷

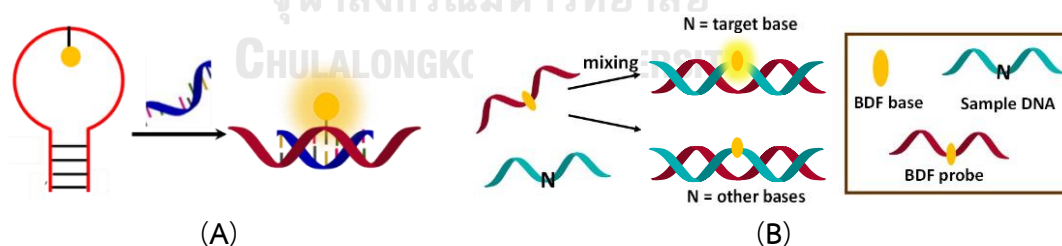


Figure 1.4 Quencher-free molecular beacons²² in the forms of (A) hairpin and (B) linear probes

Another alternative approach for quencher-free probe is the use of simple labeled probes with an external FRET donor or acceptor (such as quantum dots) or an external quencher such as graphene oxide or gold nanoparticles.²⁸⁻³⁰ Graphene oxide (GO) is a two-dimensional carbon network consisting the sp^2 -hybridized carbons that is able to interact with other aromatic compounds via π - π stacking.³¹ Single-stranded nucleic acids are shown to bind more favorably on the GO surface than double-stranded nucleic acids via the π - π stacking and hydrogen bonding interactions between the exposed nucleobases and the GO surface. Since GO is a good quencher through fluorescence resonance energy transfer (FRET) or dipole-dipole coupling effect, fluorescence-modified single stranded nucleic acid is more strongly quenched than double stranded nucleic acid.³² The combination of fluorescent-labeled nucleic acids and GO has been widely used in FRET-based biosensors to detect proteins,³³ nucleic acids,³⁴ as well as non-nucleic acid targets.¹⁵

To avoid the stem-loop structures without compromising the specificity, another type of fluorescence hybridization probe called strand displacement probe was designed. The working principle of strand displacement probe relies on an intermolecular competitive hybridization. Generally, the strand displacement probe contains two complementary nucleic acid strands – one of which carries a fluorophore and the other a quencher. Hybridization to each other resulting in the fluorescence quenching due to the close proximity of the fluorophore and the quencher. However, one of the strand is designed to be readily displaced by the DNA target that is perfectly complementary to the other strand of the probe. For example, the strand to be displaced is often made shorter than the other strand. Subsequently, in the presence of the target, the formation of a more stable hybrid between one of the probe strands and the target lead to the separation of the quencher and the fluorophore (**Figure 1.5**). Since the fluorophore and quencher can no longer interact, the enhancement of fluorescence occurs.³⁵⁻³⁶

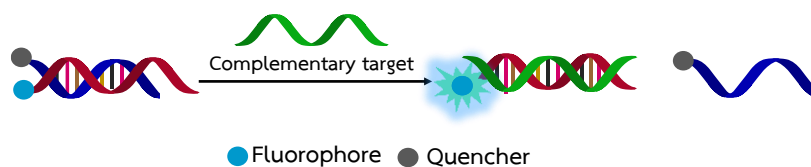


Figure 1.5 Schematic representation of strand displacement probe

1.2 Hybridization probes carrying fluorescence nucleobases

A number of fluorescent purine and pyrimidine analogues have been synthesized to be utilized as base-discriminating fluorescent nucleobases for determining nucleic acid sequences and genetic analysis.³⁷⁻³⁹ Fluorescence purine and pyrimidine analogues can be divided into three categories; 1) ring fusion modification, 2) substitution on the purine or pyrimidine ring and 3) extending purines or pyrimidines ring through conjugated fluorophore (**Figure 1.6**).⁴⁰

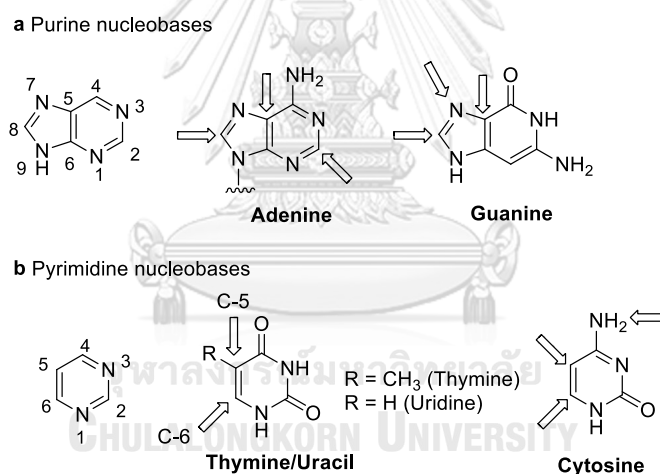


Figure 1.6 Numbering the typically modified sites of purines and pyrimidines state as arrows⁴¹

The first category is ring fusion modification which mostly occurs at N-7 and C-8 position of the five-membered ring of purines, and at C5- and C-6 position or C-4 site of pyrimidines.⁴⁰ Several ring fusion designs have been proposed. For example, extending the aromatic ring of adenine gave a tricyclic carbazole-like methoxybenzoadenine (^{MD}A) and methoxebenzozainosine (^{MD}I) that, when incorporated into DNA, can change their fluorescence upon pairing to C and T in

complementary strand, respectively.⁴² Another extended fluorophore, naphthodeazaadenine (NDA), has been employed as a FRET donor in combination with fluorescein as the FRET acceptor to detect a single nucleotide alteration in DNA. This system showed a strong fluorescent emission only in the presence of complementary base.⁴³ Besides, insertion of the phenyl ring between the five- and the six-membered rings of the purine structure⁴⁴ gave the bases xA and xG that showed a high fluorescence quantum yield. Oligonucleotides containing xG showed a highly selective fluorescence emission increase by 2–3 folds upon hybridization that depends on its pairing with adenine in the opposite strand (**Figure 1.7a**).⁴⁵

Similar expansion of the pyrimidine rings could be achieved at C5- and C-6 sites such as the highly emissive fluorescent thieno[3,4-*d*]-pyrimidines ThU that exhibited a strong quantum yield at 0.41 in water.⁴⁶ The emissive oligonucleotide bearing ThU exhibited significant fluorescence quenching upon hybridization with perfect match oligonucleotides due to partial stacking of the chromophore or photoinduced electron transfer caused by neighboring bases effect. However, fluorescence signal was significantly enhanced upon binding with DNA or RNA containing abasic site or mismatched pairing.⁴⁷⁻⁴⁸ Fusion of cytosine with pyrrole ring at C4- and C-5 positions resulted in a fluorescent nucleobase called 2*H*-pyrrolo[2,3-*d*]pyrimidin-2-one (also known as pyrrolo dC) (dF*) that was reported as early as the late 1980s by Inoue and coworkers. It selectively formed a stable dF*•C base pair similar to the canonical G•C base pair.⁴⁹ Since the base dF* was unstable during the oxidation stage required for the solid phase oligonucleotide synthesis, it must be incorporated via the phosphoramidite of the analogous furo[2,3-*d*]-pyrimidin-2(3*H*)-one (furanouracil), which could be converted to the desired or dF* by ammonia treatment during the final stage of DNA synthesis.⁵⁰ In addition, the fluorescent nucleobase 6-methylpyrrolo-dC (MepC) was similarly obtained by treating furano-dU with ammonia during the final step of DNA solid phase synthesis. The MepC containing oligonucleotide could be excited at 272 nm and 345 nm, giving the emission maxima at 470 nm that far from other biomolecules.⁵¹ It can form a stable base pair with dG. The fluorescence of MepC was quenched upon formation of a fully matched hybrid. However, the fluorescence

was enhanced in the probe-mismatched dA duplexes relative to single-stranded probe because the restriction on base stacking that could not detect in the single-stranded probes.⁵² The fluorescence nucleobase 6-phenylpyrrolocytosine (PhpC) can similarly recognize guanine in DNA and RNA. Moreover, the fluorescence was selectively quenched upon pairing with guanine.⁵³ The PhpC have been used in a wide variety of applications, for example for monitoring the biodistribution of siRNAs,⁵⁴ and for enzyme recognition as cytosine mimic (Figure 1.7b).⁵⁵

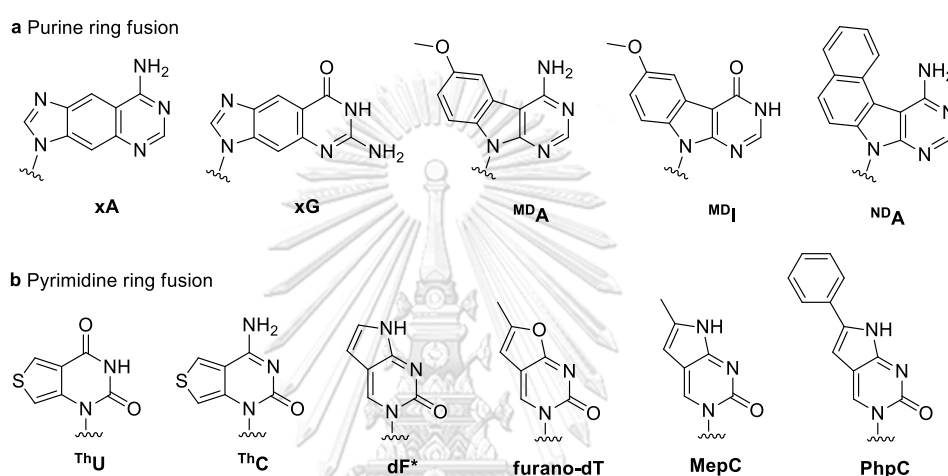


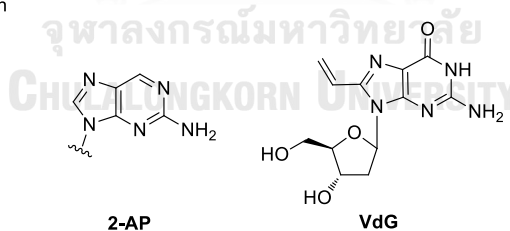
Figure 1.7 Examples of purine and pyrimidine rings fusion modifications

The second category of modification involves manipulation of substituents on the purine or pyrimidine rings to make the base fluorescence. The most well-known fluorescent nucleobase in this category is 2-aminopurine (2-AP), in which the amino group at the C-4 position of the six-membered of adenine moves to the C-2 position as reported by Ward *et. al.* in 1996.⁵⁶ The fluorescent nucleobase 2-AP specifically recognize thymine, uracil or cytosine⁵⁷ in the opposite strand. The fluorescence of 2-AP is strongly quenched when the 2-AP modified probe binds with its complementary target. The high fluorescence quantum yield and sensitivity towards base pairing make 2-AP as an important fluorescent base that has been employed in a wide range of research such as probing the structures and dynamics of nucleic acids,⁵⁸ studying the local structure and thermodynamics of trinucleotide repeat,⁵⁹ investigation of conformation and dynamics of abasic sites in DNA.⁶⁰ Conjugation of a vinyl group at C-8 position of guanine affords a new environment sensitive nucleobase 8-vinyl-2'-

deoxyguanosine (VdG). The base pairing ability of VdG with dC in complementary DNA was retained as confirmed by melting temperature. The fluorescence was quenched upon duplex formation especially when the adjacent nucleobases were guanine and thymine (**Figure 1.8a**).⁶¹

Other examples are C-5 modified pyrimidines with small five-membered ring and bicyclic heterocycles compounds such as *N*-methylindole-, benzothiophene- and benzofuran-nucleosides were synthesized through a standard Pd-catalyzed coupling of halogenated nucleoside precursors and tributylstannylated heterocycles that retain the native nucleic acid structures and functions and highly sensitive to microenvironment.⁶²⁻⁶⁴ Photophysical properties of a series of deoxyuridine functionalized with five-membered heterocycles including thiophene, furan, oxazole and thiazole were studied, which revealed remarkable photophysical properties of furan modified nucleoside (**Figure 1.8b**). Thus, the furan-labeled deoxyuridine was utilized as a building block in oligonucleotide probe for the detection of abasic sites in DNA. The fluorescence of 5-furan-modified deoxyuridine was quenched upon hybridization with complementary DNA. However, a strong fluorescent enhancement was observed by 7 folds (relative to that of perfect match hybridization) when the duplex contain an abasic site located opposite the the modified base.⁶⁴

a Purine modification



b Pyrimidine modification

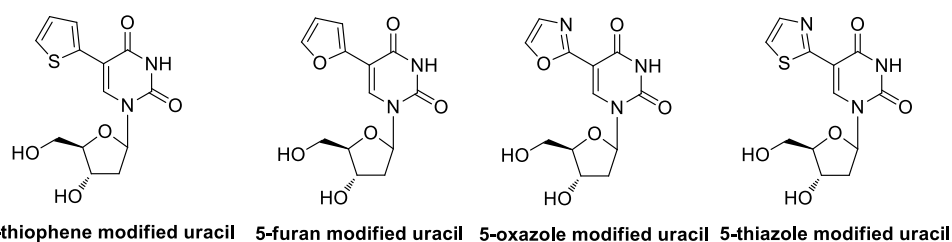
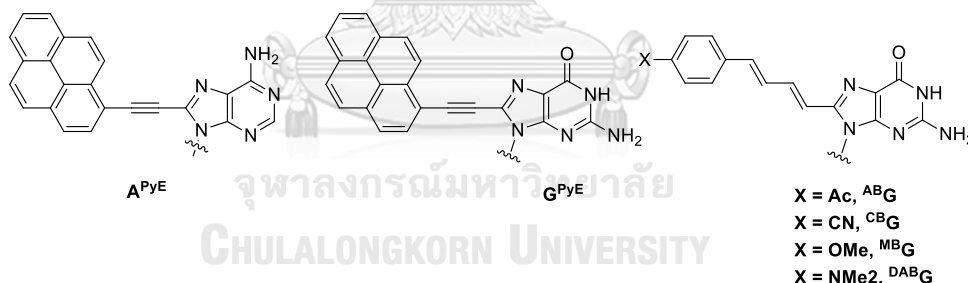


Figure 1.8 Purine and pyrimidine rings substituents modification

The last category of modification is the modification of purine or pyrimidine rings by extended conjugated fluorophores. The C2- or C8 position of purines are the typical sites that can be modified through Pd-catalyzed cross coupling reactions. Pyrene is one of the most popular fluorophores which possess high quantum efficiency and exhibits environment-sensitive fluorescence behavior whereby the fluorescence quantum yields is dependent on the polarity of the media. Quenching was observed in low polarity environment and fluorescence enhancement was observed in high polarity environment. Moreover, pyrene can form the π -stacking with aromatic units of nucleobases, and also intercalate into DNA duplexes leading to the increasing of thermostability of the duplexes. Recently, several reports on pyrene-modified in DNA and its analogues as fluorescent hybridization probes have been described.⁶⁵⁻⁶⁷ In addition, extending the π -conjugation between the nucleobases and pyrene moieties can modify the photophysical properties of the nucleobase. Usually, acetylene bridges are used to extend the conjugation providing a strong electronic coupling between the pyrene and nucleobase.⁶⁸⁻⁶⁹

a Purine ring extension by conjugated fluorophore



b Pyrimidine ring extension by conjugated fluorophore

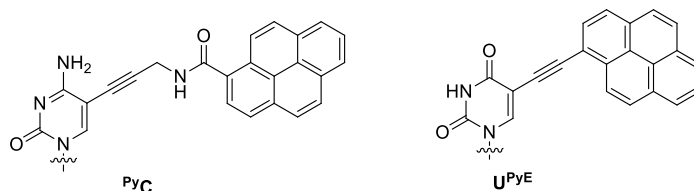


Figure 1.9 Purines and pyrimidines ring extension by conjugated fluorophores

Several modified purine analogues have been investigated in the past decades. Most notably, the fluorescent nucleoside consisting of 1-ethynylpyrene modified adenine (A^{PyE} , **Figure 1.9a**) was employed to determine conformational change in G-

quadruplexes. Incorporating the A^{PyE} at the dangling position of the G-rich oligonucleotide sequences leads to exciplex formation as a result of stacking between the pyrene chromophore and the guanine base in the quadruplex formed in the presence of potassium ion. The emission maxima shifted towards longer wavelength which can be visualized by naked eyes from blue (single-stranded DNA) to green color (G-quadruplex). The increasing in melting temperature of the G-quadruplex containing A^{PyE} (T_m in the range of 57.3–59.2 °C) relative to the natural G-quadruplex (T_m in the range of 55.9–56.4 °C) suggests that the A^{PyE} stacks with the end surface of the G-quadruplex.⁶⁹ The A^{PyE} -modified oligodeoxyadenylate can form a self duplex (A^{PyE} -poly dA) that show a characteristic emission at ca. 580 nm. Addition of coralyne, which site-selectively intercalated at the 3' sides of A^{PyE} , leads to destabilization of the self-duplex, resulting in dissociation of the A^{PyE} -poly dA self-duplex as indicated in **Figure 1.10**. The destabilizing of the self-stacking A^{PyE} -polydA was confirmed by decreasing of melting temperature of the stacked A^{PyE} by 1.5–2.0 °C upon coralyne addition. Furthermore, a decrease of fluorescence intensity as well as blue-shifting of the emission maxima wavelength from ca. 580 nm (A^{PyE} -poly dA) to 500 nm (A^{PyE} -poly dA with coralyne) were observed.⁶⁸

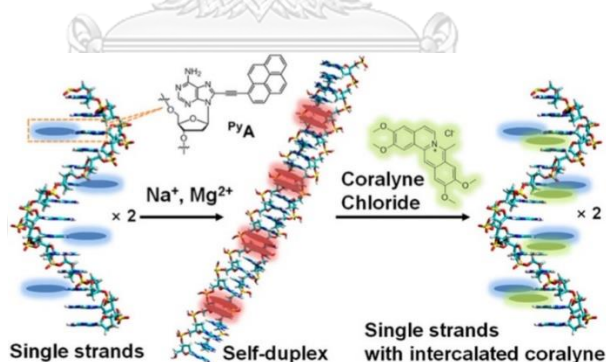


Figure 1.10 The working principle of chromophore-guided DNA disassembly⁶⁸

From all experiments with oligodeoxynucleotides reported so far, it is important to note that the A^{PyE} base showed low binding affinity and non-specific binding when incorporated into DNA as indicated by very small differences in melting temperature of mismatched duplexes by only 0.5–2.5 °C compared with complementary DNA. In addition, the fluorescence emissions of the complementary and mismatched hybrids did not show any significant difference.⁷⁰ This was explained

by the partial intercalation of the pyrene within the duplex as a result of the preference of the A^{PyE} to adopt a *syn* conformation, resulting in lowering the binding affinity as well as specificity.⁷¹⁻⁷² In an attempt to improve the ability of A^{PyE} as a base discriminating fluorescence nucleobase for the detection of single nucleotide polymorphism (SNPs), the A^{PyE}-modified conformationally restricted DNA analogue called locked nucleic acid (LNA) was developed based on the hypothesis that the conformationally constrained structure of LNA might affect to the conformation of pyrene in *anti* or *syn* conformation. Unfortunately, only small difference in the melting temperatures ($\Delta T_m = 1.0\text{--}5.0$ °C) was again observed between complementary and mismatched hybrids. In addition, very a small difference of the fluorescence emission in both complementary and mismatch hybrids were observed.⁷⁰

More examples in this area are the development of fluorescent DNA probe using two pyrene-modified nucleosides. The pyrene-modified alternating C^{Py}G^{PyE} oligonucleotides were designed to monitor the B-Z DNA transition. In the normal B-DNA conformation, the G^{PyE} adopted a *syn*-conformation resulting in the pyrene oriented in the major groove. In contrast, the C^{Py} adopted the *anti*-conformations, exposing the pyrene outside the major groove. Such arrangement resulted in the emission of blue fluorescence of pyrene monomers. At high salt concentration, the CG-alternating DNA adopts a stable Z-DNA structure, in which the pyrene units of G^{PyE} and C^{Py} were forced to locate at the same groove, resulting in π -stacking and exciplex formation and the B-Z transition was indicated by a switch from blue to bluish-green fluorescence (**Figure 1.11**).⁷³

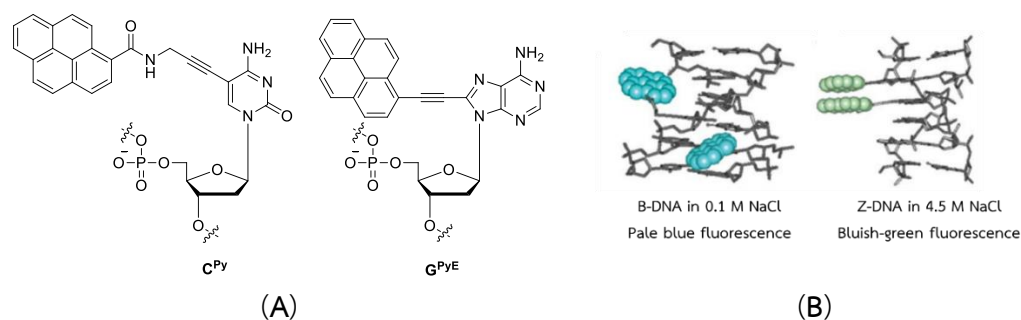


Figure 1.11 The structures of C^{Py} and G^{PyE} (A) and molecular modeling of B-DNA and Z-DNA bearing G^{PyE} and C^{Py} (B). (The molecular modeling pictures were taken from Ref. 73)

Modification of pyrimidines with pyrene at C5-position have been studied in the context of fluorescence oligonucleotide probes (**Figure 1.9b**). In contrast to A^{PyE} , pyrenecarboxamide-modified deoxyuridine and deoxycytosine via a rigid propargyl linker can be utilized as potential BDF probes for SNP typing in DNA sample containing *c-Ha-ras* and BRCA2 gene. Discrimination of the *ras* gene *c-Ha-ras* sequence containing a C/A SNP sites using pyrenecarboxamide-modified deoxyuridine (^{Py}U) showed a highly-A-allele-selective with fluorescence enhancement by 25 folds relative to single-stranded probe. No fluorescence change was observed in the corresponding C-allele sequence. In addition, the fluorescence of pyrenecarboxamide-modified deoxycytidine (^{Py}C) with BRCA2 sequences containing T/G sites was also highly specific to G-allele sequence as indicated by an increase in fluorescence quantum yield from $\Phi_F = 0.035$ (single-stranded) to $\Phi_F = 0.107$ (G-allele). The researchers proposed that the A-selective fluorescence enhancement resulted from the increased polarity around the pyrene chromophore of ^{Py}U upon duplex formation as confirmed by molecular modeling. The modeling study found that in the hybridized state, the ^{Py}U adopted the *anti*-conformation, and the pyrenecarboxamide group was exposed towards the more polar environment outside the duplex, resulting in fluorescent enhancement upon hybridization with perfect match. In the mismatched hybrid, the ^{Py}U adopted a *syn* conformation through rotation of the glycosyl bond between the ^{Py}U and the sugar ring, resulting in intercalation of the pyrene group in the more hydrophobic minor groove, and therefore a fluorescence quenching (**Figure 1.12**).²⁵

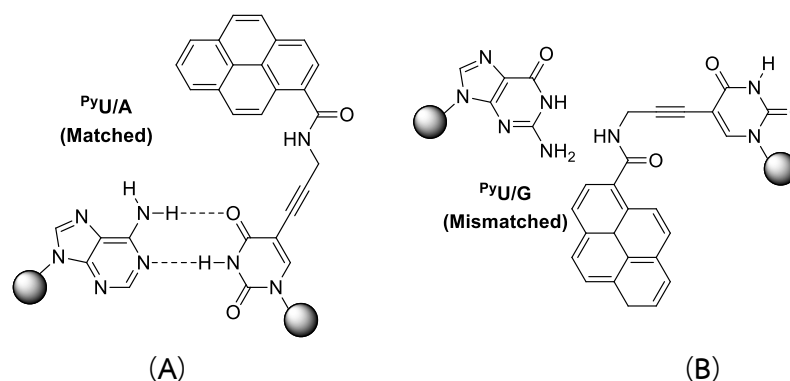


Figure 1.12 The proposed structures of the hybridization of ${}^{\text{Py}}\text{U}$ probe with its (A) complementary base pair (${}^{\text{Py}}\text{U}/\text{A}$) and (B) mismatch base pair (${}^{\text{Py}}\text{U}/\text{G}$)²³

A series of pyrene-modified pyrimidine and purine base analogues directly linked together through an ethynyl linker ($\text{Py}-\text{C}\equiv\text{C}-\text{dX}$, where X is dA, dC, dG or dU) was obtained from Sonogashira cross coupling reaction (**Figure 1.13**). The single-stranded oligonucleotide bearing a single modified nucleoside $\text{Py}-\text{C}\equiv\text{C}-\text{dX}$ exhibited distinct fluorescence spectra compared with complementary duplexes. The complementary duplexes displayed different emission maxima wavelength and fluorescence band structure indicative of the change to the electronic coupling of the pyrene moiety and the nucleobase. The $\text{Py}-\text{C}\equiv\text{C}-\text{dC}$ and $\text{Py}-\text{C}\equiv\text{C}-\text{dG}$ showed a weak electronic coupling between pyrene moiety and nucleobase rings (C and G) with the emission maxima at 408/430 nm or 430/455 nm, respectively. In cases of $\text{Py}-\text{C}\equiv\text{C}-\text{dA}$ and $\text{Py}-\text{C}\equiv\text{C}-\text{dU}$, strong electronic couplings between pyrene and nucleobase residues (A and U) were observed with a broad structure at emission maxima 447 nm and 452 nm, respectively. Fluorescence enhancement was observed in all complementary DNA duplexes, especially a more than 40 folds fluorescence increase was observed in the complementary duplex of $\text{Py}-\text{C}\equiv\text{C}-\text{dG}$.⁷⁴

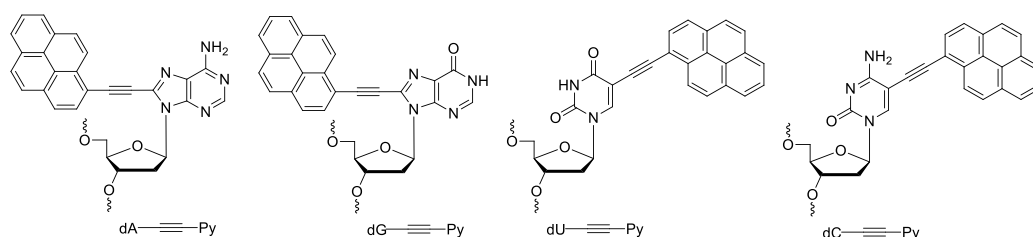


Figure 1.13 The structures of the Py-C≡C-dX modified DNA where X is dA, dG, dU or dC⁷⁴

Recently, an interesting white-light-emitting DNA oligonucleotide probes was developed. Its working principle relies on interactions between pyrene-modified uracil as a donor and Nile red-modified uracil as an acceptor. The pyrene and Nile red fluorophores were attached at 5-position of two adjacent 2'-deoxyuridine via an acetylene bridge. In the single-stranded state, the energy transfer from pyrene to Nile red occurred as shown by fluorescence quenching at pyrene emission wavelength ($\lambda_{em} = 440$ nm) upon excitation ($\lambda_{ex} = 380$ nm) with simultaneous increase of Nile red fluorescence emission ($\lambda_{em} = 665$ nm). When the complementary duplex was formed in the presence of the complementary DNA target, the fluorescence changed into white as a result of the combination of the fluorescence at 440 nm of the pyrene and the fluorescence at 665 nm of the Nile red that were separated, resulting in a less efficient energy transfer from pyrene to Nile red (**Figure 1.14**).⁷⁵

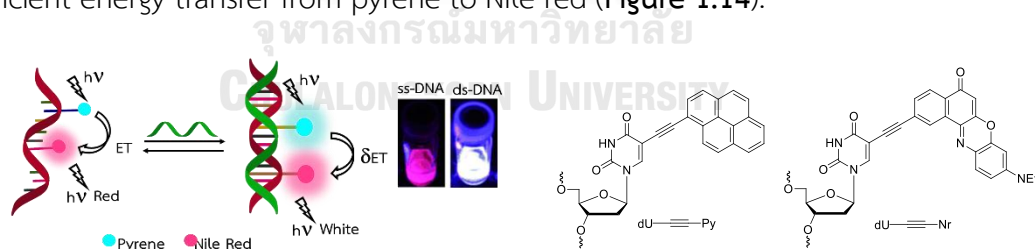


Figure 1.14 The working principle of White-Light-Emitting DNA (WED) and the structures of ethynylpyrene and ethynyl Nile red functionalized deoxyuridine⁷⁵

1.3 Peptide nucleic acid (PNA)

Unnatural oligonucleotide analogues such as peptide nucleic acid (PNA) and locked nucleic acid (LNA), have been increasingly used as biological tools. These analogues generally offer greater chemical and biological stabilities, binding affinity

and increased mismatch discrimination ability compared to DNA. Peptide nucleic acid (PNA) is a remarkable rare example of DNA analogue with an entirely re-designed synthetic backbone not consisting of the sugar-phosphate. The first example of PNA (now known as aegPNA) was introduced by Nielsen and coworkers since 1991.⁷⁶⁻⁷⁷ Unlike most other oligonucleotide analogues, the negatively-charged sugar-phosphate backbone of DNA is completely substituted with an uncharged *N*-(2-aminoethyl) glycine as the repetitive units, linked together by peptide bonds. The purine and pyrimidine nucleobases are attached to the peptide backbone via methylene carbonyl linkage (Figure 1.15).

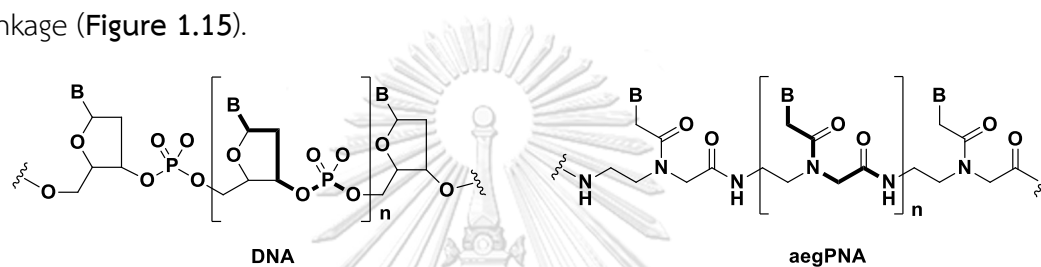


Figure 1.15 Basic structures of DNA and PNA. B = pyrimidine base (T or C) or purine bases (A or G)

The absence of repulsive electrostatic force between PNA and its complementary DNA target resulted in the higher affinity and specificity of the recognition in PNA-DNA hybrid than DNA-DNA hybrid. Despite the great DNA binding affinity of PNA probes, the specificity was not compromised as shown by the larger destabilization of single mismatched hybrids of PNA-DNA than the corresponding DNA-DNA. This makes PNA highly suitable for applications involving single mismatch detections such as discrimination of point mutations or single nucleotide polymorphisms (SNPs). Moreover, the unnatural peptide-like backbone of PNA makes it stable over a wide range of pH and temperature, and contributes to its highly resistance towards nucleases and proteases.⁷⁸⁻⁸⁰

The remarkable properties of aegPNA inspired the development of several other PNA systems over the past 25 years.⁸¹ The rather flexible structure of aegPNA means that there must be entropic penalties in the hybridization process, resulting in suboptimal binding affinities. Besides, aegPNA was experimentally shown to form

stable hybrids with DNA in both antiparallel and parallel directions, which are not desirable. Accordingly, several groups have adopted the idea of conformational restriction of the PNA molecule to develop a more effective PNA.⁸² In this respect, a novel conformationally restricted molecule called pyrrolidinyl PNA was developed by Vilaivan and co-workers in 2005.⁸³⁻⁸⁴ The pyrrolidinyl PNA structure can be divided into two parts (**Figure 1.16**). The first part is the pyrrolidine monomer carrying the four nucleobases (A, T, C and G) attached at 4-position of the pyrrolidine ring. This part is equivalent to nucleosides in DNA. The second part is a cyclic β -amino acid that acts as a spacer, which is equivalent to the phosphate group. A representative member of pyrrolidinyl PNA is acpcPNA carrying a (2'R,4'R)-prolyl-(1S,2S)-2-aminocyclopentanecarboxylic acid backbone. AcpcPNA showed an enhanced binding affinity and higher specificity towards complementary DNA over other PNA systems including the original aegPNA and the more recently developed γ -PNA.⁸⁵ Unlike aegPNA, acpcPNA can only form hybrids with DNA in antiparallel fashion owing to the conformationally constrained nature of the molecule.⁸⁶ These properties suggest the potential of acpcPNA as a candidate for development of hybridization probes for nucleic acid hybridization.

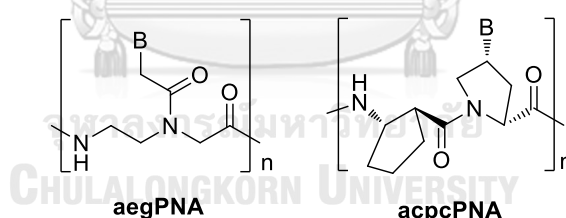


Figure 1.16 Comparison structures of aegPNA and acpcPNA. B = nucleobase (A, T, C or G)

1.4 Fluorescence hybridization probes based on peptide nucleic acid

The remarkable properties of PNA in terms of binding affinity and specificity over DNA-based probes make it a potential candidate for development of hybridization responsive fluorescence probes for DNA sequences analysis. The conjugation of bicyclic heterocycles, for example benzothiophene and benzofuran, to the C5-position of uracil was performed in aegPNA (**Figure 1.17**) with the aim to

develop fluorescence PNA probes.⁶³ The small heterobicyclic substituent minimally perturbed the hybridization efficiency, and the overall structure of the PNA as studied by circular dichroism (CD) and UV melting analysis was similar to unmodified PNA.⁸⁷ The modified-aegPNAs displayed a substantial fluorescence enhancement in the presence of both complementary and mismatched hybrids with a slightly blue-shifted fluorescence emission. Due to the unsatisfactory fluorescence discrimination of these modified aegPNA probes, graphene oxide was used to enhance the performance of benzothiophene-aegPNA by fluorescence quenching of single-stranded PNA before complementary DNA addition. The fluorescence intensity of the single stranded PNA was quenched by 3 folds in the presence of GO. Subsequent addition of the complementary DNA lead to a dramatically increased fluorescence signal by 4 folds relative to the PNA–GO complex.⁸⁸

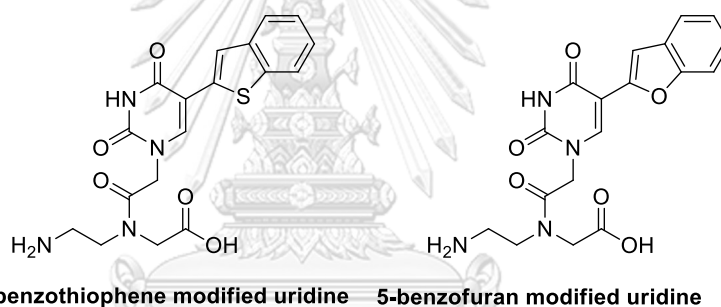


Figure 1.17 The structures of C5-modified with bicyclic heterocycles based PNA

The “G-clamp” pyrrolocytosine analogues, [bis-*ortho*-(aminoethoxy)phenyl]-pyrrolocytosine (abbreviated as boPhpC), was synthesized based on the hypothesis that this fluorescence monomer would interact with guanine by additional hydrogen bonding between the protonated amino group of the side chain of boPhpC and O4 of guanine (**Figure 1.18**).⁸⁹ The beneficial role of the additional hydrogen bonding with guanine base in DNA was confirmed by the remarkable increase of melting temperature by more than 9 °C, as well as the base discrimination ability of the boPhpC to discriminate single-base mismatch as shown by the large ΔT_m value of –13.5 °C. The fluorescence of the complementary duplex was decreased by 50% relative to the free PNA probe, which was consistent with the behavior of other pyrrolocytosine derivatives such as MepC and PhpC in DNA probes.⁵²⁻⁵³

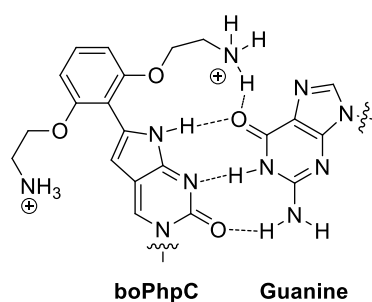


Figure 1.18 Structure of boPhpC and proposed the hydrogen bonding interaction of boPhpC with guanine base⁸⁹

Due to the high sequence-specificity of acpcPNA, the development of such PNA system as potential hybridization-responsive self-reporting fluorescence PNA probes for DNA sequence analysis have been extensively explored by Vilaivan's group.^{86,90} A pyrene-modified uracil incorporated into acpcPNA probes acts as a base discriminating fluorescence nucleobase. It gave a strong fluorescence enhancement in the presence of complementary DNA with high selectivity, showing the discrimination factors between complementary and single-mismatched hybrids up to 3–42 folds, depending on the sequences.⁹¹ Besides, modification of acpcPNA probe with fluorophores can be made easily through post-synthetic modification via a novel spacer, (3'R,4'S)-3-aminopyrrolidine-4-carboxylic acid (APC), which contains a secondary amine group that allows simple functionalization of acpcPNA with a variety of fluorophores at any predefined positions in the PNA sequence, either through amide bonds^{92,93} or via sequential reductive alkylation-click chemistry.⁹⁴ Pyrene-modified acpcPNA at internal position showed fluorescence enhancement when hybridized with complementary DNA and quenching when hybridized with mismatched DNA due to intercalation of the pyrene inside the duplex as confirmed by molecular dynamics simulation.⁹³ The acpcPNA modified with various fluorophores at the internal positions have been successfully employed as self-reporting acpcPNA probes that show fluorescence enhancement in the presence of correct DNA target. The thiazole orange (TO)-labeled acpcPNA probe was highly sensitive to the presence of complementary DNA by showing a strong fluorescence enhancement of ca. 22 folds resulted from the restricted rotation of the thiazole orange dye when intercalated into

the acpcPNA·DNA duplex. Although some non-specific fluorescence enhancement was observed as a result of binding between TO and single stranded DNA, enzymatic digestion by S1 nuclease was employed to improve the specificity of the TO-labeled acpcPNA probe to between 9 and 60 folds for complementary and less than 3.5 folds for mismatched hybrids.⁹⁴ Nile red-modified acpcPNA probes were also utilized as hybridization-responsive probes to determine the oligonucleotide secondary structure as a results of different arrangement of Nile red in single-stranded and double-stranded states.⁹⁵ In addition, a highly sequence specific doubly-end-labeled acpcPNA probes containing a fluorescent dye (FAM or TMR) and an end-stacking quencher (anthraquinone) was recently developed. The fluorescent dye was quenched by the anthraquinone in the single stranded probe. Upon duplex formation, the anthraquinone was stacked on top of the terminal base pair of the PNA-DNA duplex, resulting in its separation from the dye, and therefore fluorescence enhancement.⁹⁶ A strand displacement probe based on a fluorophore-labeled acpcPNA and a quencher-labeled DNA was also developed and demonstrated to show high mismatch discriminating ability.⁹⁷

1.5 Fluorescent oligonucleotide labeling methods

The important step for development of hybridization responsive fluorescent oligonucleotide probes are the incorporation of a fluorescent nucleobase into oligonucleotides. This can be achieved through three different approaches including i) chemical synthesis of the fluorescence monomer and incorporation into the oligonucleotides by chemical methods, ii) chemical synthesis of the fluorescence monomer and incorporation into the oligonucleotides by enzymatic methods and iii) post-synthetic modification of pre-synthesized oligonucleotides.^{40,98} This section focuses on only the chemical-based approaches which can be summarized in **Figure 1.19**.

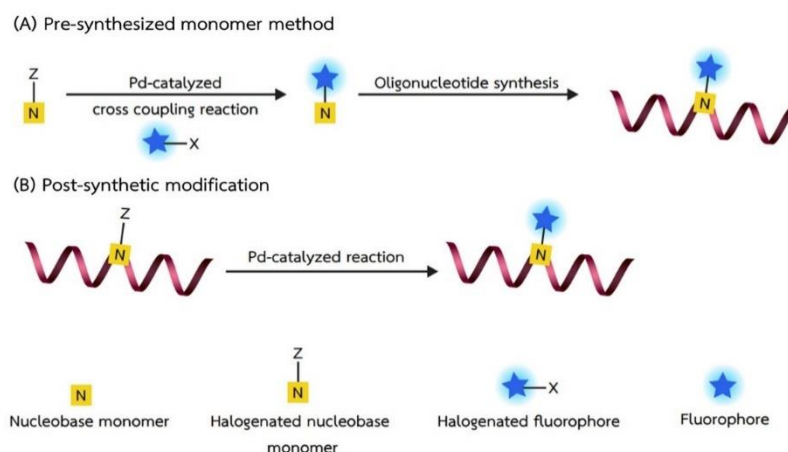


Figure 1.19 Synthetic approaches to palladium-catalyzed nucleobase functionalization

In the pre-synthesized monomer approach, the fluorescent nucleobase monomer is synthesized first as a reactive phosphoramidite, which will be subsequently introduced to the oligonucleotide via solid phase synthesis. The advantage of this method is the monomer can be incorporated site-selectively into the oligonucleotide at any desired position. Although the majority of published work employed this approach extensively,⁹⁹⁻¹⁰⁰ the methods involved the laborious and time-consuming synthesis of the modified building blocks. Moreover, the building blocks may not be stable for long-term storage, and are not always compatible with the solid phase synthesis and cleavage conditions. In addition, the coupling efficiency may be low for bulky monomers.⁴⁰ Another alternative approach that can overcome these limitations is the post-synthetic modification, whereby one or more reactive monomers are initially incorporated at the pre-defined positions of the oligonucleotides via solid phase synthesis or enzymatic methods. Next, the reactive monomer is modified via an appropriate chemical (or enzymatic) reaction. For example, oligonucleotides incorporating halogenated nucleobases can be post-synthetically modified by the palladium-catalyzed cross-coupling reactions. The 8-aryl-guanine oligonucleotides were successfully synthesized via solution-phase post-synthetic Suzuki-Miyaura cross-coupling reaction of 8-bromoguanine-containing oligonucleotide with arylboronic acids treated with $\text{Pd}(\text{OAc})_2/\text{TPPTS}$, the catalytic system, and Na_2CO_3 as base in aqueous acetonitrile at 70 °C to give the modified

oligonucleotides up to 70% yield.¹⁰¹ Post-synthetic modifications of 5-iodouracil-modified oligonucleotides with arylboronic acids under mild condition has been reported using Suzuki-Miyaura cross-coupling. The reactions between of the starting material and various functionalized boronic esters including diazine, azobenzene or benzophenone were effectively performed with 2-aminopyrimidine-4,6-diol (APD) and Pd(OAc)₂ as catalyst under Tris buffer at 37 °C with practically complete conversion.¹⁰² The water-soluble palladium complex, 2-dimethylaminopyrimidine-4,6-diol was used in copper-free Sonogashira cross-coupling reaction to incorporate a wide variety of aryl iodides into peptides/proteins bearing a terminal alkyne group in aqueous media with excellent yields. The palladium complex also utilized to functionalization an alkyne-encoded protein in *Escherichia coli* cells.¹⁰³ In addition, the peptides and proteins labeling approach was reported using a two-step labeling strategy. This approach consisted of covalently attached of *p*-iodopheny derivatives to 13-amino-acid peptide using *Escherichia coli* lipoic acid ligase A (LplA) as a reactive group subsequently bioorthogonal palladium-catalyzed Sonogashira cross-coupling with alkyne-modified fluorophore.¹⁰⁴ The copper catalyzed alkyne-azide cycloaddition (CuAAC) reaction or click chemistry is another popular method that allows effective labeling of an alkyne- or azide-modified oligonucleotide with one or more reporter molecules (usually an alkyne- or azide-modified dye). Click chemistry is particularly attractive for some fluorophores are not compatible with the solid phase synthesis or cleavage conditions.¹⁰⁵ In one example, a quencher-free stemless PNA molecular beacons carrying two pyrene was synthesized from the azide-containing PNA oligonucleotide by click reaction with 1-ethynylpyrene for studying of cystic fibrosis gene.¹⁰⁶

1.6 Objectives of this research

This research aims to develop novel hybridization-responsive fluorescence PNA probes based on the conformationally-constrained acpcPNA system previously developed in this research group by incorporation of fluorescent nucleobases into the PNA molecule. It was expected that the novel fluorescent acpcPNA probes would bind to the correct DNA target and provide fluorescence change in a sequence specific

fashion. The thesis is divided into two parts according to the modification strategies; 1) pre-synthesized monomers and 2) post-synthetic modification approaches. The first part involves the synthesis of acpcPNA probes bearing 8-(pyrene-1-yl)-ethynyl-adenine monomer (A^{PyE}) and evaluation of its performance for DNA sequence detection. The second part involves the development of new fluorescent acpcPNA probes through post-synthetic modification of iodouracil-containing acpcPNA with arylboronic acids or arylethyne via palladium-catalyzed cross couplings, as well as the evaluation of their DNA binding and fluorescence properties.

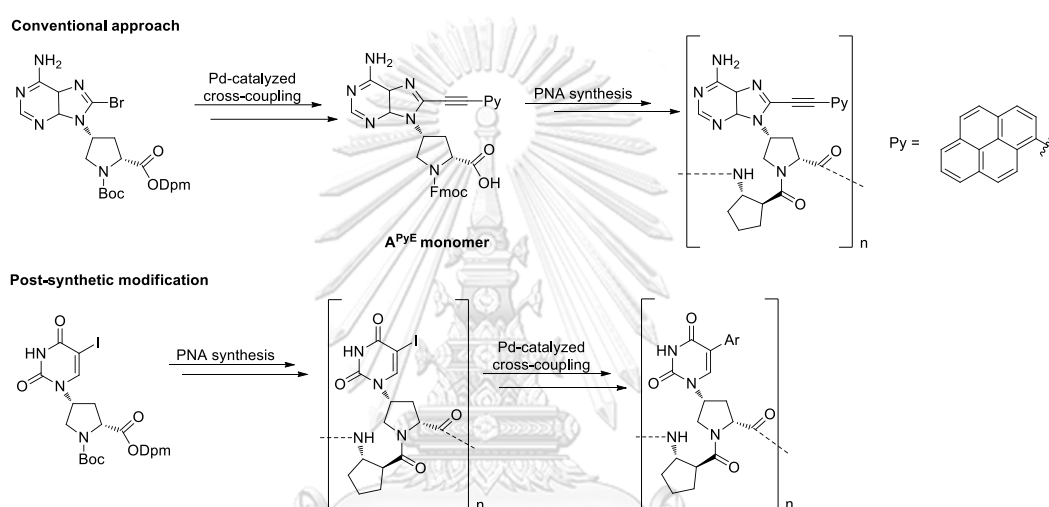


Figure 1.20 Synthetic plan for fluorescence acpcPNA probes in this work

CHAPTER II

EXPERIMENTAL SECTION

2.1 Materials and instruments

All reagent grade chemicals and solvents were purchased from standard suppliers and used as received without further purification. HPLC grade solvents for HPLC experiments were purchased from Merck and Scharlau. The reaction progress was monitored by thin layer chromatography (TLC) purchased from Merck D.C. silica gel 60 F254 0.2 mm pre-coated aluminium plates and observed spots on TLC by visualization under UV light (254 nm). Column chromatography was performed on silica gel 70-230 mesh. Graphene oxide nanocolloids (GO) were purchased from Sigma Aldrich. Reduced graphene oxide (rGO) was synthesized via hydrazine reduction of graphene oxide as previously reported.¹⁰⁷

Anhydrous *N,N*-dimethylformamide ($H_2O \leq 0.01\%$) for solid phase peptide synthesis was purchased from RCI Labscan (Thailand) and dried over activated 4Å molecular sieves before use. Tentagel S-RAM Fmoc resin (0.24 mmol/g) was used as a solid support for peptide synthesis and purchased from Fluka. Oligonucleotides were purchased from Pacific Science (Thailand) or BioDesign (Thailand). Milli-Q water in all experiments were obtained from an ultrapure water system fitted with a Millipak[®] 40 filter unit 0.22 μm , Millipore (USA).

Melting points were determined by using an electrothermal melting point apparatus model 9100. Optical rotation ($[\alpha]^D$) was measured on a Jasco P-1010 Polarimeter using sodium light (D line, 589.3 nm) and the concentrations (c) are reported as g/100 mL. Infrared spectra were recorded on Nicolet 6700 Infrared (IR) spectrometer. ¹H NMR were recorded on Varian Mercury-400 plus or Bruker Avance 400 NMR spectrometer at 400 MHz and 100 MHz for ¹³C NMR. High resolution mass spectra (HRMS) were measured on Bruker Daltonics micrOTOF mass spectrometer (Department of Chemistry, Faculty of Science, Mahidol University) for all new compounds. High resolution MALDI-TOF mass spectra (HRMS) were measured on JEOL

spiralTOF mass spectrometer model JMS-S3000 (Scientific and Technology Research Equipment Centre, Chulalongkorn University) for a new compound. Reversed phase HPLC were performed on a Waters Delta 600 HPLC equipped with a gradient pump, Water 996TM photodiode array detector and ACE 5 A71197, C18-AR, 150x4.6 mm, 5 μm particle size HPLC column for semipreparative separation or Vertisep UPS, 50x4.6 mm, 3 μm particle size HPLC column for analysis of PNA. MALDI-TOF mass spectra were performed on a Microflex MALDI-TOF mass spectrometry (Bruker Daltonics) using α -cyano-4-hydroxycinnamic acid (CCA) as a matrix. Fluorescence spectra were recorded on Cary Eclipse fluorescence spectrophotometer (Varian/Agilent Technologies). Thermal denaturation (T_m) experiments and UV-vis spectra were recorded on Cary 100 Bio UV-vis spectrophotometer (Varian/Agilent Technologies). CD spectra were determined by JASCO Model J-815 spectropolarimeter.

2.2 Synthesis of pyrrolidinyl PNA monomers, ACPC spacer

All Fmoc-protected pyrrolidinyl PNA monomers and ACPC spacer consisting of A^{Bz}, C^{Bz}, T and G monomers were synthesized according to previously published protocols.^{84, 108}

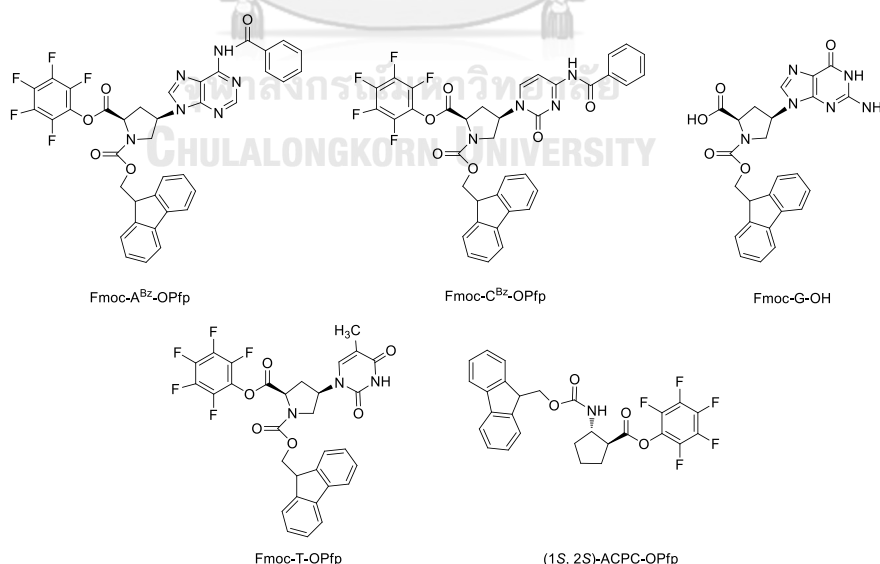


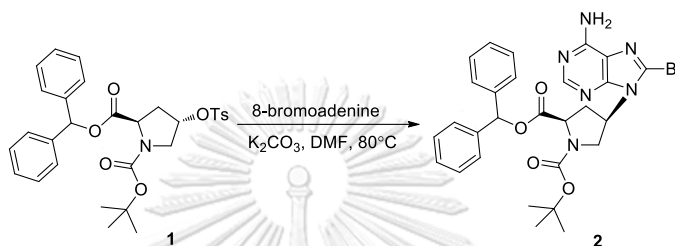
Figure 2.1 Structures of pyrrolidinyl PNA monomers and ACPC spacer for solid phase peptide synthesis

Experimental procedure

Part I: Synthesis of fluorescence acpcPNA via pre-synthesized fluorescence monomer approach

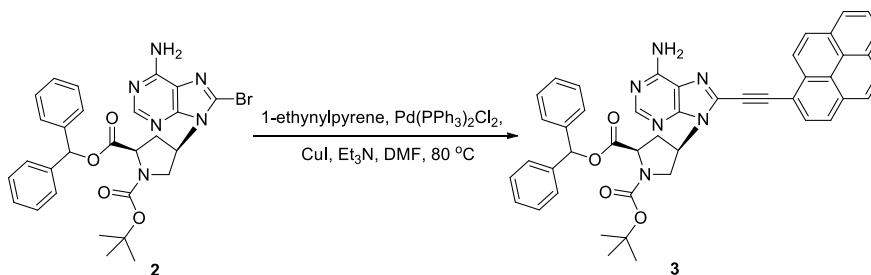
2.3 Synthesis of A^{PyE}-modified pyrrolidiny PNA monomer

2.3.1 Synthesis of *N*-*tert*-Butoxycarbonyl-*cis*-(4'*R*)-(8-bromoadenine-9-yl)-*(2'R)*-proline diphenylmethyl ester (**2**)



N-*tert*-butoxycarbonyl-*trans*-4-(*p*-tolylsulfonyloxy)-2'*R*-proline diphenylmethyl ester **1** (102.73 mg, 1.86 mmol), 8-bromoadenine¹⁰⁹ (445.2 mg, 2.10 mmol) and anhydrous K₂CO₃ (697.0 mg, 5.04 mmol) in anhydrous DMF (5 mL) was stirred under nitrogen at 80°C for 8 h. After aqueous work-up, the crude product was purified by column chromatography on silica gel using ethyl acetate/hexanes (50:50) as eluent to obtain **2** (234.1 mg, 21% yield) as an off-white solid. *R*_f = 0.18 (hexanes/ethyl acetate 50:50); m.p. 119.5–120.9 °C; [α]_D²⁵ = +43.9° (*c* = 1.14 g/100 mL, CHCl₃); *v*_{max} = 1739.9, 1693.6, 1632.8, 1595.2, 1389.7, 1155.3, 1126.4 cm⁻¹; ¹H NMR (400 MHz, CDCl₃) (**Figure A1**): δ 1.18, 1.37 (2xs, 9H, CH₃-Boc), 3.11 (m, 1H, CH₂-3'), 3.33 (m, 1H, CH₂-3'), 3.90, 4.04 (m, 2H, CH₂-5'), 4.51, 4.61 (m, 1H, CH-2'), 5.08 (m, 1H, CH-4'), 6.02 (br s, 2H, NH₂) 6.93 (s, 1H, CHPh₂), 7.21-7.39 (m, 10H, Phenyl Dpm), 8.05 (s, 1H, CH adenine), ¹³C NMR (100 MHz, CDCl₃) (**Figure A2**): δ 27.9 and 28.3 (CH₃ Boc rotamers), 31.5 and 32.4 (CH₂(3') rotamers), 47.3 and 47.6 (CH₂(5') rotamers), 54.1 and 54.5 (CH(4') rotamers), 57.6 and 57.9 (CH(2) rotamers), 77.6 and 77.8 (CH Dpm rotamers), 80.8 and 80.9 (CCH₃ Boc rotamers), 120.3 (C5 adenine), 127.1-128.5 (CH Ar Dpm), 139.5 and 139.6 (C Dpm), 151.2 (C6 adenine), 152.4 (CH(2) adenine), 153.3 and 154.1 (CO Boc rotamers), 170.47 (CO proline); HRMS (ESI⁺): *m/z* calcd for C₂₈H₂₉BrN₆O₄+H⁺: 593.1512 [M+H]⁺; found: 593.1511.

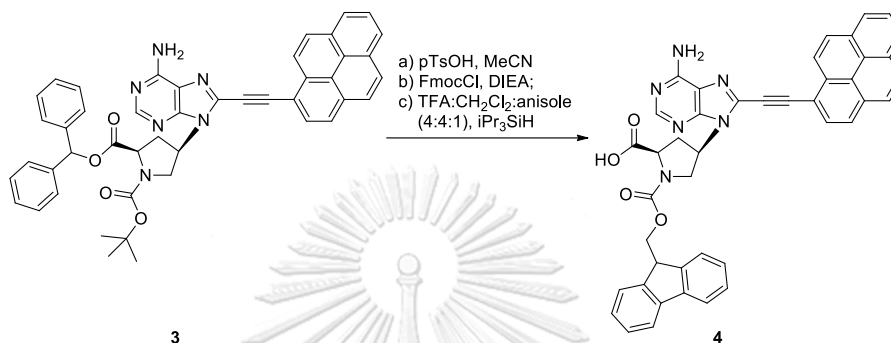
2.3.2 Synthesis of *N*-tert-Butoxycarbonyl-(4'*R*)-[8-(pyrene-1-yl)ethynyladenine-9-yl]-(2'*R*)-proline diphenylmethyl ester (**3**)



To a stirring mixture of the 8-bromoadenine intermediate **2** (159.2 mg, 0.27 mmol), Pd(PPh₃)₂Cl₂ (47.0 mg, 0.07 mmol), 1-ethynylpyrene (105.7 mg, 0.47 mmol) and CuI (16.7 mg, 0.03 mmol) in degassed DMF was added Et₃N (110 μL, 0.79 mmol) at room temperature under nitrogen. After that, the reaction mixture was heated to 80°C with stirring under nitrogen for 8 h. After completion of the reaction as monitored by TLC, the crude product was diluted with dichloromethane and washed with water, dried over Na₂SO₄ and concentrated. The crude product was purified by column chromatography on silica gel eluting with dichloromethane/methanol (100:1 to 100:7) to afford 149.2 mg (75% yield) of the desired product **3** as a brown solid. *R*_f = 0.24 (hexanes/ethyl acetate 50:50); m.p. 149.8–151.4 °C; [α]_D²⁵ = +78.5° (c = 0.26 g/100 mL, CHCl₃); IR(ATR): ν_{max} = 2200.0, 1745.0, 1690.7, 1647.0, 1389.7, 1363.0, 1152.4 cm⁻¹; ¹H NMR (400 MHz, CDCl₃) (**Figure A3**): δ 1.30, 1.50 (2xs, 9H, CH₃-Boc), 2.60 (br s, 1H, CH₂-3'), 2.90 (br s, 1H, CH₂-3'), 4.04, 4.16 (m, 2H, CH₂-5'), 4.54, 4.66 (m, 1H, CH-2'), 5.15 (m, 1H, CH-4'), 6.92 (s, 1H, CHPh₂), 7.11-7.31 (m, 10H, Phenyl Dpm), 8.00-8.28 (m, 9H, CH Pyr), 8.45 (s, 1H, CH adenine), ¹³C NMR (100 MHz, CDCl₃) (**Figure A4**): δ 28.0 and 28.4 (CH₃ Boc rotamers), 32.3 and 33.3 (CH₂(3') rotamers), 48.2 and 48.4 (CH₂(5') rotamers), 53.2 and 53.9 (CH(4') rotamers), 57.6 and 57.9 (CH(2') rotamers), 77.6 and 77.8 (CH Dpm rotamers), 81.1 and 82.6 (CCH₃ Boc rotamers), 97.5 (C11), 113.3 (C10), 119.3 (C5 adenine), 123.6 (C pyrene), 123.9 (C pyrene), 124.4 (CH(2) adenine), 124.6 (CH pyrene), 126.6 (CH pyrene), 126.8 (CH pyrene), 127.1 (CH Ar Dpm), 127.2 (CH pyrene), 128.5 (CH Ar Dpm), 129.6 (CH pyrene), 129.7 (CH pyrene), 130.1 (C pyrene), 130.5 (C pyrene), 130.9 (C pyrene), 132.5 (C pyrene), 132.7 (C pyrene), 139.6 and 139.5 (C Dpm), 139.8

(C4 adenine), 148.6 (C6 adenine), 153.8 and 153.4 (CO Boc rotamers), 170.3 (CO proline); HRMS (ESI⁺): m/z calcd for C₄₆H₃₈N₆O₄+H⁺: 739.3033 [M+H]⁺; found: 739.3039.

2.3.3 Synthesis of *N*-Fluoren-9-ylmethoxycarbonyl-(4'*R*)-[8-(pyrene-1-yl)ethynyl-adenine-9-yl]-(2'*R*)-proline (**4**)



To a solution of compound **3** (338.4 mg, 0.46 mmol) in MeCN (3 mL) was treated with *p*-toluenesulfonic acid monohydrate (591.5 mg, 3.11 mmol) at room temperature for 4 h. After the Boc-deprotection was completed as monitored by TLC, DIEA (595 mL, 3.41 mmol) was added to the reaction mixture followed by FmocCl (232.2 mg, 0.89 mmol), continued stirring at room temperature. After the reaction was consumed (as indicated by TLC), the solvent was removed under reduced pressure and the residue was purified by column chromatography on silica gel eluting with ethyl acetate/hexanes (60:40) to obtain Fmoc-protected intermediate. Then, the Fmoc/Dpm intermediate (101.6 mg, 0.12 mmol) was treated with 1:4:4 anisole:trifluoroacetic acid:CH₂Cl₂ (2 mL) and triisopropylsilane (1 drop) for 1 h at room temperature to remove the diphenylmethyl ester group (monitored by TLC). The solvents were removed by gentle stream of nitrogen, washed with diethyl ether to give a yellow solid **4** (74.4 mg, 65% yield from **3**).¹¹⁰ R_f = 0.31 (dichloromethane/methanol 9:1); m.p. decomposed at 185 °C; $[\alpha]_D^{25} = +18.7^\circ$ ($c = 0.525$ g/100 mL, DMF); IR(ATR): $\nu_{\max} = 2200.0, 1690.7, 1415.7, 1175.6, 1126.4$ cm⁻¹; ¹H NMR (400 MHz, CDCl₃) (**Figure A5**): δ 2.88 and 3.12 (m, 2H, CH₂(3') rotamers), 4.13 (m, 1H, CH Fmoc), 4.20 (m, 2H, CH₂(5') rotamers), 4.31 (m, 2H, CH₂ Fmoc), 4.47, 4.68 (2xm, 1H, CH-2' rotamers), 5.63 (m, 1H, CH(4') rotamers), 7.18-7.21 (m, 2H, CH Fmoc), 7.27-7.41 (m, 2H, CH Fmoc), 7.62-7.71 (m, 2H, CH Fmoc), 7.78-7.88 (m, 2H, CH Fmoc), 8.17-8.43 [m, 9H, c), 8.56 (s, 1H, CH-2

adenine), ^{13}C NMR (100 MHz, CDCl_3) (**Figure A6**): δ 32.6 and 33.5 ($\text{CH}_2(3')$ rotamers), 46.5 and 46.7 ($\text{CH}_2(5')$ rotamers), 48.3 (CH Fmoc), 52.6 and 53.2 ($\text{CH}(4')$ rotamers), 57.2 and 57.6 ($\text{CH}(2')$ rotamers), 66.9 and 67.3 (CH_2 Fmoc), 94.2 ($\text{C}11$), 113.8 ($\text{C}10$), 119.5 ($\text{C}5$ adenine), 119.9 (CH Ar Fmoc), 123.2 (C pyrene), 123.5 (C pyrene), 124.1 ($\text{CH}-2$ adenine), 124.9 (CH pyrene), 125.0 (CH Ar Fmoc), 125.2 (CH pyrene), 126.4 (CH pyrene), 126.5 (CH pyrene), 126.9 (CH Ar Fmoc), 127.2 (CH pyrene), 127.5 (CH Ar Fmoc), 127.7 (C pyrene), 129.2 (CH pyrene), 129.6 (CH pyrene), 130.2-133.7 (C pyrene), 140.5 (CH Ar Fmoc), 143.6 (C Ar Fmoc), 149.4 ($\text{C}8$ adenine), 151.6 ($\text{C}6$ adenine), 153.8, 153.9 (CO Fmoc), 172.5 and 173.1 (CO Proline); HRMS (ESI $^+$): m/z calcd for $\text{C}_{43}\text{H}_{30}\text{N}_6\text{O}_4+\text{Na}^+$: 717.2226 $[\text{M}+\text{Na}]^+$; found: 717.2226.

PNA sequences that were synthesized from the pre-synthesized A^{PyE} monomer (**4**) as a building block are shown in **Table 2.1**. Details of the PNA synthesis can be found in the **section 2.5**.

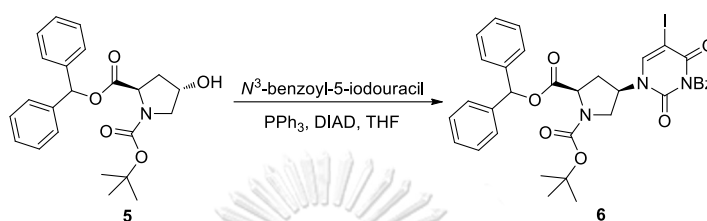
Table 2.1 Sequences of fluorescent modified-nucleobases acpcPNA by incorporating fluorescent monomers

Code of PNA	Sequence (N \rightarrow C)
T4(A^{PyE})T4	Ac-TTTTA $^{\text{PyE}}$ TTTT-LysNH $_2$
T8(A^{PyE})2_0B	Lys-TTTT A $^{\text{PyE}}$ A $^{\text{PyE}}$ TTTT-LysNH $_2$
T8(A^{PyE})2_3B	Lys-TTA $^{\text{PyE}}$ TTTA $^{\text{PyE}}$ TTT-LysNH $_2$
M12T(A^{PyE})T	Lys-AGTCATA $^{\text{PyE}}$ TA CTG-LysNH $_2$
M12A(A^{PyE})A	Lys-AGTCAAA $^{\text{PyE}}$ AACTG-LysNH $_2$
M12G(A^{PyE})G	Lys-AGTCAGA $^{\text{PyE}}$ GACTG-LysNH $_2$
M12C(A^{PyE})C	Lys-AGTCACA $^{\text{PyE}}$ CACTG-LysNH $_2$
A $^{\text{PyE}}$ M12	Lys-A $^{\text{PyE}}$ GTCATATACTG-LysNH $_2$
M10A(A^{PyE})C	Ac-GTAGAA $^{\text{PyE}}$ CACT-LysNH $_2$
M10G(A^{PyE})T	Ac-GTAGA $^{\text{PyE}}$ TCACT-LysNH $_2$
CAG(A^{PyE})	Lys-CAGCA $^{\text{PyE}}$ GCAGCAG-LysNH $_2$

Part II: Synthesis of fluorescence acpcPNA via post-synthetic modification approach

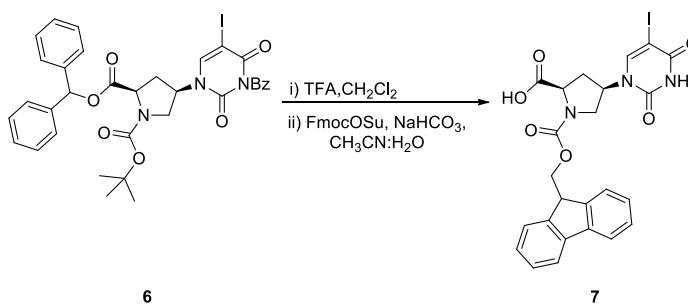
2.4 Synthesis of IU^{Bz}-modified pyrrolidinyl PNA monomer

2.4.1 Synthesis of *N*-*tert*-Butoxycarbonyl-*cis*-4-(*N*³-benzoyl-5-iodouracil-1-yl)-(2'*R*)-proline diphenylmethyl ester (**6**)



5-Iodouracil pyrrolidinyl PNA monomer **6** was synthesized from the protected hydroxyproline **5** (0.2489 g, 0.63 mmol) and *N*³-benzoyl-5-iodouracil¹¹¹ (0.2416 g, 0.71 mmol) according to a previously reported procedure⁹¹ via Mitsunobu reaction to obtain the Boc/Dpm **6** as white solid (196.1 mg, 43% yield). ¹H NMR (400 MHz, CDCl₃): δ 1.30 and 1.49 (2s, 9H; CH₃ Boc rotamers), 2.04 (m, 1H; 1 × CH₂(3')), 2.83 (m, 1H; 1 × CH₂(3')), 3.57 and 3.71 (m, 1H; 1 × CH₂(5') rotamers), 3.99 (m, 1H; 1 × CH(5') rotamers), 4.50 and 4.59 (m, 1H; CH(4') rotamers) 5.17 (m, 1H; CH(2')), 6.96 (s, 1H; CHPh₂), 7.26 (s, 1H; C(6)H Thymine), 7.36 (m, 10H; Dpm ArH), 7.48 (dd, *J* = 7.0, 7.4 Hz, 2H; CH(3,5) Bz), 7.66 (t, *J* = 7.3 Hz, 1H; CH(4) Bz), 7.86 ppm (m, 2H; CH(2,6) Bz). The spectroscopic data was consistent to the literature.⁹¹

2.4.2 Synthesis of *N*-Fluoren-9-ylmethoxycarbonyl-*cis*-(4'*R*)-(5-iodouracil-1-yl)-(2'*R*)-proline -proline (**7**)



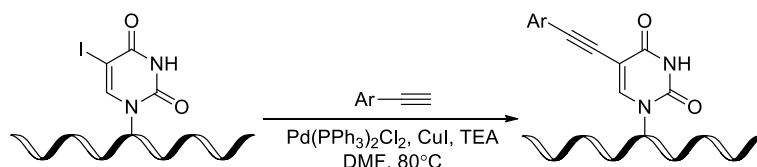
N-*tert*-Butoxycarbonyl-*cis*-4-(*N*³-benzoyl-5-iodouracil-1-yl)-D-proline diphenylmethyl ester (**6**) (232.4 mg, 0.38 mmol) was dissolved in a mixture of

trifluoroacetic acid in dichloromethane (1:1, 3 mL) then left stirring for overnight. After completing the reaction (monitored by TLC), the solvent was removed by a stream of nitrogen and the residue was washed with diethyl ether three times to obtain a precipitate. Next, the solution of the monomer was dissolved acetonitrile:H₂O (1:1) followed by NaHCO₃ (80.7 mg, 0.96 mmol) and *N*-(9-fluorenylmethoxycarbonyloxy)succinimide (146.7 mg, 0.43 mmol) with stirring. The reaction mixture was stirred at room temperature overnight. After extraction with diethyl ether, the aqueous phase was collected and purged with a stream of nitrogen gas to remove the residual ether. Acidification by conc. HCl caused precipitation of the product, which was filtered off, washed with cold water followed by diethyl ether to afford the *N*-Fmoc-protected iodouracil monomer (**7**) as a white solid (148.5 mg, 55% yield). *R_f* = 0.42 (dichloromethane/methanol 8:2); m.p. 214-217 °C; [α]_D²⁵ = -9.34° (*c* = 1.0 g/100 mL, DMF); IR(ATR): ν_{\max} = 3063.2, 1685.5, 1420.1, 1176.5 1119.7 cm⁻¹; ¹H NMR (400 MHz, DMSO-*d*₆) (**Figure A7**): δ 2.28 and 2.33 (m, 1H, CH₂(3') rotamers), 2.66 and 2.73 (m, 1H, CH₂(3') rotamers), 3.60 (m, 1H, CH₂(5') rotamers), 3.89 (m, 1H, CH₂(5') rotamers), 4.23 (m, 1H, CH Fmoc), 4.29 (m, 2H, CH₂ Fmoc), 4.44 (m, 1H, CH(2') rotamers), 4.91 (m, 1H, CH(4') rotamers), 7.35 (m, 2H, CH Fmoc), 7.43 (m, 2H, CH Fmoc), 7.67 (d, *J* = 7.7 Hz, 2H, CH Fmoc), 7.89 (d, *J* = 7.9 Hz, 2H, CH Fmoc), 8.12 (s, 1H, H₆ Thymine), 11.69 [s, 1H, NH Thymine), 12.93 (br s, 1H, OH), ¹³C NMR (100 MHz, DMSO-*d*₆) (**Figure A8**): δ 32.7 and 33.8 (CH₂(3') rotamers), 46.6 (CH Fmoc), 48.6 and 49.1 (CH₂(5') rotamers), 53.7 and 54.3 (CH(4') rotamers), 57.0 and 57.4 (CH(2') rotamers), 67.0 and 67.3 (CH₂ Fmoc), 68.9 (C₅ Thymine), 120.1 (CH Ar Fmoc), 125.2 (CH Ar Fmoc), 127.2, 127.7 (CH Ar Fmoc), 140.7 (C Ar Fmoc), 143.9 (C Ar Fmoc), 146.9 (C₆H Thymine), 150.6 (C₂ Thymine), 153.9 (CO Fmoc), 160.5 (C₄ Thymine), 172.6, 173.1 (CO Proline); HRMS (MALDI-TOF): *m/z* calcd for C₂₄H₂₀I_N₃O₆+Na⁺: 596.0294 [M+Na]⁺; found: 596.0286.

2.5 General procedure for post-synthetic modification of acpcPNA by Sonogashira reaction

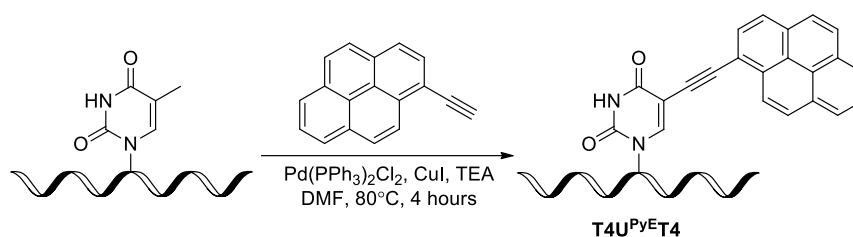
2.5.1 Post-synthetic Sonogashira reaction in solution phase

General reaction conditions:



Functionalization of 5-iodouracil acpcPNA with 1-ethynylpyrene and 2-ethynylfluorene via Sonogashira reaction were accomplished in solution phase. All reagents and 5-iodouracil-modified acpcPNA were prepared as stock solutions by dissolving in DMF: arylethyne (2.0 M), palladium(II) bis(triphenylphosphine) dichloride $[\text{Pd}(\text{PPh}_3)_2\text{Cl}_2]$ (0.025 M), copper(I) iodide $[\text{CuI}]$ (0.06 M) and triethylamine (0.2 M). The 5-iodouracil acpcPNA (0.25 μmol) was mixed with the arylethyne (500 equiv.), palladium(II) bis(triphenylphosphine) dichloride $[\text{Pd}(\text{PPh}_3)_2\text{Cl}_2]$ (2.5 equiv.), copper(I) iodide $[\text{CuI}]$ (3.0 equiv.) and triethylamine (16.3 equiv.) with a total volume of 500 μL in 1.5 mL Eppendorf tube. The reaction was performed at 80 $^\circ\text{C}$ for the specified period of time. The progress of the reaction was monitored by MALDI-TOF mass spectrometry. After completing of the reaction, the reaction mixture was centrifuged and the supernatant passed through a C18 cartridge (100 mg/1mL), followed by washing with 10% aqueous acetonitrile for several times (100 μL , 5 times). The collected fractions were freeze-dried to afford the crude arylethynyl-modified acpcPNA as a yellow solid. The crude PNA was re-dissolved in acetonitrile (120 μL) and purified by reversed phase HPLC to obtain the arylethynyl-modified acpcPNA.

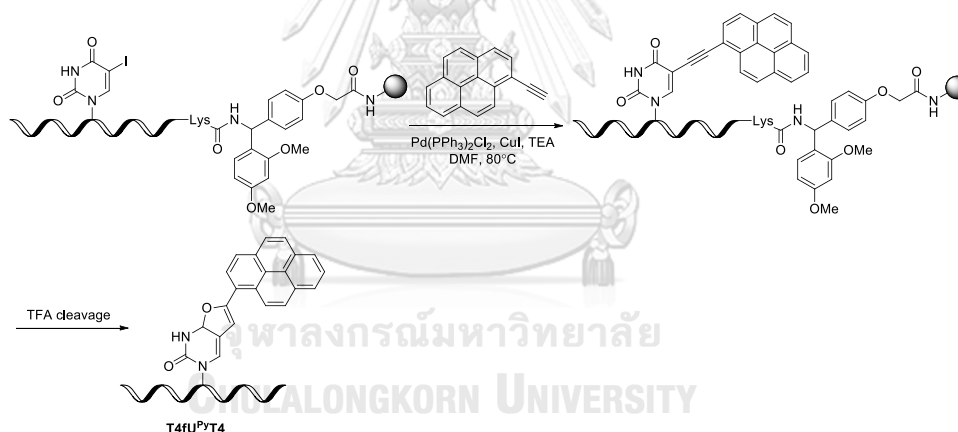
5-(pyrene-1-yl)ethynyluracil (U^{PyE}) acpcPNA



The 5-iodouracil-modified acpcPNA (0.25 μmol , 500 μM), 1-ethynylpyrene (125 μmol , 500 equiv.), $\text{Pd(PPh}_3)_2\text{Cl}_2$ (0.63 μmol , 2.5 equiv.), CuI (0.75 μmol , 3 equiv.), triethylamine (4.08 μmol , 16.3 equiv.) in DMF (500 mL) were heated for 4 hours at 80 °C to give 5-(pyrene-1-yl)ethynyluracil acpcPNA in 14.4% yield after HPLC purification.

2.5.2 Post-synthetic Sonogashira reaction on the solid phase

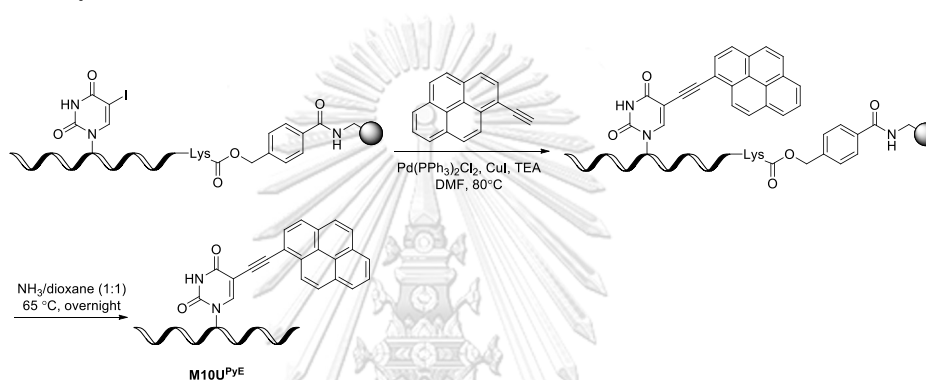
a) 5-(pyrene-1-yl)furanouracil acpcPNA via Rink amide (RAM) linker



The 5-iodouracil modified acpcPNA was first synthesized on the solid support carrying an acid-labile Fmoc-protected Rink amide (RAM) linker (see details in **section 2.7.1**). The post-synthetic Sonogashira reaction was performed on the solid support in the presence of 1-ethynylpyrene (500 equiv.), palladium(II) bis(triphenylphosphine) dichloride [$\text{Pd(PPh}_3)_2\text{Cl}_2$] (2.5 equiv.), copper(I) iodide (3.0 equiv.) and triethylamine (16.3 equiv.) in DMF (500 μL) at 80 °C for 6 hours. The reaction progress was monitored by MALDI-TOF mass spectrometry. After the reaction was completed, the resin was extensively washed with DMF and methanol to remove the excess reagents. Then, the modified PNA was next cleaved by treatment with 10% triisopropylsilane in

trifluoroacetic acid (500 $\mu\text{L} \times 30 \text{ min} \times 3$). The acid was removed by a gentle stream of nitrogen, then the PNA residue was precipitated with diethyl ether to obtain a crude PNA as yellow solid after air drying. The crude PNA was further purified by reverse phase HPLC. This was not the expected 5-(pyren-1-yl)-modified uracil but was later confirmed to be the cyclized furanouracil product.

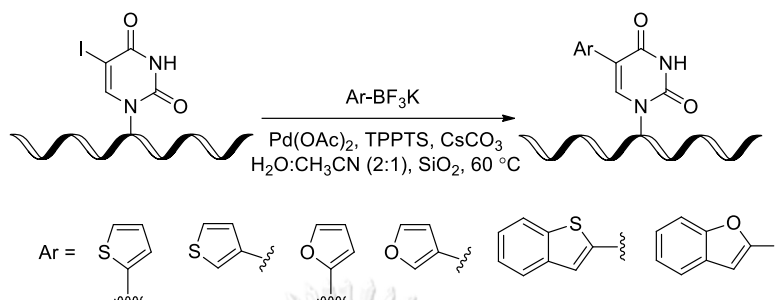
b) 5-(pyrene-1-yl)ethynyluracil acpcPNA via hydroxymethylbenzoyl (HMBA) linker



In this method, the 5-iodouracil modified acpcPNA was first synthesized on a solid support carrying a base-labile hydroxymethylbenzoyl (HMBA) linker instead of the usual Rink amide linker (see details in **section 2.7.1**). The post-synthetic Sonogashira reaction was performed with the fully protected PNA while still attached on the solid support in the presence of 1-ethynylpyrene (500 equiv.), palladium(II) bis(triphenylphosphine) dichloride [$\text{Pd}(\text{PPh}_3)_2\text{Cl}_2$] (2.5 equiv.), copper(I) iodide (3.0 equiv.) and triethylamine (16.3 equiv.) in DMF (500 μL) at 80°C for 18 hours. The reaction progress was monitored by MALDI-TOF mass spectrometry. After the reaction was completed, the resin was extensively washed with DMF to remove the excess reagents. Then, the modified PNA was cleaved by treatment with 1:1 aqueous $\text{NH}_3/\text{dioxane}$ at 65°C overnight. The solvents were removed under a stream of nitrogen and the residue was washed with diethyl ether to afford the crude product as a yellow solid, however, MALDI-TOF analysis revealed a complex mixture containing only trace of the desired product, which was not further isolated.

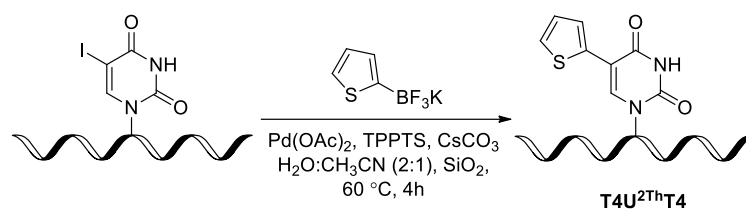
2.6 General procedure for post-synthetic modification of acpcPNA by Suzuki-Miyaura reaction in solution phase

General reaction conditions:



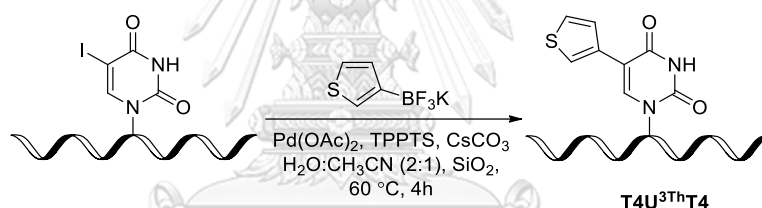
Post-synthetic modification of 5-iodouracil-modified acpcPNA with potassium aryltrifluoroborates to obtain 5-aryluracil acpcPNA were accomplished via Suzuki-Miyaura reaction. The 5-iodouracil-modified acpcPNA were dissolved in minimum amounts of Milli Q water and other reagents were prepared as stock solutions: palladium(II) acetate [$\text{Pd}(\text{OAc})_2$] (0.05 M) in acetonitrile, potassium aryltrifluoroborate (2.5 M), triphenylphosphine-3,3',3''-trisulfonic acid trisodium salt (TPPTS) (0.5 M) and cesium carbonate (0.25 M) in Milli Q water. The reagents were added to the iodouracil acpcPNA as follows: aryltrifluoroborates (100 equiv.), $\text{Pd}(\text{OAc})_2$ (2.0 equiv), TPPTS (4.0 equiv.) and cesium carbonate (3.0 equiv.) in aqueous acetonitrile ($\text{H}_2\text{O}:\text{MeCN} = 2:1$) with a total volume of 500 μL in Eppendorf tube. Catalytic amounts of SiO_2 (column chromatography grade, 4.0 mg) was next added to the resulting solution. The reaction was heated at 60 $^\circ\text{C}$ for the specified period of time. The reaction progress was monitored by MALDI-TOF mass spectrometry. After the starting 5-iodouracil acpcPNA was consumed, the reaction mixture was centrifuged and the supernatant was passed through a C18 cartridge (100 mg/1mL), followed by washing with 10% aqueous acetonitrile (5 x 100 μL). The collected fractions were lyophilized to obtain crude 5-aryluracil acpcPNA as off-white solid. The crude PNA was re-dissolved in Milli Q water (120 μL) and purified by reversed phase HPLC to afford the pure aryl-modified acpcPNA.

5-(Thiophen-2-yl)uracil (U^{2Th}) acpcPNA



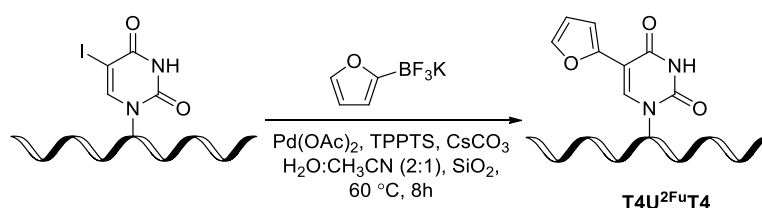
The reaction mixture containing 5-iodouracil-modified acpcPNA (0.25 μmol , 500 μM), potassium thiophene-2-trifluoroborate (25 μmol , 100 equiv.), Pd(OAc)₂ (0.5 μmol , 2 equiv.), TPPTS (1 μmol , 4 equiv.), Cs₂CO₃ (0.75 μmol , 3 equiv.) and SiO₂ (column chromatography grade, 4.0 mg) catalytic amount) in aqueous acetonitrile (H₂O:MeCN = 2:1) (total volume = 500 μL) was heated at 60 °C for 4 hours to afford 5-(thiophen-2-yl)uracil acpcPNA in 2.2% yield after HPLC purification.

5-(Thiophen-3-yl)uracil (U^{3Th}) acpcPNA



The 5-iodouracil-modified acpcPNA (0.25 μmol , 500 μM), potassium thiophene-3-trifluoroborate (25 μmol , 100 equiv.), Pd(OAc)₂ (0.5 μmol , 2 equiv.), TPPTS (1 μmol , 4 equiv.), Cs₂CO₃ (0.75 μmol , 3 equiv.) and SiO₂ (column chromatography grade, 4.0 g) were dissolved in aqueous acetonitrile (H₂O:MeCN = 2:1) for 4 hours at 60 °C to afford 5-(thiophen-3-yl)uracil acpcPNA in 10.3% yield after HPLC purification.

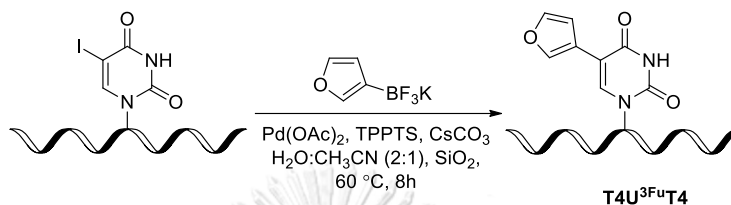
5-(Fur-2-yl)uracil (U^{2Fu}) acpcPNA



The 5-iodouracil-modified acpcPNA (0.25 μmol , 500 μM), potassium furan-2-trifluoroborate (25 μmol , 100 equiv.), Pd(OAc)₂ (0.5 μmol , 2 equiv.), TPPTS (1 μmol , 4

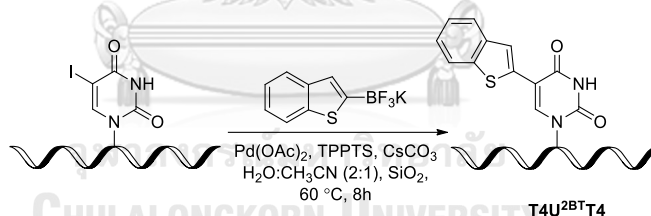
equiv.), Cs_2CO_3 (0.75 μmol , 3 equiv.) and SiO_2 (column chromatography grade, 4.0 g) were dissolved in aqueous acetonitrile ($\text{H}_2\text{O}:\text{MeCN} = 2:1$) for 8 hours at 60 °C to afford 5-(fur-2-yl)uracil acpcPNA in 30.8% yield after HPLC purification.

5-(Fur-3-yl)uracil ($\text{U}^{3\text{Fu}}$) acpcPNA

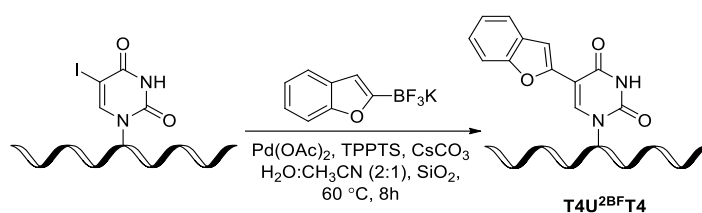


The 5-iodouracil-modified acpcPNA (0.25 μmol , 500 μM), potassium furan-3-trifluoroborate (25 μmol , 100 equiv.), $\text{Pd}(\text{OAc})_2$ (0.5 μmol , 2 equiv.), TPPTS (1 μmol , 4 equiv.), Cs_2CO_3 (0.75 mM, 3 equiv.) and SiO_2 (column chromatography grade, 4.0 g) were dissolved in aqueous acetonitrile ($\text{H}_2\text{O}:\text{MeCN} = 2:1$) for 8 hours at 60 °C to afford 5-(fur-3-yl)uracil acpcPNA in 28.0% yield after HPLC purification.

5-(Benzothiophene-2-yl)uracil ($\text{U}^{2\text{BT}}$) acpcPNA



The 5-iodouracil-modified acpcPNA (0.25 μmol , 500 μM), potassium benzothiophene-2-trifluoroborate (25 μmol , 100 equiv.), $\text{Pd}(\text{OAc})_2$ (0.5 μmol , 2 equiv.), TPPTS (1 μmol , 4 equiv.), Cs_2CO_3 (0.75 μmol , 3 equiv.) and SiO_2 (column chromatography grade, 4.0 g) were dissolved in aqueous acetonitrile ($\text{H}_2\text{O}:\text{MeCN} = 2:1$) for 8 hours at 60 °C to afford 5-(benzothiophene-2-yl)uracil acpcPNA in 2.9% yield after HPLC purification.

5-(Benzofuran-2-yl)uracil (U^{2BF}) acpcPNA

The 5-iodouracil-modified acpcPNA (0.25 μmol , 500 μM), potassium benzofuran-2-trifluoroborate (25 μmol , 100 equiv.), $\text{Pd}(\text{OAc})_2$ (0.5 μmol , 2 equiv.), TPPTS (1 μmol , 4 equiv.), Cs_2CO_3 (0.75 μmol , 3 equiv.) and SiO_2 (column chromatography grade, 4.0 g) were dissolved in aqueous acetonitrile ($\text{H}_2\text{O}:\text{MeCN} = 2:1$) for 8 hours at 60 $^\circ\text{C}$ to afford 5-(benzofuran-2-yl)uracil acpcPNA in 35.0% yield after HPLC purification.

The modified-acpcPNA successfully synthesized by post-synthetic modification according to this study are summarized in **Table 2.2**.

Table 2.2 Sequences of fluorescence modified nucleobases acpcPNA by post-synthetic modification

Code of PNA	Sequence (N \rightarrow C)	Reaction	Synthetic method
T4U ^{2Th} T4	Ac-TTTTU ^{2Th} TTTT-LysNH ₂	Suzuki-Miyaura	Solution
T4U ^{3Th} T4	Ac-TTTTU ^{3Th} TTTT-LysNH ₂	Suzuki-Miyaura	Solution
T4U ^{2Fu} T4	Ac-TTTTU ^{2Fu} TTTT-LysNH ₂	Suzuki-Miyaura	Solution
T4U ^{3Fu} T4	Ac-TTTTU ^{3Fu} TTTT-LysNH ₂	Suzuki-Miyaura	Solution
T4U ^{2BT} T4	Ac-TTTTU ^{2BT} TTTT-LysNH ₂	Suzuki-Miyaura	Solution
T8U ^{2BF} T4	Ac-TTTTU ^{2BF} TTTT-LysNH ₂	Suzuki-Miyaura	Solution
T4U ^{PyE} T4	Ac-TTTTU ^{PyE} TTTT-LysNH ₂	Sonogashira	Solution
T4fU ^{Py} T4	Ac-TTTTfU ^{Py} TTTT-LysNH ₂	Sonogashira	Solid ^a
M10U ^{PyE}	Ac-GTAGAU ^{PyE} CACT-LysNH ₂	Sonogashira	Solution
Lys2M10U ^{PyE}	Ac-Lys-GTAGAU ^{PyE} CACT-LysNH ₂	Sonogashira	Solid ^b

^a Rink amide linker. ^b HMBA linker; This modified acpcPNA was not successfully synthesized.

2.7 General procedure for the synthesis of acpcPNA

2.7.1 Solid phase synthesis of acpcPNA

All acpcPNA were synthesized via Fmoc solid phase peptide synthesis according to the same procedure as previously reported using Fmoc-protected acpcPNA monomers (A^{Bz} , T, C^{Bz} , G, U^{Bz} , A^{PyE}) and ACPC spacer at 0.5 to 1.5 μmol scales.^{84, 108, 112} One or more lysine residues were included either at C- or N-termini or both to improve aqueous solubility of the modified acpcPNA in the form of Fmoc-Lys(Boc)-OPfp or Fmoc-Lys(Mtt)-OH. The monomers were assembled on a Tentagel resin equipped with an Fmoc-protected Rink amide (RAM) linker (0.24 mmol/g, most of the cases) or hydroxymethylbenzoyl (HMBA) linker (0.25 mmol/g, for Sonogashira reaction on solid phase). The cycle of acpcPNA synthesis consists of three steps as follows:

1) Fmoc deprotection: The Fmoc protecting group was removed from the Rink amide linker, PNA monomers or spacer immobilized on the resin to allow extension of the PNA chain using 20% piperidine, 2% DBU in DMF (total volume = 100 μL) for 5 minutes.

2) Coupling: Pfp-activated Fmoc-protected lysine, acpcPNA monomers or ACPC spacer were directly coupled to the Fmoc-deprotected resin by using 4 equiv. of HOAt in 7% DIEA in DMF (30 μL) for 30-60 minutes. In cases of Fmoc-protected free carboxylic acid monomers (Fmoc-Lys(Mtt)-OH, Fmoc-G-OH, Fmoc- A^{PyE} -OH (**4**) and Fmoc- U^I -OH (**7**)), these free acid monomers (4 equiv.) were activated with HATU (3.9 equiv.) in the presence of 7% DIEA in DMF (30 μL) and were coupled on the deprotected-Fmoc resin (40 minutes for Fmoc-G-OH and Fmoc-Lys(Mtt)-OH, 1 hour for Fmoc- A^{PyE} -OH (**4**) and Fmoc- U^I -OH (**7**)).

3) Capping: The incomplete acpcPNA sequences were capped with 10% acetic anhydride/DIEA in DMF (30 μL) for 5 minutes to prevent further chain extension from the unreacted amino groups.

After each cycle, the resin was extensively washed with DMF to remove any excess reagents. The deprotection-coupling-capping cycles were repeated until the

desired PNA sequences obtained. The final *N*-terminal Fmoc group was cleaved and replaced with acetyl group. Before cleavage of the PNA from the solid support with Rink amide linker, the benzoyl protecting group on the bases A and C were removed by treatment with 1:1 aqueous ammonia/dioxane at 65 °C overnight. The acpcPNA was next cleaved from the solid support by treatment with 10% triisopropylsilane in trifluoroacetic acid (500 μ L \times 30 min \times 3). The acid was removed by a gentle stream of nitrogen and the residual PNA was repeatedly washed with diethyl ether, followed by drying to obtain a crude PNA.

For post-synthetic modification in solution phase, the 5-iodouracil acpcPNA was cleaved from the resin by TFA. The solvent was removed under stream of nitrogen gas and the crude PNA was precipitated with diethyl ether and air dried. This material was used for the next reaction without further purification. The acpcPNA synthesized on the resin carrying HMBA-linker are subjected to the post-synthetic modification reactions before simultaneous side-chain deprotection and cleavage from the resin by treatment with 1:1 aqueous ammonia/dioxane at 65 °C overnight. Since the Mtt protecting group in Fmoc-Lys(Mtt)-OH was stable under basic conditions, this protecting group must be removed by treatment with 5% TFA in dichloromethane before performing the Sonogashira coupling reaction.

2.7.2 Purification and analysis of modified acpcPNA

The crude PNA was purified by reversed phase HPLC on a column ACE 5 A71197, C18-AR, 150 \times 4.6 mm, 5 μ m particle size, monitored by UV absorbance at 310 nm. The gradient system for the purification of A^{PyE}-acpcPNA consisted of solvent A (0.1% trifluoroacetic acid in MilliQ water) and solvent B (0.1% trifluoroacetic acid in methanol) at a flow rate 0.5 mL/min. The elution was proceeded with A:B 90:10 for 5 minutes, then using linear gradient to 10:90 over 60 minutes. In the cases of more acid-labile acpcPNA obtained from post-synthetic modification including 5-(thiophen-2-yl)uracil, 5-(thiophen-3-yl)uracil, 5-(fur-2-yl)uracil, 5-(fur-3-yl)uracil, 5-(benzofuran-2-yl)uracil, 5-(benzothiophene-2-yl)uracil and 5-(pyrene-1-yl)ethynyluracil acpcPNAs, the gradient system consisted of 0.1 M TEAA buffer pH 7.0 (solvent A and acetonitrile

(solvent B) as eluent (A:B 90:10 for 5 minutes then linear gradient to 10:90 over 60 min, flow rate 0.5 mL/min). Fractions containing the desired product based on MALDI-TOF analysis were combined and lyophilized to obtain the pure PNA.

For analytical of A^{PYE}-acpcPNA, a Vertisep UPS, 50x4.6 mm, 3 μ m particle size column was used for analysis of eluting with the gradient of 0.1% trifluoroacetic acid in MilliQ water (solvent A) and 0.1% trifluoroacetic acid in methanol (solvent B) at a flow rate 0.5 mL/min with the elution gradient A:B 90:10 for 5 minutes followed by linear gradient to 10:90 over period of 35 minutes. For other post-synthetically modified acpcPNA including 5-(thiophen-2-yl)uracil, 5-(thiophen-3-yl)uracil, 5-(fur-2-yl)uracil, 5-(fur-3-yl)uracil, 5-(benzofuran-2-yl)uracil, 5-(benzothiophene-2-yl)uracil and 5-(pyrene-1-yl)ethynyluracil acpcPNAs, the elution was performed with the gradient system of 0.1 M TEAA buffer pH 7.0 (solvent A) and acetonitrile (solvent B) with a flow rate 0.5 mL/min (A:B 90:10 for 5 minutes and using linear gradient to 10:90 over 35 minutes).

2.7.3 Characterization of modified acpcPNA

The identity of the purified acpcPNA were confirmed by MALDI-TOF mass spectrometry. The samples were prepared by using 1 μ L of aqueous PNA samples mixed with the matrix solution (α -cyano-4-hydroxy-cinnamic acid, CCA in 0.1% trifluoroacetic acid in 1:1 acetonitrile:water) and deposited on a MALDI-TOF target.

2.7.4 Determination of PNA concentration

The acpcPNA concentration was determined from the absorbance at 260 nm using a Cary 100 Bio UV-vis spectrophotometer (Varian/Agilent Technologies) in 10 mM sodium phosphate buffer pH 7.0 and using this value to calculate the concentration. The extinction coefficients at 260 nm (ϵ_{260}) of the A^{PYE} base were calculated by measuring the UV-vis absorption at varying concentrations and obtain from the slope of the calibration plot between concentration (x) and absorption (y). The extinction coefficients of all nucleobases in the PNA strand was calculated from the sum of

extinction coefficients of individual nucleobase with the following values $\epsilon(\text{A}) = 10.8 \text{ mL } \mu\text{mol}^{-1} \text{ cm}^{-1}$, $\epsilon(\text{C}) = 7.4 \text{ mL } \mu\text{mol}^{-1} \text{ cm}^{-1}$, $\epsilon(\text{G}) = 11.5 \text{ mL } \mu\text{mol}^{-1} \text{ cm}^{-1}$, $\epsilon(\text{T}) = 8.8 \text{ mL } \mu\text{mol}^{-1} \text{ cm}^{-1}$, $\epsilon(\text{A}^{\text{PyE}}) = 8.3 \text{ mL } \mu\text{mol}^{-1} \text{ cm}^{-1}$. For the C5-modified uracil acpcPNA obtained from post-synthetic modification, the extinction coefficients of thymine base ($\epsilon(\text{T}) = 8.8 \text{ mL } \mu\text{mol}^{-1} \text{ cm}^{-1}$) were used to calculate the extinction coefficients value of all modified-uracil acpcPNAs. All calculations were performed by an in-house web-based software (<http://www.chemistry.sc.chula.ac.th/pna/pna.asp>).

2.8 Investigation of PNA•DNA binding

2.8.1 Fluorescence experiments

The fluorescence spectra were performed on a Cary Eclipse fluorescence spectrophotometer, Varian/Agilent Technologies at 20 °C. The samples were prepared in aqueous 10 mM sodium phosphate buffer (pH 7.0) at the specified concentrations of PNA and DNA in a 10 mm quartz cell with a Teflon stopper. The parameters were set as follows: excitation and emission slits width = 5 nm.

2.8.2 UV-vis and thermal denaturation experiments

The UV-vis absorption properties and melting temperature experiment were measured on a Cary 100 Bio UV-vis spectrophotometer (Varian/Agilent Technologies) equipped with a thermal melt system. For UV-vis experiment, the modified PNA samples were prepared under same condition as fluorescence experiments in a 10 mm quartz cell with a Teflon stopper and measured at 20 °C. For thermal denaturation experiments, the temperature was recorded at 260 nm from 20 to 90 °C with a heating rate 1.0 °C/min. The recorded temperature was corrected according to equation (1) obtained from comparison of block temperature and actual temperature inside the cell in order to obtain the more accurate temperature.¹¹³ KaliedaGraph 4.0 (Synergy Software) and Microsoft Excel (Microsoft Corporation) were used for processing the melting temperature graphs. The melting temperature (T_m) was calculated from the maximum value of the first derivative plot.

$$\text{Corrected Temperature} = (0.9696 \times T_{\text{block}}) - 0.8396 \quad (1)$$

2.8.3 Circular dichroism experiments

Circular dichroism experiments were recorded on a JASCO Model J-815 spectrometer (JASCO). The samples were prepared under same condition to the fluorescence and UV-vis experiments. The spectra were determined from 500 to 200 nm (scanning speed 200 nm/min, averaged 4 times at 25 °C) then subtracted from a spectrum of the blank (10 mM sodium phosphate buffer pH 7.0) under the same conditions.

2.8.4 Photographing

The samples were prepared at the specified concentration of PNA and DNA in 10 mM sodium phosphate buffer pH 7.0 in PCR tube. The photographs were recorded under black light (365 nm) using UV transilluminator (VILBER LOURMAT TCP-20.LM) by a digital camera (Canon EOS M) in a manual mode (ISO 100, F2.8, shutter speed 1 sec).

2.8.5 Polyacrylamide gel electrophoresis (PAGE)

The sample were prepared by mixing 0.20 nmol of acpcPNA and 0.24 nmol of DNA in 1X TBE buffer and incubated for overnight. A 20% polyacrylamide gel was prepared at the following composition: 5 mL of 40% acrylamide, 1 mL of 10x TBE buffer, 3 mL of distilled water, 10 μ L of *N,N,N',N'*-tetramethylethylenediamine (TEMED) and 12 mg of ammonium persulfate. The PAGE experiment was performed at 100 volts, 25 °C for 2.5 hours on an omniPAGE Vertical Electrophoresis System and NANOPAC-300 (Clever Scientific) power supply. The gel was visualized under UV transilluminator (VILBER LOURMAT TCP-20.LM).

CHAPTER III

RESULTS AND DISCUSSION

This dissertation focuses on the development of hybridization responsive fluorescence PNA probes. The approach used in this work involves incorporation of one or more base discriminating fluorescent nucleobases into the PNA probe. These nucleobases are intrinsically fluorescence and can form specific base pairing to natural nucleobases in DNA according to the Watson-Crick base pairing rules. In addition, the formation of the base pair may result in fluorescence change that could be utilized in DNA sensing applications.

Not all fluorescence nucleobases can form specific base pairing with natural nucleobases, and even less can change fluorescence upon formation of the base pairs.¹¹⁴ The working principle for the fluorescence change generally relies on a difference in microenvironment of the fluorophore incorporated into the probe in the single-stranded hybridized (duplex) states. Pyrene is a frequently used environment sensitive fluorophore for the design of base discriminating fluorescence nucleobase in the DNA context and promising examples in PNA have already been reported.^{91,106,115-116} In this work, natural nucleobases including adenine and uracil will be modified with an aromatic fluorophore either via a direct conjugation (without linker) or via a rigid and π -conjugated ethynyl linker. It was expected that the base pairing event may alter the electronic properties of the nucleobase, and this will be transmitted to the aromatic fluorophores that were directly attached to the nucleobase or via a π -conjugated linker, resulting in a fluorescence change. According to the high-sequence specificity and greater binding affinity of a novel class of conformationally restricted pyrrolidiny peptide nucleic acid (acpcPNA) towards DNA target, it is expected to utilize this potential ability of acpcPNA as self-reporting fluorescence probes for DNA sequence analysis in response to the fluorescence alteration in the presence of correct DNA target representation as turn on-off fluorescence. This novel fluorescently-modified acpcPNA would be advantageous as the biological tools for DNA analysis.

In general, modified nucleobases can be incorporated into oligonucleotide probes by two different approaches: 1) by employing the pre-synthesized modified monomers as the building block for the oligonucleotide synthesis^{26,66,74,91} and 2) by post-synthetic modification of the oligonucleotide carrying a reactive precursor.¹⁰¹⁻¹⁰² Both approaches will be investigated in this study in order to develop the PNA probes carrying the fluorescent nucleobases. The result and discussion would divide into two parts. The first part (**section 3.1–3.5**) describes the synthesis and hybridization properties of fluorescence acpcPNA probes carrying fluorescent nucleobases namely pyrenylethynyladenine (A^{PyE}), that was incorporated into the PNA via the pre-synthesized monomer approach. As mentioned in chapter 1 about the limitation of using A^{PyE} as a base discriminating fluorescence nucleobase in DNA in terms of low binding affinity and non-selectivity for single nucleotide polymorphisms (SNPs) detection, even when using the conformationally restricted DNA analogues such as LNA.⁷⁰ This pre-synthesized monomer approach is lengthy since it requires a separate step for synthesizing the monomer. Moreover, it lacks flexibility since changing the fluorophore requires re-synthesizing the fluorescence monomer and the PNA. In addition, the method is applicable only to fluorescence monomers that are stable towards the acidic conditions generally required for cleavage of the PNA from the solid support. The second part (**section 3.6–3.16**) relates to the development of fluorescence acpcPNA probes via a more versatile post-synthetic modification of 5-iodouracil-modified acpcPNA by palladium-catalyzed cross-coupling reactions including Suzuki-Miyaura and Sonogashira reactions that may overcome the aforementioned drawbacks of the pre-synthesized monomer approach (**Figure 3.1**).

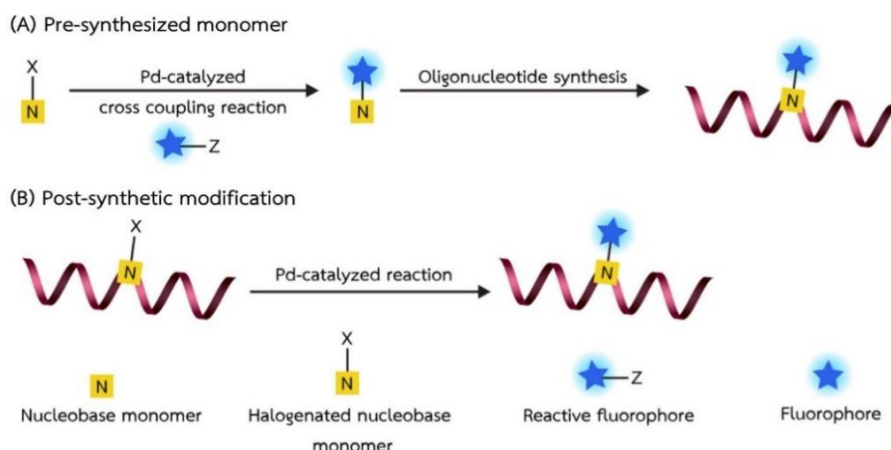


Figure 3.1 Schematic representation of the two approaches for incorporation of base discriminating fluorescence nucleobases into PNA probes.

3.1 Fluorescence acpcPNA probes incorporating pre-synthesized fluorescence monomer: Pyrenylethynyladenine (A^{PyE})

This part of the work related to the modification of C8-position of adenine base by 1-ethynylpyrene via Sonogashira reaction to form a fluorescence nucleobase monomer, namely, 8-(pyrene-1-yl)ethynyl-adenine (A^{PyE}) (**Figure 3.2**). The base A^{PyE} has been widely used as a fluorescent nucleobase in DNA^{26,117-118} However, purine bases with modification at C8 position generally adopted the *syn*-conformation, in which the Watson-Crick base pair is perturbed by partial stacking of the pyrene into the DNA duplexes resulting in low affinity and also deteriorated specificity.^{70,100} In addition, self-aggregation in multi-labeled DNA probes,¹¹⁹⁻¹²⁰ the excimer or exciplex interaction between A^{PyE} itself¹²¹⁻¹²² or A^{PyE} with nucleobases^{69,123} were the limitation of utilization A^{PyE} -based DNA probes. Thus, the A^{PyE} -based acpcPNA probe will be studied to evaluate the performance of A^{PyE} as a base discriminating fluorescence nucleobase in this high-performance PNA system.

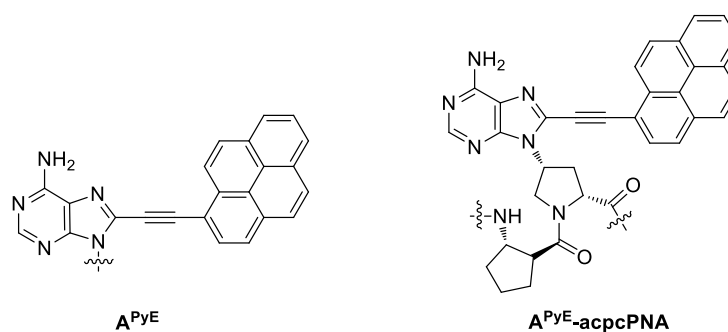


Figure 3.2 The structure of base discriminating fluorescence nucleobases, A^{PyE} , used in this work

The approach used here started from synthesizing the Fmoc-protected acpcPNA monomer carrying the A^{PyE} base. Subsequently, the fluorescent monomer was incorporated into the acpcPNA via solid phase peptide synthesis. It was proposed that the A^{PyE} should retain the ability to recognize the base thymine in the DNA target. In addition, the base pairing between A^{PyE} and dT should push the pyrene, which were connected via a rigid linker, into a more polar environment outside the duplex. As a result, the base pairing should result in fluorescence change due to the change in the environment of the fluorophore.

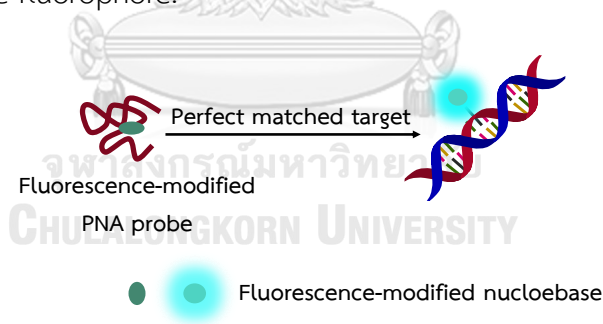


Figure 3.3 A schematic diagram of the hypothesis of this work

3.1.1 Synthesis of A^{PyE} -pyrroldinyl PNA monomer

The Fmoc-protected acpcPNA monomer bearing the A^{PyE} base (**4**) is the key building block for the synthesis of A^{PyE} -containing acpcPNA. The monomer **4** can be synthesized by coupling of 8-bromoadenine acpcPNA monomer with 1-ethynylpyrene via Sonogashira cross-coupling reaction as the key step as shown in **Figure 3.4**. The known Boc/Dpm tosylate compound (**1**) was synthesized according to a previously

reported procedure.¹²⁴ The Boc-protected 8-bromoadenine acpcPNA monomer (**2**) was synthesized from the tosylate compound (**1**) and 8-bromoadenine¹⁰⁹ to afford the corresponding 8-bromoadenine acpcPNA monomer (**2**) with inversion of configuration via adenine attack through S_N2 substitution of the tosylate **1** confirmed by ¹H NMR which showed a pattern that was consistent with previously reported compounds such as *cis*-A^{Bz} acpcPNA monomer¹²⁵ in 21% yield. The lower yield obtained may be ascribed to the possible formation of isomeric N⁷ and N⁹ substitutions as well as other side reactions such as elimination of the tosylate group on the proline ring.¹²⁶ In this case, the N⁹ substitution was confirmed by comparison in ¹H NMR signal at 8-position of adenine moiety of the Boc-protected A^{Bz} acpcPNA monomer with the Boc-protected 8-bromoadenine acpcPNA monomer (**2**). The proton signal at the 8-position of Boc-protected A^{Bz} acpcPNA monomer appeared at 7.89–7.96 ppm¹²⁵ which this signal did not detect in the Boc-protected 8-bromoadenine acpcPNA monomer (**2**). In addition, the Boc-protected 8-bromoadenine acpcPNA monomer (**2**) was also compared in ¹³C NMR of the Boc-protected 8-bromoadenine acpcPNA monomer (**2**) with 8-bromo-2'-deoxyadenosine from the literature, which showed the ¹³C NMR signal at C2 (152.4 ppm), C5 (120.3 ppm) and C6 adenine (151.2 ppm).¹²⁷ Next, the Sonogashira cross-coupling reaction between the 8-bromoadenine precursor (**2**) and 1-ethynylpyrene afforded the protected A^{PyE} intermediate (**3**) in 75% yield. The Boc protecting group in **3** was selectively removed by treatment with *p*-toluenesulfonic acid in acetonitrile to form the free amine tosylate salt, which was directly protected with FmocCl in the presence of DIEA. Finally, the Dpm protecting group was removed by a mixture of TFA:CH₂Cl₂ containing anisole (4:4:1) and 10% triisopropylsilane as scavengers for the electrophilic diphenylmethyl carbocations occurred during the acidic deprotection to provide the Fmoc-protected A^{PyE} monomer **4** in 65% yield from the Boc/Dpm protected intermediate **3**. The monomer **4** was characterized by ¹H and ¹³C NMR as well as high resolution mass spectrometry (HRMS).

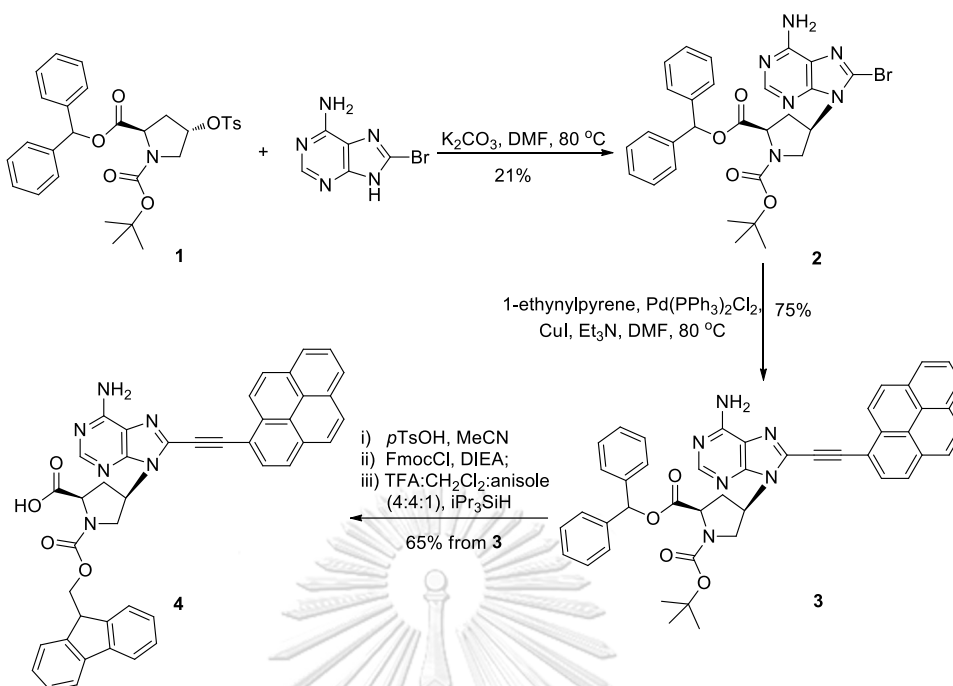


Figure 3.4 Synthesis of Fmoc-protected A^{PyE} PNA monomer

3.1.2 Synthesis of A^{PyE} -modified acpcPNA probes

The A^{PyE} -modified acpcPNA probes were manually synthesized by Fmoc solid phase peptide synthesis on a Tentagel S RAM resin from the four Fmoc-protected acpcPNA monomers (A^{Bz} , T, C^{Bz} , G and A^{PyE}) and ACPC spacer, which were alternately coupled to the solid support according to the standard protocol as previously published.^{84,108} The Fmoc-protected A^{PyE} monomer **4** was incorporated at the appropriate positions in the acpcPNA strand employing the standard HATU activation protocol as described in Chapter II. It is interesting to note that protection of the exocyclic amino group of A^{PyE} was not necessary during the PNA synthesis. After completing the PNA synthesis, the benzoyl protecting group on adenine and cytosine were removed by treatment with 1:1 aqueous ammonia/dioxane at 65 °C overnight. Subsequently, the fluorescently-modified acpcPNA probes were cleaved from the solid support using TFA containing 10% triisopropylsilane and the crude PNA was purified by reversed phase HPLC. The characterization data and isolated yields of all A^{PyE} -PNA synthesized in this study are shown in **Table 3.1**.

Table 3.1 Sequences and characterization data of fluorescence-modified acpcPNA probes.

Code of PNA	Sequence (N→C)	t_R (min) ^a	Yield (%) ^b	m/z (calcd)	m/z (found) ^c
T4(A ^{PyE})T4	Ac-TTTTA ^{PyE} TTTT-LysNH ₂	37.4	8.1	3413.4	3413.5
T8(A ^{PyE})2_0B	Lys-TTTT A ^{PyE} A ^{PyE} TTTT-LysNH ₂	38.8	2.6	4065.9	4064.8
T8(A ^{PyE})2_3B	Lys-TTA ^{PyE} TTTA ^{PyE} TTT-LysNH ₂	35.6	2.6	4065.9	4064.1
M12T(A ^{PyE})T	Lys-AGTCATA ^{PyE} TACTG-LysNH ₂	34.9	4.4	4543.7	4542.1
M12A(A ^{PyE})A	Lys-AGTCAAA ^{PyE} AACTG-LysNH ₂	34.4	2.0	4561.7	4563.1
M12G(A ^{PyE})G	Lys-AGTCAGA ^{PyE} GACTG-LysNH ₂	29.4	1.4	4593.7	4593.1
M12C(A ^{PyE})C	Lys-AGTCACA ^{PyE} CACTG-LysNH ₂	34.3	2.6	4513.7	4512.1
A ^{PyE} M12	Lys-A ^{PyE} GTCATATACTG-LysNH ₂	36.7	3.1	4543.7	4541.6
M10A(A ^{PyE})C	Ac-GTAGAA ^{PyE} CACT-LysNH ₂	35.9	6.4	3792.8	3789.2
M10G(A ^{PyE})T	Ac-GTAGA ^{PyE} TCACT-LysNH ₂	37.6	6.0	3779.0	3779.0
CAG(A ^{PyE})	Lys-CAGCA ^{PyE} GCAGCAG-LysNH ₂	35.9	4.2	4477.6	4477.3

^aSee HPLC conditions in experimental section. ^bIsolated yield after HPLC. ^cMALDI-TOF mass spectrometry in linear positive ion mode using α -cyano-4-hydroxycinnamic acid as a matrix.

3.2 Thermal stability of A^{PyE}-modified acpcPNA with DNA

3.2.1 Determination of thermal stability of A^{PyE}-modified acpcPNA

Melting temperature (T_m) is a common technique used to estimate the DNA duplex stability by monitoring the absorbance at 260 nm (A_{260}) at various temperatures. At a sufficiently high temperature, the hydrogen bonds between nucleobases are broken and the base stacking are also disrupted, resulting in a noticeable increase of A_{260} . Since the melting of the duplex is generally an all-or-none process, the plot between absorbance and temperature appears as a sigmoidal curve – so-called “melting curve”. The melting temperature is defined as a temperature that 50% of the duplex exist in single-stranded form and the other half as intact duplex. In practice, T_m is the temperature at the steepest part of the melting curve, which could be deduced from the maxima of the first derivative plot of the melting curve.

The stability of the duplex formed between the A^{PyE}-modified acpcPNA probes and DNA targets were determined by T_m measurement to investigate the binding affinity and sequence specificity of the A^{PyE}-modified acpcPNA probes towards their DNA targets. These thermal stability data are summarized in **Table 3.2**.

Table 3.2 Thermal stability data of A^{PyE}-modified acpcPNA probes and their DNA hybrids (Condition: 1.0 μ M PNA, 1.2 μ M DNA, 10 mM phosphate buffer pH 7.0).

Entry	PNA	DNA	DNA sequence ^a (5'→3')	T_m (°C)	ΔT_m (°C)	Notes
1	T4(A ^{PyE})T4	dA8T	AAAA I AAAA	61.6	-	ds, complementary
2		dA9	AAAAA A AAA	36.4	-25.2	ds, mismatched A
3		dA8G	AAAAG A AAA	28.3	-33.3	ds, mismatched G
4		dA8C	AAAAC A AAA	35.0	-26.6	ds, mismatched C
5	T8(A ^{PyE}) ₂ _0B	dA4TTA4	AAAA I AAAA	76.0	-	ds, complementary
6		dA10	AAAAA A AAAA	62.2	-13.8	ds, double mismatched
7		dA4TA5	AAAA I AAAA	53.7	-22.3	ds, single mismatched
8	T8(A ^{PyE}) ₂ _3B	dA3TA3TA2	AAA I AAATAA	60.8	-	ds, complementary
9		dA10	AAAAA A AAAA	<20	>40.8	ds, double mismatched
10		dA3TA6	AAA I AAAAAA	<20	>40.8	ds, single mismatched
11	M12T(A ^{PyE})T	dcompM12T	CAGTA I ATGACT	74.7	-	ds, complementary
12		dsmAM12T	CAGTAA A TGACT	48.6	-26.1	ds, mismatched A
13		dsmGM12T	CAGTAG A TGACT	38.0	-36.7	ds, mismatched G
14		dsmCM12T	CAGTAC A TGACT	40.0	-34.7	ds, mismatched C
15	M12A(A ^{PyE})A	dcompM12A	CAGTT I TTGACT	59.0	-	ds, complementary
16		dsmAM12A	CAGTT A TTGACT	47.3	-11.7	ds, mismatched A
17		dsmGM12A	CAGTT G TTGACT	45.7	-13.3	ds, mismatched G
18		dsmCM12A	CAGTT C TTGACT	47.7	-11.3	ds, mismatched C
19	M12G(A ^{PyE})G	dcompM12G	CAGTC I CTGACT	60.6	-	ds, complementary
20		dsmAM12G	CAGTCA A CTGACT	38.8	-21.8	ds, mismatched A
21		dsmGM12G	CAGTC G CTGACT	55.3	-5.3	ds, mismatched G
22		dsmCM12G	CAGTC C CTGACT	59.4	-8.8	ds, mismatched C

^aMismatched bases in the DNA sequence are indicated as bold font. Complementary bases in DNA sequence are indicated by underlying. Φ represents as abasic site position in DNA.

Table 3.2 Thermal stability data of A^{PyE}-modified acpcPNA probes and their DNA hybrids (Condition: 1.0 μ M PNA, 1.2 μ M DNA, 10 mM phosphate buffer pH 7.0). (Continued)

Entry	PNA	DNA	DNA sequence ^a (5'→3')	T _m (°C)	Δ T _m (°C)	Notes
23		dcompM12C	CAGTGTGTGACT	64.2	–	ds, complementary
24		dsmAM12C	CAGTGAGTGACT	59.0	–5.2	ds, mismatched A
25		dsmGM12C	CAGTGGGTGACT	55.2	–9.0	ds, mismatched G
26		dsmCM12C	CAGTGCCTGACT	61.2	–3.0	ds, mismatched C
27	M12C(A ^{PyE})C	din8M12C	CAGTGTGAGACT	58.2	–6.0	ds, indirect mismatch
28		din4M12C	CAGAGTGTGACT	44.7	–19.5	ds, indirect mismatch
29		ddsM12C	CAGTTTTTGACT	33.1	–31.1	ds, double mismatched
30		dcompM10AC	AGTG <u>I</u> TCTAC	54.4	–	ds, complementary
31		dsmAM10AC	AGTGATCTAC	46.0	–8.4	ds, mismatched A
32	M10A(A ^{PyE})C	dsmGM10AC	AGTGGTCTAC	42.8	–11.6	ds, mismatched G
33		dsmCM10AC	AGTGCTCTAC	48.8	–5.6	ds, mismatched C
34		dabasicM10AC	AGTG Φ TCTAC	48.6	–5.8	ds, direct abasic site
35		dcompM10GT	AGTG <u>A</u> ICTAC	49.6	–	ds, complementary
36		dsmAM10GT	AGTGA <u>A</u> CTAC	37.8	–11.8	ds, mismatched A
37	M10G(A ^{PyE})T	dsmGM10GT	AGTGAGCTAC	36.2	–13.4	ds, mismatched G
38		dsmCM10GT	AGTGACCTAC	39.0	–10.6	ds, mismatched C
39		dcompM12ter	CAGTATATGACT	80.4	–	ds, complementary
40		dsmAM12ter	CAGTATATGACA	77.6	–2.8	ds, mismatched A
41	A ^{PyE} M12	dsmGM12ter	CAGTATATGACG	78.8	–1.6	ds, mismatched G
42		dsmCM12ter	CAGTATATGACC	78.6	–1.8	ds, mismatched C
43		d(CTG) ₃	CTGCTGCTG	44.0	–	ds, short DNA
44	CAG(A ^{PyE})	d(CTG) ₄	CTGCTGCTGCTG	69.6	–	ds, complementary
45		d(CTG) ₅	CTGCTGCTGCTGCTG	73.6	–	ds, long DNA

^aMismatched bases in the DNA sequence are indicated as bold font. Complementary bases in DNA sequence are indicated by underlying. Φ represents as abasic site position in DNA.

3.2.2 Thermal stability of homothymine acpcPNA bearing A^{PyE} base

In the homothymine sequence [T4(A^{PyE})T4], thermal stability data indicated that the A^{PyE} base in A^{PyE}-modified acpcPNA specifically recognize thymine base in the

DNA strand. The complementary hybrid **T4(A^{PyE})T4•dA8T** showed the highest melting temperature ($T_m = 61.6$ °C). On the other hand, hybridization between the same PNA and mismatched DNA sequences exhibited much lower T_m values when compared to the complementary hybrid, **T4(A^{PyE})T4•dA9** = 36.4 °C; **T4(A^{PyE})T4•dA8G** = 28.3 °C; **T4(A^{PyE})T4•dA8C** = 35.0 °C. The large difference between melting temperatures of complementary and mismatched hybrid (ΔT_m in the range of 25.2 to 33.3 °C) suggested that the A^{PyE} base in acpcPNA can specifically recognize the base thymine in DNA, which is in accordance with the Watson-crick base pairing rules.

In addition, the thermal stabilities of acpcPNA probes carrying two A^{PyE} residues and their complementary as well as mismatched DNA targets were also studied. The two A^{PyE} bases were placed at adjacent positions [**T8(A^{PyE})2_0B**] or separated by three bases [**T8(A^{PyE})2_3B**]. As expected, the complementary hybrids were more stable than the mismatched hybrids as shown by a sharp decrease in the melting temperature by 13.8–40.8 °C (entries 5–10, **Table 3.2**). The large decrease of T_m suggests that the A^{PyE} base in A^{PyE}-modified acpcPNA could specifically recognize thymine base in the DNA strand, which is in good agreement with the results obtained from the single-A^{PyE}-modified acpcPNA.

3.2.3 Thermal stability of mix-base acpcPNA bearing A^{PyE}

The effects of neighboring nucleobases were next investigated in mix-base 12 mer A^{PyE}-modified acpcPNA: **M12T(A^{PyE})T**, **M12A(A^{PyE})A**, **M12G(A^{PyE})G** and **M12C(A^{PyE})C**, and mix-base 10 mer A^{PyE}-modified acpcPNA: **M10A(A^{PyE})C** and **M10G(A^{PyE})T** (entries 11–38, **Table 3.2**). The T_m data again confirm that the acpcPNA probes **M12X(A^{PyE})X** (X = T, A, G and C) can form stable hybrids with their complementary DNA targets as indicated by high T_m values ranging from 49.6–74.4 °C, depending on sequences. Importantly, PNA binding with its mismatched DNA exhibited lower T_m values in the range of 33.1–61.2 °C (depending on sequences). Moreover, the thermal stability was decreased even further with double-mismatched DNA targets as shown by a much further reduced melting temperature ($T_m = 33.1$ °C, entry 29, **Table**

3.2). In addition, DNA carrying abasic site at the position directly opposite to the A^{PyE} base revealed the decreasing of melting temperature by 5.8 °C relative to complementary hybrid. This value is in the same range as those observed in the single mismatched hybrids.

In addition, terminally modified A^{PyE} acpcPNA was investigated in comparison with internally-labeled [$A^{PyE}M12$ vs $M12T(A^{PyE})T$]. For complementary DNA hybrids, the T_m value of terminally-labeled acpcPNA $A^{PyE}M12$ was considerably higher than the internally-modified acpcPNA $M12T(A^{PyE})T$ (80.4 °C vs 74.7 °C, respectively). The higher stability of the complementary hybrid of terminally A^{PyE} -modified PNA than internally A^{PyE} -modified acpcPNA suggest that the incorporation of A^{PyE} base at internal positions might destabilize the duplex or the A^{PyE} base at terminal positions might stabilize the duplex, or both. To gain further insight in this observed phenomenon, the T_m were compared with unmodified acpcPNA with **T4AT4** sequence,¹⁰⁸ **T4AT4.dA8T** = 66.8 °C; **T4(A^{PyE})T4.dA8T** = 61.6 °C. The lower T_m value of **T4(A^{PyE})T4** compared with the unmodified PNA, **T4AT4**, suggested that the unfavorable steric effect of pyrene substituent group on adenine base might disturb the duplex of A^{PyE} -acpcPNA and complementary DNA. Interestingly, all single base mismatched hybrid of terminally-labeled acpcPNA $A^{PyE}M12$ when the mismatched base was positioned opposite the A^{PyE} base showed similar melting temperature to the complementary hybrid (entries 11–14 and entries 39–42, **Table 3.2**). The data suggested that the pyrene at the terminal position might stack on top of the terminal base pairs, leading to more stable and non-discriminative hybridization as previously observed in terminally pyrene-labeled DNA.^{91,93,123}

The acpcPNA probe **CAG(A^{PyE})** was designed to detect DNA carrying trinucleotide repeat sequences. High melting temperature were obtained in the cases of fully complementary and longer complementary DNA targets [**d(CTG)₄** = 69.6 °C and **d(CTG)₅** = 73.6 °C, respectively]. The higher stability of the hybrid with long DNA target even when the numbers of base pairs were identical may result from base stacking of the hanging base at the end of the PNA-DNA duplex. For a shorter complementary DNA target [**d(CTG)₃**], however, lower melting temperature was

observed due to the smaller number of base pairs formed with the PNA probe ($T_m = 44.0$ °C).

According to the T_m results, it can be concluded that the A^{PyE} base in acpcPNA probes can specifically recognize the base thymine in DNA in a broad sequence context. The A^{PyE} -modified acpcPNA probe can therefore effectively discriminate between complementary and mismatch DNA targets according to the observed difference in melting temperatures. The much larger decrease in T_m values of mismatched DNA hybrids of A^{PyE} -modified acpcPNA ranging from 5.2–36.7 °C is in sharp contrast to A^{PyE} -labeled DNA, which displayed poor binding affinity and non-specific binding. This is supported by the lower T_m value upon binding with complementary DNA at 44.5–53.5 °C and only slightly decreased by 0.5–2.5 °C in the presence of mismatch DNA⁷⁰ due to partial intercalation of the pyrene moiety, leading to the observed low binding specificity. Hence, the A^{PyE} -modified acpcPNA has fulfilled one of the basic criteria required to be applied as a probe for DNA sequencing analysis. Next, the optical properties of A^{PyE} -modified acpcPNA probes both in single-stranded form and after hybridization with complementary and various mismatched DNA targets will be investigated with UV-vis and fluorescence spectrophotometry as well as circular dichroism (CD) to obtain the information about the secondary structure of the duplexes.

3.3 Optical properties of A^{PyE} -modified acpcPNA with DNA

3.3.1 Optical properties of homothymine A^{PyE} acpcPNA

The generality of A^{PyE} as base discriminating fluorescence acpcPNA probes upon hybridization with various DNA targets were next determined. The homothymine PNA carrying one A^{PyE} unit at the middle position of the PNA strand was selected as the model sequence in this investigation. In the presence of complementary DNA, the absorption maxima wavelength at 420 nm of the single-stranded PNA remained the same but with increasing in magnitude. This is in accordance to the previous spectroscopic data of A^{PyE} -DNA probes that a new absorption peak was observed at 420 nm upon duplex formation.⁷⁴ For UV absorption spectra of single mismatched

DNA, however, the absorption maxima shifted to a longer wavelength relative to single-stranded PNA (Figure 3.5A). The UV absorption data suggested that the A^{PyE} base may adopt different orientations upon binding with complementary and mismatched targets.

The fluorescence spectra of single-stranded PNA showed a high fluorescence intensity as revealed by a high quantum yield ($\Phi_F = 0.333$) with the emission maxima at 453 nm. Upon addition of complementary DNA, the fluorescence was enhanced by 1.56 folds relative to single-stranded PNA with emission wavelength shifting into a shorter wavelength at 438 nm. In the mismatched dC and dG DNA hybrid, the fluorescence was decreased by 0.64 and 0.75 folds, respectively. Moreover, hybridization of A^{PyE}-dA mismatched exhibited a smaller decrease in fluorescence (Figure 3.5B). According to the results, A^{PyE} acts as a base discriminating fluorescence nucleobase whereby the discrimination ability of thymine base from other mismatch bases by showing the enhancement in fluorescence upon base-pairing to its complementary base.

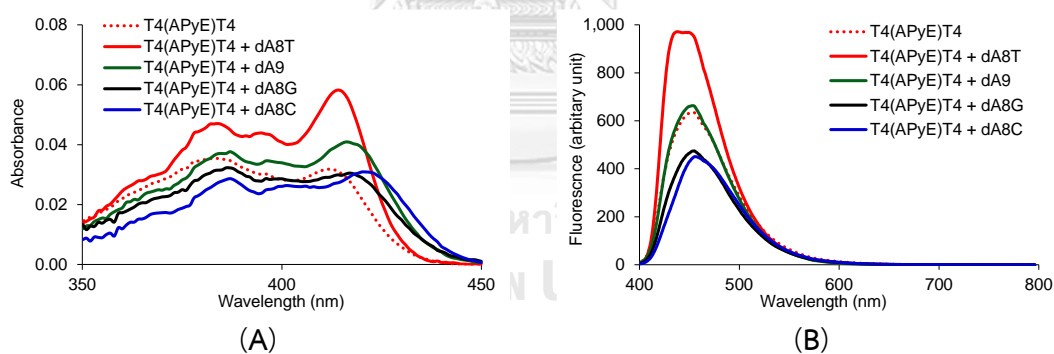


Figure 3.5 (A) UV-vis and (B) fluorescence spectra of **T4(A^{PyE})T4** and its DNA hybrids. Conditions: 1.0 μM PNA, 1.2 μM DNA, 10 mM sodium phosphate buffer pH 7.0, λ_{ex} 376 nm

3.3.2 Effects of neighboring bases to base pairing and optical properties of A^{PyE}

The next study focused on the effects of neighboring nucleobases to the fluorescent properties of A^{PyE} in acpcPNA. The experiments were performed with 12

mer mix-base sequences carrying different bases adjacent, **M12T(A^{PyE})T**, **M12A(A^{PyE})A**, **M12G(A^{PyE})G** and **M12C(A^{PyE})C** and 10 mer mix-base sequences carrying different flanking bases **M10A(A^{PyE})C** and **M10G(A^{PyE})T**.

In the experiment involving 12 mer PNA sequences, the UV absorption spectra exhibited a small blue-shifting (ca. 2–4 nm) from single-stranded PNA when hybridized with complementary DNA. In contrast, hybridization with single base mismatch DNA carrying the mismatch base directly opposite to the A^{PyE} resulted in pronounced red-shifted UV absorption spectra (λ_{abs} of single stranded PNA: 414–419 nm, complementary duplexes: 412–419 nm, single mismatched duplexes: 419–426 nm). Interestingly, the UV absorption spectra of “indirect mismatch” duplexes carrying the mismatched not directly opposite to the A^{PyE} base were remarkably similar to the complementary hybrid, *i.e.* without red-shifting (**Figure 3.6**).

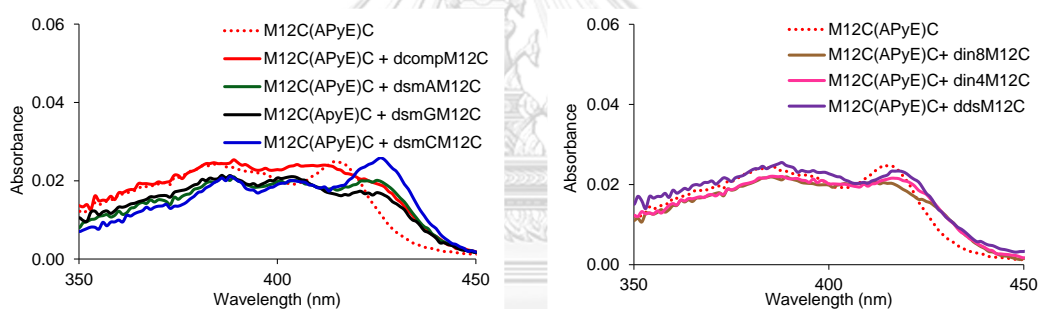


Figure 3.6 UV-vis spectra of **M12C(A^{PyE})C** and its DNA hybrids. Conditions: 1.0 μM PNA, 1.2 μM DNA, 10 mM sodium phosphate buffer pH 7.0

To provide further insight about the arrangement of the A^{PyE} within the duplex, circular dichroism spectroscopy (CD) was used to study the conformation and interaction of pyrene inside the duplex. In the direct mismatched hybrid, CD spectra showed a distinct negative band at ca. 320 nm which was in the pyrene absorption region (**Figure 3.7B**). Such band was not observed in the complementary and indirect mismatched duplexes (**Figure 3.7A** and **3.7C**). The CD supported that the A^{PyE} in these hybrids were adopting different conformations. It was proposed that in the complementary or indirect mismatched duplexes, base pairing of A^{PyE} and thymine base occurred through the usual hydrogen-bonding. On the other hand, in the single mismatched hybrids having the mismatch base opposite to the A^{PyE}, the pyrene moiety

may instead bury into the base stack of the duplex, resulting in the observed red-shifted absorption and induced CD spectra.

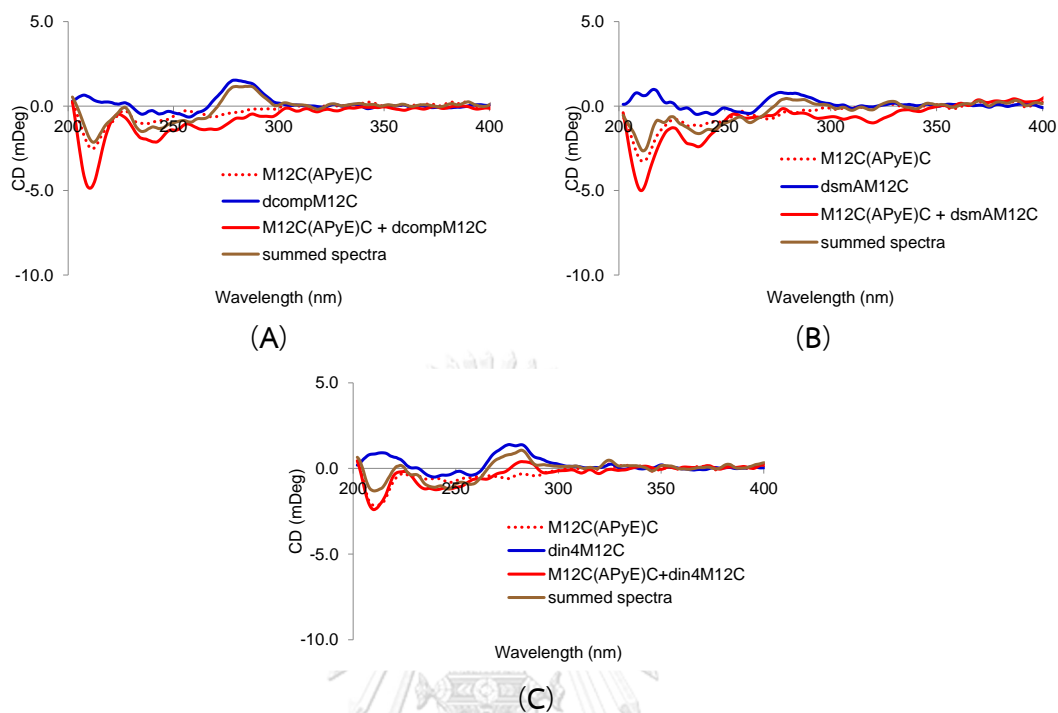


Figure 3.7 CD spectra of M12C(A^{PyE})C with (A) dcompM12C (complementary), (B) dsmAM12C (single mismatch) and, (C) din4M12C (indirect single mismatch). Conditions: 1.0 μM PNA, 1.2 μM DNA in 10 mM phosphate buffer pH 7.0

The fluorescence of single stranded A^{PyE}-modified PNA with different adjacent bases was influenced by the flanking bases, especially in cases of G/G and C/C due to the photoinduced electron transfer between the modified base and its flanking bases.¹²⁸ Reduction of the fluorescence quantum yield by 2–4 folds was observed when the flanking bases were G/G and C/C compared with T/T and A/A (Table 3.3). Upon binding with complementary DNA, the enhancement of fluorescence by 1.5–2.8-fold relative to the single-stranded A^{PyE} PNA was observed as a result of a strong hydrogen bonding between A^{PyE} and thymine, which forced the pyrene to expose outside the duplex thereby causing the observed fluorescence enhancement. In contrast, the presence of single mismatched DNA caused the fluorescence quantum yield to decrease compared to the single stranded PNA probe (Figure 3.8). Indirect and double mismatch binding caused relatively minor fluorescence reduction

(0.62–0.73-fold) or even unchanged when compared to the direct mismatch. Obviously, the intercalation of the A^{PyE} is less likely in these cases, and the duplex may not be even fully formed in these cases (**Figure 3.8**).

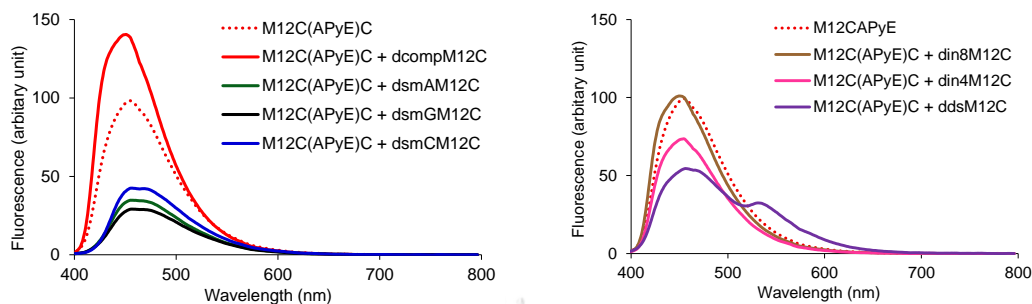


Figure 3.8 Fluorescence spectra of M12C(A^{PyE})C and its DNA hybrids. Conditions: 1.0 μM PNA, 1.2 μM DNA, 10 mM sodium phosphate buffer pH 7.0, λ_{ex} 376 nm

In addition, two 10 mer mix-base sequences with different flanking bases (A/C and G/T) also showed the same trend of fluorescence spectra as observed in the 12 mer PNA. In both cases, the fluorescence enhancement of complementary duplexes and fluorescence reduction of mismatched duplexes were confirmed (**Figure 3.9A**). DNA containing abasic site located directly opposite to the A^{PyE} base in the PNA strand also demonstrated the red-shifting in UV absorption (**Figure 3.9B**) similar to the direct mismatched hybrids described above. Again, CD spectra suggested that the pyrene was placed inside the duplex in the cases of hybrids carrying a mismatched base or abasic site directly opposite to the A^{PyE} as shown by the negative band around 320 nm in (**Figure 3.9C**, entry 29 in **Table 3.3**).

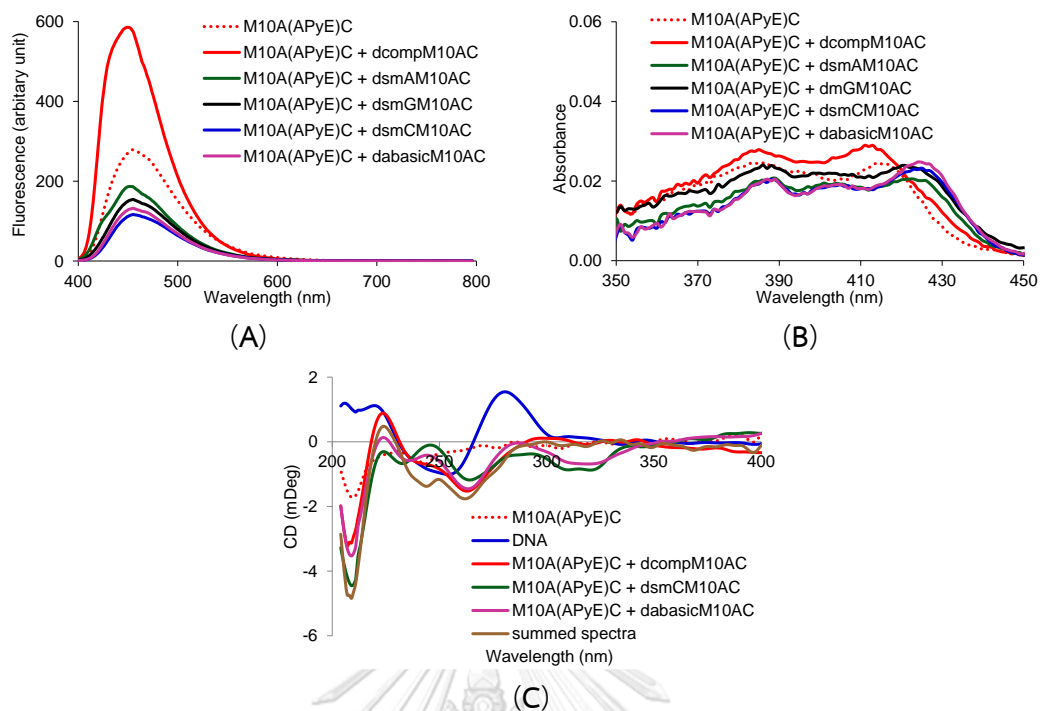


Figure 3.9 (A) Fluorescence, (B) UV-vis and (C) CD spectra of **M10A(A^{PyE})C** and its DNA hybrids. Conditions: 1.0 μM PNA, 1.2 μM DNA, 10 mM sodium phosphate buffer pH 7.0, λ_{ex} 376 nm

The absorption wavelength shifting and CD data suggested that the enhancement or reduction of fluorescence upon hybrid with DNA targets resulted from different orientations of the pyrene chromophore in the perfect matched and mismatched duplexes (*anti* vs *syn*, respectively). Briefly, pyrene is a planar, hydrophobic chromophore and should prefer stacking inside the DNA duplex to avoid contact with water. However, this would prevent the A^{PyE} base to form hydrogen bonds with the opposite thymine base. Hybridization of A^{PyE}-PNA with complementary or indirect mismatched DNA required that the A^{PyE} should adopt the *anti*-conformation to allow base pairing with the opposite dT in the DNA strand. This led to the fluorescence enhancement because the strong base pairing necessarily forced the pyrene to expose to the aqueous environment. In cases of direct single base mismatch or abasic site, the A^{PyE} should adopt the *syn*-conformation so that the pyrene chromophore can stack inside the PNA•DNA duplex to avoid contact with aqueous environment. This is possible without breaking the hydrogen bonds since the A^{PyE} did

not form any hydrogen bonds under these circumstances. Stacking of pyrene inside DNA duplexes was known to result in reduction of fluorescence,^{123,129-130} and this is fully consistent with the fluorescence reduction observed in the case of mismatched and abasic duplexes. The results are quite different to previous work on A^{PyE}-based DNA probe that was shown to be unable to discriminate T from other DNA bases in the target strand. In these cases, the pyrene chromophore always adopt *syn*-orientation allowing pyrene, a hydrophobic unit, to intercalate within the duplex to minimize contact with water regardless of the identity of the opposite nucleobase.⁷⁰ The A^{PyE} containing acpcPNA can therefore be used as a hybridization responsive fluorescence PNA probe whereby the fluorescence of which depends on the environment around the modified base rather than global sensing of the formation of duplex. **Table 3.3** summarizes optical data of all mix-base A^{PyE}-PNA with its DNA hybrids.

Table 3.3 Optical properties of A^{PyE}-modified acpcPNA probes and their DNA hybrids (Condition: 1.0 μ M PNA, 1.2 μ M DNA, 10 mM phosphate buffer pH 7.0, λ_{ex} 376 nm).

Entry	PNA	DNA	F/F_0^a	$\lambda_{abs}/\lambda_{em}^b$ (nm)	Φ_f^c	Notes
1		-	-	416/455	0.187	ss
2		dcompM12T	2.68	414/447	0.374	ds, complementary
3	M12T(A ^{PyE})T	dsmAM12T	1.17	420/453	0.313	ds, mismatched A
4		dsmGM12T	0.77	423/455	0.221	ds, mismatched G
5		dsmCM12T	1.02	425/455	0.267	ds, mismatched C
6		-	-	417/457	0.163	ss
7		dcompM12A	2.71	413/448	0.264	ds, complementary
8	M12A(A ^{PyE})A	dsmAM12A	1.25	423/454	0.229	ds, mismatched A
9		dsmGM12A	1.10	423/454	0.220	ds, mismatched G
10		dsmCM12A	1.11	423/455	0.235	ds, mismatched C

^aM12T(A^{PyE})T, $\lambda_{em} = 447$ nm, M12A(A^{PyE})A, $\lambda_{em} = 448$ nm, M12G(A^{PyE})G, $\lambda_{em} = 455$ nm, M12C(A^{PyE})C, $\lambda_{em} = 451$ nm, $\lambda_{em} = 449$ nm, M10G(A^{PyE})T, $\lambda_{em} = 449$ nm. ^bOnly the longest wavelength was shown for λ_{abs} . ^cQuantum yields were measured by using quinine sulfate as a standard ($\Phi_f = 0.546$).

Table 3.3 Optical properties of A^{PyE}-modified acpcPNA probes and their DNA hybrids (Condition: 1.0 μ M PNA, 1.2 μ M DNA, 10 mM phosphate buffer pH 7.0, λ_{ex} 376 nm). (Continued)

Entry	PNA	DNA	F/F_0^a	$\lambda_{abs}/\lambda_{em}^b$ (nm)	Φ_F^c	Notes
11		-	-	419/498	0.050	ss
12	M12G(A ^{PyE})G	dcompM12G	2.78	419/457	0.077	ds, complementary
13		dsmAM12G	1.27	423/482	0.062	ds, mismatched A
14		dsmGM12G	0.99	423/496	0.053	ds, mismatched G
15		dsmCM12G	1.25	421/495	0.061	ds, mismatched C
16		-	-	-	414/455	0.078
17	M12C(A ^{PyE})C	dcompM12C	1.52	412/451	0.113	ds, complementary
18		dsmAM12C	0.35	425/455	0.042	ds, mismatched A
19		dsmGM12C	0.28	421/456	0.033	ds, mismatched G
20		dsmCM12C	0.42	426/457	0.059	ds, mismatched C
21		din8M12C	1.01	412/450	0.092	ds, indirect mismatch
22		din4M12C	0.73	417/454	0.067	ds, indirect mismatch
23		ddsM12C	0.62	417/456	0.063	ds, double mismatched
24		-	-	-	416/455	0.227
25	M10A(A ^{PyE})C	dcompM10AC	2.27	412/449	0.389	ds, complementary
26		dsmAM10AC	0.68	422/452	0.211	ds, mismatched A
27		dsmGM10AC	0.57	421/455	0.139	ds, mismatched G
28		dsmCM10AC	0.40	425/455	0.145	ds, mismatched C
29		dabasicM10AC	0.44	424/455	0.167	ds, direct abasic site
30	-	-	-	416/457	0.094	ss
31	M10G(A ^{PyE})T	dcompM10GT	5.18	415/449	0.304	ds, complementary
32		dsmAM10GT	1.37	419/455	0.161	ds, mismatched A
33		dsmGM10GT	1.33	419/454	0.164	ds, mismatched G
34		dsmCM10GT	1.83	422/455	0.202	ds, mismatched C

^aM12T(A^{PyE})T, λ_{em} = 447 nm, M12A(A^{PyE})A, λ_{em} = 448 nm, M12G(A^{PyE})G, λ_{em} = 455 nm, M12C(A^{PyE})C, λ_{em} = 451 nm, λ_{em} = 449 nm, M10G(A^{PyE})T, λ_{em} = 449 nm. ^bOnly the longest wavelength was shown for λ_{abs} . ^cQuantum yields were measured by using quinine sulfate as a standard (Φ_F = 0.546).

3.3.3 Effects of position of A^{PyE} in the PNA strand (internal vs terminal)

The effects of labelling position of A^{PyE} in the single-stranded PNA were studied in terms of melting temperature (see **section 3.2.3**) and optical properties. Two acpcPNA sequences having the same sequence except for the replacement of the N-terminal A with A^{PyE} for the terminally-modified probe [A^{PyE}M12] and the replacement of internal A with A^{PyE} for the internally-modified probe [M12T(A^{PyE})T] were compared. The fluorescence quantum yield of the terminally-modified single-stranded PNA was much smaller than the internally-modified PNA by 5 folds (0.040 vs 0.187, respectively). This may be explained by the quenching effect of the neighboring guanine at the N-terminus adjacent to the terminal A^{PyE}. Addition DNA caused a small increase in fluorescence. Interestingly, the fluorescence emission was significantly red-shifted from 455 nm to 471–479 nm regardless of the identity of the base opposite to the A^{PyE} (**Table 3.4**). This fluorescence change is quite distinctive from the internally-modified PNA M12T(A^{PyE})T having the same sequence except for the position of the A^{PyE} base and may suggest that the A^{PyE} might adopt the *syn*-conformation so that the pyrene part could stack on top of the PNA-DNA duplex. Since the fluorescence change is not so selective as shown by the large fluorescence increase in the case of A mismatch, the terminal position is not the appropriate place for making a good hybridization responsive PNA probe.

Table 3.4 Optical properties of A^{PyE}-modified acpcPNA probes and their DNA hybrids (Condition: 1.0 μ M PNA, 1.2 μ M DNA, 10 mM phosphate buffer pH 7.0, λ_{ex} 376 nm).

Entry	PNA	DNA	F/F_0^a	$\lambda_{\text{abs}}/\lambda_{\text{em}}^b$ (nm)	Φ_F^c	Notes
1		-	-	414/455	0.040	ss
2		dcompM12ter	1.81	413/476	0.081	ds, complementary
3	A ^{PyE} M12	dsmAM12ter	1.56	415/471	0.068	ds, mismatched A
4		dsmGM12ter	0.76	415/474	0.045	ds, mismatched G
5		dsmCM12ter	0.96	414/479	0.062	ds, mismatched C

^aA^{PyE}M12, $\lambda_{\text{em}} = 476$ nm. ^bOnly the longest wavelength was shown for λ_{abs} . ^cQuantum yields were measured by using quinine sulfate as a standard ($\Phi_F = 0.546$).

3.4 Improving the discrimination of A^{PyE} modified acpcPNA probes using graphene oxide

The modest discrimination factors due to the high fluorescence background of single-stranded A^{PyE}-modified PNA is the limitation of the current PNA probes. Therefore, a method for reducing the background signal further was required in order to improve the discrimination ability. One way to achieve this goal was to employ nanomaterials as external quenchers. Graphene oxide (GO) and reduced graphene oxide (rGO) were utilized in this work to quench the background signal.¹³¹ The nanomaterial-based fluorescent platform probes display sensitive, rapid and specific detection of several biomolecules,^{15,132} including DNA.¹³³ It is known from the studies with oligonucleotides that in the presence of the GO/rGO nanoquencher, the rather non-specific π - π interaction between the fluorophore-labeled single stranded oligonucleotides and the GO/rGO resulted in fluorescence quenching. Duplex DNA, on the other hand, show much lower tendency for similar π - π interaction since the nucleobases formed stable base pairs and base stacks inside the duplex therefore the fluorescence signal of fluorescence-labeled duplex DNA was not quenched in the same way.¹³¹⁻¹³⁴ If the affinity of the two DNA strands can overcome the association of the single stranded DNA and the GO, addition of complementary DNA will result in competitive formation of duplexes. This will lead to dissociation of the single stranded probe from the quencher with concomitant restoration of fluorescence signal due to the separation of the fluorophore from the quencher. This principle has been used extensively for DNA sequence detection with DNA as well as PNA probes.¹³⁵⁻¹³⁸ **Figure 3.10** represents the concept of the use of GO/rGO together with A^{PyE}-modified PNA probes in order to reduce the background signal and to improve the specificity of the DNA detection further.

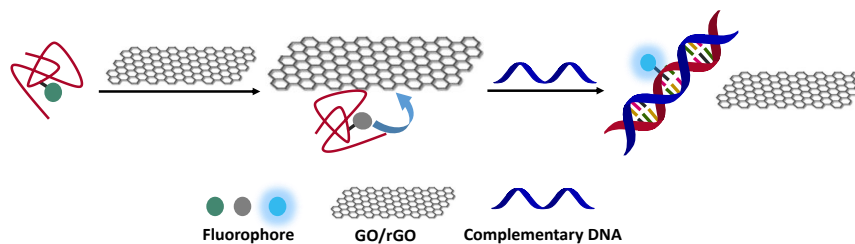


Figure 3.10 The concept of using GO or rGO as nanoquenchers to improve the performance of fluorescence hybridization probe detection

Firstly, the fluorescence quenching of GO/rGO with single-stranded PNA probe **M12T(A^{PyE})T** was investigated. The fluorescence was reduced upon increasing the concentration of the quenchers. The appropriate concentration of the quenchers at 0.2 $\mu\text{g}/\text{mL}$ was chosen, which was sufficient to reduce the fluorescence signal by more than 90% (**Figure 3.11**). GO was slightly more effective than rGO in terms of the ability to quench the fluorescence of A^{PyE}-modified PNA probe.

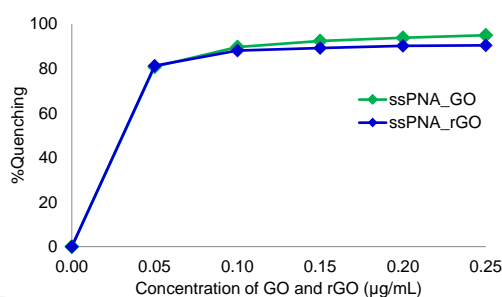


Figure 3.11 Percentage fluorescence quenching of single-stranded PNA **M12T(A^{PyE})T** by GO (green) or rGO (blue). Conditions: 0.1 μM PNA, 0.1 μM DNA, 10 mM Tris HCl pH 7.4, λ_{ex} 376 nm. The fluorescence intensity was measured after incubating the ssPNA with GO/rGO for 1 h.

The fluorescence signal restoration after addition of complementary DNA to the complex of A^{PyE}-PNA and GO/rGO was subsequently examined. Addition of complementary DNA resulted in a dramatic increase of the fluorescence signal. However, the signal restoration could not reach the original level (71% vs 47%, for rGO and GO, respectively) (**Figure 3.12A**). The signal restoration was not complete under the reaction time (1 hour) at the stoichiometric concentration of the sample performed

in this experiment. In addition, the fluorescence quantum yield of A^{PyE}-rGO hybrid with complementary DNA was also slightly reduced ($\Phi_F = 0.287$, Φ_F of free probe = 0.056) compared to the control experiment without rGO ($\Phi_F = 0.374$, Φ_F of free probe = 0.187).

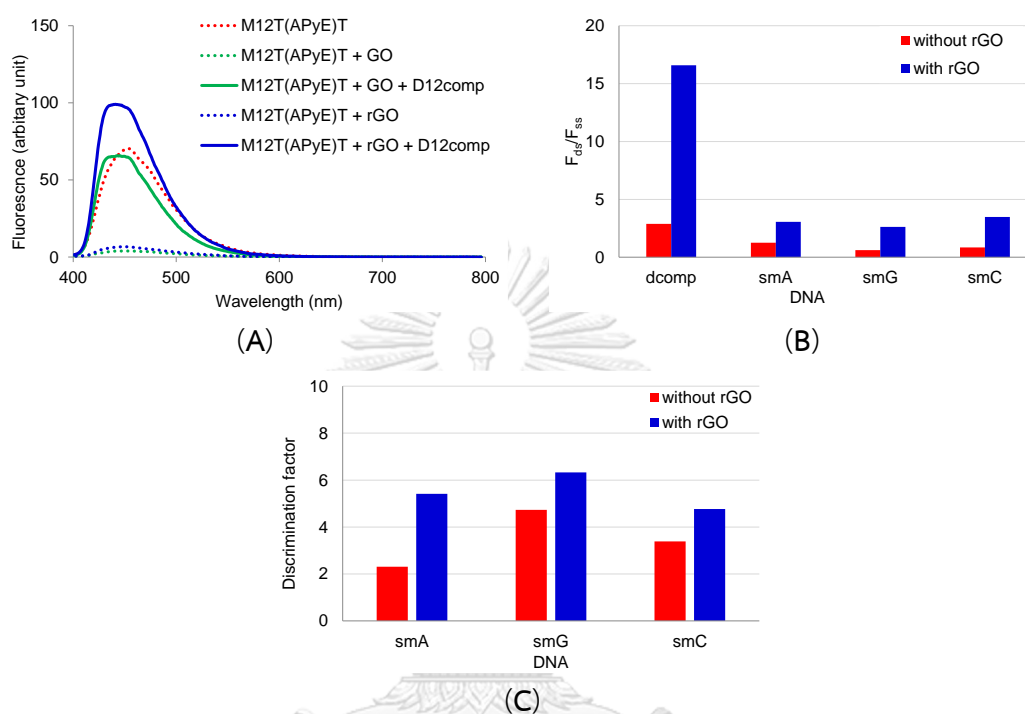


Figure 3.12 (A) Fluorescence spectra of PNA M12T(A^{PyE})T before and after addition of GO or rGO, and after addition of GO/rGO and complementary DNA, (B) The discrimination graph compared between without/with rGO in the presence of DNA and (C) The discrimination graph defined as complementary divided by mismatched hybrid. Conditions: 0.1 μM PNA, 0.5 μM DNA, GO/rGO = 0.2 $\mu\text{g/mL}$, 10 mM Tris HCl pH 7.4, λ_{ex} 376 nm, λ_{em} 438 nm. The fluorescence intensity was measured after incubating the ssPNA with GO/rGO for 1 h.

Due to the higher level of fluorescence restoration, rGO was chosen as the nanoquencher for further selectivity studies with single base mismatch DNA targets. The fluorescence intensity of single mismatched hybrids was not decreased much in the presence of rGO, suggesting that the fluorescence of the single mismatched hybrids was not effectively quenched by the rGO. This, together with the lower background of single stranded PNA (F_0), explain the observed increase in F/F_0 (Figure

3.12B). Nevertheless, the discrimination factor (defined as F/F_0 of complementary divided by F/F_0 of mismatched hybrid) in the presence of rGO was still higher than without using rGO as shown in **Figure 3.12C** and **Table 3.5**.

Table 3.5 Fluorescence emission ratio of the **M12T(A^{PyE})T**-rGO complex in the presence of DNA. (Condition: 0.1 μM PNA, 0.5 μM DNA, 0.2 $\mu\text{g/mL}$ rGO, 10 mM Tris HCl pH 7.4, λ_{ex} 376 nm, λ_{em} 438 nm. The fluorescence intensity was measured after incubated ssPNA with rGO for 1 hour.)

Entry	DNA	F/F_0 at 438 nm		Discrimination factor	
		Without rGO	With rGO	Without rGO	With rGO
1	Complementary DNA	2.9	16.6	1.0	1.0
2	Single mismatched A	1.3	3.1	2.2	5.4
3	Single mismatched G	0.6	2.6	4.7	6.3
4	Single mismatched C	0.9	3.5	3.4	4.8

Thus, the use of rGO as an external nanoquencher could improve the performance of the A^{PyE}-modified PNA probe further.

3.5 Applications of A^{PyE} modified acpcPNA as color-shifting probes

While the fluorescence emission wavelength of the complementary DNA hybrids of A^{PyE}-modified acpcPNA are similar or only slightly blue-shifted from the single stranded probe (**Table 3.3**), an exception was observed in the case of **M12G(A^{PyE})G** probe. This particular sequence exhibited a remarkably long wavelength emission maxima in the single stranded form (entry 11, **Table 3.3**) which was in contrast to other flanking bases (λ_{em} : T/T = 455 nm, A/A = 457 nm and C/C = 455 nm). Interestingly, the positions of the guanine adjacent to the A^{PyE} showed a dramatic effect to the emission wavelength of the single stranded probe (guanine located at N terminus side (**M10G(A^{PyE})T**, λ_{em} = 457 nm) and C-terminus side (**CAG(A^{PyE})**, λ_{em} = 498 nm). Thus, the most distinctive switching of fluorescence emission maxima was observed when guanine residue was placed at C-terminus side of the A^{PyE} base.

Hybridization with complementary DNA gave a duplex that exhibit fluorescence emission maxima at 457 nm which was similar to other A^{PyE}PNA-DNA hybrids, thereby causing a remarkable blue-shifting of the emission maxima by 41 nm. This pronounced change in the emission maxima wavelength resulted in an observable fluorescence color change from green to blue-green under UV light. Such wavelength shift and color change were not observed with single mismatched DNA targets. The remarkable wavelength shifting properties were observed only in the presence of complementary DNA targets, therefore the A^{PyE}-modified acpcPNA probe may be useful as a hybridization responsive probe for DNA sequences analysis that can change color in addition to fluorescence intensity. This was demonstrated in the application for the detection of CAG/CTG trinucleotide repeats.¹³⁹ The CAG/CTG trinucleotide repeats disorders are the major class in genetic disorders by the CAG expansion in the coding region causing several well-known heritable neurological and neuromuscular disorders including Huntington's disease (HD), spinobulbar muscular atrophy (SBMA, Kennedy's disease), spinocerebellar ataxias (SCA) types 1, 2, 3, 6, 7, 17 and dentatorubropallidoluysian atrophy (DRPLA).¹⁴⁰ Detection of CAG/CTG repeats have been extensively studied with several techniques such as electrochemical methods¹⁴¹ and fluorescent probes.¹⁴² In this study, the CAG(A^{PyE}) PNA probe with the length of 12 mer was investigated. The single-stranded PNA probe exhibited a particularly long emission maxima wavelength at 498 nm similar to the M12G(A^{PyE})G probe and exhibited a green fluorescence under UV light (365 nm). In the presence of DNA with the trinucleotide repeat sequences, [d(CTG)₃, d(CTG)₄ and d(CTG)₅], the fluorescence was enhanced by 2.5 folds with a blue-shifting ca. 45 nm relative to single-stranded PNA. The fluorescence intensity ratio and fluorescence quantum yield are summarized in **Table 3.6**.

Table 3.6 Optical properties of A^{PyE}-modified acpcPNA probes and their DNA hybrids (Condition: 1.0 μM PNA, 1.2 μM DNA, 10 mM phosphate buffer pH 7.0, λ_{ex} 376 nm).

Entry	PNA	DNA	F/F_0^a	$\lambda_{\text{abs}}/\lambda_{\text{em}}^b$ (nm)	Φ_F^c	Notes
1		-	-	417/498	0.047	ss
2	CAG(A ^{PyE})	d(CTG) ₃	2.38	414/457	0.070	ds, short DNA
3		d(CTG) ₄	2.55	413/454	0.066	ds, complementary
4		d(CTG) ₅	2.48	413/455	0.065	ds, long DNA

^aCAG(A^{PyE}), $\lambda_{\text{em}} = 454$ nm. ^bOnly the longest wavelength was shown for λ_{abs} . ^cQuantum yields were measured by using quinine sulfate as a standard ($\Phi_F = 0.546$).

Furthermore, the CD spectra confirmed the formation of PNA•DNA hybrid as revealed the dominant positive peak at 286 nm in the CD spectra (Figure 3.13B). The color shifting upon addition of DNA could be observed by naked eyes under UV exposure (Figure 3.13C). Polyacrylamide gel electrophoresis also confirmed the formation of blue-fluorescence PNA-DNA hybrids in all cases (Figure 3.13D).

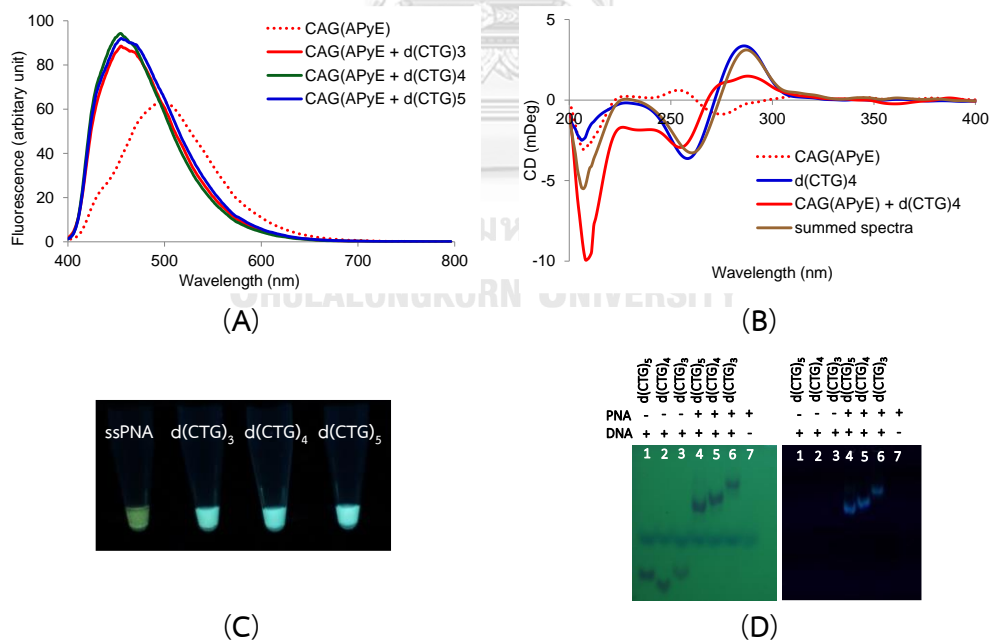


Figure 3.13 (A) Fluorescence spectra, (B) CD spectra, (C) photograph, and (D) gel electrophoresis of CAG(A^{PyE}) and its DNA hybrids under UV light. Conditions: 1.0 μM PNA, 1.2 μM DNA, 10 mM phosphate buffer pH 7.0, λ_{ex} 376 nm

Unfortunately, the remarkably red-shifting of the single-stranded PNA probe was most noticeable only when guanine was present adjacent to the A^{PyE} toward the C-terminus of the PNA probes. When the neighboring G was placed towards the N-terminus (entries 30–34, **Table 3.3**), the red-shift was not so pronounced and therefore the color-shifting is quite sequence dependent. To overcome the limitation, the double labeling of the acpcPNA probe with two A^{PyE} residues was examined in order to employ the monomer-excimer switching principle as a mechanism to induce the wavelength shift.^{26,121-122} It was proposed that in the single-stranded state, the two pyrene fluorophores from the two A^{PyE} bases were forced into close proximity since the hydrophobic structure of PNA preferred to form a compact structure to minimize the contact with aqueous environment leading to the emission of excimer. Hybridization with complementary DNA causes the two pyrenes to separate, resulting in the disappearance of the excimer emission and formation of the monomer emission. According to this design, the color shifting phenomena should be general regardless of the base sequence of the PNA probe. **Table 3.7** summarizes optical data of the double-labeling A^{PyE}-PNA with its DNA hybrids.

Table 3.7 Optical properties of A^{PyE}-modified acpcPNA probes and their DNA hybrids (Condition: 1.0 μ M PNA, 1.2 μ M DNA, 10 mM phosphate buffer pH 7.0, λ_{ex} 376 nm).

Entry	PNA	DNA	F/F_0^a	$\lambda_{abs}/\lambda_{em}^b$ (nm)	Φ_F^c	Notes
1		-	1.0	385/491	0.178	ss
2	T8A ^{PyE} 2_0B	dA4TTA4	0.95	385/494	0.177	ds, complementary
3		dA10	0.80	385/482	0.188	ds, double mismatched
4		dA4TA5	0.90	386/480	0.179	ds, single mismatched
5		-	1.0	386/484	0.097	ss
6	T8A ^{PyE} 2_3B	dA3TA3TA2	2.03	385/455	0.114	ds, complementary
7		dA10	0.50	387/455	0.062	ds, double mismatched
8		dA3TA6	1.43	386/487	0.099	ds, single mismatched

^aT8A^{PyE}2_0B, λ_{em} = 494 nm, T8A^{PyE}2_3B, λ_{em} = 455 nm. ^bOnly the longest wavelength was shown for λ_{abs} .

^cQuantum yields were measured by using quinine sulfate as a standard (Φ_F = 0.546).

To verify the proposed design, the double- A^{PyE} -modified acpcPNA probes were synthesized. Two different probes, each carried two A^{PyE} residues at different positions were compared. In one case, the two A^{PyE} were placed at the adjacent position [T8(A^{PyE})2_0B] and the other were separated by three bases [T8(A^{PyE})2_3B]. The fluorescence spectra of the two PNA probes revealed a distinctive red-shifted emission due to the formation of excimer as expected. However, the distance between those two A^{PyE} labels strongly affected the discrimination ability of the probes. In case of T8(A^{PyE})2_0B probe, the fluorescence spectra of the single stranded probe and all of its DNA hybrids were similar (Figure 3.14A). In contrast, the blue-shifted spectra as well as 2-fold fluorescence enhancement relative to the single stranded PNA probe was observed with the T8(A^{PyE})2_3B probe in the presence of its complementary DNA. The level of discrimination was not perfect since single mismatched hybrid gave similar fluorescence change to complementary hybrid. However, with double mismatched DNA target, the fluorescence became similar to single stranded probe. It is quite possible that the level of discrimination could be further improved by increasing the stringency of the hybridization conditions, for example by increasing temperature, salt concentration or by employing S1 nuclease.^{94,143-144} The color shifting of the emission could be visualized under UV light (Figure 3.14B).

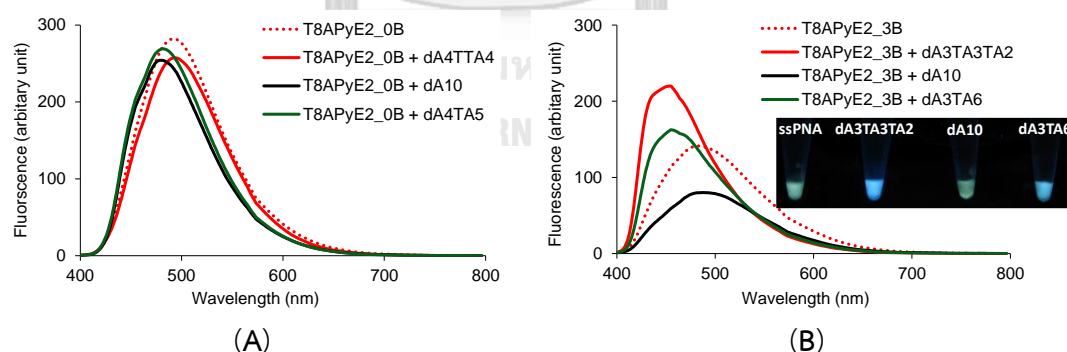


Figure 3.14 Fluorescence spectra of (A) T8A^{PyE}2_0B and (B) T8A^{PyE}2_3B with DNA. In set shows a photograph of T8A^{PyE}2_3B with DNA. Conditions: 1.0 μ M PNA, 1.2 μ M DNA, 10 mM phosphate buffer pH 7.0, λ_{ex} 376 nm

3.6 Fluorescence acpcPNA probes synthesized via post-synthetic modification

Fluorescence oligonucleotides bearing modified nucleobases have been prepared by various methods. Typically, fluorescence nucleobases can be incorporated into oligonucleotides by the conventional approach that involves chemical synthesis of the modified nucleobase building block which is subsequently incorporated into the oligonucleotide through solid phase synthesis. This approach has some limitations, for example, the incompatibility and instability of some functional groups in the building block during the solid phase synthesis and cleavage step,¹⁴⁵ In addition, lower coupling efficiency is frequently observed due to steric hindrance when using bulky building block.^{40,102} An alternative approach is to incorporate the modified nucleobases enzymatically by DNA polymerase using modified nucleoside triphosphates (dNTPs or NTPs).⁹⁸ However, the selection of modified (d)NTPs that is compatible with the enzymatic reactions is limited and may not be easily predicted.^{40,98,146-147} Another powerful approach for preparing fluorescence oligonucleotides is via post-synthetic modification. The obvious advantages of this approach over the pre-formed monomer approach is that there is no need to synthesize new monomers and changing of the fluorophore can be easily made without the need to re-synthesize the whole sequence. In addition, the method is highly suitable for certain modifications that may not be stable under the DNA/PNA synthesis, deprotection or cleavage conditions.

One of the most promising approaches for post-synthetic modification of DNA oligonucleotides involves incorporation of one or more halogenated nucleosides at predefined positions in the oligonucleotide sequence followed by a palladium-catalyzed cross coupling. This synthetic approach allows convenient functionalization of oligonucleotides with a variety of fluorescence dyes onto the readily accessible oligonucleotides carrying halogenated nucleobases. For example, a successful modification of oligonucleotides bearing a single 8-bromoguanine residue with several arylboronic acids.¹⁰¹ Although such Pd-catalyzed reactions for nucleoside monomers⁴¹ as well as post-synthetic approaches for the synthesis of more complex oligonucleotides on solid support in organic media has been well developed,¹⁴⁸ the

corresponding solution phase reaction under aqueous conditions has only been recently realized.^{101,102,149} Thus, this part of the work involved the adaptation of similar post-synthetic palladium-catalyzed reactions to synthesize fluorescence acpcPNA probes with a wide variety of fluorophores. The synthesis started with synthesizing the Fmoc-protected 5-iodouracil acpcPNA monomer as a reactive building block. This halogenated monomer was subsequently incorporated at a predefined position on the acpcPNA through solid phase peptide synthesis. Afterward, modifications with the fluorophore were performed in solution phase after cleavage of the PNA from the solid support using Suzuki-Miyaura or Sonogashira cross-couplings (**Figure 3.15**). It was proposed that the Watson-Crick base pairing ability of the modified-uracil in acpcPNA should be retained, and that the intrinsically fluorescence modified nucleobase should give fluorescence alteration upon binding with complementary nucleobases in the DNA target strand.



Figure 3.15 A schematic showing the post-synthetic modification of acpcPNA through palladium-catalyzed reactions

3.6.1 Synthesis of U^I-acpcPNA monomer

The Fmoc-protected 5-iodouracil acpcPNA monomer (**7**, U^I) was required as a protected building block for the synthesis of U^I-modified acpcPNA. The Boc-protected U^I intermediate **6** was synthesized through the Mitsunobu reaction of the known Boc/Dpm hydroxyproline¹²⁵ (**5**) with *N*³-benzoyl-5-iodouracil¹¹¹ according to the previously reported procedure.⁹¹ All protecting groups in **6** was subsequently removed by treatment with trifluoroacetic acid in dichloromethane (1:1). After solvent removal and precipitation with diethyl ether, the intermediate free amino acid was protected by FmocOSu/NaHCO₃ in aqueous acetonitrile to obtain the desired Fmoc-protected U^I monomer (**7**) in 55% yield starting from the Boc/Dpm intermediate (**6**). The identity of

the Fmoc-protected monomer (**7**) was confirmed by ^1H and ^{13}C NMR and also MALDI-HRMS.

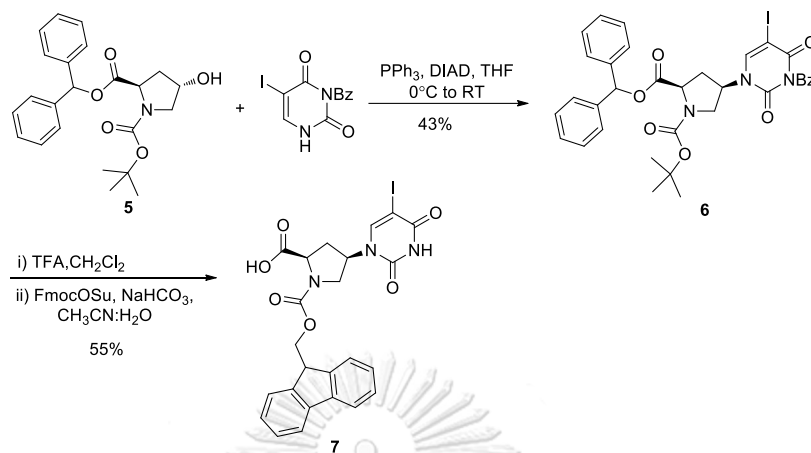


Figure 3.16 Synthesis of Fmoc-protect U¹ monomer

3.6.2 Synthesis of 5-iodouracil-containing acpcPNA

The Fmoc-protected 5-iodouracil acpcPNA monomer was incorporated into the internal position of the acpcPNA using the standard HATU activation protocol as described in Chapter II. After completing the acpcPNA synthesis, the U¹-acpcPNA was cleaved from the solid support by TFA. The crude PNA was used for post-synthetic Sonogashira and Suzuki-Miyaura cross-couplings without further purification other than evaporation of the TFA followed by ether precipitation. The sequences and MALDI-TOF characterization data of the U¹-modified acpcPNA synthesized in this study are shown in **Table 3.8**.

Table 3.8 Sequences and characterization data of U¹-acpcPNA

Code of PNA	Sequence (N→C)	<i>m/z</i> (calcd)	<i>m/z</i> (found) ^a
TU ¹ T	Ac-TU ¹ T-Lys-NH ₂	1297.2	1296.4
T4U ¹ T4	Ac-TTTTU ¹ TTTT-LysNH ₂	3291.3	3292.6
M10U ¹	Ac-GTAGAU ¹ CACT-LysNH ₂	3670.5	3668.6
Lys2M10U ¹	Ac-Lys-GTAGAU ¹ CACT-LysNH ₂	3798.9	3800.4

^aMALDI-TOF mass spectrometry in linear positive ion mode using α -cyano-4-hydroxycinnamic acid as a matrix.

3.7 Post-synthetic modification of acpcPNA by Sonogashira reaction

This part focuses on the synthesis of acpcPNA carrying 1-ethynylpyrene-modified uracil at C5 position [5-(pyrene-1-yl)ethynyl-uracil, U^{PyE}] through post-synthetic Sonogashira reaction. The U^{PyE} monomer was reported to be one of the most distinguished base discriminating fluorescence nucleobase in DNA probes that showed the excellent discrimination ability towards SNPs detection,¹⁵⁰ and it has been utilized as a displacement probe to discriminate single base mismatch in target RNAs.¹⁵¹ The U^{PyE} DNA or RNA monomers can be synthesized as a pre-formed fluorophore-labeled monomer by joining the 5-iodouracil nucleobase with 1-ethynylpyrene using the Sonogashira cross coupling.^{139,150} However, the time-consuming synthesis of that of pre-formed monomer can be avoided by a semi-automated approach in the solid phase reported by Wagenknecht *et. al.* consisting four steps; i) oligonucleotide synthesis on the solid support (CPG); ii) insertion of 2'-deoxy-5-iodouridine; iii) removal of the synthesis column from the synthesizer for manual Sonogashira coupling on the solid support (manually); iv) resuming the automated DNA synthesis.¹⁴⁸ Both of these approaches are not suitable for the synthesis of U^{PyE}-containing acpcPNA due to the instability of the U^{PyE} monomer towards even mildly acidic conditions necessary for the cleavage of PNA from the solid support. To prevent the formation of the undesired cyclized product during PNA cleavage under acidic condition (see **section 3.9.1**), the modification by Sonogashira reaction should be performed after cleavage of the PNA from the solid support. In the next sections, the synthesis of U^{PyE}-modified acpcPNA via post-synthetic Sonogashira coupling, as well as the hybridization as well as optical properties of the U^{PyE}-modified acpcPNA with DNA will be investigated.

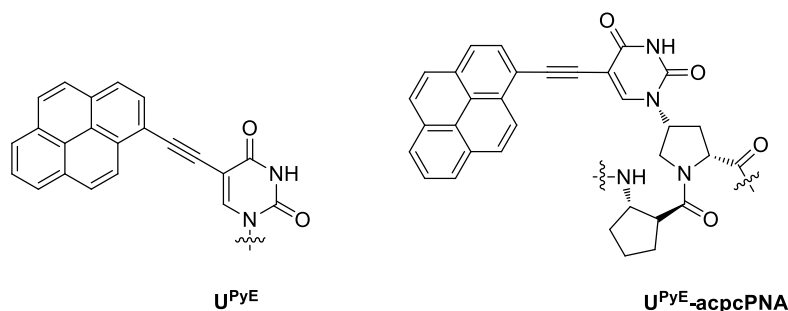


Figure 3.17 The structures of base discriminating fluorescence nucleobase, U^{PyE} in this work

3.8 Post-synthetic Sonogashira reaction of acpcPNA in the solution phase

3.8.1 Post-synthetic Sonogashira reaction of homothymine U^{PyE}-modified acpcPNA

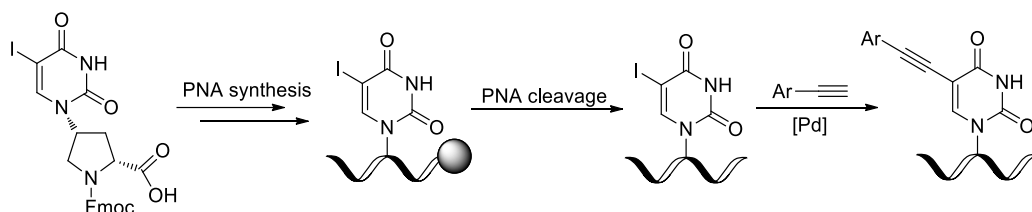


Figure 3.18 The post-synthetic approach for the introduction 5-(pyrene-1-yl)ethynyl-uracil (U^{PyE}) into acpcPNA

Initial studies were focused on the Sonogashira cross-coupling reaction between phenylacetylene or 1-ethynylpyrene and model acpcPNA with 5-iodouracil-modified homothymine sequences [TU^TT and T4U^TT4] in aqueous media. The catalyst system Pd(OAc)₂·[DMADHP]₂ consisting of a water-soluble ligand 2-(dimethylamino)-4,6-dihydropyrimidine (DMADHP) and palladium(II) acetate in potassium phosphate buffer and sodium ascorbate as a reducing agent was initially chosen according to the previously published success on the similar functionalization of protein.¹⁰⁴ The DMADHP ligand was synthesized according to the method by Wombacher *et al.*¹⁰⁴ Next, the Sonogashira reactions between the short PNA sequence TU^TT and phenylacetylene were performed in water using a pre-formed Pd(OAc)₂·[DMADHP]₂ complex in the presence of K₂HPO₄·3H₂O and sodium ascorbate as a reducing agent at 37 °C for 20 minutes (monitored by MALDI-TOF mass spectrometry). The mass spectrum showed the peak of the desired product at $m/z = 1271.4$ (m/z calcd = 1271.2, **Figure 3.19B**) therefore this condition was further used with 1-ethynylpyrene. The starting material was consumed as indicated by the decrease of the starting U^T-PNA peak height. Unfortunately, the deiodinated product TU^T (m/z found = 1171.4; calcd = 1170.3) was observed as the major product and only trace of the product peak was observed ($m/z = 1396.4$, **Figure 3.19C**).

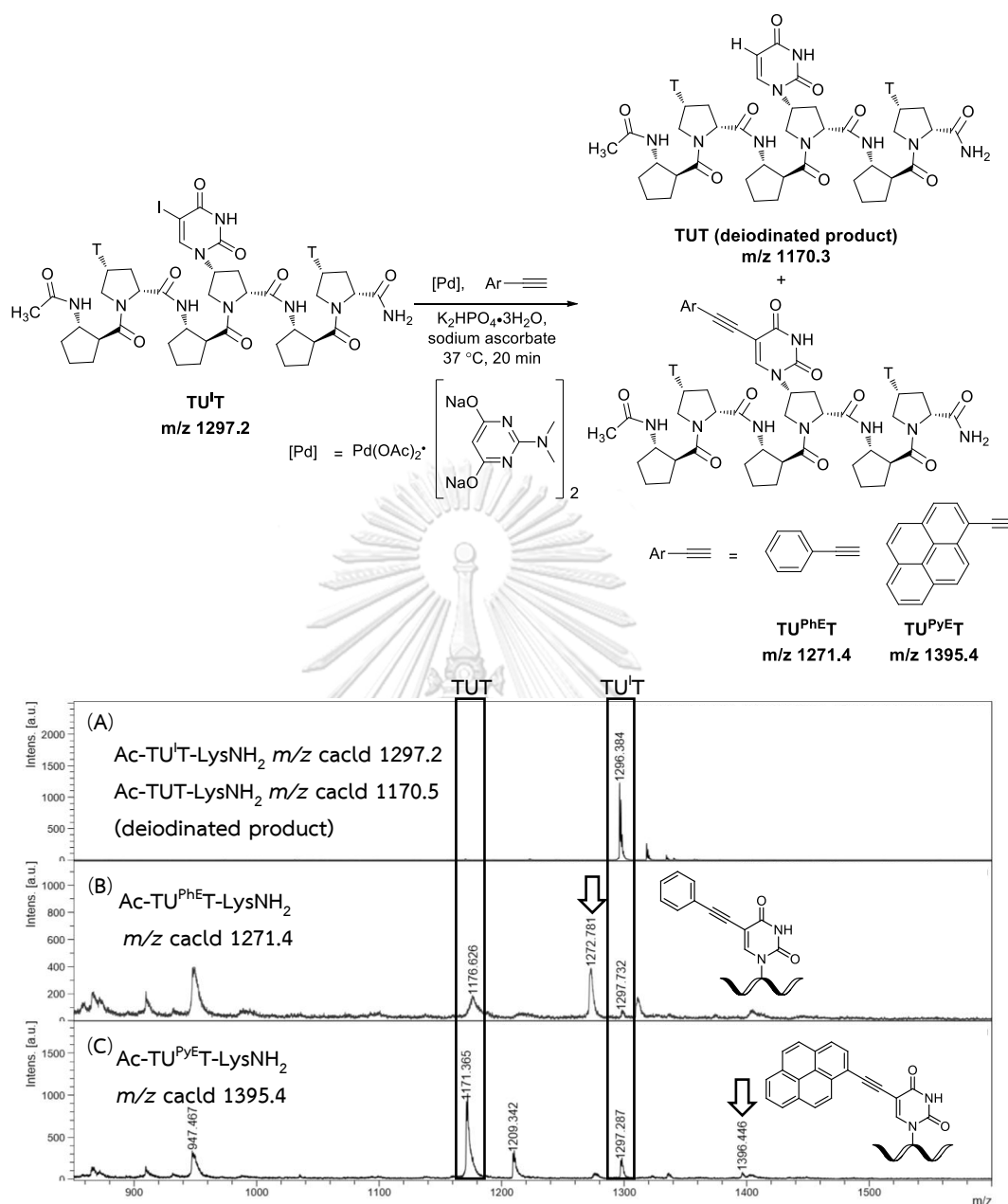
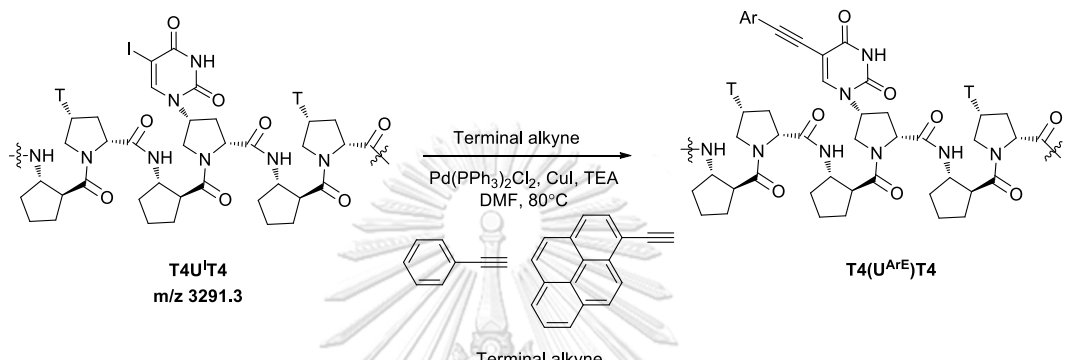


Figure 3.19 MALDI-TOF mass spectra of (A) starting material **TU^T**, (B) and (C) post-synthetic Sonogashira reaction between **TU^T** and alkyne/fluorophores proceeded in the $Pd(OAc)_2 \cdot [DMADHP]_2$ complex. Arrows indicated the mass of the product peak. (Condition: 600 equiv. alkyne/fluorophore, 4.0 equiv. $Pd(OAc)_2 \cdot [DMADHP]_2$, 700 equiv. $K_2HPO_4 \cdot 3H_2O$, 17.0 equiv., sodium ascorbate, 37 °C)

Next, the condition was changed to the standard Sonogashira cross-coupling condition employing $Pd(PPh_3)_2Cl_2$ and CuI catalytic system in organic solvent (DMF) as

in the synthesis of A^{PyE} monomer (see **section 2.3.2**). The conditions optimization for post-synthetic Sonogashira reaction using by the long PNA sequence **T4U^IT4** and either phenylacetylene or 1-ethynylpyrene as model terminal alkynes are summarized in **Table 3.9**.

Table 3.9 Optimization of post-synthetic Sonogashira reaction of acpcPNA



Entry	Scale (nmol)	Terminal alkyne (equiv.)		Condition ^a		
		Phenylacetylene	1-ethynylpyrene	Pd(PPh ₃) ₂ Cl ₂ (equiv.)	CuI (equiv.)	Et ₃ N (equiv.)
1	10	1.5	-	0.2	0.1	3.0
2	10	100	-	2.5	3.0	16.3
3	10	500	-	2.5	3.0	16.3
4	10	-	500	2.5	3.0	16.3
5	50	-	500	2.5	3.0	16.3
6	250	-	500	2.5	3.0	16.3

^aThe reaction progress was monitored by MALDI-TOF mass spectrometry.

Firstly, the standard condition used for the synthesis of A^{PyE} monomer was employed but the reaction did not proceed as shown by the presence of unchanged starting material after the reaction was performed at 80 °C for 2 hours (**Figure 3.20B**). Thus, more equivalents of all reagents were added to push the reaction forward, which provided the expected product after heating at 80 °C for 2 hours as indicated by a mass peak at $m/z = 3266.7$. However, the remaining starting material along with the deiodinated product **T4UT4** were still observed (entry 2, **Table 3.9**, **Figure 3.20C**).

Next, the amount of phenylacetylene was increased to 500 equiv., whereby the starting material was completely consumed without the contamination of the deiodinated product (entry 3, **Table 3.9**, **Figure 3.20D**).

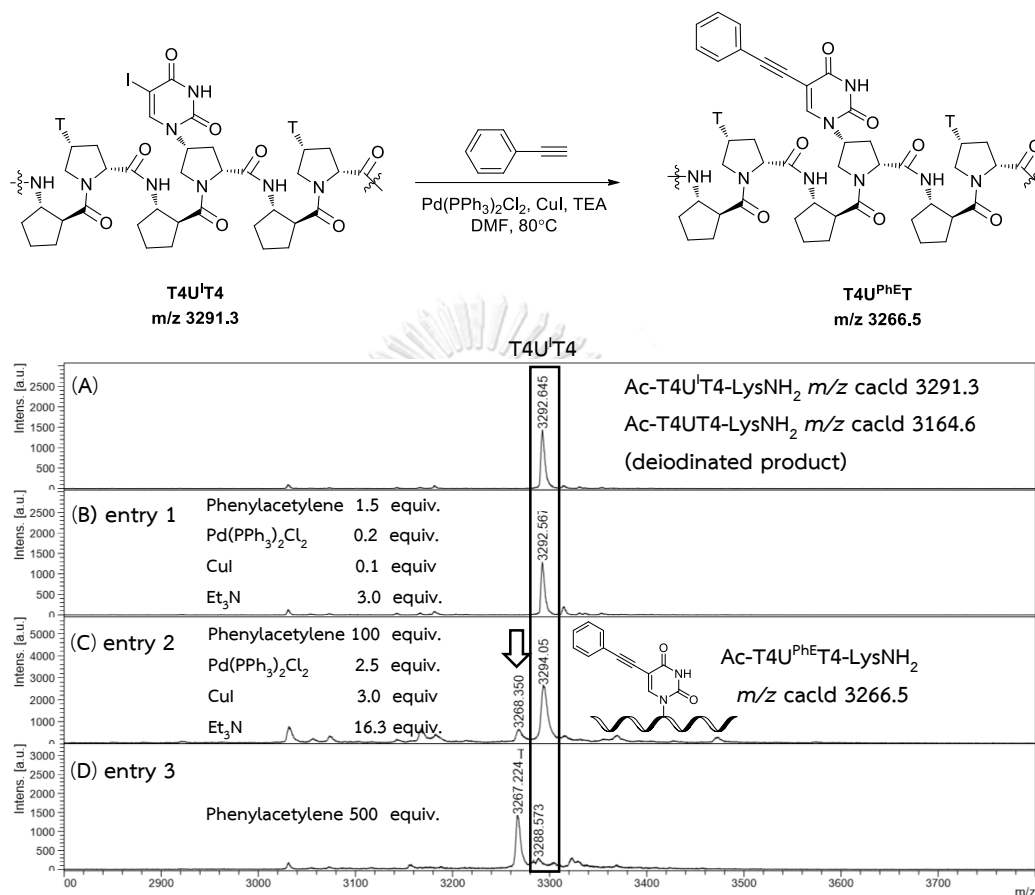


Figure 3.20 MALDI-TOF mass spectra of (A) starting material **T4U^IT4** and (B)-(D) post-synthetic Sonogashira reaction performed under the catalytic system of $\text{Pd}(\text{PPh}_3)_2\text{Cl}_2$, CuI and triethylamine. The product peak was indicated by an arrow. The entry number referred to the entry number in **Table 3.9**.

Thus, this optimal condition was applied to the reaction between **T4U^IT4** and 1-ethynylpyrene at 10 nmol scale, and the expected product, **T4U^{PYE}T4** (m/z calcd = 3389.7) was successfully formed (entry 4, **Table 3.9**, **Figure 3.21B**). After that, the scale of the reaction was increased to 50 nmol and 250 nmol of starting material in order to produce sufficient quantities of the modified acpcPNA for investigation in hybridization and optical properties. The scale-up reactions were also efficient as monitored by MALDI-TOF mass spectrometry (**Figure 3.21C** and **3.21D**).

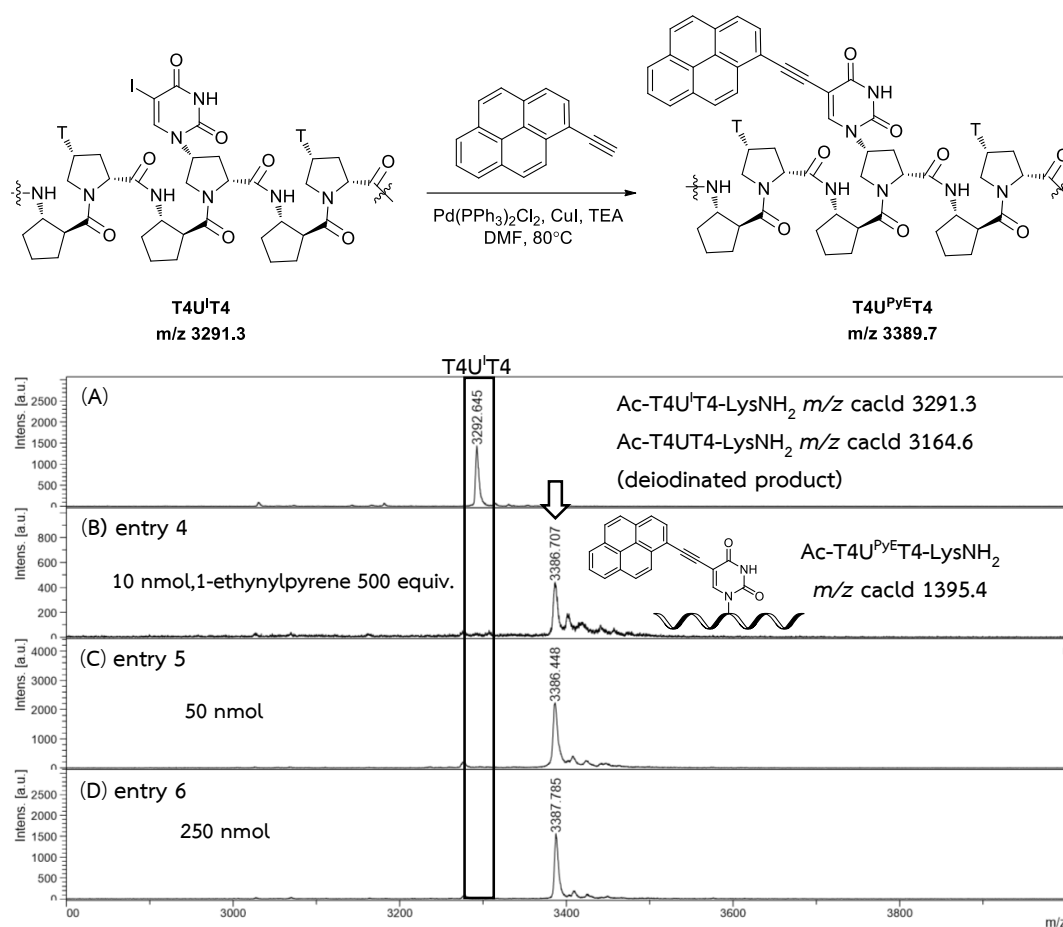


Figure 3.21 MALDI-TOF mass spectra of (A) starting material T4U^TT4, (B) post-synthetic Sonogashira reaction between T4U^TT4 and 1-ethynylpyrene and (C)-(D) the scale-up reactions between T4U^TT4 and 1-ethynylpyrene performed under the catalytic system of Pd(PPh₃)₂Cl₂, CuI and triethylamine. The entry number referred to the entry number in Table 3.9.

The mechanism of Sonogashira cross coupling reaction is depicted in Figure 3.22. The reaction started with an inactive palladium(II) catalyst that was activated by reduction with copper(I) iodide to form a palladium(0) complex. Then, the active palladium(0) complex reacted with 5-iodouracil at C5-halogen bond via oxidative addition resulting in the Ar-(PPh₃)₂Pd(II)-I complex **B**. This complex reacted with copper acetylide that produced from the copper catalytic cycle afforded intermediate **C**. Finally, the final product **D** was produced via reductive elimination as well as the palladium(0) catalyst regeneration.¹⁵² The deiodinated product was probably

originated from the same Pd-containing intermediate for the desired Sonogashira reaction obtained by oxidative insertion reaction of the Pd into the C-I bond. However, instead of reacting further with the rather bulky 1-ethynylpyrene it underwent a protodepalladation reaction to form the deiodinated substrate instead of the desired cross-coupling product.

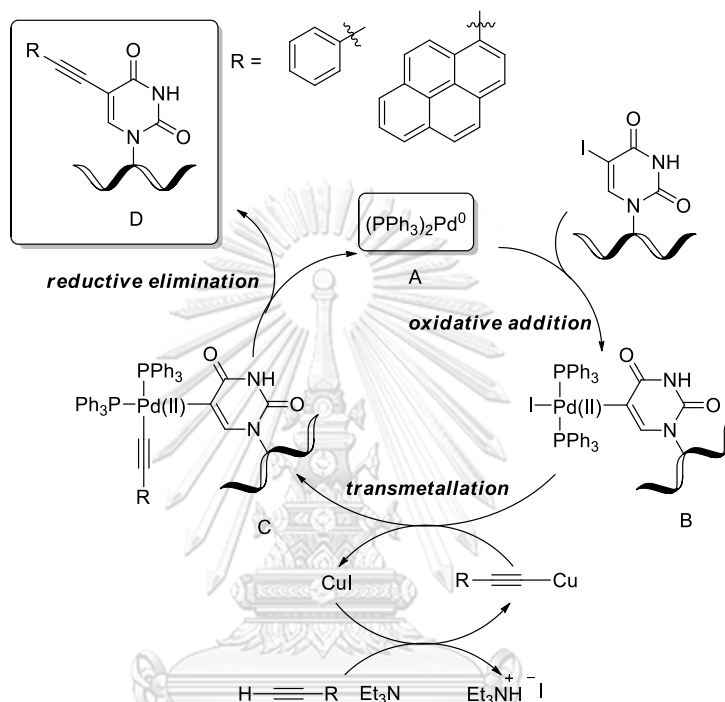


Figure 3.22 The mechanism of Sonogashira cross coupling reaction between T4U^IT4 and 1-ethynylpyrene

3.8.2 Post-synthetic Sonogashira reaction of mix-base U^{PyE}-modified acpcPNA

Additionally, the post-synthetic Sonogashira reaction of the mix-base sequence PNA M10U^I with 1-ethynylpyrene was also performed. Before PNA cleavage from the solid support, the benzoyl protecting group on the nucleobases side chain were removed by treatment with 1:1 aqueous ammonia/dioxane at 65 °C overnight. The M10U^I was directly used for the post-synthetic Sonogashira reaction after cleavage from the resin without purification. The reaction was also successful as shown by a complete reaction after 4 hours at 80 °C under same conditions (Figure 3.23). Unfortunately, purification of the M10U^{PyE} by reversed phase HPLC was not successful

because of the poor solubility of $M10U^{PyE}$ in aqueous acetonitrile. Thus, the hybridization properties of $M10U^{PyE}$ cannot be determined.

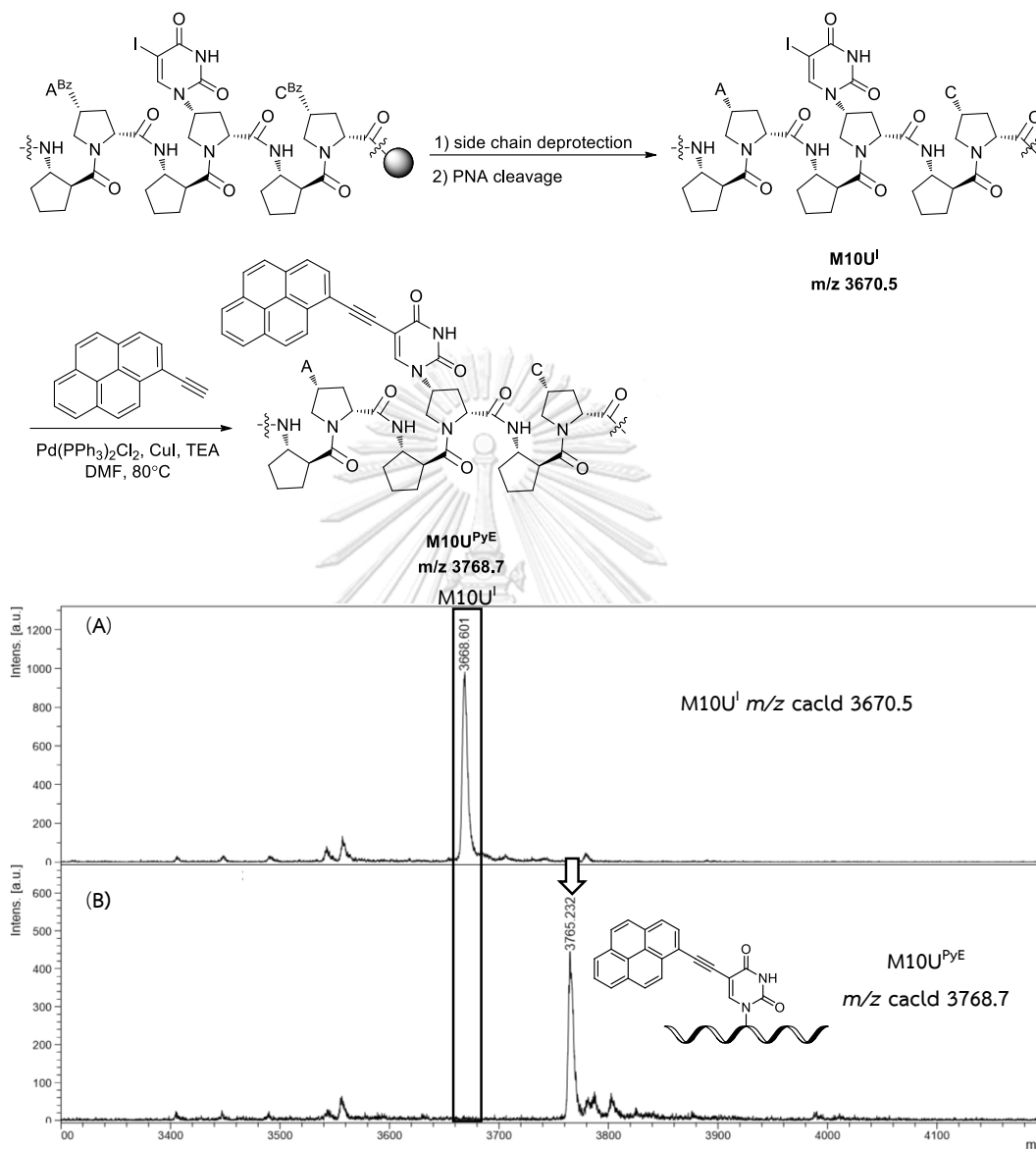


Figure 3.23 MALDI-TOF mass spectra of (A) starting material $M10U^I$ and (B) post-synthetic Sonogashira reaction between $M10U^I$ and 1-ethynylpyrene. (Condition: 500 equiv. 1-ethynylpyrene, 2.5 equiv. $Pd(PPh_3)_2Cl_2$, 3.0 equiv., 16.3 equiv. triethylamine in DMF, 80 °C, 4 hours)

3.9 Post-synthetic Sonogashira reaction on the solid phase

3.9.1 Attempted synthesis of 5-(pyrene-1-yl)ethynyl-uracil acpcPNA in solid phase via Rink amide (RAM) linker

Due to the inconvenience in solution phase synthesis in terms of removing the excess reagents from the reaction and requirement of the clean-up step using C18-cartridge column to eliminate the inorganic salt before HPLC purification, the solid phase synthesis was investigated in order to solve those problems. The 5-iodouracil acpcPNA attached on the acid labile Rink amide (RAM) linker was reacted with 1-ethynylpyrene under the same condition as in the solution phase synthesis, which showed a complete reaction as monitored by MALDI-TOF mass spectrometry (**Figure 3.24**). After the starting iodinated acpcPNA was completely consumed, the modified PNA was treated with trifluoroacetic acid in the presence of 10% triisopropylsilane (TIPS) to scavenge the undesired electrophilic carbocations that might react with the electron-rich pyrene. The modified-acpcPNA was then purified and characterized by reversed phase HPLC and MALDI-TOF mass spectrometry. However, although a product with the expected mass was obtained, subsequent thermal and spectroscopic studies (see **section 3.11** and **3.12**) revealed that it was not the desired 5-(pyrene-1-yl)ethynyl-uracil acpcPNA, but the cyclization product pyrene-substituted furanouracil (fU^{Py}) acpcPNA was obtained instead.

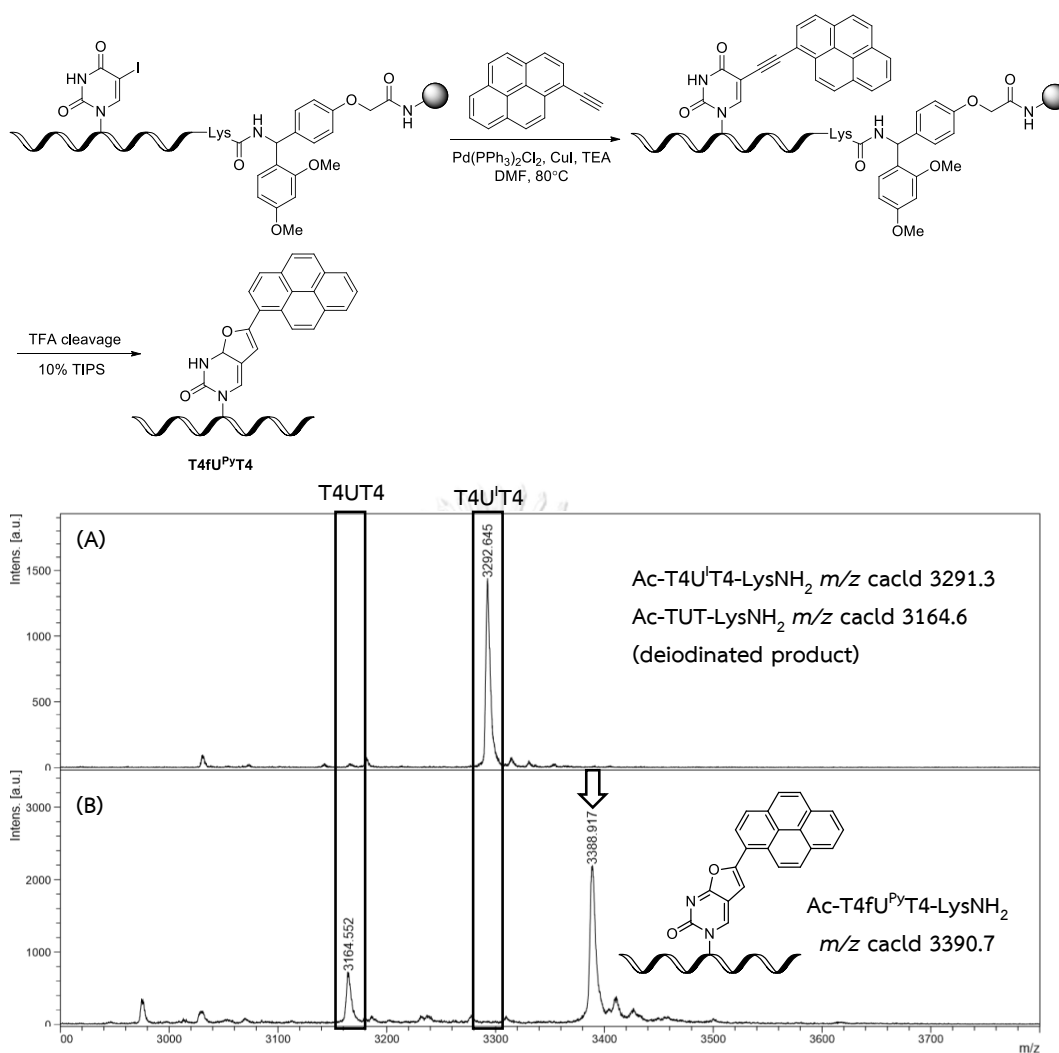


Figure 3.24 MALDI-TOF mass spectra of (A) starting material and (B) post-synthetic Sonogashira reaction between T4U^TT4 and 1-ethynylpyrene using solid phase synthesis. (Condition: 500 equiv. 1-ethynylpyrene, 2.5 equiv. Pd(PPh₃)₂Cl₂, 3.0 equiv., 16.3 equiv. triethylamine in DMF, 80 °C, 6 hours)

The formation of the pyrenyl-furanopyrimidine (abbreviated as fU^{Py}) was explained by the intramolecular cyclization of 5-(pyrene-1-yl)ethynyl-uracil during the cleavage of the under acidic condition. Similar reactions have been reported in DNA oligonucleotides for the cyclization of 5-alkynyluracil to furanopyrimidine catalyzed by AgNO₃ via the *5-endo-dig* cyclization whereby the carbon-carbon triple bond was attacked by the O⁴ oxygen atom of the uracil moiety as illustrated in **Figure 3.25**.¹⁵³

The acid probably activated the triple bond by protonation to form a vinyl carbocation intermediate that underwent a rapid cyclization.¹⁵⁴

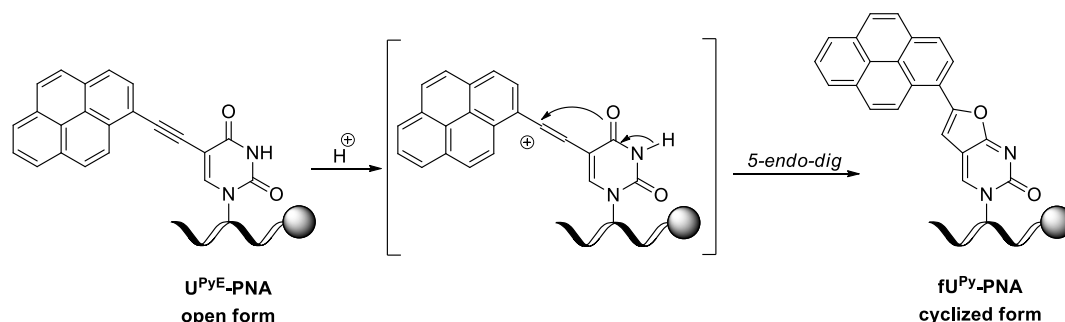


Figure 3.25 The possible mechanism of cyclization through 5-*endo-dig* annulation of 5-(pyrene-1-yl)ethynyl-uracil under acidic condition based on Agrofoglio's hypothesis

3.9.2 Attempted synthesis of 5-(pyrene-1-yl)ethynyl-uracil acpcPNA in solid phase via hydroxymethylbenzoyl (HMBA) linker

Due to the undesired cyclization product under acidic condition as described in the last section, the nucleophile-labile hydroxymethylbenzoyl (HMBA) linker¹⁵⁵ was utilized as solid support instead of the usual Rink amide linker. This linker can be easily cleaved through nucleophilic substitution reaction at the carbonyl group. In this experiment, two lysine residues were included at both N- and C-termini of 5-iodouracil acpcPNA (**Lys2M10U**) to improve aqueous solubility of the modified acpcPNA using Fmoc-Lys(Mtt)-OH. The Mtt protecting group was removed under mild acidic condition without cleavage of the PNA from the solid support. The Sonogashira cross coupling reaction was next performed with the PNA attached on-resin that still carried the nucleobase protecting groups. The reaction was allowed to proceed under the same condition as described above for 8 hours. Cleavage of the PNA from the solid support was achieved by treatment with aqueous NH_3 /dioxane at 65 °C overnight. Unfortunately, even though the peak corresponded to the product was obtained, the reaction was quite messy, and a number of side products were observed (**Figure 3.26**). As a result, this approach has not been pursued further.

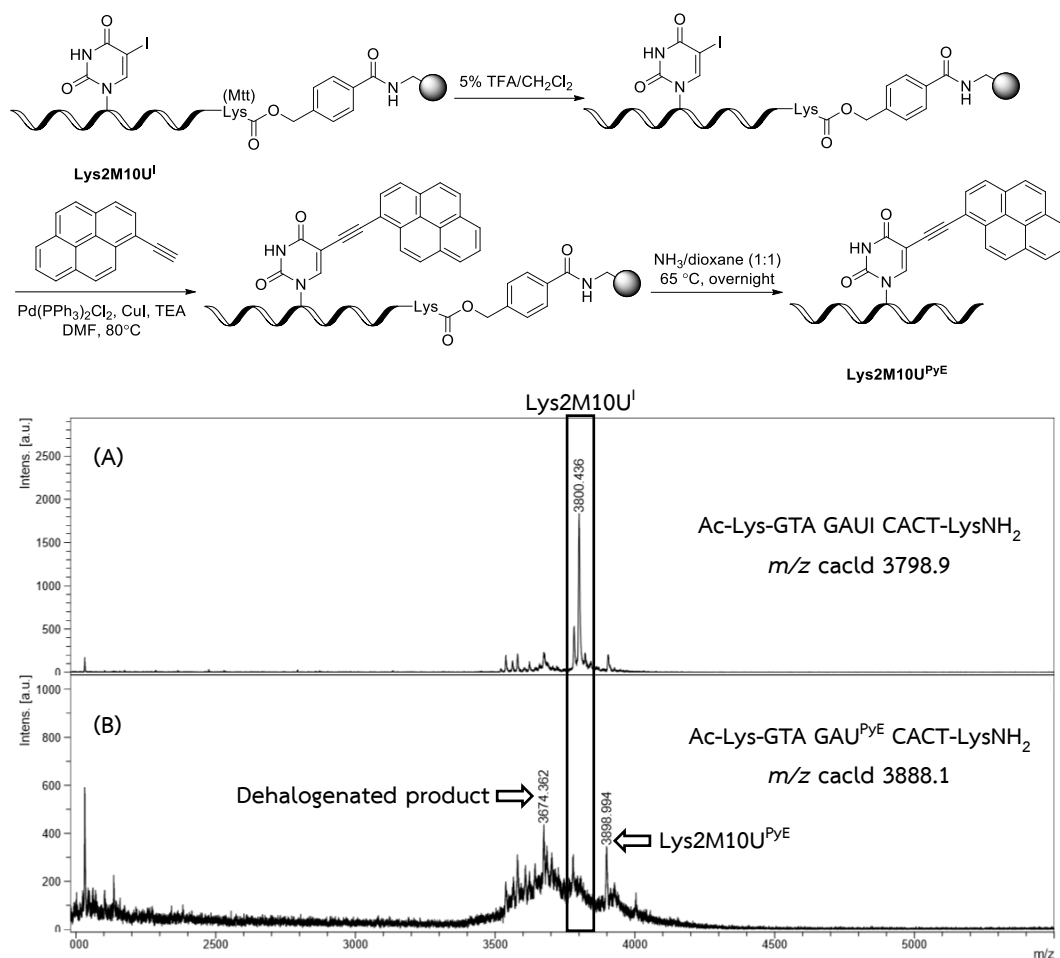


Figure 3.26 MALDI-TOF mass spectra of post-synthetic Sonogashira cross coupling reaction between **Lys2M10U^I** and 1-ethynylpyrene performing through HMBA linker

3.10 Purification and characterization of pyrene-modified acpcPNA derived from post-synthetic modification

The crude U^{PyE}-modified acpcPNA obtained from the post-synthetic modification reaction was cleaned-up by passing through a C18 cartridge followed by washing with 10% aqueous acetonitrile. After that, the collected fractions were combined and freeze-dry to give the crude PNA and re-dissolved to purify by reverse phase HPLC eluting with a gradient system of 0.1 M TEAA buffer pH 7.0 and acetonitrile. Fractions containing the pure PNA examined by MALDI-TOF MS were combined and lyophilized then –the pure PNA was re-dissolved in 120 μL of DMSO. For **T4(fU^{Py})T4** obtained from the post-synthetic Sonogashira reaction on the solid phase via Rink

amide (RAM) linker was cleaved from the solid support after completing the reaction using TFA containing 10% triisopropylsilane. Then, the crude PNA was purified by reverse phase HPLC eluting with a gradient system of 0.1 M TEAA buffer pH 7.0 and acetonitrile which therefore combined the collected fractions and lyophilized. The concentration of the modified-acpcPNAs were determined by UV/Vis spectrophotometry and characterized by MALDI-TOF mass spectrometry. The characterization data and isolated yields of all pyrene-modified acpcPNA probes derived from post-synthetic Sonogashira cross-coupling are summarized in **Table 3.10**.

Table 3.10 Sequences and characterization data of pyrene-modified acpcPNA probes obtained from post-synthetic Sonogashira reaction.

Code of PNA	Sequence (N→C)	t _R (min) ^a	Yield (%) ^b	m/z (calcd)	m/z (found) ^c
T4U ^{PyE} T4	Ac-TTTTU ^{PyE} TTTT-LysNH ₂	25.8	14.4	3389.7	3384.5
T4fU ^{Py} T4	Ac-TTTTfU ^{Py} TTTT-LysNH ₂	26.7	10.3	3390.7	3388.9

^aSee HPLC conditions in experimental section. ^bIsolated yield after HPLC. ^cMALDI-TOF mass spectrometry in linear positive ion mode using α -cyano-4-hydroxycinnamic acid as a matrix.

3.11 Thermal stability of DNA hybrids of pyrene-modified acpcPNA

UV melting experiments of the hybrids between the pyrene-modified acpcPNA probes and DNA targets were performed to investigate the hybridization properties in terms of thermal stability and sequence specificity with its DNA targets. The thermal stability data are shown in **Table 3.11**.

Table 3.11 Thermal stability data of pyrene-modified acpcPNA and their DNA hybrids. (Condition: 1.0 μM PNA, 1.2 μM DNA, 10 mM phosphate buffer pH 7.0).

Entry	PNA	DNA	DNA sequence ^a (5'→3')	T_m (°C)	ΔT_m (°C)	Notes
1		dA9	AAAA <u>A</u> AAAA	65.1	–	ds, complementary
2	T4U^{PyE}T4	dA8T	AAAATAAAA	35.1	–30.0	ds, mismatched T
3		dA8G	AAAAGAAAA	<20.0	>45.1	ds, mismatched G
4		dA8C	AAAACAAAA	40.5	–24.6	ds, mismatched C
5		dA9	AAAA <u>A</u> AAAA	<20.0	>24.6	ds, complementary
6	T4fUPyT4	dA8T	AAAATAAAA	<20.0	>24.6	ds, mismatched T
7		dA8G	AAAAGAAAA	44.6	–	ds, mismatched G
8		dA8C	AAAACAAAA	<20.0	>24.6	ds, mismatched C

^aMismatched bases in the DNA sequence are indicated as bold font. Complementary bases in DNA sequence are indicated by underlying.

As expected, the complementary PNA·DNA duplex **T4U^{PyE}T4·dA9** displayed the strongest binding affinity as shown by the highest melting temperature at 65.1 °C. This T_m value is relatively low in comparison with the unmodified T9 acpcPNA with **dA9**, which showed a T_m value of 82.0 °C,¹⁰⁸ which indicated the negative effect of the steric bulk of the pyrene to the stability of the duplex. The mismatched hybrid with **T4(U^{PyE})T4** showed either much lower melting temperature values compared to the complementary hybrid (**T4U^{PyE}T4·dA8T** = 35.1 and **T4U^{PyE}T4·dA8C** = 40.5 °C) or no sigmoidal transition at all in the case of **T4U^{PyE}T4·dA8T** duplex. The significant decrease in thermal stability of mismatched PNA·DNA hybrids by 45.1 to 24.6 °C when compared to the complementary hybrid clearly indicated the specific base pairing between U^{PyE} in acpcPNA and dA in the DNA strand.

On the other hand, no sigmoidal transition was observed at all in the cases of hybrids between **T4fU^{Py}T4** and **dA9**, **dA8T** and **dA8C**, indicating the absence of base pairing between fU^{Py} in acpcPNA and dA, dT or dT in DNA. Only in the case of **T4U^{PyE}T4·dA8G** that a weak sigmoidal transition was observed with a T_m value of 44.6 °C. It became evidence according to the T_m data and base recognition pattern that

the two "U^{PyE}"-modified acpcPNA sequences obtained from the post-synthetic Sonogashira reaction in solution and solid phase are different. The specific base pairing to **dA8G** rather than **dA8T** and **dA8C** confirmed that the furanouracil acpcPNA **T4fU^{Py}T4** was formed instead of the expected **T4U^{PyE}T4** under the solid phase synthesis condition. The formation of the furanouracil was explained by the acid-induced cyclization (section 3.9.1) This cyclized uracil could only form a stable base pairing with guanine but not adenine as depicted in **Figure 3.27**.¹⁵⁶

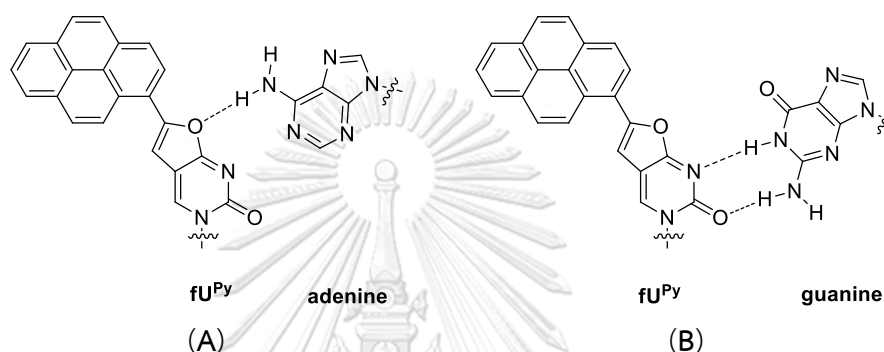


Figure 3.27 Hydrogen bonds formation of **(A)** fU^{Py}·dA and **(B)** fU^{Py}·dG¹⁵⁶

Based on the T_m results, it can be concluded that the U^{PyE}-labeled acpcPNA can distinguish dA from other bases in the DNA targets and could be useful as a fluorescence DNA probe. Additionally, the cyclized furanouracil acpcPNA (fU^{Py}-acpcPNA) can be produced when the U^{PyE}-modified acpcPNA was subjected to acidic conditions. This fU^{Py}-labeled acpcPNA can distinguish dG from other bases in the DNA targets and could also be useful as another fluorescence DNA probe, which will be experimentally confirmed in the next section.

3.12 Optical properties of pyrene-modified acpcPNA probes

The optical properties of the pyrene-modified acpcPNA derivatives in the absence and presence of various DNA targets are summarized in **Table 3.12**.

Table 3.12 Optical properties of pyrene-modified acpcPNA probes and their DNA hybrids (Condition: 1.0 μM PNA, 1.2 μM DNA, 10 mM phosphate buffer pH 7.0, λ_{ex} 385 nm).

Entry	PNA	DNA	F/F_0^a	$\lambda_{\text{abs}}/\lambda_{\text{em}}$ (nm)	Φ_F^b	Notes
1		-	-	374/433	0.069	ss
2		dA9	5.16	396/456	0.253	ds, complementary
3	T4U ^{PyE} T4	dA8T	2.31	398/455	0.116	ds, mismatched T
4		dA8G	1.44	397/450	0.081	ds, mismatched G
5		dA8C	2.11	397/450	0.127	ds, mismatched C
6		-	-	392/480	0.181	ss
7		dA9	0.87	396/482	0.204	ds, complementary
8	T4fU ^{PyE} T4	dA8T	0.86	395/483	0.186	ds, mismatched T
9		dA8G	1.07	397/489	0.230	ds, mismatched G
10		dA8C	0.89	392/481	0.194	ds, mismatched C

^aT4U^{PyE}T4, $\lambda_{\text{em}} = 447$ nm, T4fU^{PyE}T4, $\lambda_{\text{em}} = 489$ nm. ^bQuantum yields were measured by using quinine sulfate as a standard ($\Phi_F = 0.546$).

The ability of U^{PyE} as base discriminating fluoresce nucleobase upon binding with various DNA targets were studied. The absorption spectra of single-stranded PNA displayed characteristic major absorption maxima at 374 and 395 nm of pyrene, which is consistent with previous reports on U^{PyE}-modified DNA probes.^{148,150} In the complementary DNA hybrid T4U^{PyE}T4•dA9, a strong hyperchromism was observed at 396 nm. The same hyperchromism was also observed in the mismatched DNA hybrids (T4U^{PyE}T4•dA8T, T4U^{PyE}T4•dA8G and T4U^{PyE}T4•dA8C). The absorption maxima of single-mismatched hybrids were only slightly red-shifted by 1-2 nm relative to the complementary hybrid. This is different from previous work on U^{PyE}-DNA probes that showed a more significant red-shifting by 5 nm from complementary duplex (Figure 3.28B).¹⁵⁰ CD spectra was used to investigate the conformation of pyrene upon duplex formation. CD spectra confirmed the formation of a hybrid between T4U^{PyE}T4 and its complementary DNA, but not single mismatched DNA (Figure 3.28C and 3.28D). No

CD signals were observed in the pyrene absorption region for both complementary and single mismatched hybrids of **T4U^{PyE}T4**. This is different from the CD spectra of U^{PyE}-modified DNA reported by Kim and co-workers, whereby the CD spectra clearly exhibited a small negative band at 398 nm in the complementary DNA hybrid. A slightly red-shifted CD band was observed at 402 nm for single base mismatched hybrid, which was explained by the interaction of pyrene with adjacent nucleobases in the duplex.¹⁵⁰

The fluorescence intensity and fluorescence quantum yield of the pyrene-modified uracil acpcPNAs and their corresponding DNA hybrids are summarized in **Table 3.12**. Upon exciting at 385 nm, the single-stranded **T4U^{PyE}T4** showed a weak fluorescence emission, which translated into a low fluorescence quantum yield ($\Phi_F = 0.069$) with the emission maxima at 433 nm. In the presence of complementary DNA, the fluorescence was increased by 5.16 folds relative to single-stranded PNA and the fluorescence quantum yield was also increased from 0.069 to 0.253. In addition, the emission wavelength red-shifted for 433 to 456 nm, which is in good agreement with another study with U^{PyE}-modified DNA by Berlin *et al.*,¹⁵⁷ who explained the strong bathochromic shift phenomena upon hybridization as resulting from the exciplex formation of pyrene with nucleobases. Similar phenomenon may occur in U^{PyE}-modified acpcPNA duplexes, whereby the pyrene might involve in the stacking with the neighboring nucleobases.¹⁵⁷ In the presence of single-mismatch DNA, the fluorescence intensity was much smaller when compared with perfect matched hybrid. The fluorescence emission ratio (F/F_0) of the remaining mismatch DNA (**dA8T**, **dA8G** and **dA8C**) were 2.31, 1.44 and 2.11, respectively (**Figure 3.28A**). The results suggest that the U^{PyE} base in modified acpcPNA can differentiate adenine from other non-complementary nucleobases not only by T_m but also by fluorescence enhancement.

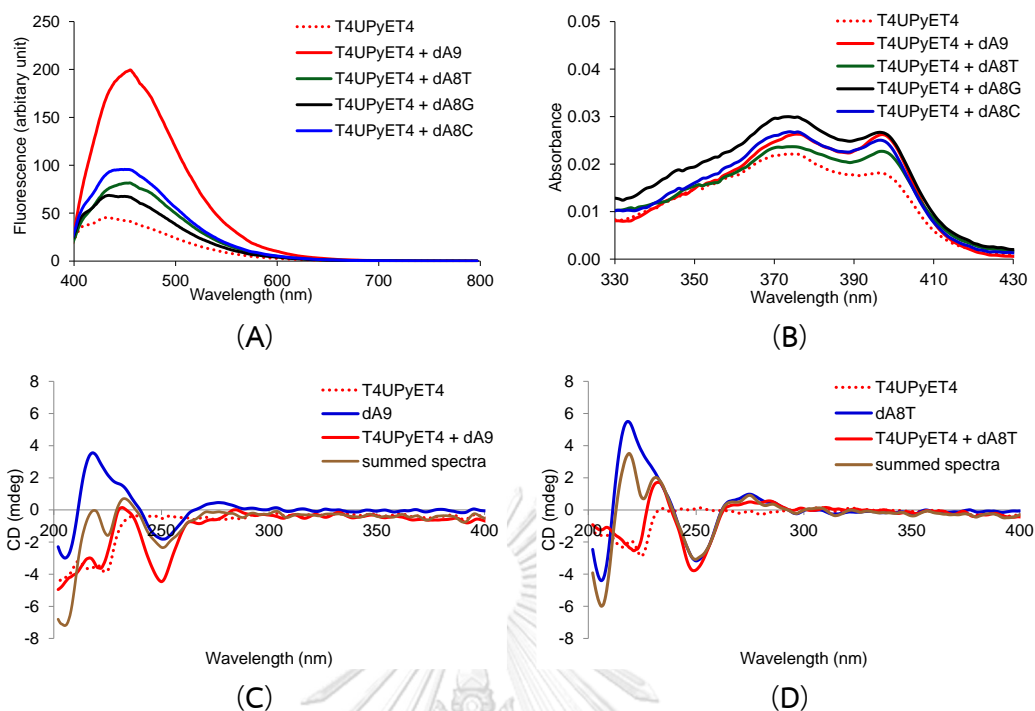


Figure 3.28 (A) Fluorescence, (B) UV-vis and (C)–(D) CD spectra of $T4UPyET4$ and its DNA hybrids. Conditions: $1.0 \mu\text{M}$ PNA, $1.2 \mu\text{M}$ DNA, 10 mM sodium phosphate buffer $\text{pH } 7.0$, $\lambda_{\text{ex}} 385 \text{ nm}$

Next, the optical properties of the cyclized version of U^{PyE} , namely pyrenyl-furanouracil [$T4fU^{PyE}T4$] were investigated. The absorption spectra of single-stranded $T4fU^{PyE}T4$ PNA displayed a single broadened and more red-shifted band ($\lambda_{\text{max}} = 394 \text{ nm}$) relative to $T4UPyET4$. This spectrum is distinctively different from $T4UPyET4$, in which no shoulder was observed indicating different structures of the two pyrene-modified acpcPNAs. In the presence of complementary (**dA9**) and mismatched (**dA8G**, **dA8T**, **dA8C**) DNA, the UV absorption maxima were further red-shifted (**Figure 3.29B**). CD spectra of $T4fU^{PyE}T4$ with **dA9** and **dA8T** confirmed that the duplex was not formed.

The fluorescence properties of $T4fU^{PyE}T4$ in the absence and presence of DNA was studied next. The maximum emission of the single stranded probe appeared at 480 nm with a moderate fluorescence quantum yield ($\Phi_F = 0.181$, **Table 3.12**). This value was higher than that of $T4UPyET4$. In all DNA hybrids, only small change in fluorescence intensity was observed. The fluorescence intensity change in the

mismatched hybrids was slightly decreased to 0.87, 0.86, and 0.89 folds relative to single-stranded **T4fU^{Py}T4** for **dA9**, **dA8T** and **dA8C**, respectively. Interestingly, the fluorescence was slightly enhanced by 1.07 folds in the "complementary" with **dA8G**. This is accompanied by a pronounced red-shifting of the emission maxima by 9 nm relative to the single-stranded PNA (**Figure 3.29A**). The thermal stability and fluorescence results suggested that the pyrenyl furanouracil (fU^{Py}) in acpcPNA can distinguish dG from other nucleobases in DNA, although the change is rather small when compared to U^{PyE}.

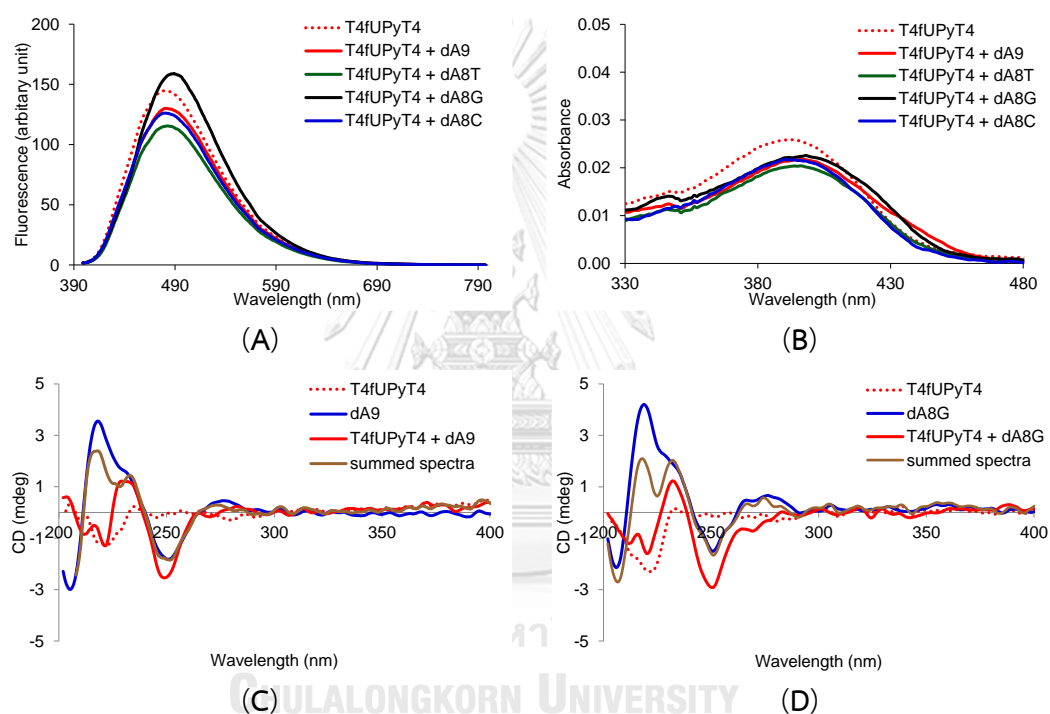


Figure 3.29 (A) Fluorescence, (B) UV-vis and (C)–(D) CD spectra of **T4fU^{Py}T4** and its DNA hybrids. Conditions: 1.0 μM PNA, 1.2 μM DNA, 10 mM sodium phosphate buffer pH 7.0, λ_{ex} 385 nm

3.13 Post-synthetic modification of acpcPNA by Suzuki-Miyaura reaction in solution phase

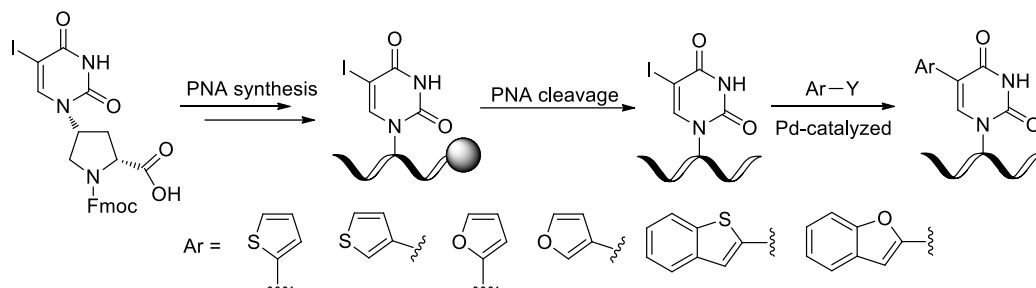


Figure 3.30 A method to incorporate C5-heteroaromatic substituent into iodouracil-containing acpcPNA

This section involves the development and application of post-synthetic Suzuki-Miyaura reaction approach for the synthesis of fluorescence acpcPNA probes bearing a uracil base modified at the C5 position by a heteroaromatic ring such as thiophene, furan and their benzo-annulated derivatives. This was inspired by a pioneering report by Manderville *et. al.* on the modification of 8-bromoguanine-containing oligonucleotides including dimer, trimer, decamer and 15mer under the catalysis of $\text{Pd}(\text{OAc})_2$ and tris(3-sulfonatophenyl)phosphane trisodium salt (TPPTS) in the aqueous acetonitrile system to obtain the fluorescently-labeled benzothiophene and phenyl analogues DNA probes in good yield.¹⁰¹ In another work, a simple one-step synthesis of the photoswitchable oligonucleotides have been reported by a highly specific reaction of the 5-iodouracil modified-oligonucleotide (15 mer and 19 mer) with several boronic acids using $\text{Pd}(\text{OAc})_2$ and TPPTS catalytic system to afford the photoswitch anchored DNA in moderate yield.¹⁵⁸ In a related study, a DNA modification under mild conditions by using the combination of $\text{Pd}(\text{OAc})_2$ /2-aminopyrimidine-4,6-diol in aqueous buffer condition that exhibited broad functional group tolerance as reported by Davis and coworkers. Under this condition, it was reported that the dehalogenation by-product was not detected.¹⁰² Thus, these methods were applied for functionalization of acpcPNA carrying 5-iodouracil with several heteroaromatic compounds to generate fluorescence probes that will be further studied for DNA binding affinity and optical properties (**Figure 3.31**).

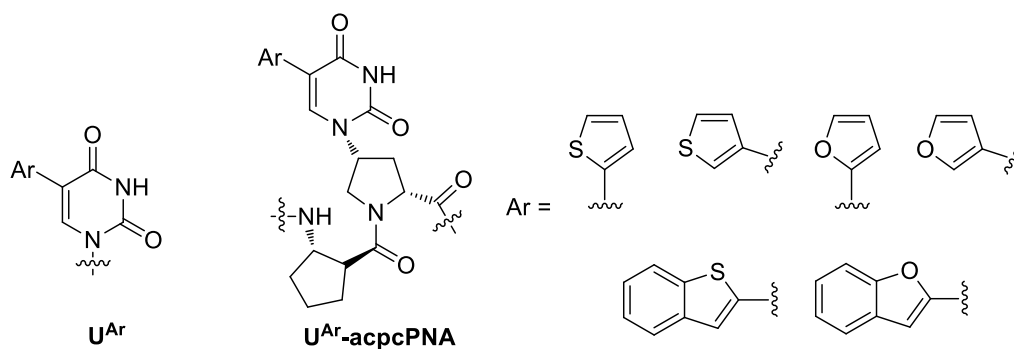
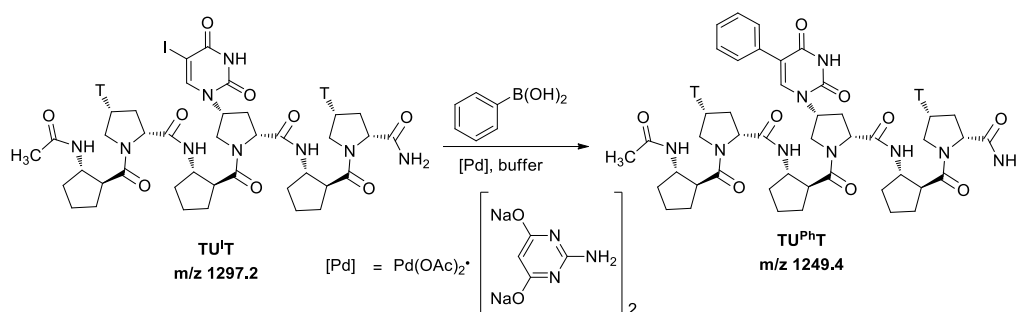
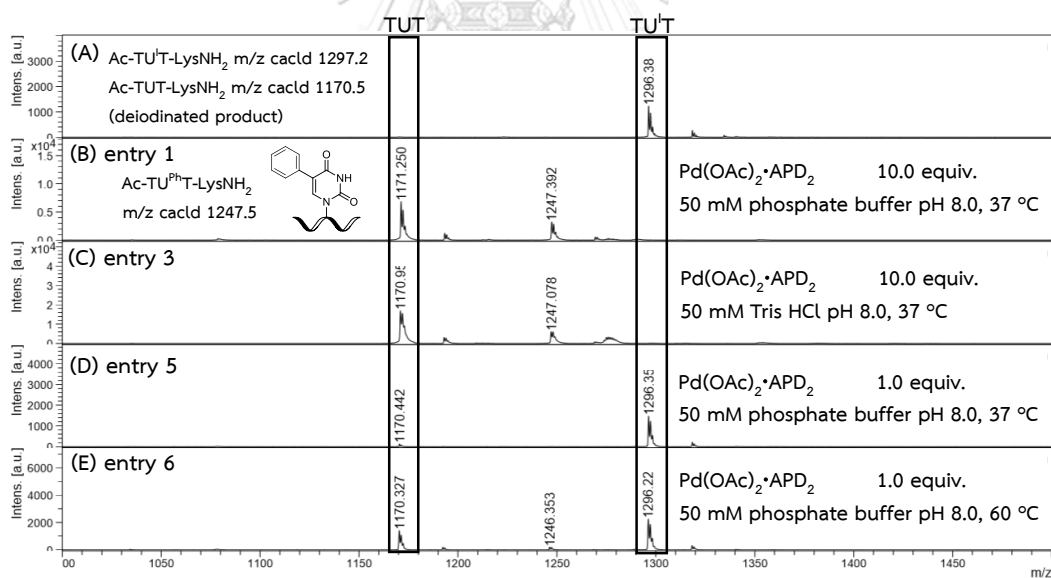


Figure 3.31 The structures of C5-modified uracil-acpcPNA bearing heteroaromatic substituents proposed in this work

Firstly, a model 3 mer 5-iodouracil (U^I)-modified acpcPNA $TU^I T$ ($m/z = 1297.2$) was employed as a substrate together with phenylboronic acid employing the catalyst system consisting of $Pd(OAc)_2$ and 2-aminopyrimidine-4,6-diolate (APD) using a condition similar to a previous report on post-synthetic Suzuki-Miyaura reaction on DNA.¹⁰² The conditions for post-synthetic Suzuki-Miyaura reaction of acpcPNA with phenylboronic acid were tested under different buffer systems as well as a range of pH values as shown in **Table 3.13**. The success of the reaction was monitored by MALDI-TOF mass analysis (**Figure 3.32**).

Table 3.13 Optimization of post-synthetic Suzuki-Miyaura reaction of acpcPNA

Entry	PhB(OH) ₂ (equiv.)	[Pd] (equiv.)	Temp (°C)	Time (hr)	Condition
1	100	10.0	37	5	50 mM phosphate buffer pH 8.0
2	100	10.0	37	5	50 mM Tris acetate EDTA buffer pH 8.0
3	100	10.0	37	5	50 mM Tris HCl pH 8.0
4	100	10.0	37	5	50 mM Tris HCl pH 8.5
5	100	1.0	37	5	50 mM phosphate buffer pH 8.0
6	100	1.0	60	5	50 mM phosphate buffer pH 8.0

**Figure 3.32** MALDI-TOF mass spectra of (A) starting material $\text{TU}^{\text{U}}\text{T}$ and (B)-(E) post-synthetic Suzuki-Miyaura coupling of $\text{TU}^{\text{U}}\text{T}$ with phenylboronic acid under buffer conditions. The entry number referred to the entry number in **Table 3.13**.

According to the MALDI-TOF mass spectra, all conditions were not effective for the Suzuki-Miyaura reaction between U¹-acpcPNA and phenylboronic acid. In all cases,

the starting material was consumed, but the deiodinated product **TUT** ($m/z = 1170.3$, entries 1–4, **Table 3.13**, **Figure 3.32B** and **3.32C**) was obtained as the major product, with only little, if any, of the expected product **TU^{Ph}T** ($m/z = 1249.4$) was formed. Changing the amount of catalyst, increasing temperature as well as using different buffers and pH values were not effective in reducing the amount of deiodinated product (entries 5–6, **Table 3.13**, **Figure 3.32D** and **3.32E**). Thus, potassium aryltrifluoroborates (ArBF_3K) was employed instead of arylboronic acid increase the reactivity of the nucleophile.¹⁵⁹ According to the literature, boronic acids are susceptible to oxidation, protodeboronation and homocoupling under Suzuki-Miyaura cross-coupling condition.¹⁶⁰ The utilization of the arylboronic acid in the Suzuki-Miyaura cross-coupling reaction was therefore not quite efficient and could generate homocoupling and oxidation products.

The use of air stable potassium aryltrifluoroborates (ArBF_3K)¹⁶¹⁻¹⁶² which generated aryl boronic acid in situ could reduce the side products¹⁶³ by slowly releasing the reactive boronic acid species, leading to a more productive reaction.¹⁶⁰ There are several reports on using ArBF_3K for the Suzuki–Miyaura cross-coupling to obtain the biaryl cross-coupling product in high purity.¹⁶³⁻¹⁶⁵ In this experiment, while *p*-tolyltrifluoroborate and 3-thienyltrifluoroborate were effective nucleophiles when used in combination with the $\text{Pd}(\text{OAc})_2/\text{APD}$ catalyst system in phosphate buffer pH 8.0 at 60 °C as shown by the formation of the expected major product under a short reaction time (15 minutes) (**Figure 3.33**). However, the deiodinated product was still significantly formed when PhBF_3K was used as the nucleophile (**Figure 3.33C**), therefore the reactivity of nucleophiles may not be the only critical factor that contribute to the success of the cross-coupling reaction. Furthermore, the reactions performed with long PNA sequences were not quite as effective as in the case of short PNA models.

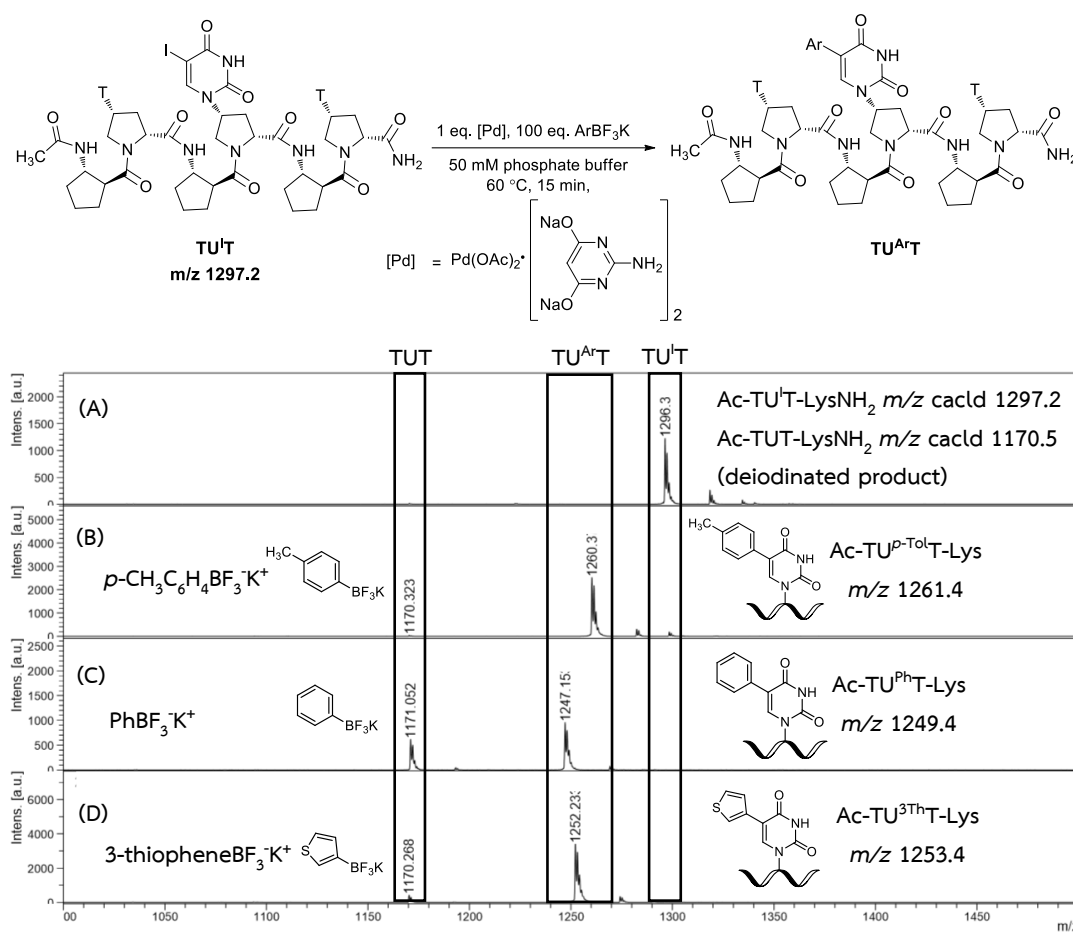
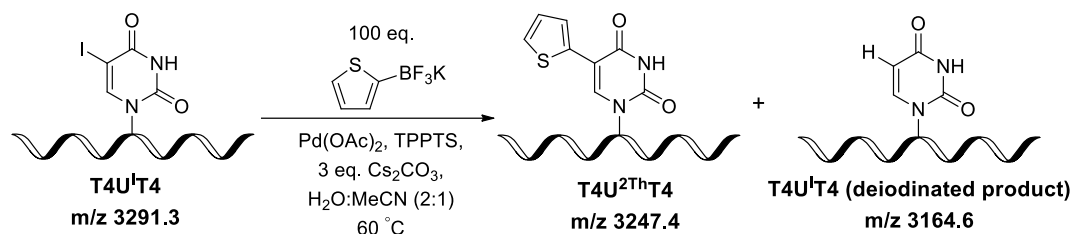


Figure 3.33 MALDI-TOF mass spectra of (A) starting material and (B)-(D) post-synthetic Suzuki-Miyaura coupling of TU^T with different organoboron compounds

Next, the palladium complex was changed to a combination of $Pd(OAc)_2$ with a water-soluble ligand tris(3-sulfonatophenyl)phosphane trisodium salt (TPPTS)¹⁶⁶ that has been successfully applied as a ligand for Suzuki-Miyaura cross-coupling reaction between 8-aryl-bromo-2'-deoxyguanosine (8-BrdG) and aryl boronic acids to form 8-aryl-2'-deoxyguanosine (8-ArdG) in an excellent yields.¹⁶⁷ This catalysis system was also effective with other purine and pyrimidine nucleosides, including those incorporated into oligonucleotides.¹⁶⁷⁻¹⁶⁹ The reaction was optimized using a longer acpcPNA sequence with potassium 2-thiophenetrifluoroborates as a model under various conditions as shown in **Table 3.14**.

Table 3.14 Optimization of post-synthetic Suzuki-Miyaura reaction of acpcPNA containing 5-iodouracil



Entry	Scale (nmol)	Pd(OAc) ₂ (equiv.)	TPPTS (equiv.)	with SiO ₂ ^a
1	10	1	4	no
2	10	1	4	yes
3	50	1	4	yes
4	50	2	4	yes
5	250	2	4	yes

^aThe reaction progress was monitored by MALDI-TOF mass spectrometry.

When the reaction between $\text{T4U}^{\text{I}}\text{T4}$ and potassium 2-thiophenetrifluoroborate was performed under the Pd(OAc)₂/TPPTS catalyst system with Cs₂CO₃ as a base in the presence of water/acetonitrile (2:1) at 60 °C (entry 1, **Table 3.14**), no desired cross-coupling product was observed. Only the deiodinated product was formed (**Figure 3.34B**). Molander *et. al.* reported that the hydrolysis of aryltrifluoroborates can be to the corresponding boronic acids can be initiated by silica gel¹⁷⁰⁻¹⁷¹ which acted as a fluorophile.¹⁵⁹ According to these previous reported on the active role of silica gel as fluorophiles, trace amounts of silica gel was used as an additive to increase the reaction efficiency. To our delight, the formation of dehalogenated product was reduced in the presence of silica gel, and the starting U^I-PNA was cleanly converted to the desired product as shown by MALDI-TOF mass spectra (entry 2, **Table 3.14**, **Figure 3.34C**). Based on the successful model reaction described above, the reaction was scaled up to 50 nmol. Under the same conditions

as employed at a small scale (10 nmol), the rate of the reaction was very slow and the deiodinated product was observed (entry 3, **Table 3.14**, **Figure 3.34D**). Thus, the amount of Pd(OAc)₂ was increased to 2.0 equiv. Under this condition, complete conversion was observed in 1 hour with only trace of deiodinated product was observed (entries 4, **Table 3.14**, **Figure 3.34E**).

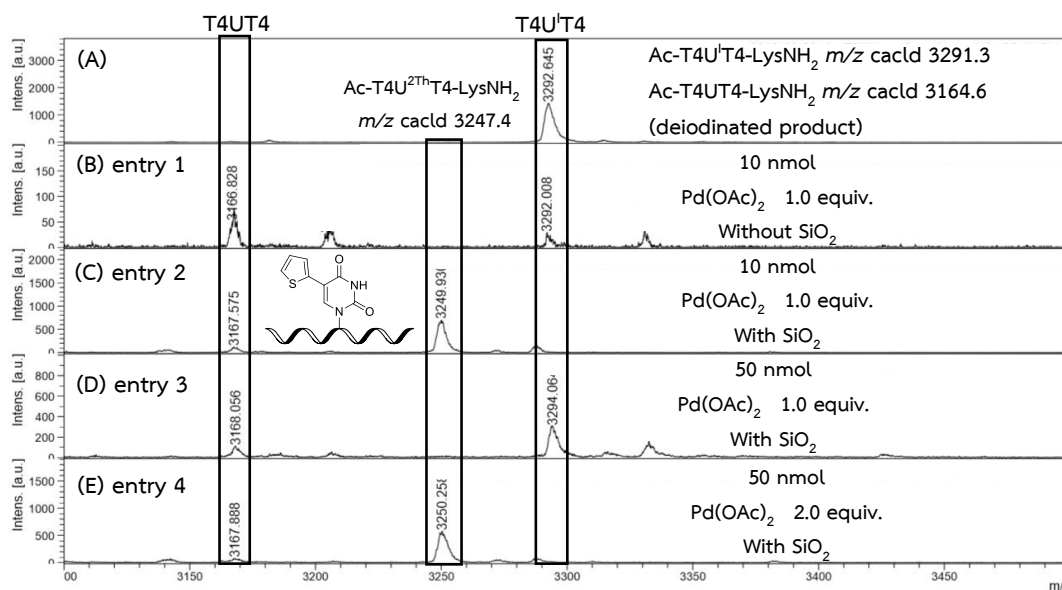


Figure 3.34 MALDI-TOF mass spectra of T4U^{2Th}T4 from Suzuki-Miyaura coupling in the absence and presence of SiO₂. The product was indicated by an arrow. The entry number referred to the entry number in **Table 3.14**.

According to the optimized conditions, the catalytic system of 2 equiv. Pd(OAc)₂ and 4 equiv. TPPS in the presence of 3.0 equiv. Cs₂CO₃ dissolved in water/acetonitrile (2:1) at 60 °C containing SiO₂ were chosen as the optimal conditions (entry 5, **Table 3.14**, **Figure 3.35B**).

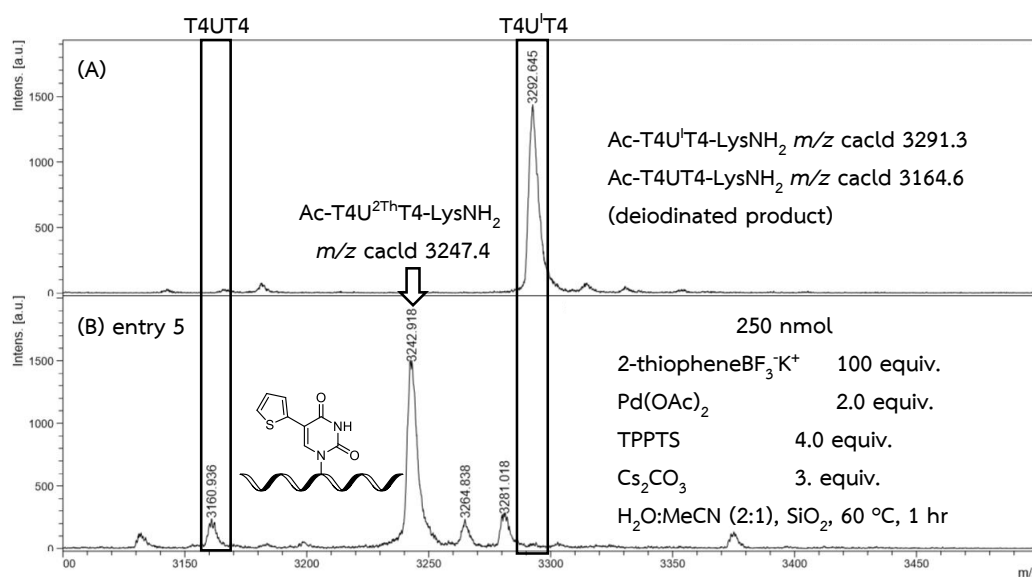


Figure 3.35 MALDI-TOF mass spectra of T4U^{2Th}T4 from Suzuki-Miyaura coupling in 250 nmol scale. The product was indicated by an arrow. The entry number referred to the entry number in **Table 3.14**.

To test the generality of the new condition, other aryltrifluoroborates were used to modify acpcPNA; with various thiophene and furan derivatives. In all cases, the reaction proceeded practically completely as indicated by MALDI-TOF mass spectrometry (**Figure 3.36**).

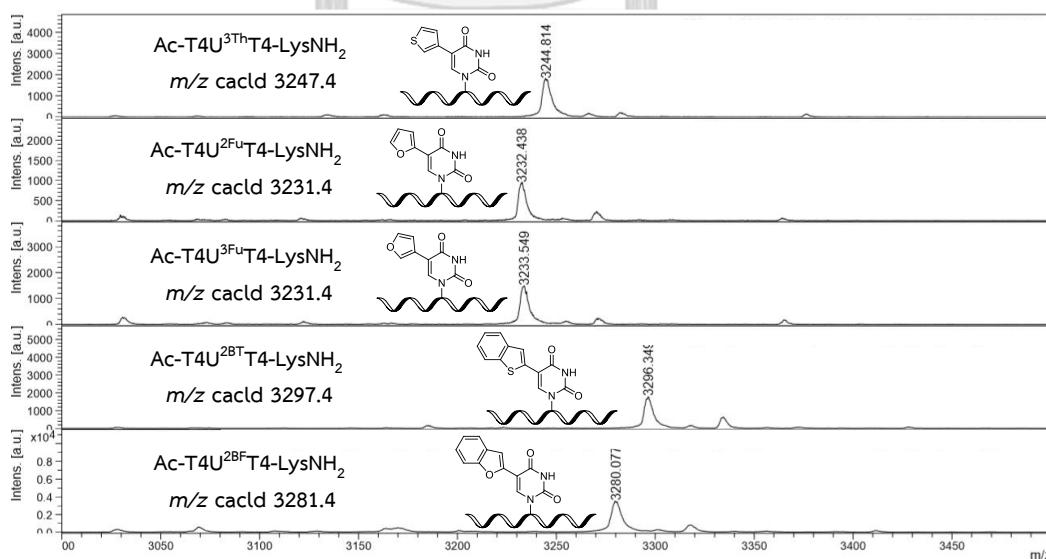


Figure 3.36 MALDI-TOF mass spectra of T4U^{Ar}T4 from Suzuki-Miyaura coupling in 250 nmol scale

3.14 Purification and characterization of C5-aryl-modified uracil acpcPNA derived from post-synthetic modification

The crude 5-aryl-modified uracil acpcPNAs obtained from the post-synthetic modification reaction were cleaned-up by passing through a C18 cartridge then washing with 10% aqueous acetonitrile and lyophilized to afford the crude PNA. The crude PNAs were purified by reversed phase HPLC eluting with a gradient system of 0.1 M TEAA buffer pH 7.0 and acetonitrile. Fractions containing the pure PNA as determined by MALDI-TOF mass analysis were combined and lyophilized to give the 5-aryl-modified uracil acpcPNA. The obtained pure modified PNAs were re-dissolved and the concentration of the modified-acpcPNA measured by UV/Vis spectrophotometry. The characterization data and isolated yields of all modified acpcPNA probes obtained from post-synthetic Suzuki-Miyaura cross-coupling are shown in **Table 3.15**.

Table 3.15 Sequences and characterization data of C5-aryl-modified uracil acpcPNA probes.

Code of PNA	Sequence (N→C)	t_R (min) ^a	Yield (%) ^b	m/z (calcd)	m/z (found) ^c
T4U ^{2Th} T4	Ac-TTTTU ^{2Th} TTTT-LysNH ₂	24.3	2.2	3247.4	3246.4
T4U ^{3Th} T4	Ac-TTTTU ^{3Th} TTTT-LysNH ₂	23.1	10.3	3247.4	3248.5
T4U ^{2Fu} T4	Ac-TTTTU ^{2Fu} TTTT-LysNH ₂	22.4	30.8	3231.4	3232.8
T4U ^{3Fu} T4	Ac-TTTTU ^{3Fu} TTTT-LysNH ₂	23.2	28.0	3231.4	3232.3
T4U ^{2BT} T4	Ac-TTTTU ^{2BT} TTTT-LysNH ₂	23.9	2.9	3297.4	3296.9
T8U ^{2BF} T4	Ac-TTTTU ^{2BF} TTTT-LysNH ₂	23.6	35.0	3281.4	3281.9

^aSee HPLC conditions in experimental section. ^bIsolated yield after HPLC. ^cMALDI-TOF mass spectrometry in linear positive ion mode using α -cyano-4-hydroxycinnamic acid as a matrix.

3.15 Thermal stability of DNA hybrids of C5-aryl-modified uracil acpcPNA probes

The duplex stability of C5-aryl-modified uracil acpcPNA probes with DNA targets were examined to investigate the binding affinity and base pairing specificity of the C5-

modified uracil acpcPNA probes towards DNA targets. The melting temperature data are summarized in **Table 3.16**.

Table 3.16 Thermal stability data of C5-aryl-modified uracil acpcPNA and their DNA hybrids. (Condition: 1.0 μM PNA, 1.2 μM DNA, 10 mM phosphate buffer pH 7.0).

Entry	PNA	DNA	DNA sequence ^a (5'→3')	T_m (°C)	ΔT_m (°C)	Notes
1	T4U ^{2Th} -T4	dA9	AAAA <u>A</u> AAAA	78.2	–	ds, complementary
2		dA8T	AAAATAAAA	52.4	–25.8	ds, mismatched T
3		dA8G	AAAAGAAAA	41.6	–36.6	ds, mismatched G
4		dA8C	AAAACAAAA	50.6	–27.6	ds, mismatched C
5	T4U ^{3Th} -T4	dA9	AAAA <u>A</u> AAAA	78.0	–	ds, complementary
6		dA8T	AAAATAAAA	51.6	–26.4	ds, mismatched T
7		dA8G	AAAAGAAAA	44.8	–33.2	ds, mismatched G
8		dA8C	AAAACAAAA	49.2	–28.8	ds, mismatched C
9	T4U ^{2Fu} -T4	dA9	AAAA <u>A</u> AAAA	83.2	–	ds, complementary
10		dA8T	AAAATAAAA	52.8	–30.4	ds, mismatched T
11		dA8G	AAAAGAAAA	46.6	–36.6	ds, mismatched G
12		dA8C	AAAACAAAA	51.6	–31.6	ds, mismatched C
13		dmG	AAAG <u>A</u> GAAA	<20.0	–63.2	ds, double mismatched
14		dabasic	AAAA <u>Φ</u> AAAA	58.4	–24.8	ds, abasic site
15	T4U ^{3Fu} -T4	dA9	AAAA <u>A</u> AAAA	74.8	–	ds, complementary
16		dA8T	AAAATAAAA	48.6	–26.2	ds, mismatched T
17		dA8G	AAAAGAAAA	40.6	–34.2	ds, mismatched G
18		dA8C	AAAACAAAA	50.0	–4.8	ds, mismatched C
19	T4U ^{2BT} -T4	dA9	AAAA <u>A</u> AAAA	77.0	–	ds, complementary
20		dA8T	AAAATAAAA	46.8	–30.9	ds, mismatched T
21		dA8G	AAAAGAAAA	42.0	–35.7	ds, mismatched G
22		dA8C	AAAACAAAA	49.2	–28.5	ds, mismatched C
23	T4U ^{2BF} -T4	dA9	AAAA <u>A</u> AAAA	65.1	–	ds, complementary
24		dA8T	AAAATAAAA	<20.0	–45.1	ds, mismatched T
25		dA8G	AAAAGAAAA	<20.0	–45.1	ds, mismatched G
26		dA8C	AAAACAAAA	<20.0	–45.1	ds, mismatched C

^aMismatched bases in the DNA sequence are indicated in bold. Complementary bases in DNA sequence are indicated by underlining. Φ represents as abasic site position in DNA.

The T_m data of **T4U^{Ar}T4** and their DNA hybrids indicated that all C5-modified uracil derivatives in acpcPNAs could specifically recognize adenine in the DNA targets as shown by the highest T_m values (**T4U^{2Th}T4•dA9** = 78.2 °C; **T4U^{3Th}T4•dA9** = 78.0 °C; **T4U^{2Fu}T4•dA9** = 83.2 °C; **T4U^{3Fu}T4•dA9** = 74.8 °C; **T4U^{2BT}T4•dA9** = 77.0 °C and **T4U^{2BF}T4•dA9** = 77.0 °C). These values are only slightly smaller (by 4.0–7.2 °C) when compared to the thermal stability of the unmodified T9 acpcPNA duplex (T_m = 82.0 °C),¹⁰⁸ indicating that the modification minimally perturbed to the duplex stability. An exception was observed with **T4U^{2Fu}T4•dA9**, whereby the T_m was slightly higher than the corresponding unmodified duplex by 1.2 °C. This may be due to the favorable stacking of the 2-furan moiety with DNA nucleobases. This behavior is in accordance to the previously published for a 2-furan-modified DNA that can form a stable hybrid with complementary DNA as shown by the similar T_m melting curves of the modified and unmodified duplexes.⁶² Additionally, DNA containing abasic site located on the direct opposite to the 2-furan modified uracil base showed the reduction of T_m value by 24.8 °C compared with complementary DNA. However, this abasic hybrid was in fact more stable than single base mismatched hybrid. Comparison with the furan-labeled deoxyuridine in DNA published by Tor *et. al.*,⁶⁴ the hybridization between the modified DNA and abasic site DNA was more stable than the corresponding unmodified duplex by 4.0 °C. They suggested that the unpaired 2-furan modified uracil nucleobase might adopt the *syn*-conformation leading to the stacking of the furan moiety within the duplex.⁶⁴ In contrast, mismatched duplexes of the same PNA displayed much lower T_m values ranging from 40.6–52.8 °C (**Table 3.16**). The large difference of T_m values relative to complementary duplex (in the range of 25.8–36.6 °C) confirmed that all C5-modified uracils in acpcPNA can specifically recognize adenine in the DNA strand.

3.16 Optical properties of fluorescence C5-aryl-modified uracil acpcPNA probes with DNA

In this section, optical properties of the C5-heteroaryl-modified acpcPNA probes in the absence and presence of DNAs will be studied by UV-Vis and

fluorescence spectrophotometry. The secondary structures of the duplexes were also studied by circular dichroism (CD) spectroscopy. For acpcPNA carrying 2-thiophene and 2-furan substituted uracil, the single-stranded probes showed a small absorption band at 320 nm similar to previously published reports in the case of DNA.^{62, 64} In the presence of complementary DNA, the absorption spectra did not significantly change. The acpcPNA carrying 3-thiophene and 3-furan substituted uracil did not show significant UV absorption beyond 300 nm. The acpcPNA $T4U^{2BT}T4$ bearing a benzothiophene substituent displayed a maximum absorption wavelength at 340 nm, which was not changed in the presence of DNA. The $T4U^{2BF}T4$ probe showed a blue-shifted signal at 287 nm that does not change much in the presence of either complementary or mismatched DNA (Figure 3.37).

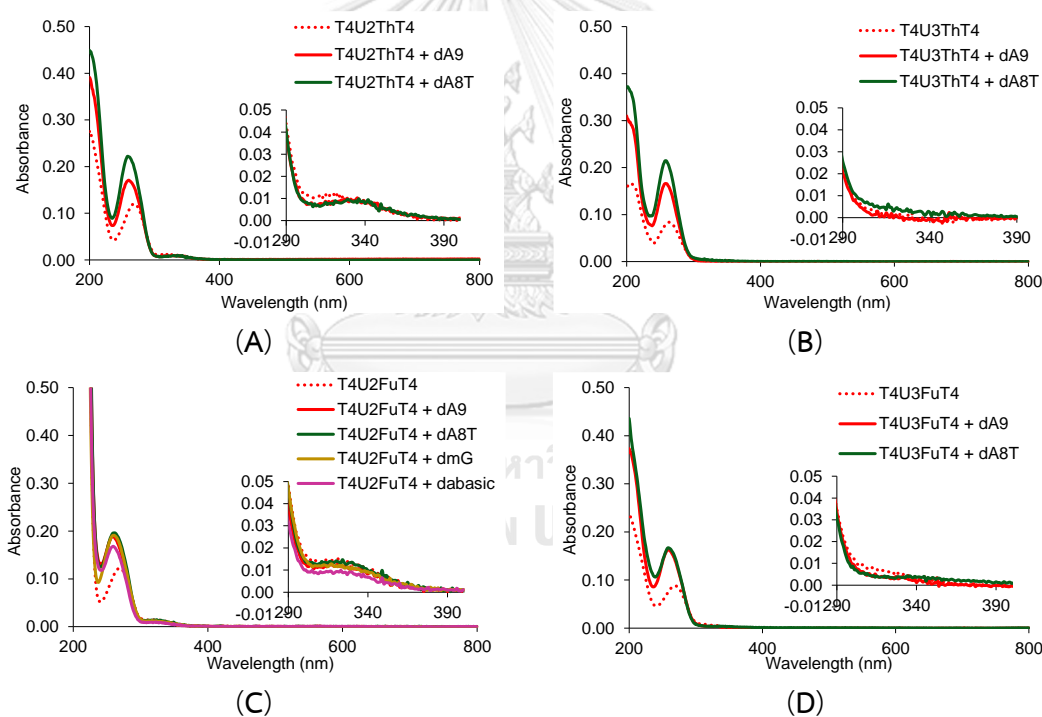


Figure 3.37 UV-vis spectra of (A) $T4U^{2Th}T4$, (B) $T4U^{3-Th}T4$, (C) $T4U^{2Fu}T4$, (D) $T4U^{3Fu}T4$, (E) $T4U^{2BT}T4$ and (F) $T4U^{2BF}T4$ and its DNA hybrids. Conditions: 1.0 μM PNA, 1.2 μM DNA, 10 mM sodium phosphate buffer pH 7.0

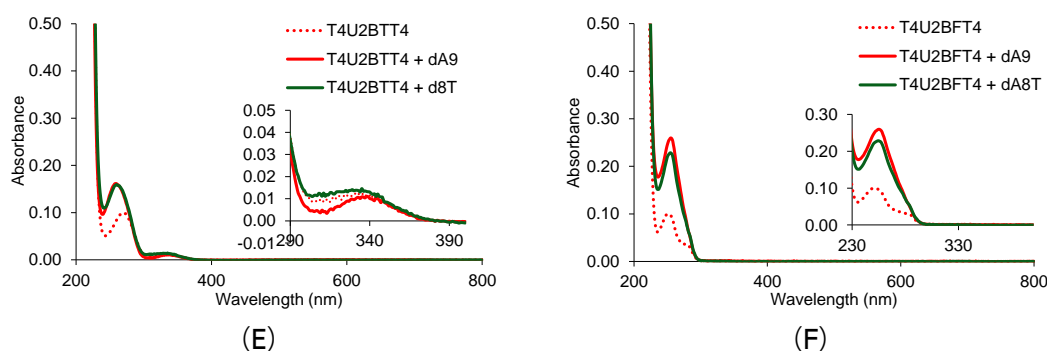


Figure 3.37 UV-vis spectra of (A) $T4U^{2Th}T4$, (B) $T4U^{3-Th}T4$, (C) $T4U^{2Fu}T4$, (D) $T4U^{3Fu}T4$, (E) $T4U^{2BT}T4$ and (F) $T4U^{2BF}T4$ and its DNA hybrids. Conditions: 1.0 μM PNA, 1.2 μM DNA, 10 mM sodium phosphate buffer pH 7.0 (Continued)

Next, the fluorescence properties of the C5-heteroaryl modified acpcPNAs were studied in the absence and presence of DNA targets. The data are summarized in **Table 3.17**.

Table 3.17 Optical properties of C5-aryl-modified uracil acpcPNA and their DNA hybrids (Condition: 1.0 μM PNA, 1.2 μM DNA, 10 mM phosphate buffer pH 7.0, λ_{ex} 330 nm).

Entry	PNA	DNA	F/F_0^a	λ_{em} (nm)	Φ_F^b	Notes
1		-	-	444	0.045	ss
2	$T4U^{2Th}T4$	dA9	3.35	428	0.130	ds, complementary
3		dA8T	3.82	429	0.137	ds, mismatched T
4		dA8G	3.14	432	0.105	ds, mismatched G
5		dA8C	3.15	432	0.106	ds, mismatched C
6			-	-	412	0.058
7	$T4U^{3Th}T4$	dA9	2.81	401	0.043	ds, complementary
8		dA8T	2.38	407	0.032	ds, mismatched T
9		dA8G	2.69	404	0.044	ds, mismatched G
10		dA8C	2.13	402	0.039	ds, mismatched C

^a $T4U^{2Th}T4$, $\lambda_{\text{em}} = 428$ nm, $T4U^{3Th}T4$, $\lambda_{\text{em}} = 401$ nm, $T4U^{2Fu}T4$, $\lambda_{\text{em}} = 419$ nm, $T4U^{3Fu}T4$, $\lambda_{\text{em}} = 399$ nm, $T4U^{2BT}T4$, $\lambda_{\text{em}} = 438$ nm, $T4U^{2BF}T4$, $\lambda_{\text{em}} = 421$ nm. ^bQuantum yields were measured by using quinine sulfate as a standard ($\Phi_F = 0.546$).

Table 3.17 Optical properties of C5-aryl-modified uracil acpcPNA and their DNA hybrids (Condition: 1.0 μM PNA, 1.2 μM DNA, 10 mM phosphate buffer pH 7.0, λ_{ex} 330 nm). (Continued)

Entry	PNA	DNA	F/F_0^a	λ_{em} (nm)	Φ_{F}^b	Notes
11		-	-	432	0.025	ss
12		dA9	7.36	419	0.207	ds, complementary
13		dA8T	9.05	418	0.206	ds, mismatched T
14	T4U ^{2Fu} T4	dA8G	6.49	420	0.130	ds, mismatched G
15		dA8C	9.09	418	0.214	ds, mismatched C
16		dmG	1.47	428	0.047	ds, double mismatched
17		dabasic	9.52	418	0.364	ds, abasic site
18		-	-	414	0.045	ss
19		dA9	2.74	399	0.099	ds, complementary
20	T4U ^{3Fu} T4	dA8T	2.30	400	0.078	ds, mismatched T
21		dA8G	2.08	407	0.049	ds, mismatched G
22		dA8C	2.34	403	0.088	ds, mismatched C
23		-	-	453	0.087	ss
24		dA9	1.72	438	0.176	ds, complementary
25	T4U ^{2BT} T4	dA8T	1.51	445	0.117	ds, mismatched T
26		dA8G	1.39	449	0.108	ds, mismatched G
27		dA8C	1.38	446	0.115	ds, mismatched C
28		-	-	439	0.171	ss
29		dA9	2.92	421	0.184	ds, complementary
30	T4U ^{2BF} T4	dA8T	2.82	420	0.105	ds, mismatched T
31		dA8G	2.75	424	0.101	ds, mismatched G
32		dA8C	2.56	422	0.123	ds, mismatched C

^aT4U^{2Th}T4, $\lambda_{\text{em}} = 428$ nm, T4U^{3Th}T4, $\lambda_{\text{em}} = 401$ nm, T4U^{2Fu}T4, $\lambda_{\text{em}} = 419$ nm, T4U^{3Fu}T4, $\lambda_{\text{em}} = 399$ nm, T4U^{2BT}T4, $\lambda_{\text{em}} = 438$ nm, T4U^{2BF}T4, $\lambda_{\text{em}} = 421$ nm. ^bQuantum yields were measured by using quinine sulfate as a standard ($\Phi_{\text{F}} = 0.546$).

The fluorescence quantum yields of all 5-aryl-modified acpcPNAs were rather low in the single stranded form for the furan and thiophene substituents ($\Phi_{\text{F}} = 0.025$ -

0.045). Higher quantum yields were observed with benzofuran (0.171) and benzothiophene ($\Phi_f = 0.087$) substituents (entries 23 and 27, **Table 3.17**). In the presence of either complementary or mismatched DNA, the fluorescence intensities of both **T4U^{2Th}T4** and **T4U^{3Th}T4** were enhanced by 2-4 folds relative to the corresponding single-stranded PNA. Interestingly, the **T4U^{2Th}T4** displayed a distinct blue-shifted emission wavelength by 10 nm from the single-stranded probe as shown by the normalized fluorescence spectra in **Figure 3.38**. On the other hand, no significant wavelength shifting was observed in the duplexes of **T4U^{3Th}T4** with DNA targets (**Figure 3.39**).

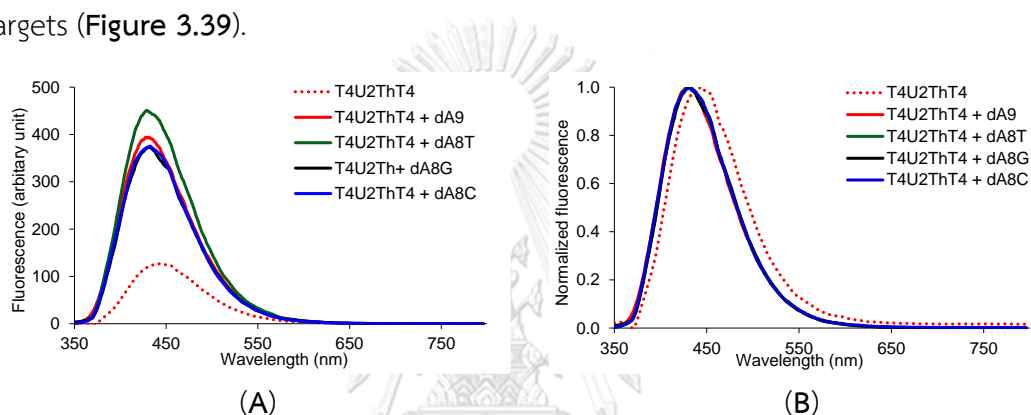


Figure 3.38 (A) Fluorescence spectra and (B) normalized fluorescence of **T4U^{2Th}T4** with its DNA hybrids. Conditions: 1.0 μM PNA, 1.2 μM DNA, 10 mM sodium phosphate buffer pH 7.0, λ_{ex} 330 nm

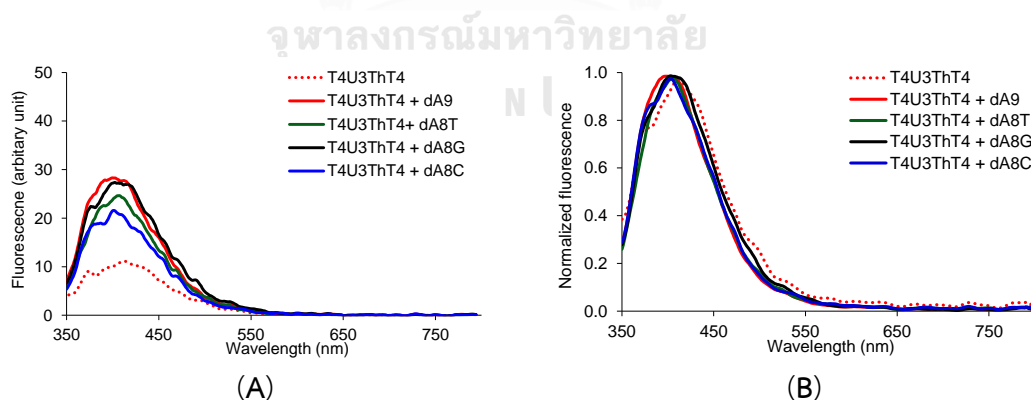


Figure 3.39 (A) Fluorescence spectra and (B) normalized fluorescence spectra of **T4U^{3Th}T4** with its DNA hybrids. Conditions: 1.0 μM PNA, 1.2 μM DNA, 10 mM sodium phosphate buffer pH 7.0, λ_{ex} 330 nm

In the cases of 2- and 3-furan modification, fluorescence enhancement were similarly observed for both complementary and mismatched hybrids. Interestingly, the fluorescence intensity of all DNA hybrids of the 2-furan-modified acpcPNA probe **T4U^{2Fu}T4** increased dramatically by a factor 6.5–9.1. Much less fluorescence increase (2.08–2.74 folds) were observed with the 3-furan-modified acpcPNA probe **T4U^{3Fu}T4**. Unfortunately, in all cases, the complementary and single mismatched hybrids gave comparable signals. The non-discriminating fluorescence increase could be attributed to the formation of the relatively stable single mismatched duplexes. When another mismatch was introduced as in the case of indirect double mismatch DNA sequence 5'- AAAGAGAAA-3' (**dmG**), the fluorescence became almost the same as single stranded probe, indicating that the fluorescence increase was specific to the formation of PNA-DNA duplexes. Blue-shifting of the fluorescence emission was observed in the DNA hybrids of both **T4U^{2Fu}T4** and **T4U^{3Fu}T4** by 7–15 nm relative to single-stranded PNA (**Figure 3.40** and **3.41**). Such blue shifting was not observed in the double mismatched hybrid **T4U^{2Fu}T4·dmG**. This suggests the connection between the fluorescence intensity increase and wavelength shifting with the PNA-DNA hybrid formation. The hybrid with DNA target containing an abasic site directly located opposite to 2-furan-modified uracil in **T4U^{2Fu}T4** showed a 9.52 folds fluorescence enhancement with wavelength shifting into shorter wavelength. The fluorescence intensity in this case was higher than complementary and single base mismatch DNAs. Comparison to the published reported of 2-furan-modified DNA, the fluorescence of the similar furan-modified uracil DNA probes was enhanced by 7 folds in the duplex carrying an abasic site in the opposite strand. However, the fluorescence emission was significantly quenched upon formation of complementary duplex. This behavior was in sharp contrast to acpcPNA bearing 2-furan moiety, whereby the fluorescence emission was increased both complementary and abasic site DNA. It can be concluded that the behavior of the furan-modified uracil in DNA and acpcPNA are not the same, which may suggest the different arrangement of the base in different types of duplexes.

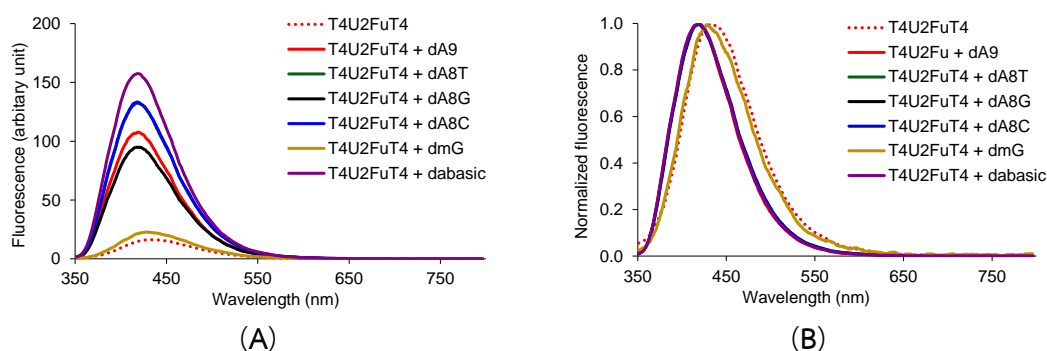


Figure 3.40 (A) Fluorescence spectra and (B) normalized fluorescence of $T4U^{2Fu}T4$ with its DNA hybrids. Conditions: $1.0 \mu\text{M}$ PNA, $1.2 \mu\text{M}$ DNA, 10 mM sodium phosphate buffer pH 7.0, λ_{ex} 330 nm

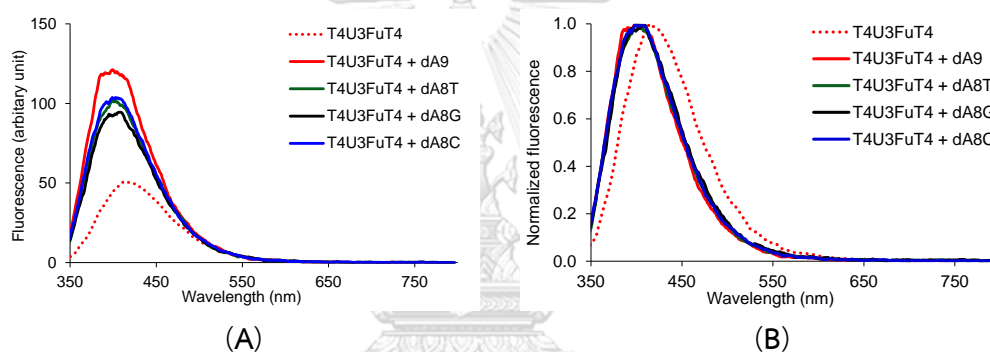


Figure 3.41 (A) Fluorescence spectra and (B) normalized fluorescence of $T4U^{3Fu}T4$ with its DNA hybrids. Conditions: $1.0 \mu\text{M}$ PNA, $1.2 \mu\text{M}$ DNA, 10 mM sodium phosphate buffer pH 7.0, λ_{ex} 330 nm

CHULALONGKORN UNIVERSITY

The circular dichroism (CD) was used to investigate the hybrid formation of 2-furan modified acpcPNA probes. In all cases, the CD spectra exhibited two dominant negative bands at 250 and 270 nm with a small positive band at 286 nm (**Figure 3.42**). Based on the CD spectra, it appeared that the 2-furan moiety may arrange in the same conformation in all types of hybrids, which is consistent with the insignificant difference of the UV absorption and fluorescence among these hybrids (**Figure 3.37C**).

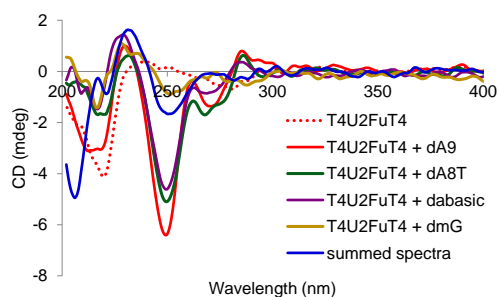


Figure 3.42 CD spectra of $T4U^{2Fu}T4$ with its DNA hybrids. Conditions: 1.0 μM PNA, 1.2 μM DNA, 10 mM sodium phosphate buffer pH 7.0. The sum spectra were obtained by combining the CD spectra of $T4U^{2Fu}T4$ and **dA9**, which should represent the spectrum to be observed if there were no interactions between the PNA and DNA.

Previous work with benzothiophene and benzofuran-modified uracil acpPNA flanked by T residues exhibited an increase in fluorescence intensity when hybridized to both complementary and mismatched DNA.^{87,88,172} Similarly, acpPNA modified with benzothiophene [$T4U^{2BT}T4$] and benzofuran [$T4U^{2BF}T4$] displayed a fluorescence enhancement upon duplex formation, showing the fluorescence emission ratio of $T4U^{2BT}T4$ in the presence of DNA in the range of 1.39–1.72 folds. Likewise, the fluorescence emission ratios of $T4U^{2BF}T4$ in the presence of DNA addition were 2.56–2.92 folds. Again, no difference in fluorescence were observed between complementary and single mismatched (Figure 3.43–3.44). The maximum emission wavelength of both modified-acpPNA was shifted into the shorter wavelength, which is in good agreement to what already observed in thiophene and furan-modified probes. The benzofuran-modified acpPNA provided a more pronounced blue-shifting of fluorescence emission maxima than the benzothiophene-modified acpPNA upon duplex formation with DNA (benzofuran: 20–23 nm; benzothiophene: 6–17 nm).

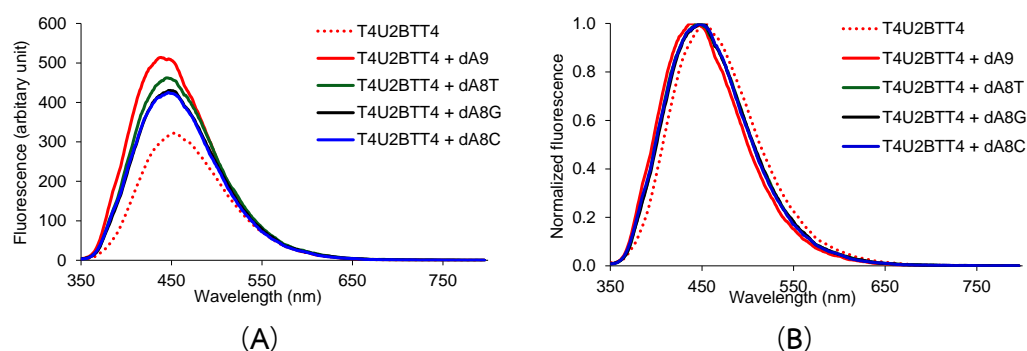


Figure 3.43 (A) Fluorescence and (B) UV-vis of $T4U^{2BT}T4$ and its DNA hybrids. Conditions: $1.0 \mu\text{M}$ PNA, $1.2 \mu\text{M}$ DNA, 10 mM sodium phosphate buffer pH 7.0, $\lambda_{\text{ex}} 330 \text{ nm}$

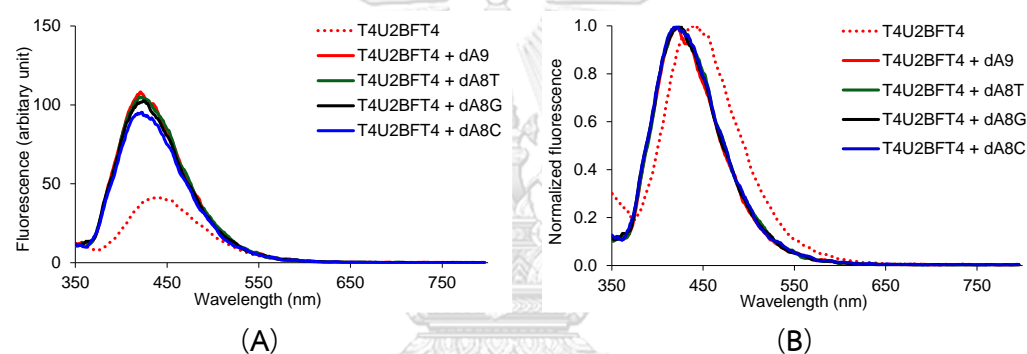


Figure 3.44 (A) Fluorescence and (B) UV-vis and of $T4U^{2BF}T4$ and its DNA hybrids. Conditions: $1.0 \mu\text{M}$ PNA, $1.2 \mu\text{M}$ DNA, 10 mM sodium phosphate buffer pH 7.0, $\lambda_{\text{ex}} 330 \text{ nm}$

In summary, fluorescence C5-aryl-modified uracil acpcPNA probes were successfully synthesized by post-synthetic Suzuki-Miyaura reaction between iodouracil-modified acpcPNA and aryltrifluoroborate. All C5-heteroaryl-modified uracil PNA probes showed the expected fluorescence increase when hybridized with DNA. The most pronounced fluorescence change was observed with the probe $T4U^{2Fu}T4$. In addition, the hybridization also caused significant blue-shifting of the emission maxima for certain probes. Unfortunately, the specificity in all cases is not sufficient to allow distinguishing between complementary and single mismatch DNA target.

CHAPTER IV

CONCLUSION

In this work, novel fluorescent hybridization responsive fluorescence acpcPNA probes were developed by incorporating base discriminating fluorescent nucleobases into acpcPNA. The requirement for the base discriminating fluorescent nucleobase is that it must selectively form Watson-Crick base pairing with one of the four natural nucleobases. In addition, the fluorescence properties of the fluorescence nucleobase should be sensitive to the base pairing states or to local environment, for example the presence of base stacks in DNA duplexes. The research consists of two sections which were divided by the synthetic approaches used for the incorporation of the fluorescent nucleobase into the PNA probe which include

1) Introducing the fluorescent monomer building block into the probes via a pre-formed monomer approach - This part focused on chemical installation of a fluorescent nucleobase 8-(pyrene-1-yl)ethynyl-adenine (A^{PyE}) into acpcPNA through a solid phase chemistry.

2) Modification the probes bearing a reactive precursor to create the fluorescent nucleobase via a post-synthetic modification approach- This part involves the development methodologies for conversion of a halogenated nucleobase – 5-iodouracil – previously incorporated into acpcPNA to 5-aryl- or 5-arylalkynyluracil via a post-synthetic modification through palladium-catalyzed cross coupling reactions including Suzuki-Miyaura and Sonogashira reactions.

In the first part, the acpcPNA monomer bearing an ethynylpyrene-modified adenine (A^{PyE}) base was successfully synthesized through Sonogashira cross-coupling reaction from 1-ethynylpyrene and 8-bromoadenine acpcPNA monomer. The monomer was incorporated into acpcPNA by standard solid phase peptide synthesis. The A^{PyE} base retained the Watson-Crick base pairing ability by specifically recognizing the thymine base in the opposite DNA strand as confirmed by melting temperature (T_m) data. The melting temperature showed that the A^{PyE} -acpcPNA could form a more

stable hybridization with complementary DNA targets carrying dT directly opposite to the A^{PyE} than other mismatched hybrids. The probes exhibit fluorescence in the range of 449-498 nm upon excitation at 376 nm. The fluorescence quantum yield and emission wavelengths of single-stranded A^{PyE}-modified acpcPNA are influenced by the flanking nucleobases. More specifically, G/G and C/C as bases adjacent with the reduction of fluorescence quantum yield by 2-4 folds relative to flanking T/T and A/A. Moreover, the sequences bearing G adjacent to the A^{PyE} at the C-terminal side gave a remarkable red-shifted fluorescence emission in the single stranded form. In the presence of perfect match DNA, the fluorescence of all A^{PyE}-modified acpcPNA probes was enhanced (1.5-5.2 folds, depending on the sequence). This is accompanied by blue-shifting of the emission wavelength, which is most pronounced in the probe bearing a G adjacent to A^{PyE} towards the C-terminus. Induction of a mismatch or abasic site DNA that were positioned to be directly opposite to the A^{PyE} base resulted in a decrease in fluorescence intensity relative to the single stranded probe. It was proposed based on CD and UV-vis studies that the orientations of the A^{PyE} base in the complementary and mismatched/abasic duplexes were different. In the complementary duplex, the Watson-Crick base pairing was formed, and the pyrene part was forced to expose to the aqueous environment, resulting in the observed fluorescence increase. On the other hand, the absence of hydrogen bonding in the case of mismatched duplexes allows the A^{PyE} to adopt a different orientation whereby the pyrene became stacked within the duplex to avoid contact with water. The base pairing ability of A^{PyE} incorporated into acpcPNA is substantially different from the case of DNA previously reported by several other groups. In DNA, the A^{PyE} gave low discrimination ability among the four nucleobases in terms of both thermal stability and fluorescence properties. This is due to the preference of the A^{PyE} to adopt a *syn*-conformation and thus the pyrene always remain buried within the duplex. The stronger binding affinity of acpcPNA towards DNA apparently force the A^{PyE} to adopt the *anti*-conformation that allows the Watson-Crick base pairing with the opposite dT. A^{PyE}-modified acpcPNA was used as fluorescence probe to determine trinucleotide repeats sequence in DNA not only by fluorescence intensity change but also by fluorescence color change from green to blue. In addition, the performance of A^{PyE}-

modified acpcPNA probes for DNA sequences discrimination was further improved by using reduced graphene oxide as an external quencher to reduce the background fluorescence of the single-stranded PNA probes.

The second part concerns about the development of post-synthetic modification strategy for incorporating of fluorescent nucleobases into acpcPNA with the aim to create new fluorescence acpcPNA probes. According to this approach, the fluorophores will be incorporated into the probe bearing a reactive group after cleavage from the solid support. This approach not only allows the variation of the fluorophores to be easily performed without the need to synthesize the monomer nor the PNA, but it also allows the synthesis of probes bearing sensitive nucleobases that cannot be incorporated by the standard solid phase conditions. The reactive building block 5-iodouracil was firstly incorporated into acpcPNA at a predefined position via solid phase peptide synthesis. After cleavage of the reactive 5-iodouracil-modified acpcPNA from the solid support, it was further modified through palladium-catalyzed cross-coupling reactions *i.e.* Suzuki-Miyaura and Sonogashira reactions. Post-synthetic Sonogashira reaction with 1-ethynylpyrene in solution phase allows the synthesis of acpcPNA probes bearing 5-ethynylpyrene-modified uracil (U^{PyE}) that could not be obtained from the solid phase synthesis approach due to the susceptibility of the U^{PyE} base to cyclize into the corresponding furanocytosine. The U^{PyE} -modified acpcPNA can form a stable hybrid with complementary DNA by showing a high melting temperature (T_m), indicating that the U^{PyE} base in acpcPNA could specifically recognize adenine in the complementary DNA similar to what already reported in the DNA system. The fluorescence signal was increased by 5.2 folds in the complementary hybrid. Hybrids with single base mismatched DNA (T, G and C) showed a large decrease in T_m values compared to the complementary duplex. In addition, the fluorescence intensity change was much smaller (1.4-2.3 folds relative to the single-stranded acpcPNA probe). These experiments suggested that the 5-ethynylpyrene-modified uracil (U^{PyE}) is sensitive to the local environment and can be used as a base discriminating fluorescent nucleobase (BDF) for DNA sequence analysis. Attempts to perform the post-synthetic modification on the solid support failed because the acidic

conditions required for cleavage of the PNA from the solid support induced a 5-*endo-dig* cyclization to form a novel pyrenylfuranouracil (fU^{Py}) base. The fU^{Py} can form more stable base pair with dG than other nucleobases as shown by melting temperature analysis. However, the stability of the pfU^{Py}·dG pair was much lower than that of conventional pG·dA pair due to the reduced number of hydrogen bonding. In addition, a small fluorescence increase was observed in the complementary duplex with pfU^{Py}·dG pair, and small fluorescence quenching was also observed in other mismatched pairs, indicating that the furanouracil may be useful for future development of fluorescence probes.

Finally, post-synthetic Suzuki-Miyaura cross-coupling reaction in the solution phase was also successfully performed on the same 5-iodouracil-modified acpcPNA reactive precursor and various heteroaromatic nucleophiles. The reaction of PNA with various aryltrifluoroborates under the catalysis of Pd(OAc)₂ and TPPTS provided a convenient access to a variety of 5-aryl-modified uracil acpcPNAs in high yield. All 5-aryl-modified uracil base in acpcPNA probes were shown to retain the Watson-Crick base pairing ability with A as revealed by the much higher T_m values compared to the mismatched bases (T, G and C). Moreover, the T_m data suggested that the stability of the acpcPNA carrying these 5-aryl-modified uracils were similar or only slightly lower than unmodified PNA, suggesting the minimal perturbation of the PNA-DNA hybridization. Unfortunately, all modified acpcPNA probes exhibited non-discriminative fluorescence enhancement upon binding with both complementary and mismatched DNA targets. The largest fluorescence increase (6.49-9.52 folds relative to the single stranded PNA probe) was observed in the 2-furyl modification. The non-discriminating behavior might be explained by the relatively high stability of the mismatched duplexes. The similar UV, CD and fluorescence spectra of the complementary and mismatched hybrids suggest that the nucleobases seem to adopt similar orientations in the duplex, which is clearly different from the case of A^{PyE} discussed above.

In a broader context, this study revealed that the behavior of the same modified nucleobase in acpcPNA may not necessarily be the same with DNA or other NA

analogues. The post-synthetic modification approach developed also opens up a new and efficient way to rapidly generate various modified acpcPNA probes which could lead to other new probes with superior performance in the future.



REFERENCES

1. Du, Y.; Dong, S. Nucleic Acid Biosensors: Recent Advances and Perspectives. *Anal. Chem.* **2017**, *89*, 189-215.
2. Zhao, Y.; Wang, H.; Tang, W.; Hu, S.; Li, N.; Liu, F. An in situ Assembly of a DNA-Streptavidin Dendrimer Nanostructure: A New Amplified Quartz Crystal Microbalance Platform for Nucleic Acid Sensing. *Chem. Commun.* **2015**, *51*, 10660-10663.
3. Makra, I.; Brajnovits, A.; Jagerszki, G.; Furjes, P.; Gyurcsanyi, R. E. Potentiometric Sensing of Nucleic Acids Using Chemically Modified Nanopores. *Nanoscale* **2017**, *9*, 739-747.
4. He, D.; Hai, L.; Wang, H.; Wu, R.; Li, H.-W. Enzyme-Free Quantification of Exosomal Microrna by the Target-Triggered Assembly of the Polymer Dnazyme Nanostructure. *Analyst* **2018**, *143*, 813-816.
5. Karmakar, S.; Hrdlicka, P. J. DNA Strands with Alternating Incorporations of LNA and 2'-O-(pyren-1-yl)methyluridine: : SNP-Discriminating RNA Detection Probes. *Chem. Sci.* **2013**, *4*, 3447-3454.
6. Wang, K.; Huang, J.; Yang, X.; He, X.; Liu, J. Recent Advances in Fluorescent Nucleic Acid Probes for Living Cell Studies. *Analyst* **2013**, *138*, 62-71.
7. Du, Y.; Lim, B. J.; Li, B.; Jiang, Y. S.; Sessler, J. L.; Ellington, A. D. Reagentless, Ratiometric Electrochemical DNA Sensors with Improved Robustness and Reproducibility. *Anal. Chem.* **2014**, *86*, 8010-6.
8. Hvastkovs, E. G.; Buttry, D. A. Recent Advances in Electrochemical DNA Hybridization Sensors. *Analyst* **2010**, *135*, 1817-29.
9. Huang, T. J.; Liu, M.; Knight, L. D.; Grody, W. W.; Miller, J. F.; Ho, C. M. An Electrochemical Detection Scheme for Identification of Single Nucleotide Polymorphisms Using Hairpin-Forming Probes. *Nucleic Acids Res.* **2002**, *30*, e55.
10. Milkani, E.; Khaing, A. M.; Morais, S.; Lambert, C. R.; McGimpsey, W. G. SPR-based Single Nucleotide Mismatch Biosensor. *Anal. Methods* **2011**, *3*, 122-132.

11. Fong, K. E.; Yung, L.-Y. L. Localized Surface Plasmon Resonance: A Unique Property of Plasmonic Nanoparticles for Nucleic Acid Detection. *Nanoscale* **2013**, *5*, 12043-12071.
12. Marin, A. G.; Garcia-Mendiola, T.; Bernabeu, C. N.; Hernandez, M. J.; Piqueras, J.; Pau, J. L.; Pariente, F.; Lorenzo, E. Gallium Plasmonic Nanoparticles for Label-Free DNA and Single Nucleotide Polymorphism Sensing. *Nanoscale* **2016**, *8*, 9842-9851.
13. Brown, R. C.; Li, Z.; Rutter, A. J.; Mu, X.; Weeks, O. H.; Smith, K.; Weeks, I. Development and Application of a Novel Acridinium Ester for Use as a Chemiluminescent Emitter in Nucleic Acid Hybridisation Assays Using Chemiluminescence Quenching. *Org. Biomol. Chem.* **2009**, *7*, 386-94.
14. Ali, Z.; Wang, J.; Tang, Y.; Liu, B.; He, N.; Li, Z. Simultaneous Detection of Multiple Viruses Based on Chemiluminescence and Magnetic Separation. *Biomater. Sci.* **2017**, *5*, 57-66.
15. Liu, Z.; Chen, S.; Liu, B.; Wu, J.; Zhou, Y.; He, L.; Ding, J.; Liu, J. Intracellular Detection of ATP Using an Aptamer Beacon Covalently Linked to Graphene Oxide Resisting Nonspecific Probe Displacement. *Anal. Chem.* **2014**, *86*, 12229-12235.
16. Zhang, N.; Appella, D. H. Colorimetric Detection of Anthrax DNA with a Peptide Nucleic Acid Sandwich-Hybridization Assay. *J. Am. Chem. Soc.* **2007**, *129*, 8424-8425.
17. Teengam, P.; Siangproh, W.; Tuantranont, A.; Vilaivan, T.; Chailapakul, O.; Henry, C. S. Multiplex Paper-Based Colorimetric DNA Sensor Using PyrrolidinyI Peptide Nucleic Acid-Induced AgNPs Aggregation for Detecting MERS-CoV, MTB, and HPV Oligonucleotides. *Anal. Chem.* **2017**, *89*, 5428-5435.
18. Juskowiak, B. Nucleic Acid-based Fluorescent Probes and their Analytical Potential. *Anal. Bioanal. Chem.* **2011**, *399*, 3157-76.
19. Tyagi, S.; Kramer, F. R. Molecular Beacons: Probes that Fluoresce Upon Hybridization. *Nat. Biotechnol.* **1996**, *14*, 303-308.
20. Li, Y.; Zhou, X.; Ye, D. Molecular Beacons: An Optimal Multifunctional Biological Probe. *Biochem. Biophys. Res. Commun.* **2008**, *373*, 457-461.
21. Varghese, R.; Wagenknecht, H.-A. Red-White-Blue Emission Switching Molecular Beacons: Ratiometric Multicolour DNA Hybridization Probes. *Org. Biomol. Chem.* **2010**, *8*, 526-528.

22. Venkatesan, N.; Seo, Y. J.; Kim, B. H. Quencher-Free Molecular Beacons: A New Strategy in Fluorescence Based Nucleic Acid Analysis. *Chem. Soc. Rev.* **2008**, *37*, 648-663.
23. Okamoto, A.; Saito, Y.; Saito, I. Design of Base-Discriminating Fluorescent Nucleosides. *J. Photochem. Photobiol., C* **2005**, *6*, 108-122.
24. Saito, Y.; Kanatani, K.; Ochi, Y.; Okamoto, A.; Saito, I. Design of Base-Discriminating Fluorescent (BDF) Nucleobase for SNP Typing. *Nucleic Acids Symp Ser (Oxf)* **2004**, 243-244.
25. Okamoto, A.; Kanatani, K.; Saito, I. Pyrene-Labeled Base-Discriminating Fluorescent DNA Probes for Homogeneous SNP Typing. *J. Am. Chem. Soc.* **2004**, *126*, 4820-4827.
26. Hwang, G. T.; Seo, Y. J.; Kim, B. H. Pyrene-Labeled Deoxyuridine and Deoxyadenosine: Fluorescent Discriminating Phenomena in their Oligonucleotides. *Tetrahedron Lett.* **2005**, *46*, 1475-1477.
27. Wagner, C.; Rist, M.; Mayer-Enthart, E.; Wagenknecht, H.-A. 1-Ethynylpyrene-Modified Guanine and Cytosine as Optical Labels for DNA Hybridization. *Org. Biomol. Chem.* **2005**, *3*, 2062-2063.
28. Chen, G.; Song, F.; Xiong, X.; Peng, X. Fluorescent Nanosensors Based on Fluorescence Resonance Energy Transfer (FRET). *Ind. Eng. Chem. Res.* **2013**, *52*, 11228-11245.
29. Wang, H.; Yang, R.; Yang, L.; Tan, W. Nucleic Acid Conjugated Nanomaterials for Enhanced Molecular Recognition. *ACS Nano* **2009**, *3*, 2451-2460.
30. Lee, J.; Kim, J.; Kim, S.; Min, D.-H. Biosensors Based on Graphene Oxide and Its Biomedical Application. *Adv. Drug Delivery Rev.* **2016**, *105*, 275-287.
31. Kim, J.; Cote, L. J.; Kim, F.; Huang, J. Visualizing Graphene Based Sheets by Fluorescence Quenching Microscopy. *J. Am. Chem. Soc.* **2010**, *132*, 260-267.
32. Chang, H.; Tang, L.; Wang, Y.; Jiang, J.; Li, J. Graphene Fluorescence Resonance Energy Transfer Aptasensor for the Thrombin Detection. *Anal. Chem.* **2010**, *82*, 2341-2346.

33. Lu, C.-H.; Li, J.; Zhang, X.-L.; Zheng, A.-X.; Yang, H.-H.; Chen, X.; Chen, G.-N. General Approach for Monitoring Peptide–Protein Interactions Based on Graphene–Peptide Complex. *Anal. Chem.* **2011**, *83*, 7276–7282.
34. Li, F.; Huang, Y.; Yang, Q.; Zhong, Z.; Li, D.; Wang, L.; Song, S.; Fan, C. A Graphene-Enhanced Molecular Beacon for Homogeneous DNA Detection. *Nanoscale* **2010**, *2*, 1021–1026.
35. Ranasinghe, R. T.; Brown, T. Fluorescence Based Strategies for Genetic Analysis. *Chem Commun* **2005**, 5487–5502.
36. Li, Q.; Luan, G.; Guo, Q.; Liang, J. A New Class of Homogeneous Nucleic Acid Probes Based on Specific Displacement Hybridization. *Nucleic Acids Res.* **2002**, *30*, E5.
37. Ingale, S. A.; Pujari, S. S.; Sirivolu, V. R.; Ding, P.; Xiong, H.; Mei, H.; Seela, F. 7-Deazapurine and 8-Aza-7-deazapurine Nucleoside and Oligonucleotide Pyrene “Click” Conjugates: Synthesis, Nucleobase Controlled Fluorescence Quenching, and Duplex Stability. *J. Org. Chem.* **2012**, *77*, 188–199.
38. Blanchard, D. J. M.; Fadock, K. L.; Sproviero, M.; Deore, P. S.; Cservenyi, T. Z.; Manderville, R. A.; Sharma, P.; Wetmore, S. D. Photophysical Properties of Push-Pull 8-Aryl-Deoxyguanosine Probes within Duplex and G-Quadruplex Structures. *J. Mater. Chem. C* **2016**, *4*, 2915–2924.
39. Manderville, R. A.; Wetmore, S. D. C-Linked 8-Aryl Guanine Nucleobase Adducts: Biological Outcomes and Utility as Fluorescent Probes. *Chem. Sci.* **2016**, *7*, 3482–3493.
40. Xu, W.; Chan, K. M.; Kool, E. T. Fluorescent Nucleobases as Tools for Studying DNA and Rna. *Nat. Chem.* **2017**, *9*, 1043–1055.
41. Shaughnessy, K. Palladium-Catalyzed Modification of Unprotected Nucleosides, Nucleotides, and Oligonucleotides. *Molecules* **2015**, *20*, 9419.
42. Okamoto, A.; Tanaka, K.; Fukuta, T.; Saito, I. Design of Base-Discriminating Fluorescent Nucleoside and Its Application to T/C SNP Typing. *J. Am. Chem. Soc.* **2003**, *125*, 9296–9297.
43. Okamoto, A.; Tanaka, K.; Fukuta, T.; Saito, I. Cytosine Detection by a Fluorescein-Labeled Probe Containing Base-Discriminating Fluorescent Nucleobase. *ChemBioChem* **2004**, *5*, 958–963.

44. Leonard, N. J.; Sprecker, M. A.; Morrice, A. G. Defined Dimensional Changes in Enzyme Substrates and Cofactors. Synthesis of *lin*-Benzoadenosine and Enzymic Evaluation of Derivatives of the Benzopurines. *J. Am. Chem. Soc.* **1976**, *98*, 3987-3994.
45. Krueger, A. T.; Kool, E. T. Fluorescence of Size-Expanded DNA Bases: Reporting on DNA Sequence and Structure with an Unnatural Genetic Set. *J. Am. Chem. Soc.* **2008**, *130*, 3989-3999.
46. Shin, D.; Sinkeldam, R. W.; Tor, Y. Emissive RNA Alphabet. *J. Am. Chem. Soc.* **2011**, *133*, 14912-14915.
47. Srivatsan, S. G.; Weizman, H.; Tor, Y. A Highly Fluorescent Nucleoside Analog Based on Thieno[3,4-D]Pyrimidine Senses Mismatched Pairing. *Org. Biomol. Chem.* **2008**, *6*, 1334-1338.
48. Srivatsan, S. G.; Greco, N. J.; Tor, Y. A Highly Emissive Fluorescent Nucleoside that Signals the Activity of Toxic Ribosome-Inactivating Proteins. *Angew. Chem.* **2008**, *120*, 6763-6767.
49. Inoue, H.; Imura, A.; Ohtsuka, E. Synthesis of Dodecadeoxyribonucleotides Containing a Pyrrolo[2, 3-d]pyrimidine Nucleoside and their Base-pairing Ability. *Nippon Kagaku Kaishi* **1987**, *1987*, 1214-1220.
50. Woo, J.; Meyer, J. R. B.; Gamper, H. B. G/C-Modified Oligodeoxynucleotides with Selective Complementarity: Synthesis and Hybridization Properties. *Nucleic Acids Res.* **1996**, *24*, 2470-2475.
51. Berry, D. A.; Jung, K.-Y.; Wise, D. S.; Sercel, A. D.; Pearson, W. H.; Mackie, H.; Randolph, J. B.; Somers, R. L. Pyrrolo-dc and Pyrrolo-C: Fluorescent Analogs of Cytidine and 2'-Deoxycytidine for the Study of Oligonucleotides. *Tetrahedron Lett.* **2004**, *45*, 2457-2461.
52. Liu, C.; Martin, C. T. Promoter Clearance by T7 RNA Polymerase: Initial Bubble Collapse and Transcript Dissociation Monitored by Base Analog Fluorescence. *J. Biol. Chem.* **2002**, *277*, 2725-2731.
53. Hudson, R. H. E.; Ghorbani-Choghamarani, A. Selective Fluorometric Detection of Guanosine-Containing Sequences by 6-Phenylpyrrolocytidine in DNA. *Synlett* **2007**, *2007*, 0870-0873.

54. Wahba, A. S.; Azizi, F.; Deleavey, G. F.; Brown, C.; Robert, F.; Carrier, M.; Kalota, A.; Gewirtz, A. M.; Pelletier, J.; Hudson, R. H.; Damha, M. J. Phenylpyrrolocytosine as an Unobtrusive Base Modification for Monitoring Activity and Cellular Trafficking of siRNA. *ACS Chem. Biol.* **2011**, *6*, 912-919.
55. Wahba, A. S.; Esmaili, A.; Damha, M. J.; Hudson, R. H. E. A Single-Label Phenylpyrrolocytidine Provides a Molecular Beacon-Like Response Reporting HIV-1 RT RNase H Activity. *Nucleic Acids Res.* **2010**, *38*, 1048-1056.
56. Ward, D. C.; Reich, E.; Stryer, L. Fluorescence Studies of Nucleotides and Polynucleotides: I. Formycin, 2-Aminopurine Riboside, 2,6-Diaminopurine Riboside, and their Derivatives. *J. Biol. Chem.* **1969**, *244*, 1228-1237.
57. Sowers, L. C.; Boulard, Y.; Fazakerley, G. V. Multiple Structures for the 2-Aminopurine–Cytosine Mismatch. *Biochemistry* **2000**, *39*, 7613-7620.
58. Hardman, S. J. O.; Thompson, K. C. Influence of Base Stacking and Hydrogen Bonding on the Fluorescence of 2-Aminopurine and Pyrrolocytosine in Nucleic Acids. *Biochemistry* **2006**, *45*, 9145-9155.
59. Degtyareva, N. N.; Reddish, M. J.; Sengupta, B.; Petty, J. T. Structural Studies of a Trinucleotide Repeat Sequence Using 2-Aminopurine. *Biochemistry* **2009**, *48*, 2340-2346.
60. Rachofsky, E. L.; Seibert, E.; Stivers, J. T.; Osman, R.; Ross, J. B. A. Conformation and Dynamics of Abasic Sites in DNA Investigated by Time-Resolved Fluorescence of 2-Aminopurine. *Biochemistry* **2001**, *40*, 957-967.
61. Nadler, A.; Strohmeier, J.; Diederichsen, U. 8-Vinyl-2'-deoxyguanosine as a Fluorescent 2'-Deoxyguanosine Mimic for Investigating DNA Hybridization and Topology. *Angew. Chem., Int. Ed.* **2011**, *50*, 5392-5396.
62. Greco, N. J.; Tor, Y. Furan Decorated Nucleoside Analogues as Fluorescent Probes: Synthesis, Photophysical Evaluation, and Site-Specific Incorporation. *Tetrahedron* **2007**, *63*, 3515-3527.
63. Tanpure, A. A.; Pawar, M. G.; Srivatsan, S. G. Fluorescent Nucleoside Analogs: Probes for Investigating Nucleic Acid Structure and Function. *Isr. J. Chem.* **2013**, *53*, 366-378.

64. Greco, N. J.; Tor, Y. Simple Fluorescent Pyrimidine Analogues Detect The Presence of DNA Abasic Sites. *J. Am. Chem. Soc.* **2005**, *127*, 10784-10785.
65. Yamana, K.; Zako, H.; Asazuma, K.; Iwase, R.; Nakano, H.; Murakami, A. Fluorescence Detection of Specific RNA Sequences Using 2'-Pyrene-Modified Oligoribonucleotides *Angew. Chem., Int. Ed. Engl.* **2001**, *40*, 1104-1106.
66. Saito, Y.; Miyauchi, Y.; Okamoto, A.; Saito, I. Base-Discriminating Fluorescent (BDF) Nucleoside: Distinction of Thymine by Fluorescence Quenching. *Chem Commun* **2004**, 1704-1705.
67. Saito, Y.; Miyauchi, Y.; Okamoto, A.; Saito, I. Synthesis and Properties of Novel Base-Discriminating Fluorescent (BDF) Nucleosides: A Highly Polarity-Sensitive Fluorophore for SNP Typing. *Tetrahedron Lett.* **2004**, *45*, 7827-7831.
68. Kim, K. T.; Choi, T. S.; Kim, K. Y.; Kim, H. I.; Kim, B. H. Disassembly of Chromophore-Guided DNA Duplexes through Site-Selective Binding of Coralyne to Pyrene-Modified Adenine Bases. *ChemPlusChem* **2016**, *81*, 590-593.
69. Seo, Y. J.; Lee, I. J.; Yi, J. W.; Kim, B. H. Probing the Stable G-Quadruplex Transition Using Quencher-Free End-Stacking Ethynyl Pyrene-Adenosine. *Chem. Commun.* **2007**, 2817-2819.
70. Kaura, M.; Kumar, P.; Hrdlicka, P. J. Synthesis, Hybridization Characteristics, and Fluorescence Properties of Oligonucleotides Modified with Nucleobase-Functionalized Locked Nucleic Acid Adenosine and Cytidine Monomers. *J. Org. Chem.* **2014**, *79*, 6256-6268.
71. Kumar, T. S.; Madsen, A. S.; Østergaard, M. E.; Sau, S. P.; Wengel, J.; Hrdlicka, P. J. Functionalized 2'-Amino-L-LNA: Directed Positioning of Intercalators for DNA Targeting. *J. Org. Chem.* **2009**, *74*, 1070-1081.
72. Dohno, C.; Saito, I. Discrimination of Single-Nucleotide Alterations by G-Specific Fluorescence Quenching. *ChemBioChem* **2005**, *6*, 1075-1081.
73. Okamoto, A.; Ochi, Y.; Saito, I. Fluorometric Sensing of the Salt-Induced B-Z DNA Transition by Combination of Two Pyrene-Labeled Nucleobases. *Chem. Commun.* **2005**, 1128-1130.

74. Mayer, E.; Valis, L.; Wagner, C.; Rist, M.; Amann, N.; Wagenknecht, H. A. 1-Ethynylpyrene as a Tunable and Versatile Molecular Beacon for DNA. *ChemBioChem* **2004**, *5*, 865-868.
75. Varghese, R.; Wagenknecht, H.-A. White-Light-Emitting DNA (WED). *Chem. Eur. J.* **2009**, *15*, 9307-9310.
76. Nielsen, P.; Egholm, M.; Berg, R.; Buchardt, O. Sequence-Selective Recognition of DNA by Strand Displacement with a Thymine-Substituted Polyamide. *Science* **1991**, *254*, 1497-1500.
77. Hyrup, B.; Nielsen, P. E. Peptide Nucleic Acids (PNA): Synthesis, Properties and Potential Applications. *Bioorg. Med. Chem.* **1996**, *4*, 5-23.
78. Paulasova, P.; Pellestor, F. The Peptide Nucleic Acids (PNAs): A New Generation of Probes for Genetic and Cytogenetic Analyses. *Ann. Genet.* **2004**, *47*, 349-358.
79. Eugen, U.; Anusch, P.; Gerhard, B.; W., W. D. PNA: Synthetic Polyamide Nucleic Acids with Unusual Binding Properties. *Angew. Chem., Int. Ed.* **1998**, *37*, 2796-2823.
80. Egholm, M.; Buchardt, O.; Christensen, L.; Behrens, C.; Freier, S. M.; Driver, D. A.; Berg, R. H.; Kim, S. K.; Norden, B.; Nielsen, P. E. PNA Hybridizes to Complementary Oligonucleotides Obeying the Watson-Crick Hydrogen-Bonding Rules. *Nature* **1993**, *365*, 566.
81. Roberto, C.; Stefano, S.; Tullia, T.; Filbert, T.; Alex, M.; Rosangela, M. Peptide Nucleic Acids with a Structurally Biased Backbone. Updated Review and Emerging Challenges. *Curr. Top. Dev. Biol.* **2011**, *11*, 1535-1554.
82. Pokorski, J. K.; Witschi, M. A.; Purnell, B. L.; Appella, D. H. (*S,S*)-trans-Cyclopentane-Constrained Peptide Nucleic Acids. A General Backbone Modification that Improves Binding Affinity and Sequence Specificity. *J. Am. Chem. Soc.* **2004**, *126*, 15067-15073.
83. Suparpprom, C.; Srisuwannaket, C.; Sangvanich, P.; Vilaivan, T. Synthesis and Oligodeoxynucleotide Binding Properties of PyrrolidinyI Peptide Nucleic Acids Bearing Prolyl-2-Aminocyclopentanecarboxylic Acid (ACPC) Backbones. *Tetrahedron Lett.* **2005**, *46*, 2833-2837.

84. Vilaivan, C.; Srisuwannaket, C.; Ananthanawat, C.; Suparpprom, C.; Kawakami, J.; Yamaguchi, Y.; Tanaka, Y.; Vilaivan, T. Pyrrolidinyl Peptide Nucleic Acid with α/β -Peptide Backbone: A Conformationally Constrained PNA with Unusual Hybridization Properties. *Artif DNA PNA XNA* **2011**, *2*, 50-59.
85. Dragulescu-Andrasi, A.; Rapireddy, S.; Frezza, B. M.; Gayathri, C.; Gil, R. R.; Ly, D. H. A Simple γ -Backbone Modification Preorganizes Peptide Nucleic Acid into a Helical Structure. *J. Am. Chem. Soc.* **2006**, *128*, 10258-10267.
86. Vilaivan, T. Pyrrolidinyl PNA with α/β -Dipeptide Backbone: From Development to Applications. *Acc. Chem. Res.* **2015**, *48*, 1645-56.
87. Sabale, P. M.; Srivatsan, S. G. Responsive Fluorescent PNA Analogue as a Tool for Detecting G-quadruplex Motifs of Oncogenes and Activity of Toxic Ribosome-Inactivating Proteins. *ChemBioChem* **2016**, *17*, 1665-1673.
88. Sabale, P. M.; George, J. T.; Srivatsan, S. G. A Base-Modified PNA-Graphene Oxide Platform as a Turn-On Fluorescence Sensor for the Detection of Human Telomeric Repeats. *Nanoscale* **2014**, *6*, 10460-10469.
89. Wojciechowski, F.; Hudson, R. H. E. Fluorescence and Hybridization Properties of Peptide Nucleic Acid Containing a Substituted Phenylpyrrolocytosine Designed to Engage Guanine with an Additional H-Bond. *J. Am. Chem. Soc.* **2008**, *130*, 12574-12575.
90. Vilaivan, T. Fluorogenic PNA Probes. *Beilstein J. Org. Chem.* **2018**, *14*, 253-281.
91. Boonlua, C.; Vilaivan, C.; Wagenknecht, H. A.; Vilaivan, T. 5-(Pyren-1-yl)uracil as a Base-Discriminating Fluorescent Nucleobase in Pyrrolidinyl Peptide Nucleic Acids. *Chem. Asian J.* **2011**, *6*, 3251-3259.
92. Reenabthue, N.; Boonlua, C.; Vilaivan, C.; Vilaivan, T.; Suparpprom, C. 3-Aminopyrrolidine-4-Carboxylic Acid as Versatile Handle for Internal Labeling of Pyrrolidinyl PNA. *Bioorg. Med. Chem. Lett.* **2011**, *21*, 6465-6469.
93. Boonlua, C.; Ditmangklo, B.; Reenabthue, N.; Suparpprom, C.; Poomsuk, N.; Siriwong, K.; Vilaivan, T. Pyrene-Labeled Pyrrolidinyl Peptide Nucleic Acid as a Hybridization-Responsive DNA Probe: Comparison Between Internal and Terminal Labeling. *RSC Adv.* **2014**, *4*, 8817-8827.

94. Ditmangklo, B.; Boonlua, C.; Suparpprom, C.; Vilaivan, T. Reductive Alkylation and Sequential Reductive Alkylation-Click Chemistry for On-Solid-Support Modification of Pyrrolidinyl Peptide Nucleic Acid. *Bioconjugate Chem.* **2013**, *24*, 614-625.
95. Yotapan, N.; Charoenpakdee, C.; Wathanathavorn, P.; Ditmangklo, B.; Wagenknecht, H.-A.; Vilaivan, T. Synthesis and Optical Properties of Pyrrolidinyl Peptide Nucleic Acid Carrying a Clicked Nile Red Label. *Beilstein J. Org. Chem.* **2014**, *10*, 2166-2174.
96. Yotapan, N.; Nim-anussornkul, D.; Vilaivan, T. Pyrrolidinyl Peptide Nucleic Acid Terminally Labeled with Fluorophore and End-Stacking Quencher as a Probe for Highly Specific DNA Sequence Discrimination. *Tetrahedron* **2016**, *72*, 7992-7999.
97. Boonlua, C.; Charoenpakdee, C.; Vilaivan, T.; Praneenarat, T. Preparation and Performance Evaluation of a Pyrrolidinyl Peptide Nucleic-Acid-Based Displacement Probe as a DNA Sensor. *ChemistrySelect* **2016**, *1*, 5691-5697.
98. Hocek, M. Synthesis of Base-Modified 2'-Deoxyribonucleoside Triphosphates and their Use in Enzymatic Synthesis of Modified DNA for Applications in Bioanalysis and Chemical Biology. *J. Org. Chem.* **2014**, *79*, 9914-9921.
99. Sinkeldam, R. W.; Greco, N. J.; Tor, Y. Fluorescent Analogs of Biomolecular Building Blocks: Design, Properties, and Applications. *Chem. Rev.* **2010**, *110*, 2579-2619.
100. Teo, Y. N.; Kool, E. T. DNA-Multichromophore Systems. *Chem. Rev.* **2012**, *112*, 4221-4245.
101. Omumi, A.; Beach, D. G.; Baker, M.; Gabryelski, W.; Manderville, R. A. Postsynthetic Guanine Arylation of DNA by Suzuki-Miyaura Cross-Coupling. *J. Am. Chem. Soc.* **2011**, *133*, 42-50.
102. Lercher, L.; McGouran, J. F.; Kessler, B. M.; Schofield, C. J.; Davis, B. G. DNA Modification under Mild Conditions by Suzuki-Miyaura Cross-Coupling for the Generation of Functional Probes. *Angew. Chem., Int. Ed.* **2013**, *52*, 10553-10558.
103. Li, N.; Lim, R. K. V.; Edwardraja, S.; Lin, Q. Copper-Free Sonogashira Cross-Coupling for Functionalization of Alkyne-Encoded Proteins in Aqueous Medium and in Bacterial Cells. *J. Am. Chem. Soc.* **2011**, *133*, 15316-15319.

104. Hauke, S.; Best, M.; Schmidt, T. T.; Baalman, M.; Krause, A.; Wombacher, R. Two-Step Protein Labeling Utilizing Lipoic Acid Ligase and Sonogashira Cross-Coupling. *Bioconjugate Chem.* **2014**, *25*, 1632-1637.
105. El-Sagheer, A. H.; Brown, T. Click Chemistry with DNA. *Chem. Soc. Rev.* **2010**, *39*, 1388-1405.
106. Wang, X.; Hudson, R. H. E. PNA Molecular Beacons Assembled by Post-Synthetic Click Chemistry Functionalization. *ChemBioChem* **2015**, *16*, 2156-2161.
107. Cao, N.; Zhang, Y. Study of Reduced Graphene Oxide Preparation by Hummers' Method and Related Characterization. *J. Nanomater.* **2015**, *2015*, 5.
108. Vilaivan, T.; Srisuwannaket, C. Hybridization of Pyrrolidinyl Peptide Nucleic Acids and DNA: Selectivity, Base-Pairing Specificity, and Direction of Binding. *Org. Lett.* **2006**, *8*, 1897-1900.
109. Bang, E. K.; Won, J.; Moon, D.; Lee, J. Y.; Kim, B. H. A Self-Complementary Nucleoside: Synthesis, Solid-State Structure, and Fluorescence Behavior. *Chem. Asian J.* **2011**, *6*, 2048-2054.
110. Mansawat, W.; Boonlua, C.; Siriwong, K.; Vilaivan, T. Clicked Polycyclic Aromatic Hydrocarbon as a Hybridization-Responsive Fluorescent Artificial Nucleobase in Pyrrolidinyl Peptide Nucleic Acids. *Tetrahedron* **2012**, *68*, 3988-3995.
111. Mešičić, A.; Harej, A.; Klobučar, M.; Glavač, D.; Cetina, M.; Pavelić, S. K.; Raić-Malić, S. Discovery of New Acid Ceramidase-Targeted Acyclic 5-Alkynyl and 5-Heteroaryl Uracil Nucleosides. *ACS Med. Chem. Lett.* **2015**, *6*, 1150-1155.
112. Srisuwannaket, C. Synthesis and DNA-Binding Properties of Novel Peptide Nucleic Acids Bearing (1S,2S)-2-Aminocyclopentane Carboxylic Acid Spacer. Chulalongkorn University, Thailand, 2005.
113. Ngamviriyavong, P. Synthesis of Peptide Nucleic Acid Containing Aminoethyl Linkers. Chulalongkorn University, Thailand, 2004.
114. Wilhelmsson, L. M. Fluorescent Nucleic Acid Base Analogues. *Quarterly Reviews of Biophysics* **2010**, *43*, 159-183.
115. Maneelun, N.; Vilaivan, T. Dual Pyrene-Labeled Pyrrolidinyl Peptide Nucleic Acid as an Excimer-To-Monomer Switching Probe for DNA Sequence Detection. *Tetrahedron* **2013**, *69*, 10805-10810.

116. Manicardi, A.; Guidi, L.; Ghidini, A.; Corradini, R. Pyrene-Modified PNAs: Stacking Interactions and Selective Excimer Emission in PNA2DNA Triplexes. *Beilstein J. Org. Chem.* **2014**, *10*, 1495-503.
117. Seo, Y. J.; Jeong, H. S.; Bang, E.-K.; Hwang, G. T.; Jung, J. H.; Jang, S. K.; Kim, B. H. Cholesterol-Linked Fluorescent Molecular Beacons with Enhanced Cell Permeability. *Bioconjugate Chem.* **2006**, *17*, 1151-1155.
118. Mayer, E.; Valis, L.; Wagner, C.; Rist, M.; Amann, N.; Wagenknecht, H. A. 1-Ethynylpyrene as a Tunable and Versatile Molecular Beacon for DNA. *ChemBioChem* **2004**, *5*, 865-868.
119. Kim, K. T.; Heo, W.; Joo, T.; Kim, B. H. Photophysical and Structural Investigation of a PyA-Modified Adenine Cluster: Its Potential Use for Fluorescent DNA Probes Exhibiting Distinct Emission Color Changes. *Org. Biomol. Chem.* **2015**, *13*, 8470-8478.
120. Seo, Y. J.; Rhee, H.; Joo, T.; Kim, B. H. Self-Duplex Formation of an A^{Py}-Substituted Oligodeoxyadenylate and Its Unique Fluorescence. *J. Am. Chem. Soc.* **2007**, *129*, 5244-5247.
121. Seo, Y. J.; Hwang, G. T.; Kim, B. H. Quencher-Free Molecular Beacon Systems with Two Pyrene Units in the Stem Region. *Tetrahedron Lett.* **2006**, *47*, 4037-4039.
122. Lee, I. J.; Kim, B. H. Monitoring i-motif Transitions Through the Exciplex Emission of a Fluorescent Probe Incorporating Two ^{Py}A Units. *Chem. Commun.* **2012**, *48*, 2074-2076.
123. Seo, Y. J.; Ryu, J. H.; Kim, B. H. Quencher-Free, End-Stacking Oligonucleotides for Probing Single-Base Mismatches in DNA. *Org. Lett.* **2005**, *7*, 4931-3.
124. Lowe, G.; Vilaivan, T. Amino Acids Bearing Nucleobases for the Synthesis of Novel Peptide Nucleic Acids. *J. Chem. Soc., Perkin Trans. 1* **1997**, 539-546.
125. Suparpprom, C. Synthesis and Nucleic Acid Binding Properties of Novel Peptide Nucleic Acids Carrying Beta Amino Acid Spacer. Chulalongkorn University, Thailand, 2006.
126. Hartsel, S. A.; Marshall, W. S. Synthesis of 9-(4-Thioxylofuranosyl)adenine via a Novel Glycosylation Reaction. *Tetrahedron Lett.* **1998**, *39*, 205-208.

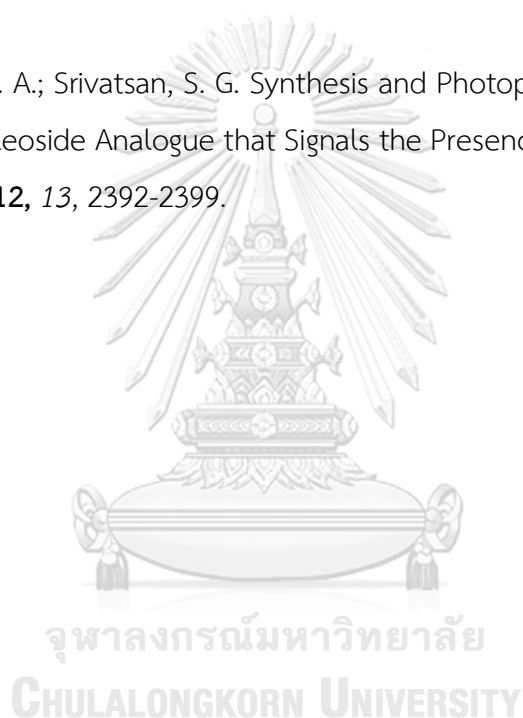
127. Clima, L.; Bannwarth, W. Building-Block Approach for the Straightforward Incorporation of a New FRET (Fluorescence-Resonance-Energy Transfer) System into Synthetic DNA. *Helv. Chim. Acta* **2008**, *91*, 165-175.
128. Mechanisms and Dynamics of Fluorescence Quenching. In *Principles of Fluorescence Spectroscopy*, Lakowicz, J. R., Ed. Springer US: Boston, MA, 2006; pp 331-351.
129. Wilson, J. N.; Cho, Y.; Tan, S.; Cuppoletti, A.; Kool, E. T. Quenching of Fluorescent Nucleobases by Neighboring DNA: The "Insulator" Concept. *ChemBioChem* **2008**, *9*, 279-285.
130. Avirah, R. R.; Schuster, G. B. Fluorescence Quenching by Intercalation of a Pyrene Group Tethered to an N4-modified Cytosine in Duplex DNA. *Photochem. Photobiol.* **2013**, *89*, 332-335.
131. Liu, Z.; Liu, B.; Ding, J.; Liu, J. Fluorescent Sensors Using DNA-Functionalized Graphene Oxide. *Anal. Bioanal. Chem.* **2014**, *406*, 6885-6902.
132. Lu, C. H.; Yang, H. H.; Zhu, C. L.; Chen, X.; Chen, G. N. A Graphene Platform for Sensing Biomolecules. *Angew. Chem., Int. Ed.* **2009**, *48*, 4785-4787.
133. He, S.; Song, B.; Li, D.; Zhu, C.; Qi, W.; Wen, Y.; Wang, L.; Song, S.; Fang, H.; Fan, C. A Graphene Nanoprobe for Rapid, Sensitive, and Multicolor Fluorescent DNA Analysis. *Adv. Funct. Mater.* **2010**, *20*, 453-459.
134. Songwei, Z.; Liang, C.; Yu, W.; Junlang, C. Exploration on the Mechanism of DNA Adsorption on Graphene and Graphene Oxide via Molecular Simulations. *J. Phys. D: Appl. Phys.* **2015**, *48*, 275402.
135. Kotikam, V.; Fernandes, M.; Kumar, V. A. Comparing the Interactions of DNA, Polyamide (PNA) and Polycarbamate Nucleic Acid (PCNA) Oligomers with Graphene Oxide (GO). *Phys. Chem. Chem. Phys.* **2012**, *14*, 15003-15006.
136. Guo, S.; Du, D.; Tang, L.; Ning, Y.; Yao, Q.; Zhang, G.-J. PNA-Assembled Graphene Oxide for Sensitive and Selective Detection Of DNA. *Analyst* **2013**, *138*, 3216-3220.
137. Lee, J.; Park, G.; Min, D.-H. A Biosensor for The Detection of Single Base Mismatches in Microrna. *Chem. Commun.* **2015**, *51*, 14597-14600.
138. Liu, B.; Sun, Z.; Zhang, X.; Liu, J. Mechanisms of DNA Sensing on Graphene Oxide. *Anal. Chem.* **2013**, *85*, 7987-7993.

139. Kim, K. T.; Veedu, R. N.; Seo, Y. J.; Kim, B. H. Quencher-Free Molecular Beacons as Probes for Oligonucleotides Containing CAG Repeat Sequences. *Chem. Commun.* **2014**, *50*, 1561-1563.
140. Krench, M.; Littleton, J. T., Chapter Six - Neurotoxicity Pathways in Drosophila Models of the Polyglutamine Disorders. In *Current Topics in Developmental Biology*, Pick, L., Ed. Academic Press: 2017; Vol. 121, pp 201-223.
141. Li, J.; Liu, Y.; Zhu, X.; Chang, G.; He, H.; Zhang, X.; Wang, S. A Novel Electrochemical Biosensor Based on a Double-Signal Technique for d(CAG)_n Trinucleotide Repeats. *ACS Appl. Mater. Interfaces* **2017**, *9*, 44231-44240.
142. Fujimoto, J.; Bando, T.; Minoshima, M.; Uchida, S.; Iwasaki, M.; Shinohara, K.-i.; Sugiyama, H. Detection of Triplet Repeat Sequences in the Double-Stranded DNA Using Pyrene-Functionalized Pyrrole-Imidazole Polyamides with Rigid Linkers. *Bioorg. Med. Chem.* **2008**, *16*, 5899-5907.
143. Komiyama, M.; Ye, S.; Liang; Yamamoto, Y.; Tomita, T.; Zhou, J.-M.; Aburatani, H. PNA for One-Base Differentiating Protection of DNA from Nuclease and Its Use for SNPs Detection. *J. Am. Chem. Soc.* **2003**, *125*, 3758-3762.
144. Ye, S.; Miyajima, Y.; Ohnishi, T.; Yamamoto, Y.; Komiyama, M. Combination of Peptide Nucleic Acid Beacon and Nuclease S1 for Clear-Cut Genotyping of Single Nucleotide Polymorphisms. *Anal. Biochem.* **2007**, *363*, 300-302.
145. Krotz, A. H.; Rentel, C.; Gorman, D.; Olsen, P.; Gaus, H. J.; McArdle, J. V.; Scozzari, A. N. Solution Stability and Degradation Pathway of Deoxyribonucleoside Phosphoramidites in Acetonitrile. *Nucleosides, Nucleotides Nucleic Acids* **2004**, *23*, 767-775.
146. Morales, J. C.; Kool, E. T. Minor Groove Interactions between Polymerase and DNA: More Essential to Replication than Watson-Crick Hydrogen Bonds? *J. Am. Chem. Soc.* **1999**, *121*, 2323-2324.
147. Spratt, T. E. Identification of Hydrogen Bonds between Escherichia coli DNA Polymerase I (Klenow fragment) and the Minor Groove of DNA by Amino Acid Substitution of the Polymerase and Atomic Substitution of the DNA. *Biochemistry* **2001**, *40*, 2647-2652.

148. Rist, M.; Amann, N.; Wagenknecht, H. A. Preparation of 1-Ethynylpyrene-Modified DNA via Sonogashira-Type Solid-Phase Couplings and Characterization of the Fluorescence Properties for Electron-Transfer Studies. *Eur. J. Org. Chem.* **2003**, *2003*, 2498-2504.
149. Chalker, J. M.; Wood, C. S. C.; Davis, B. G. A Convenient Catalyst for Aqueous and Protein Suzuki–Miyaura Cross-Coupling. *J. Am. Chem. Soc.* **2009**, *131*, 16346-16347.
150. Hwang, G. T.; Seo, Y. J.; Kim, S. J.; Kim, B. H. Fluorescent Oligonucleotide Incorporating 5-(1-Ethynylpyrenyl)-2'-Deoxyuridine: Sequence-Specific Fluorescence Changes upon Duplex Formation. *Tetrahedron Lett.* **2004**, *45*, 3543-3546.
151. Lee, H. J.; Go, G. H.; Ro, J. J.; Kim, B. H. Detection of Cofilin Mrna By Hybridization-Sensitive Double-Stranded Fluorescent Probes. *RSC Adv.* **2018**, *8*, 7514-7517.
152. Sonogashira, K. Development of Pd–Cu Catalyzed Cross-Coupling of Terminal Acetylenes with sp^2 -Carbon Halides. *J. Organomet. Chem.* **2002**, *653*, 46-49.
153. Aucagne, V.; Amblard, F.; Agrofoglio, L. A. Highly Efficient $AgNO_3$ -Catalyzed Preparation of Substituted Furano-pyrimidine Nucleosides. *Synlett* **2004**, *2004*, 2406-2408.
154. Hudson, R. H. E.; Ghorbani-Choghamarani, A. Oligodeoxynucleotides Incorporating Structurally Simple 5-Alkynyl-2'-Deoxyuridines Fluorometrically Respond to Hybridization. *Org. Biomol. Chem.* **2007**, *5*, 1845-1848.
155. Axel, S.; Morten, M.; Renil, M.; Hans, P.; Klaus, B. Direct Solid-Phase Glycosylations of Peptide Templates on a Novel PEG-Based Resin. *Angew. Chem., Int. Ed. Engl.* **1997**, *36*, 1976-1978.
156. Ettles, C. M. Progress Toward Synthesis of Molecular Beacons Incorporating Dabcyl Analog Quenchers. Electronic Thesis and Dissertation Repository, The University of Western Ontario, 2013.
157. Malakhov, A. D.; Malakhova, E. V.; Kuznitsova, S. V.; Grechishnikova, I. V.; Prokhorenko, I. A.; Skorobogaty, M. V.; Korshun, V. A.; Berlin, Y. A. Synthesis and Fluorescent Properties of 5-(1-Pyrenylethynyl)-2'-Deoxyuridine-Containing Oligodeoxynucleotides. *Russ. J. Bioorg. Chem.* **2000**, *26*, 34-44.

158. Hana, C.; Andres, J. Nucleoside-Based Diarylethene Photoswitches and Their Facile Incorporation into Photoswitchable DNA. *Angew. Chem., Int. Ed.* **2013**, *52*, 3186-3190.
159. Darses, S.; Genet, J.-P. Potassium Organotrifluoroborates: New Perspectives in Organic Synthesis. *Chem. Rev.* **2008**, *108*, 288-325.
160. Lennox, A. J.; Lloyd-Jones, G. C. The Slow-Release Strategy in Suzuki–Miyaura Coupling. *Isr. J. Chem.* **2010**, *50*, 664-674.
161. Darses, S.; Genêt, J.-P.; Brayer, J.-L.; Demoute, J.-P. Cross-Coupling Reactions of Arenediazonium Tetrafluoroborates with Potassium Aryl- or Alkenyltrifluoroborates Catalyzed By Palladium. *Tetrahedron Lett.* **1997**, *38*, 4393-4396.
162. Molander, G.; Canturk, B. Organotrifluoroborates and Monocoordinated Palladium Complexes as Catalysts-A Perfect Combination for Suzuki–Miyaura Coupling. *Angew. Chem., Int. Ed.* **2009**, *48*, 9240-9261.
163. Butters, M.; Harvey, J.; Jover, J.; Lennox, A. J.; Lloyd-Jones, G. C.; Murray, P. Aryl Trifluoroborates in Suzuki–Miyaura Coupling: The Roles of Endogenous Aryl Boronic Acid and Fluoride. *Angew. Chem., Int. Ed.* **2010**, *49*, 5156-5160.
164. Lennox, A. J.; Lloyd-Jones, G. C. Organotrifluoroborate Hydrolysis: Boronic Acid Release Mechanism and an Acid–Base Paradox in Cross-Coupling. *J. Am. Chem. Soc.* **2012**, *134*, 7431-7441.
165. Batey, R. A.; Quach, T. D. Synthesis and Cross-Coupling Reactions of Tetraalkylammonium Organotrifluoroborate Salts. *Tetrahedron Lett.* **2001**, *42*, 9099-9103.
166. Shaughnessy, K. H. Beyond TPPTS: New Approaches to the Development of Efficient Palladium-Catalyzed Aqueous-Phase Cross-Coupling Reactions. *Eur. J. Org. Chem.* **2006**, *2006*, 1827-1835.
167. Western, E. C.; Daft, J. R.; Johnson, E. M.; Gannett, P. M.; Shaughnessy, K. H. Efficient One-Step Suzuki Arylation of Unprotected Halonucleosides, Using Water-Soluble Palladium Catalysts. *J. Org. Chem.* **2003**, *68*, 6767-6774.
168. Vongsutilers, V.; Daft, J.; Shaughnessy, K.; Gannett, P. A General Synthesis of C8-Aryl-purine Phosphoramidites. *Molecules* **2009**, *14*, 3339.

169. Capek, P.; Pohl, R.; Hocek, M. Cross-Coupling Reactions of Unprotected Halopurine Bases, Nucleosides, Nucleotides and Nucleoside Triphosphates with 4-Boronophenylalanine in Water. Synthesis of (purin-8-yl)- and (purin-6-yl)Phenylalanines. *Org. Biomol. Chem.* **2006**, *4*, 2278-2284.
170. Molander, G. A.; Ellis, N. M. Linchpin Synthons: Metalation of Aryl Bromides Bearing a Potassium Trifluoroborate Moiety. *J. Org. Chem.* **2006**, *71*, 7491-7493.
171. Molander, G. A.; Cavalcanti, L. N.; Canturk, B.; Pan, P.-S.; Kennedy, L. E. Efficient Hydrolysis of Organotrifluoroborates via Silica Gel and Water. *J. Org. Chem.* **2009**, *74*, 7364-7369.
172. Tanpure, A. A.; Srivatsan, S. G. Synthesis and Photophysical Characterisation of a Fluorescent Nucleoside Analogue that Signals the Presence of an Abasic Site in RNA. *ChemBioChem* **2012**, *13*, 2392-2399.





APPENDIX

จุฬาลงกรณ์มหาวิทยาลัย
CHULALONGKORN UNIVERSITY

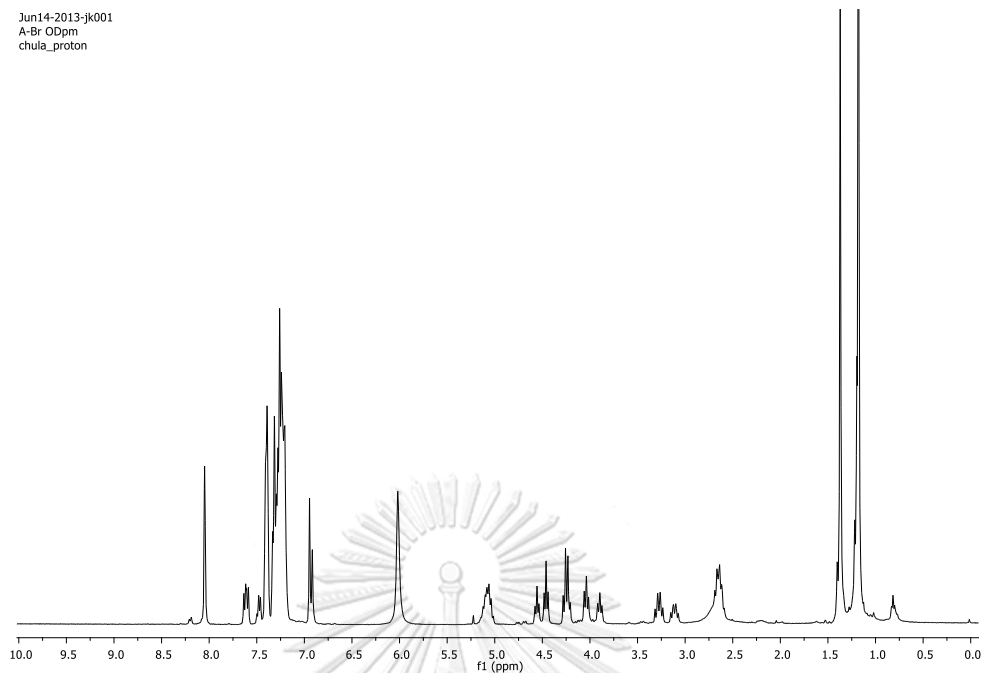


Figure A1. ^1H NMR (CDCl_3 , 400 MHz) of *N*-tert-Butoxycarbonyl-*trans*-(4'*R*)-(8-bromoadenine-9-yl)-(2'*R*)-proline diphenylmethyl ester (**2**)

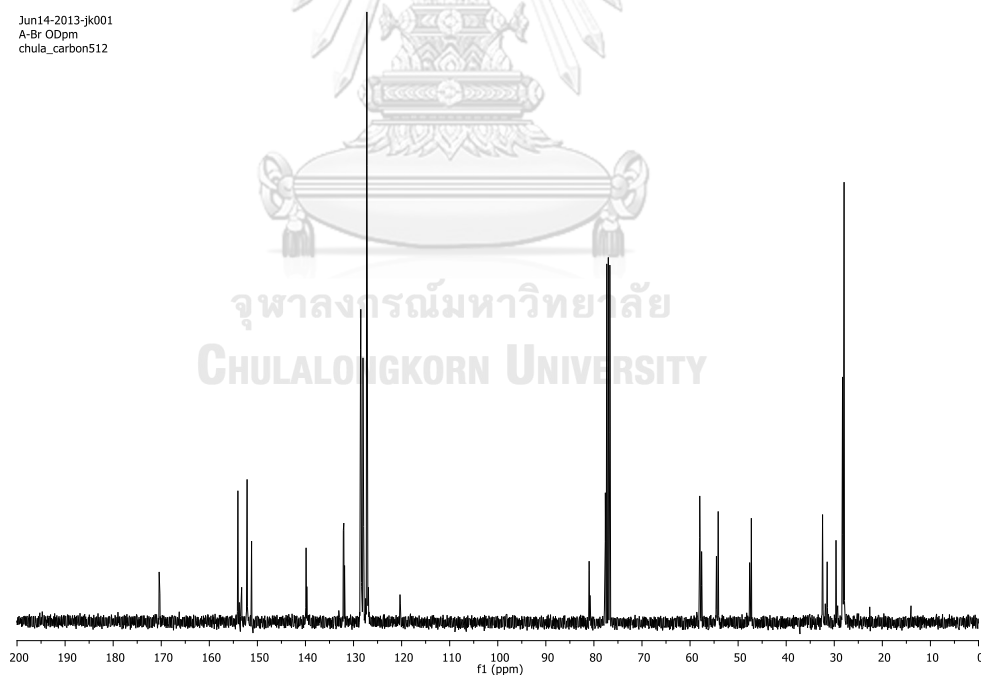


Figure A2. ^{13}C NMR (CDCl_3 , 100 MHz) of *N*-tert-Butoxycarbonyl-*trans*-(4'*R*)-(8-bromoadenine-9-yl)-(2'*R*)-proline dienylnmethyl ester (**2**)

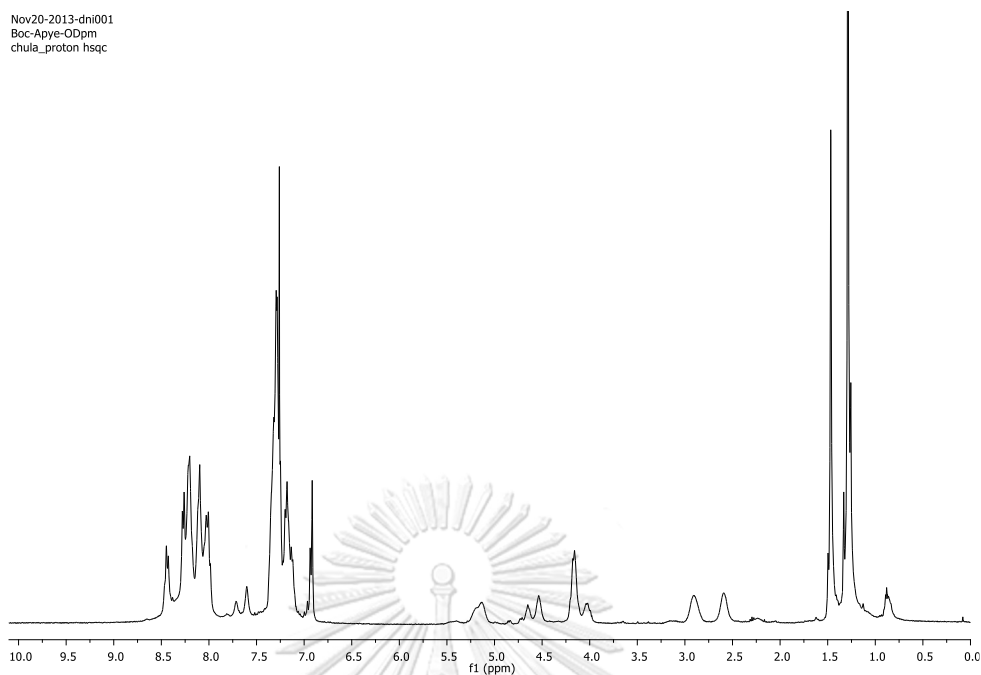


Figure A3. ^1H NMR (CDCl_3 , 400 MHz) of *N*-*tert*-Butoxycarbonyl-(4'*R*)-[8-(pyrene-1-yl)ethynyladenine-9-yl]-(2'*R*)-proline diphenylmethyl ester (**3**)

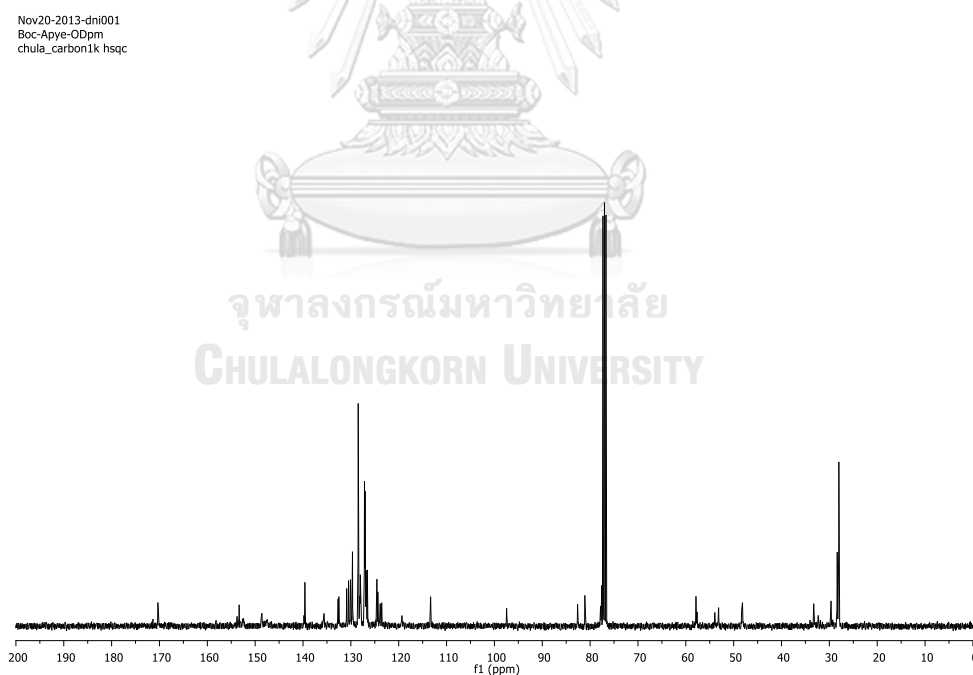


Figure A4. ^{13}C NMR (CDCl_3 , 100 MHz) of *N*-*tert*-Butoxycarbonyl-(4'*R*)-[8-(pyrene-1-yl)ethynyladenine-9-yl]-(2'*R*)-proline diphenylmethyl ester (**3**)

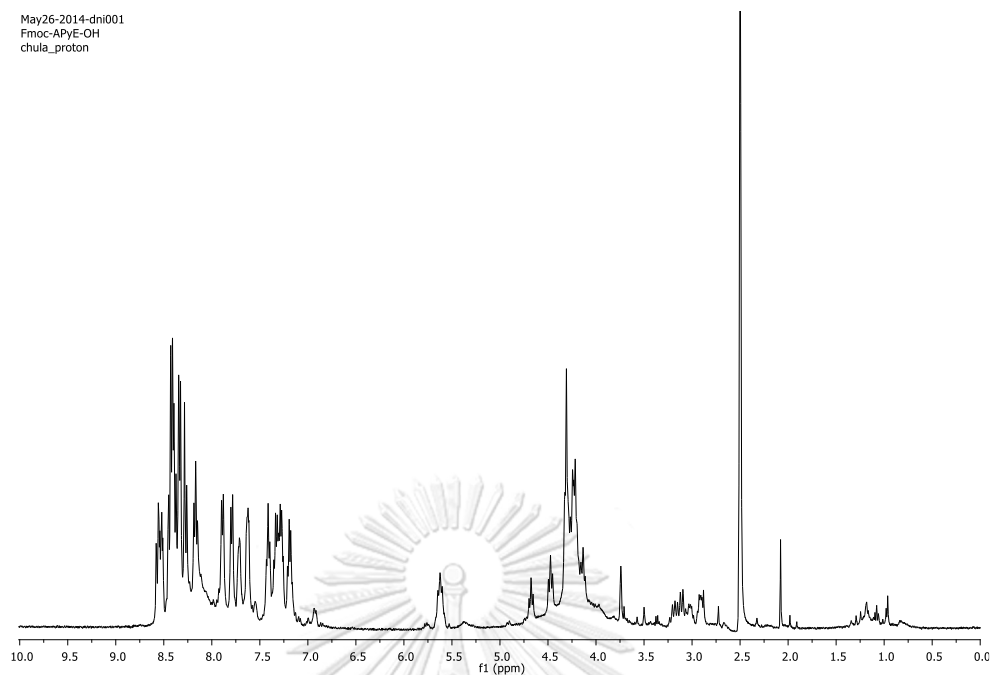


Figure A5. ^1H NMR (CDCl_3 , 400 MHz) of *N*-Fluoren-9-ylmethoxycarbonyl-(4'*R*)-[8-(pyrene-1-yl)ethynyladenine-9-yl]-(2'*R*)-proline (**4**)

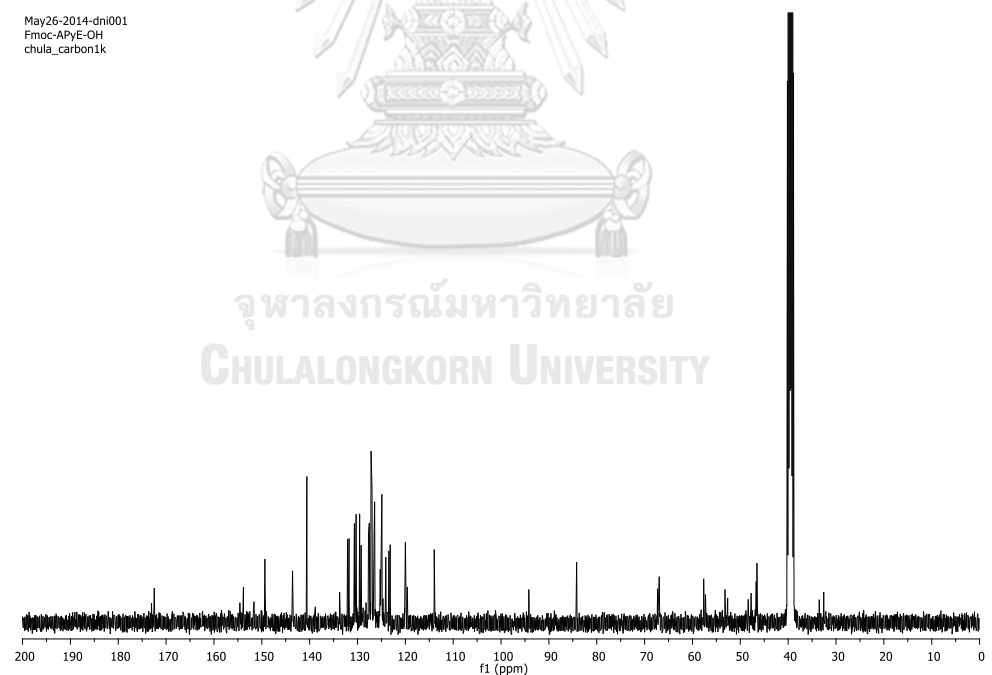


Figure A6. ^{13}C NMR ($\text{DMSO-}d_6$, 100 MHz) of *N*-Fluoren-9-ylmethoxycarbonyl-(4'*R*)-[8-(pyrene-1-yl)ethynyladenine-9-yl]-(2'*R*)-proline (**4**)

Mar29-2018-dni002
Fmoc-UI-OH_2 10 mg
chula_proton8

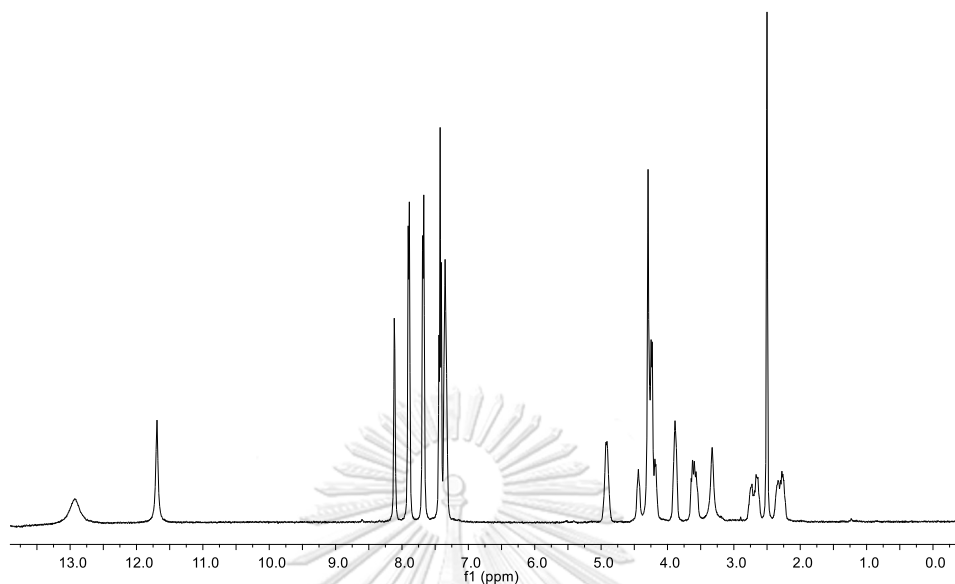


Figure A7. ^1H NMR (CDCl_3 , 400 MHz) of *N*-Fluorenylmethoxycarbonyl-*cis*-(4'*R*)-(5-iodouracil-1-yl)-(2'*R*)-proline (**7**)

Mar29-2018-dni002
Fmoc-UI-OH_2 10 mg
chula_carbon3k

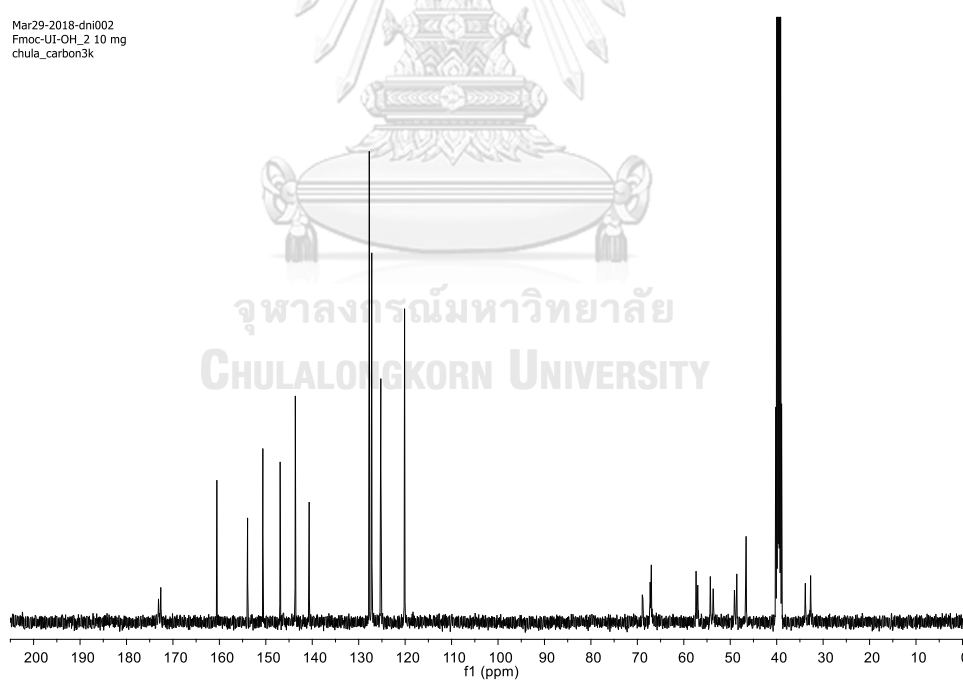


Figure A8. ^{13}C NMR ($\text{DMSO-}d_6$, 100 MHz) of *N*-Fluorenylmethoxycarbonyl-*cis*-(4'*R*)-(5-iodouracil-1-yl)-(2'*R*)-proline (**7**)

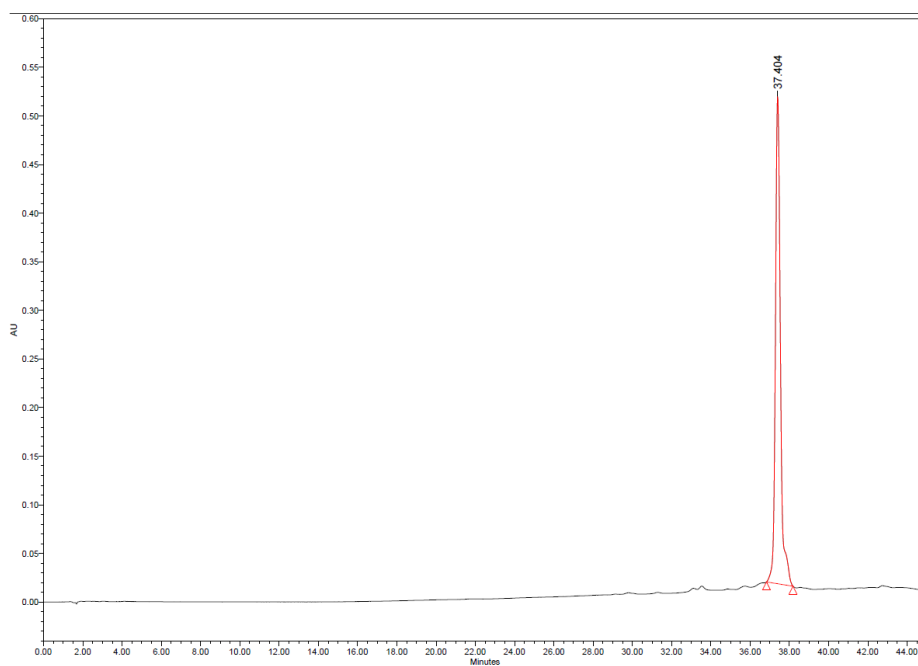


Figure A9. Analytical HPLC chromatogram of T4(A^{PyE})T4

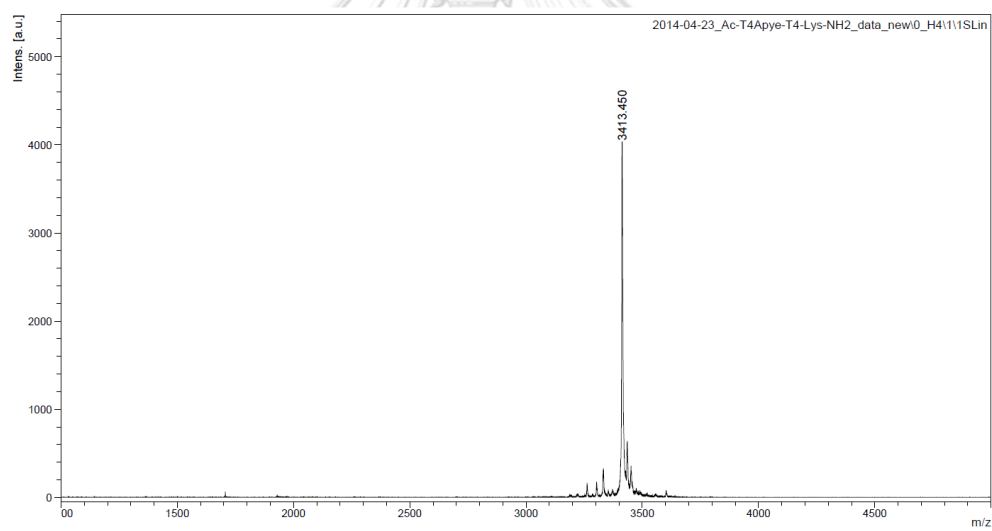


Figure A10. MALDI-TOF mass spectrum of T4(A^{PyE})T4 (calcd for $[M \cdot H]^+ = 3413.4$)

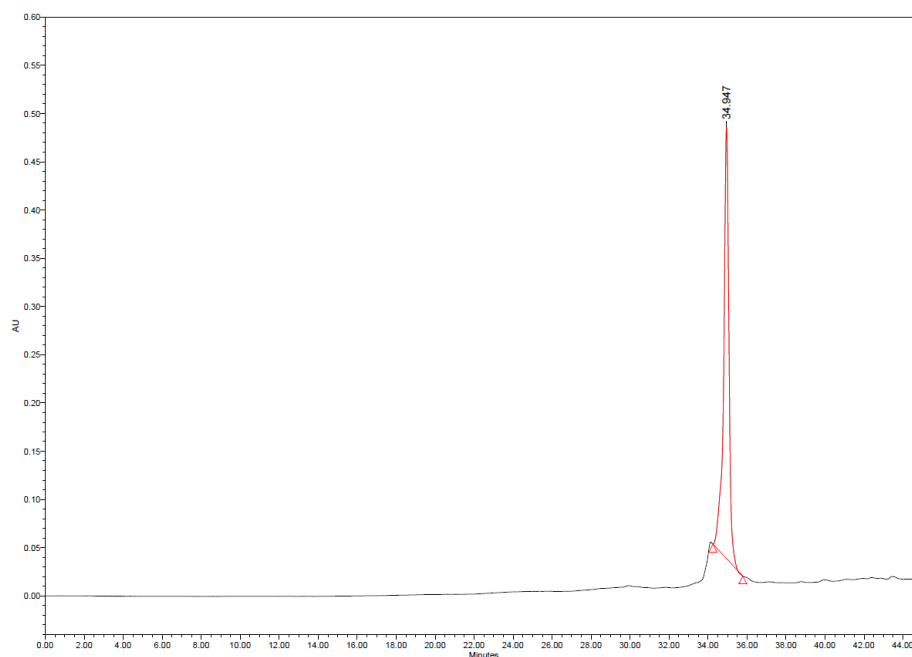


Figure A11. Analytical HPLC chromatogram of M12T(A^{PyE})T

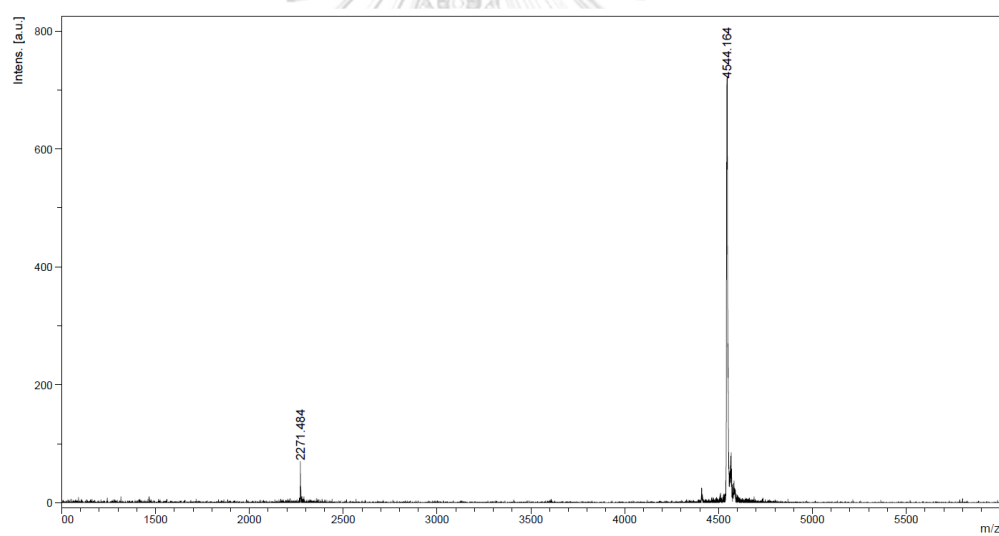


Figure A12. MALDI-TOF mass spectrum of M12T(A^{PyE})T (calcd for $[M \cdot H]^+ = 4543.7$)

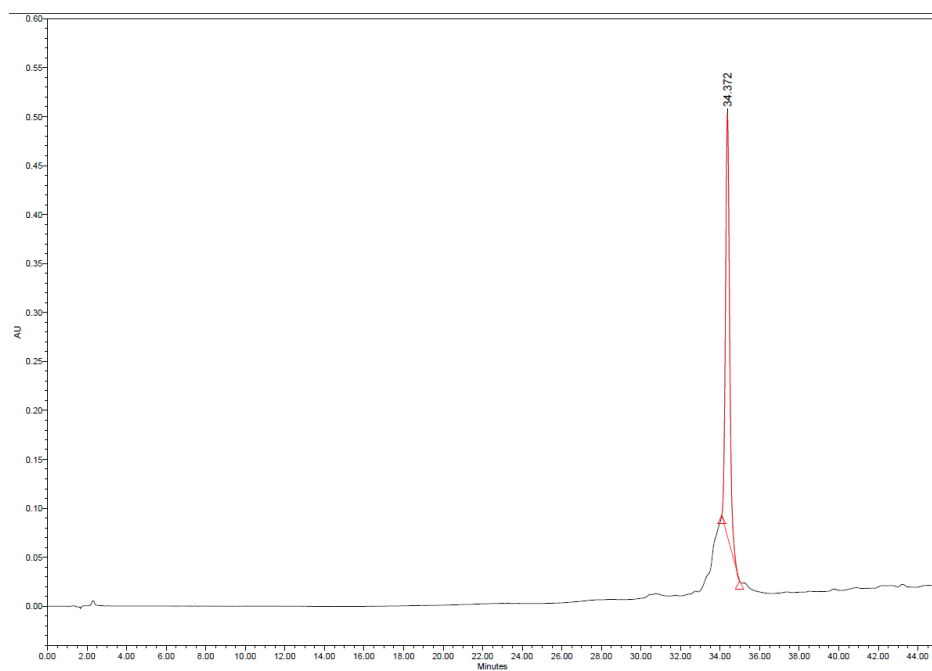


Figure A13. Analytical HPLC chromatogram of M12A(A^{PyE})A

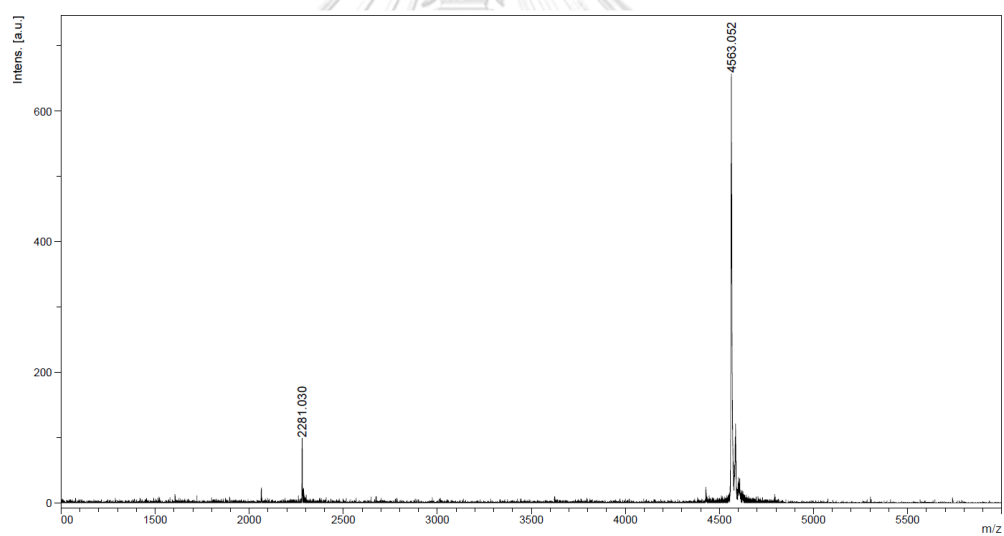


Figure A14. MALDI-TOF mass spectrum of M12A(A^{PyE})A (calcd for $[M \cdot H]^+ = 4561.7$)

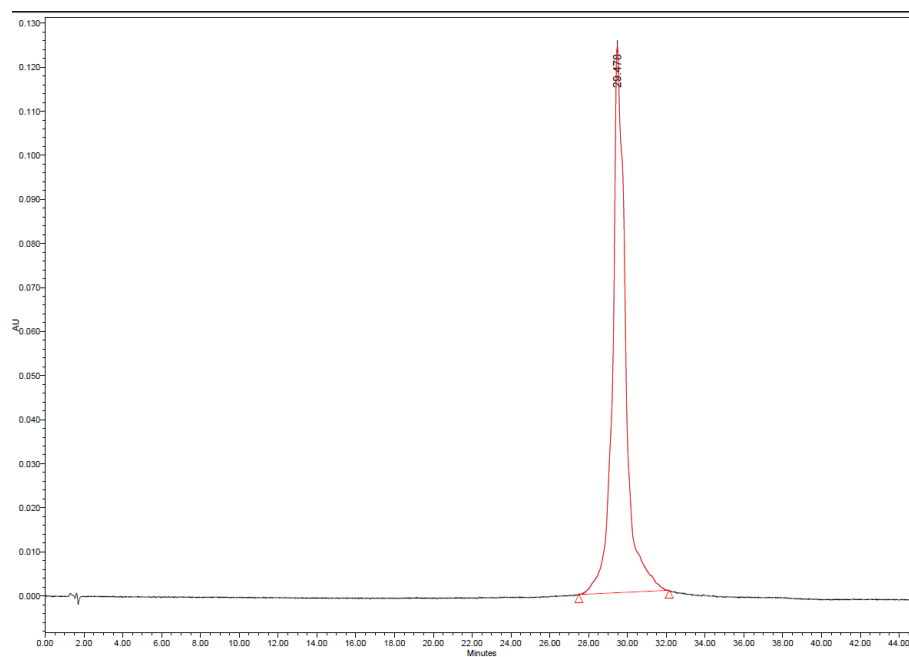


Figure A15. Analytical HPLC chromatogram of M12G(A^{PyE})G

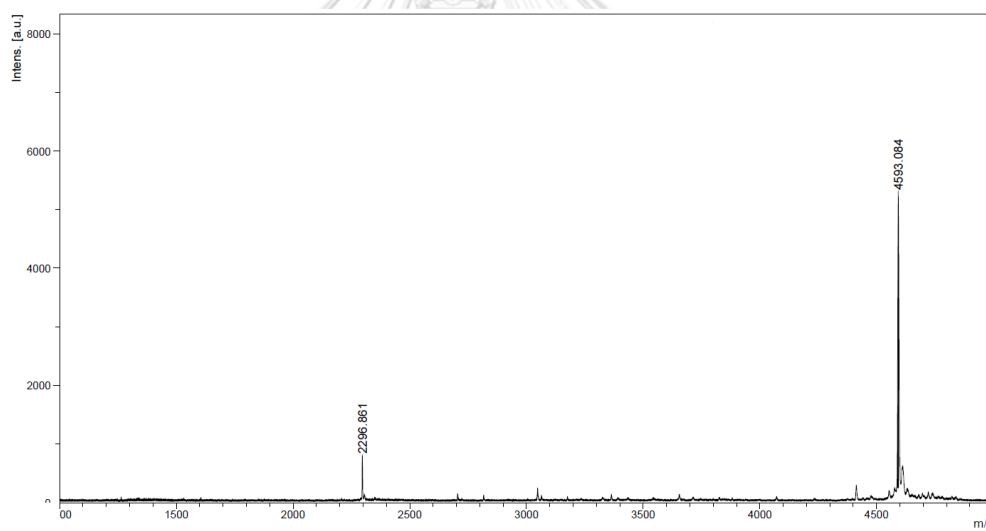


Figure A16. MALDI-TOF mass spectrum of M12G(A^{PyE})G (calcd for [M·H]⁺ = 4593.7)

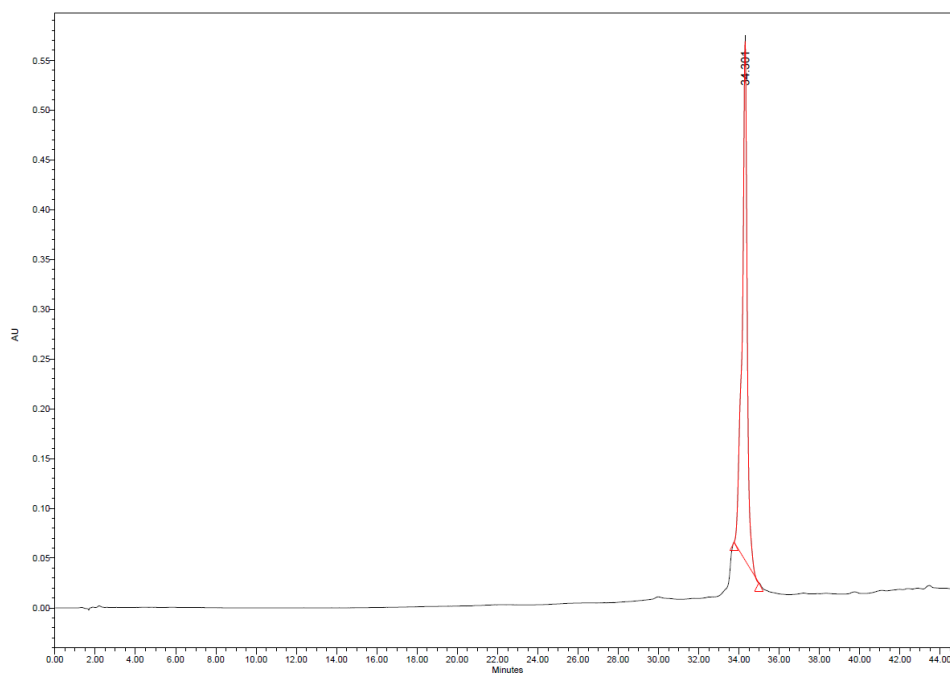


Figure A17. Analytical HPLC chromatogram of $M12C(A^{PyE})C$

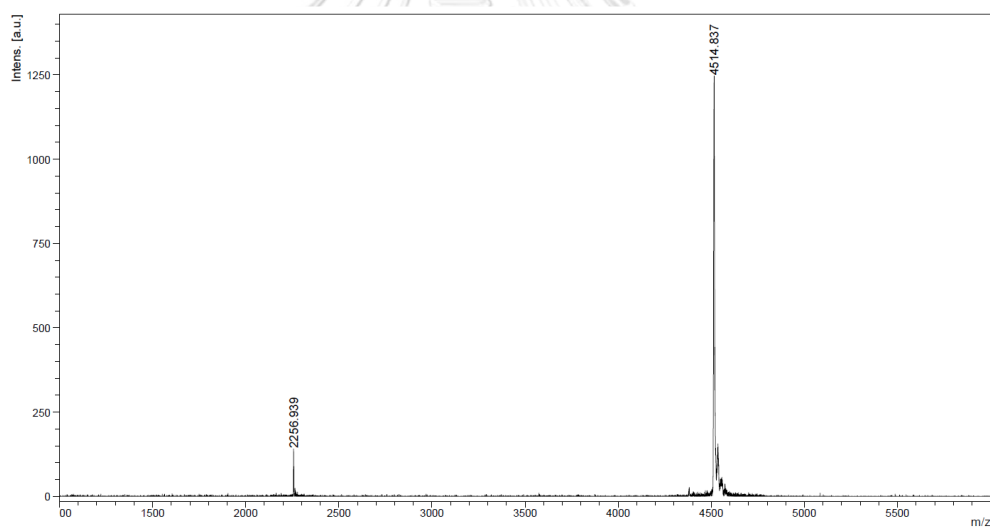


Figure A18. MALDI-TOF mass spectrum of $M12C(A^{PyE})C$ (calcd for $[M \cdot H]^+ = 4513.7$)

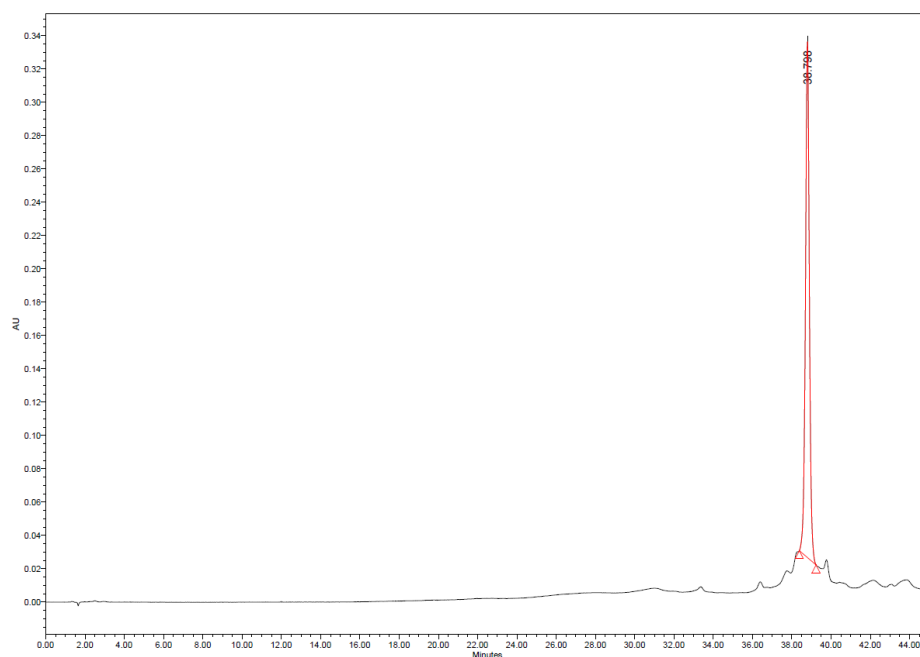


Figure A19. Analytical HPLC chromatogram of T8(A^{PyE})₂_0B

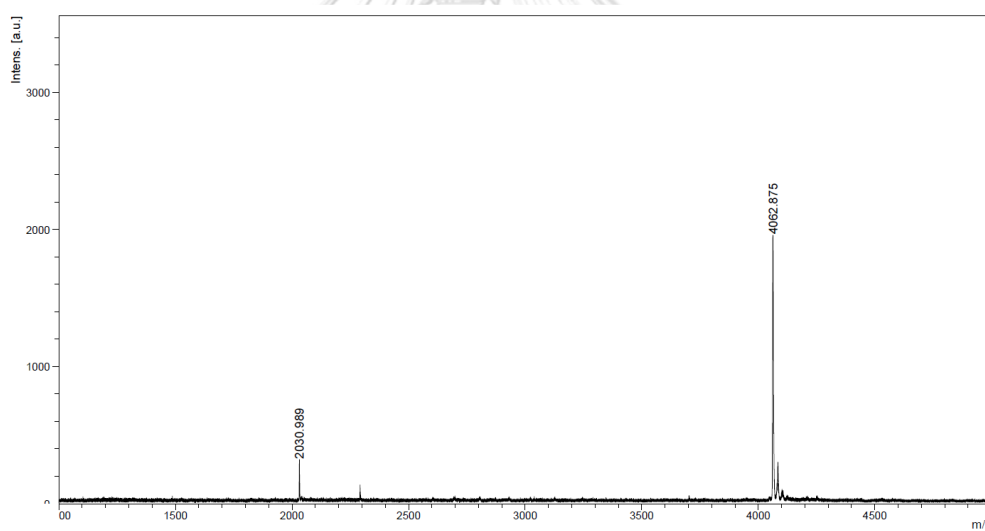


Figure A20. MALDI-TOF mass spectrum of T8(A^{PyE})₂_0B (calcd for [M·H]⁺ = 4065.9)

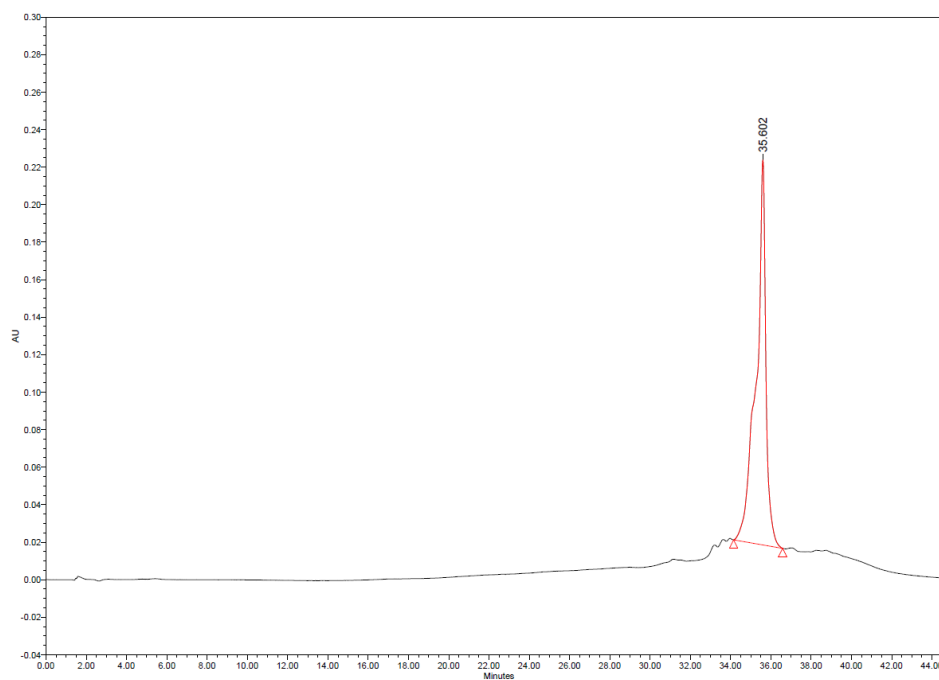


Figure A21. Analytical HPLC chromatogram of T8(A^{PyE})₂_3B

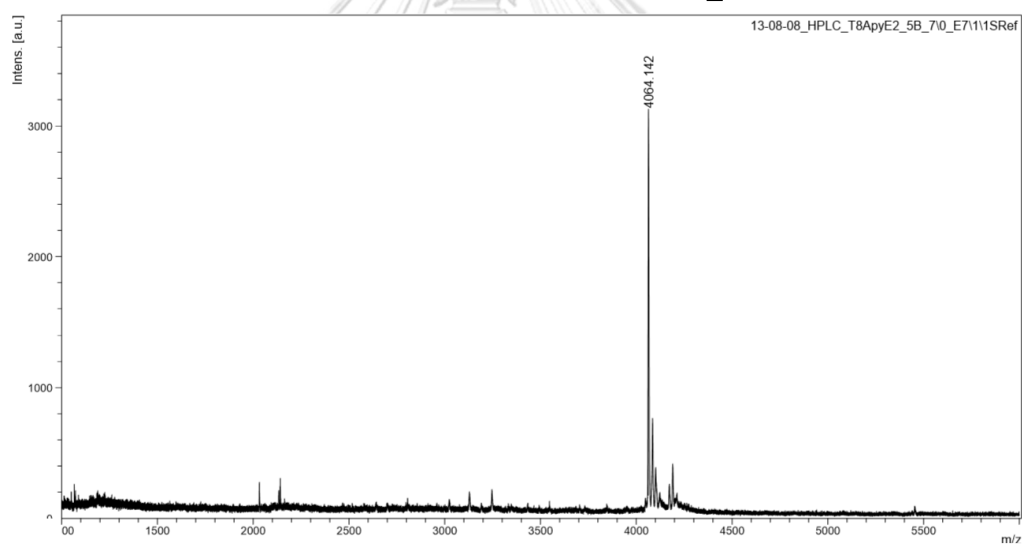


Figure A22. MALDI-TOF mass spectrum of T8(A^{PyE})₂_3B (calcd for [M•H]⁺ = 4065.9)

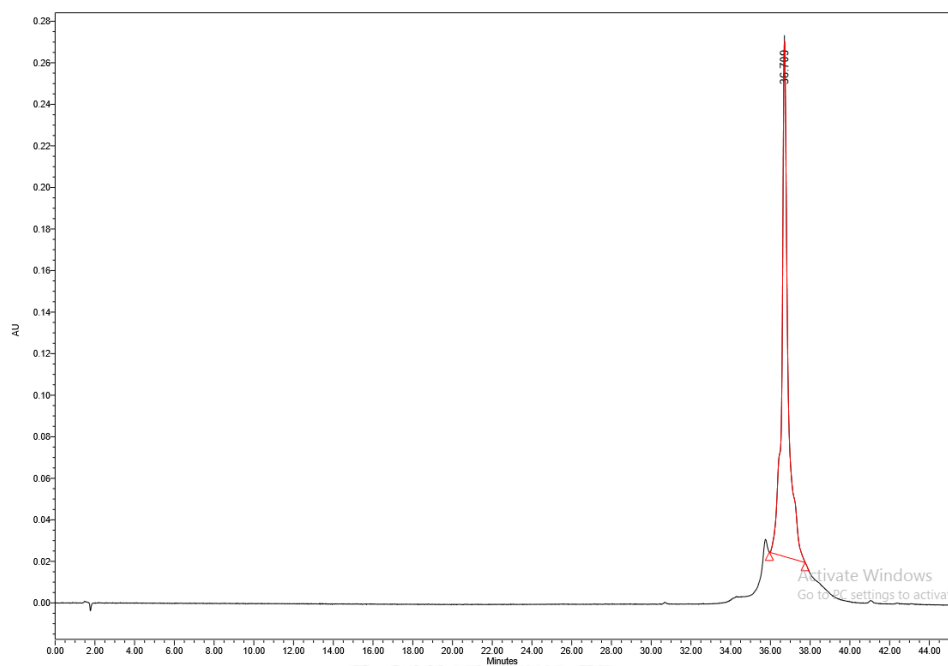


Figure A23. Analytical HPLC chromatogram of A^{PyE}M12

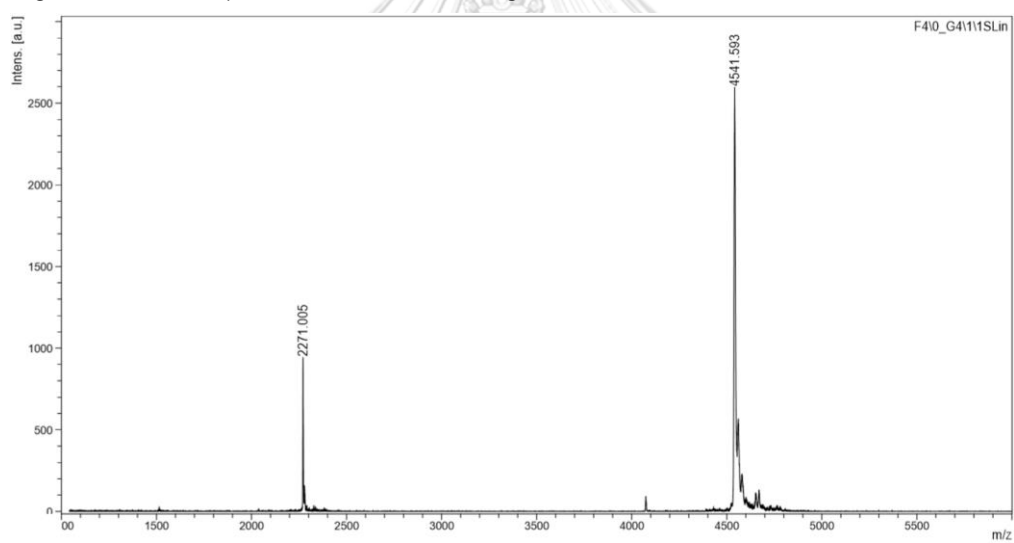


Figure A24. MALDI-TOF mass spectrum of A^{PyE}M12 (calcd for $[M \cdot H]^+ = 4543.7$)

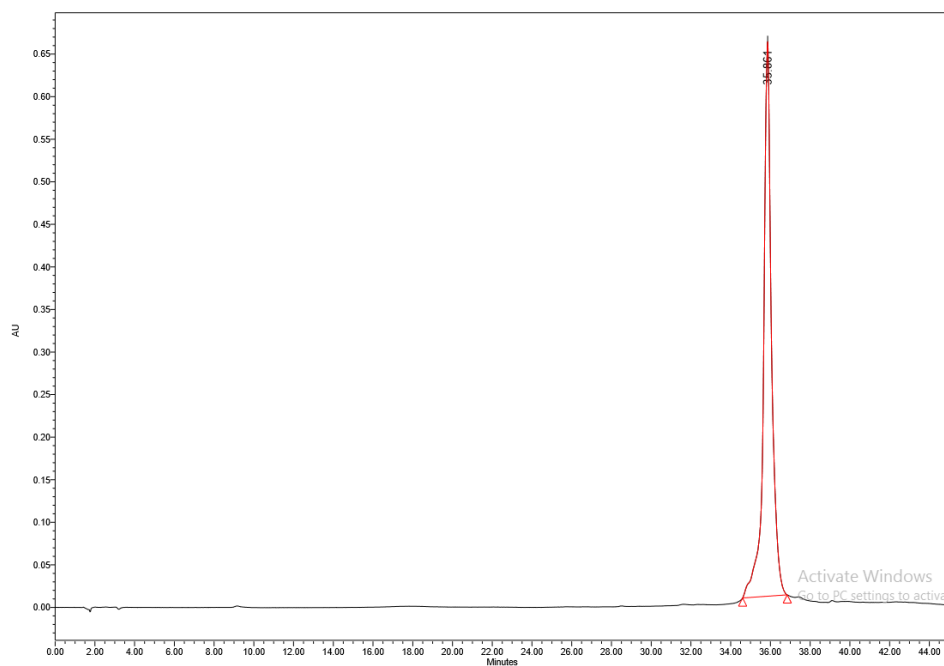


Figure A25. Analytical HPLC chromatogram of M10A(A^{PyE})C

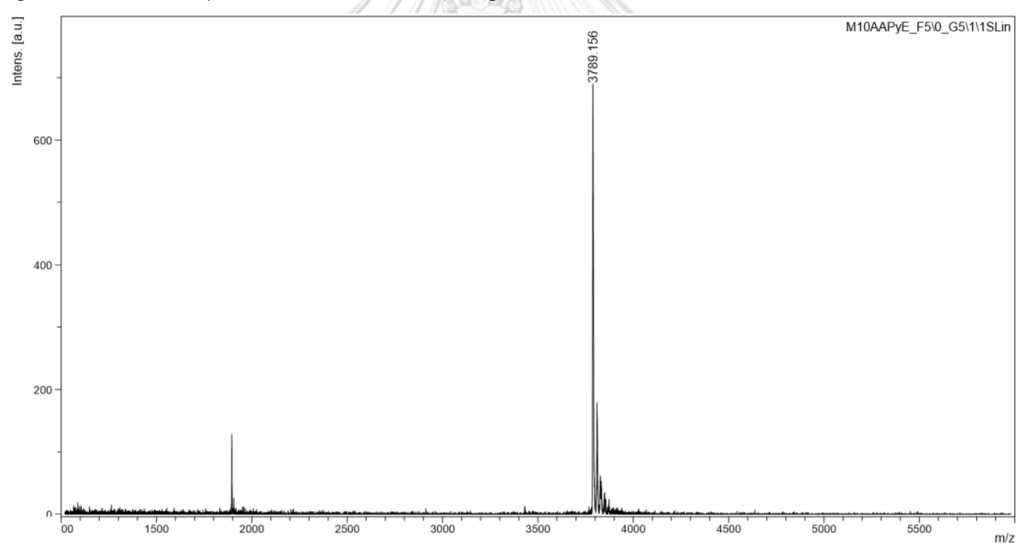


Figure A26. MALDI-TOF mass spectrum of M10A(A^{PyE})C (calcd for [M+H]⁺ = 3792.8)

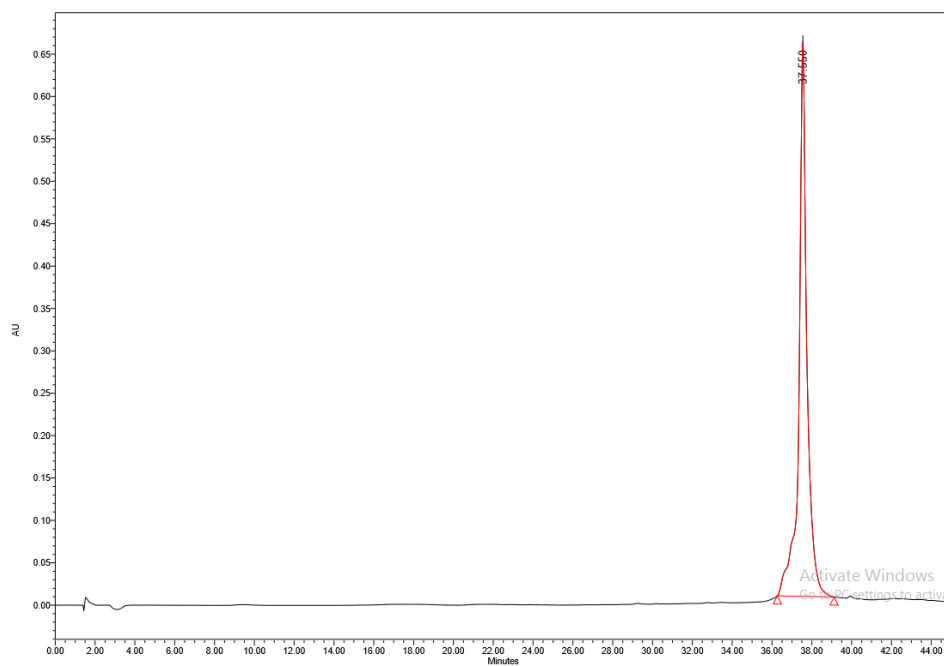


Figure A27. Analytical HPLC chromatogram of M10G(A^{PyE})T

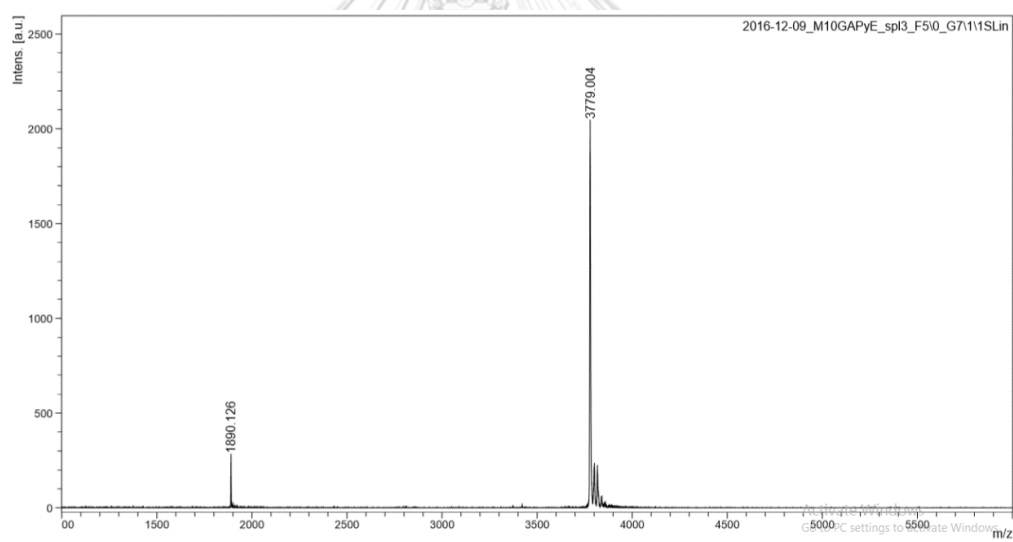


Figure A28. MALDI-TOF mass spectrum of M10G(A^{PyE})T (calcd for $[M \cdot H]^+ = 3779.0$)

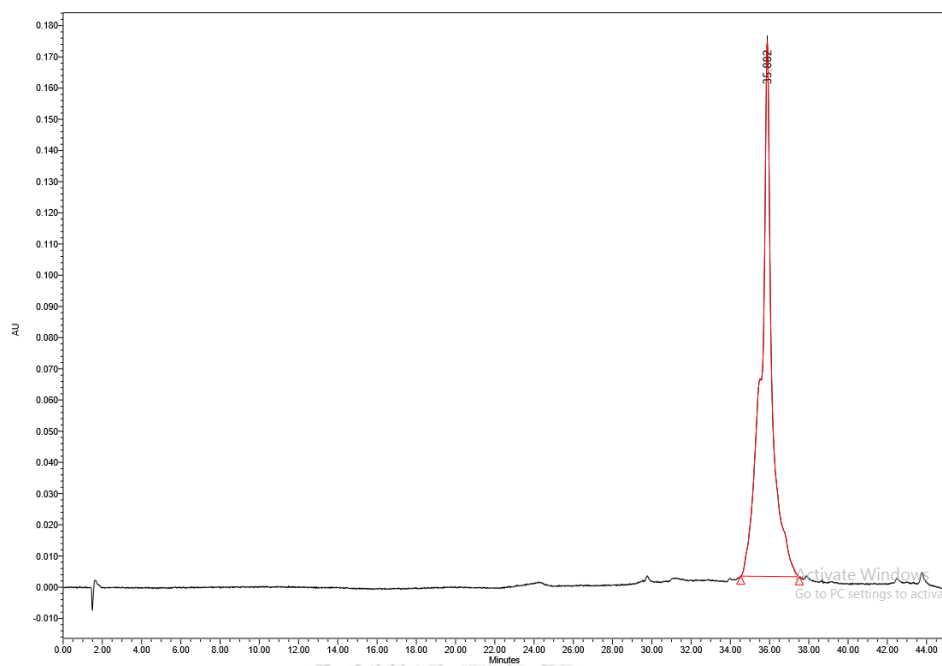


Figure A29. Analytical HPLC chromatogram of $\text{CAG}(\text{A}^{\text{PyE}})$

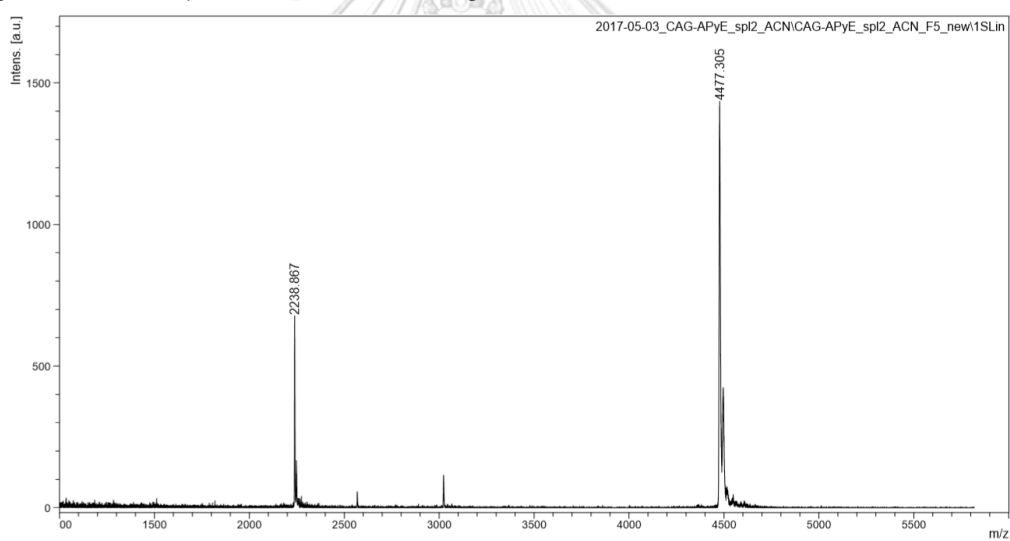


Figure A30. MALDI-TOF mass spectrum of $\text{CAG}(\text{A}^{\text{PyE}})$ (calcd for $[\text{M}\cdot\text{H}]^+ = 4477.6$)

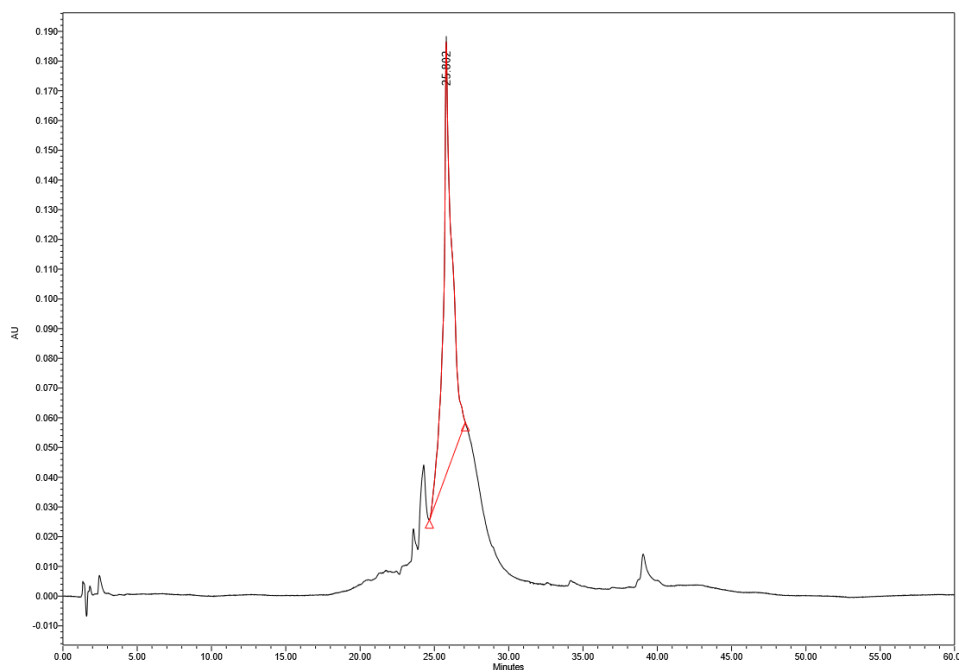


Figure A31. Analytical HPLC chromatogram of T4U^{PyE}-T4

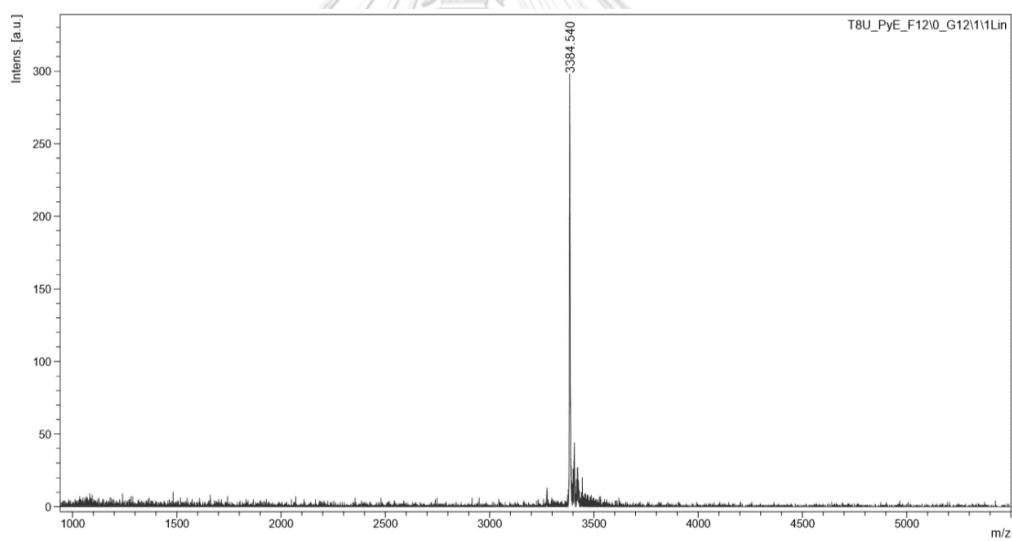


Figure A32. MALDI-TOF mass spectrum of T4U^{PyE}-T4 (calcd for $[M \cdot H]^+ = 3389.7$)

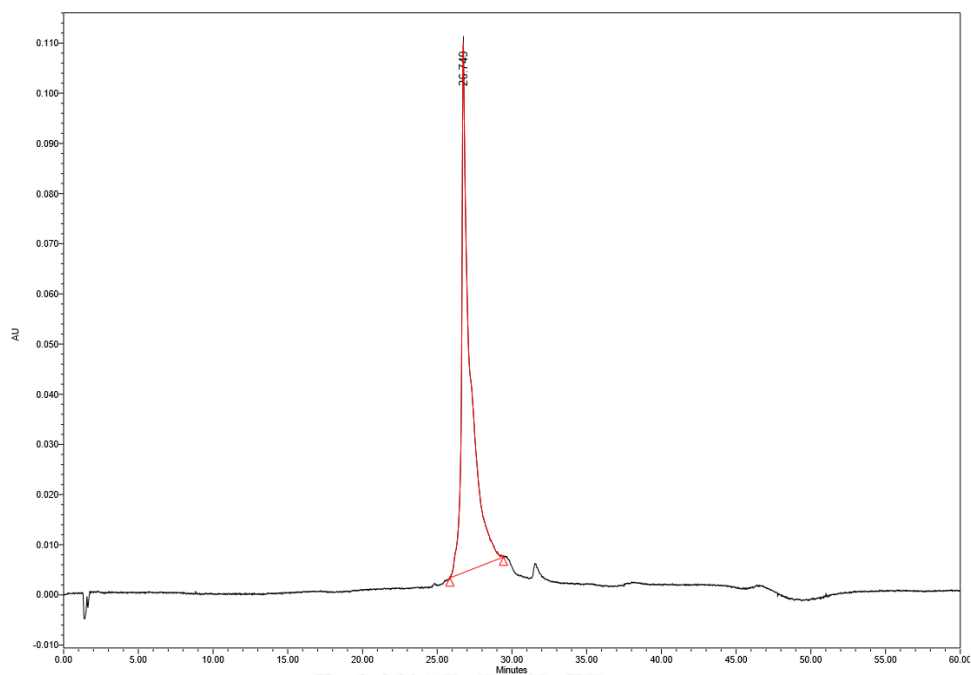


Figure A33. Analytical HPLC chromatogram of T4fU^{Py}T4

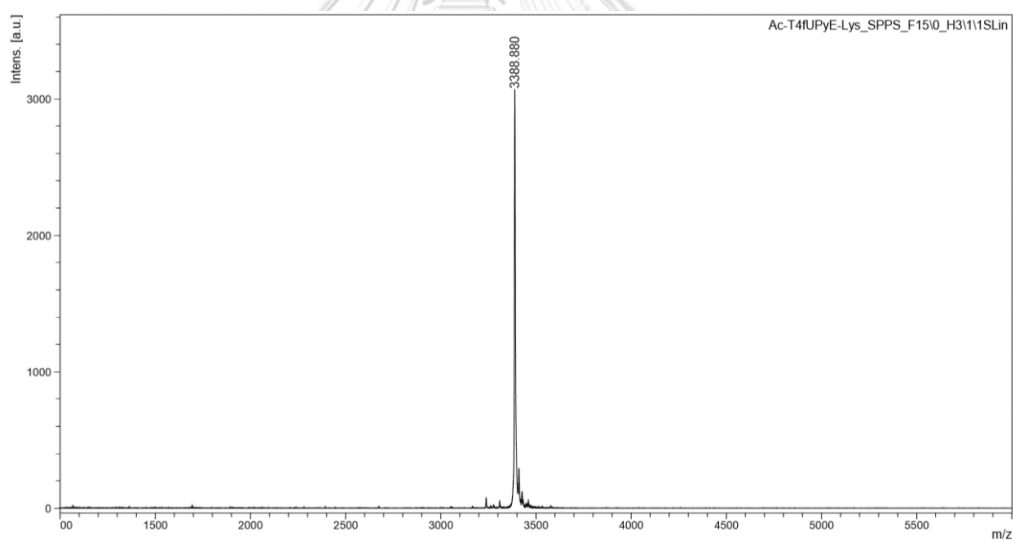


Figure A34. MALDI-TOF mass spectrum of T4fU^{Py}T4 (calcd for $[M+H]^+ = 3390.7$)

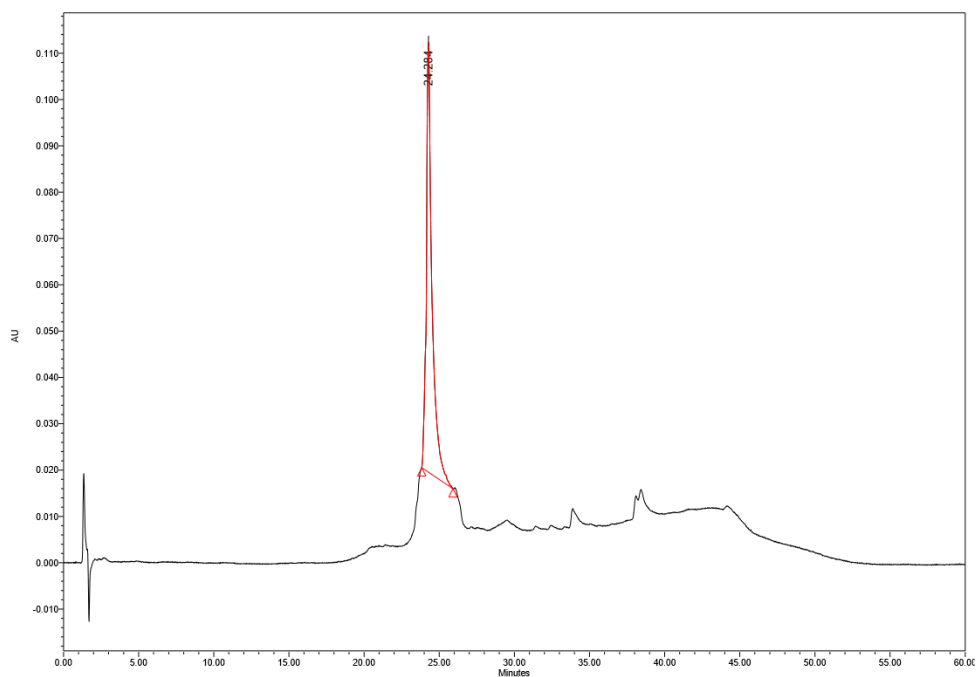


Figure A35. Analytical HPLC chromatogram of T4U^{2Th}T4

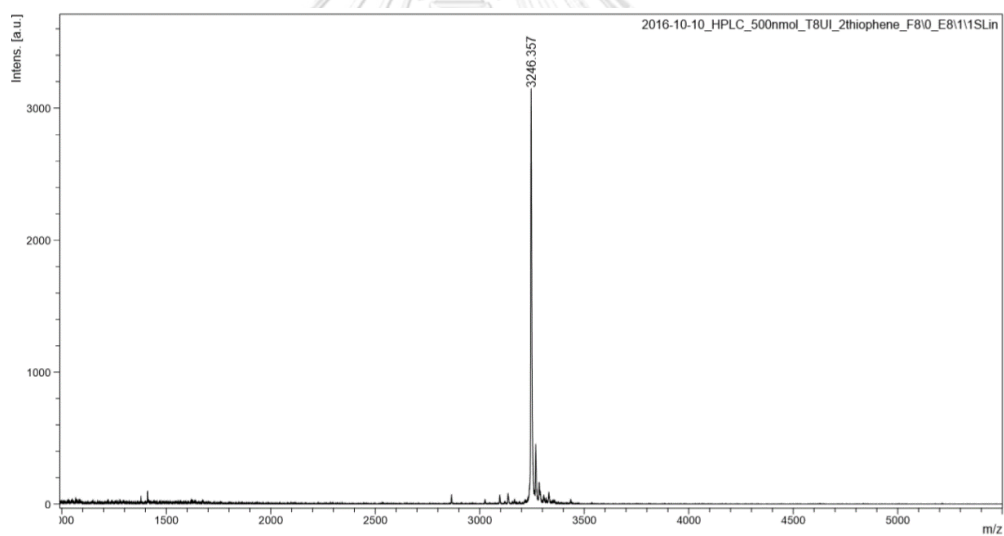


Figure A36. MALDI-TOF mass spectrum of T4U^{2Th}T4 (calcd for $[M \cdot H]^+ = 3247.4$)

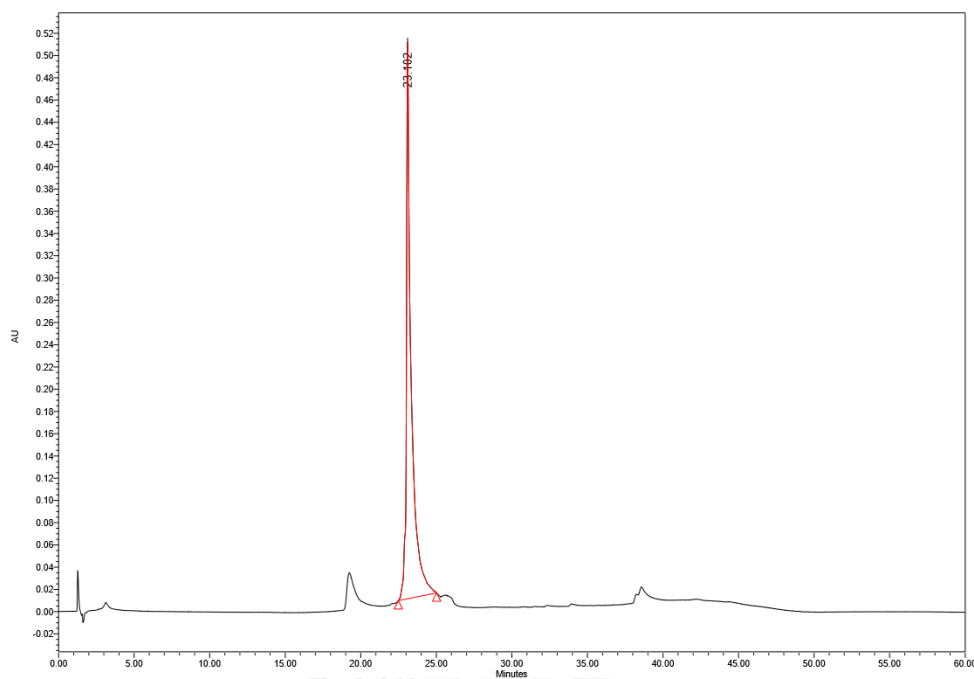


Figure A37. Analytical HPLC chromatogram of T4U^{3Th}T4

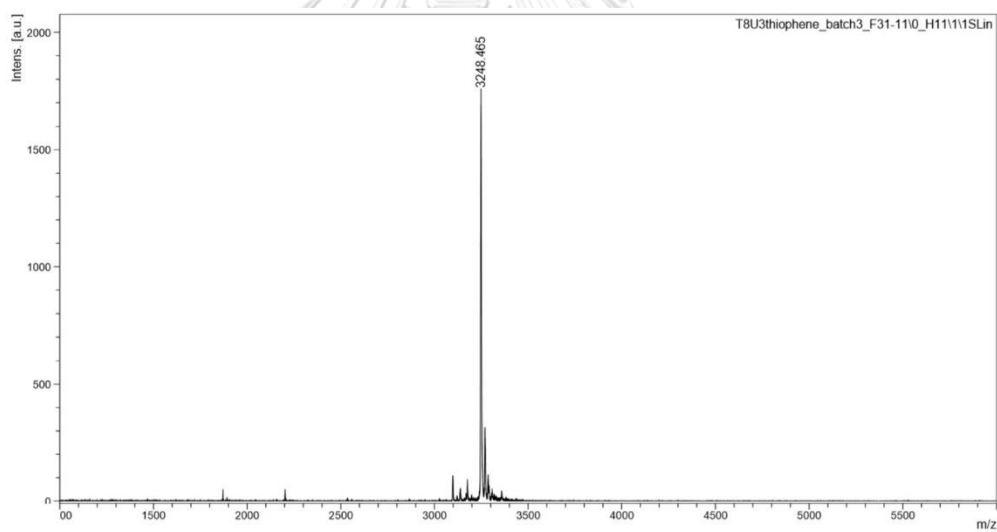


Figure A38. MALDI-TOF mass spectrum of T4U^{3Th}T4 (calcd for $[M \cdot H]^+$ = 3247.4)

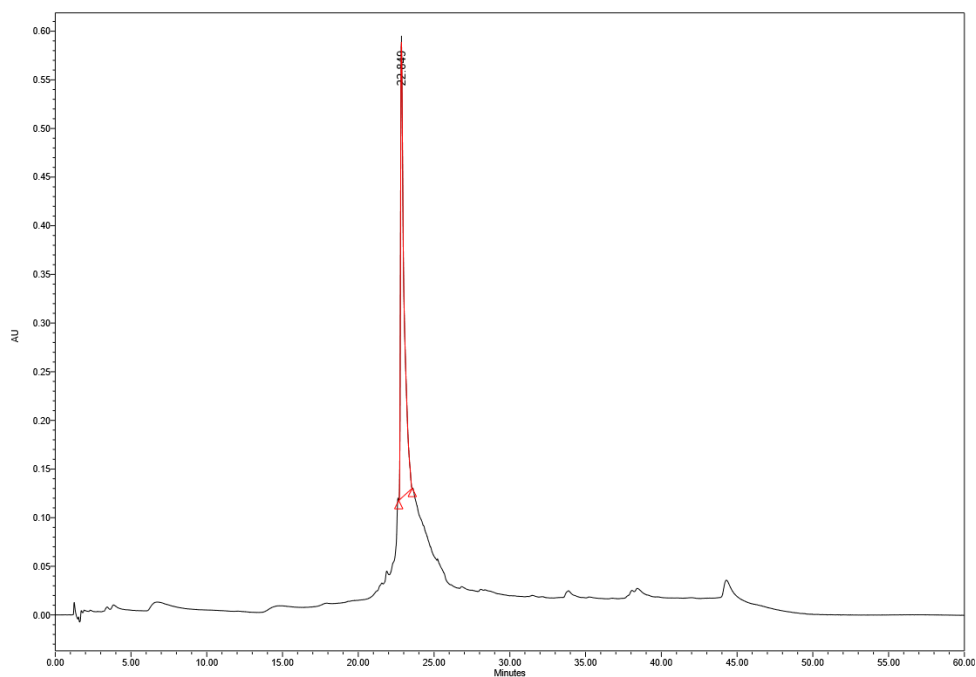


Figure A39. Analytical HPLC chromatogram of T4U^{2Fu}T4

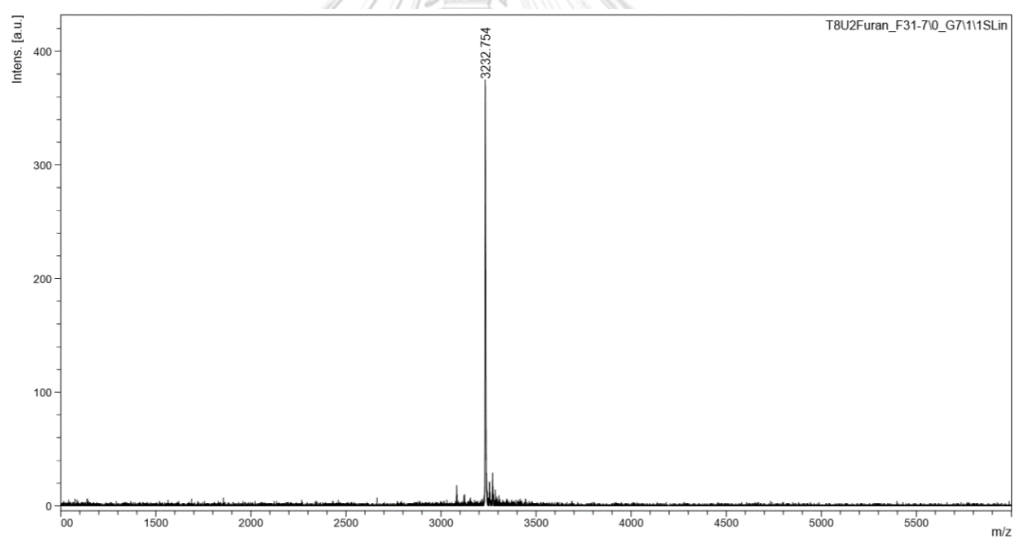


Figure A40. MALDI-TOF mass spectrum of T4U^{2Fu}T4 (calcd for $[M \cdot H]^+ = 3231.4$)

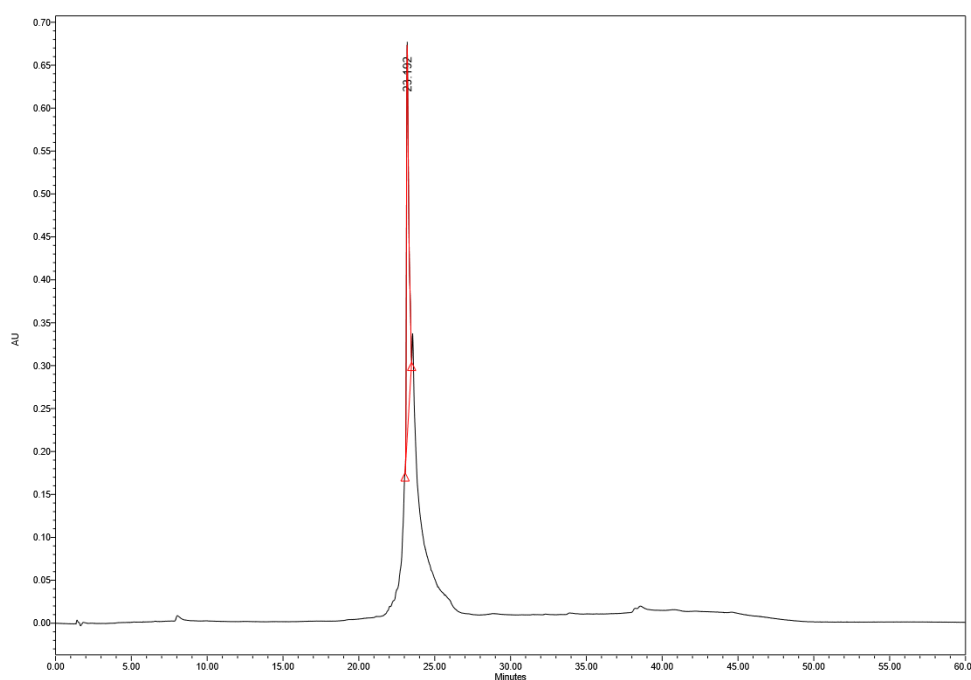


Figure A41. Analytical HPLC chromatogram of T4U^{3Fu}T4

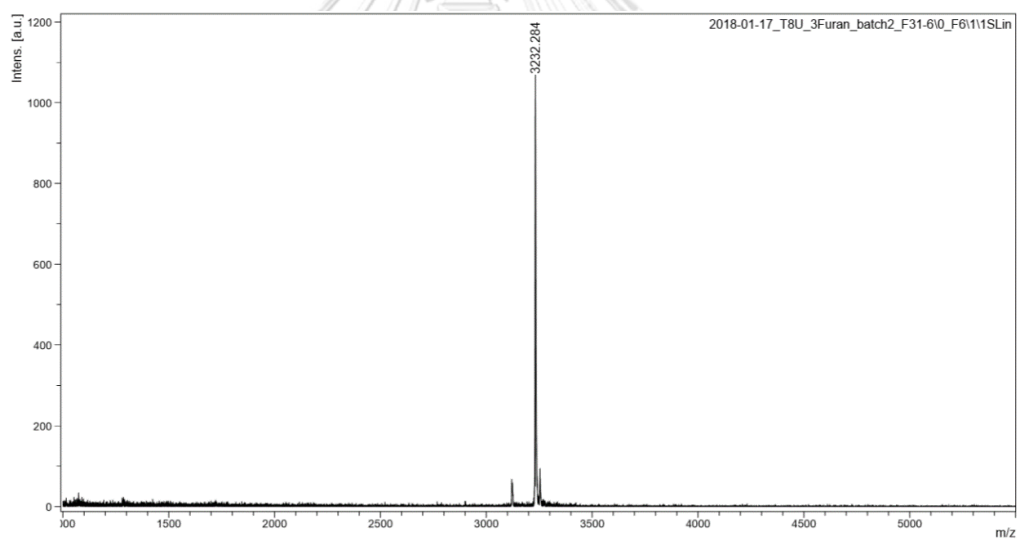


Figure A42. MALDI-TOF mass spectrum of T4U^{3Fu}T4 (calcd for $[M \cdot H]^+$ = 3231.4)

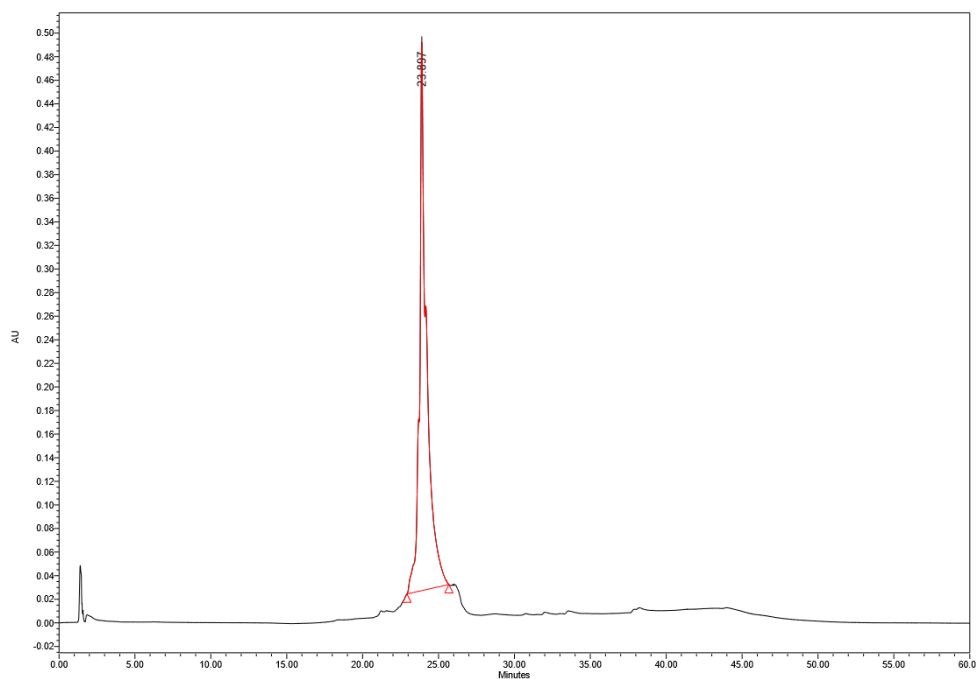


Figure A43. Analytical HPLC chromatogram of T4U^{2BT}T4

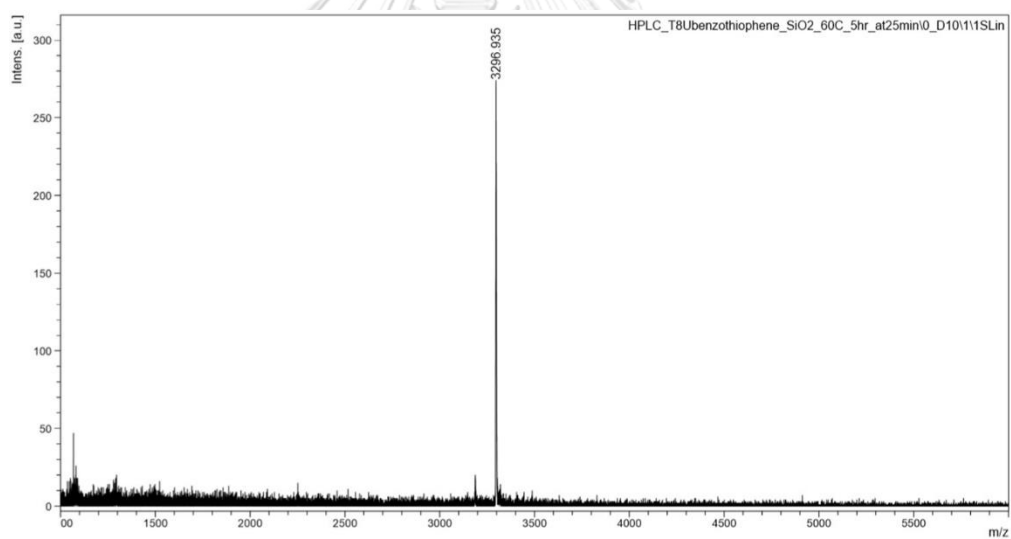


Figure A44. MALDI-TOF mass spectrum of T4U^{2BT}T4 (calcd for $[M \cdot H]^+ = 3297.4$)

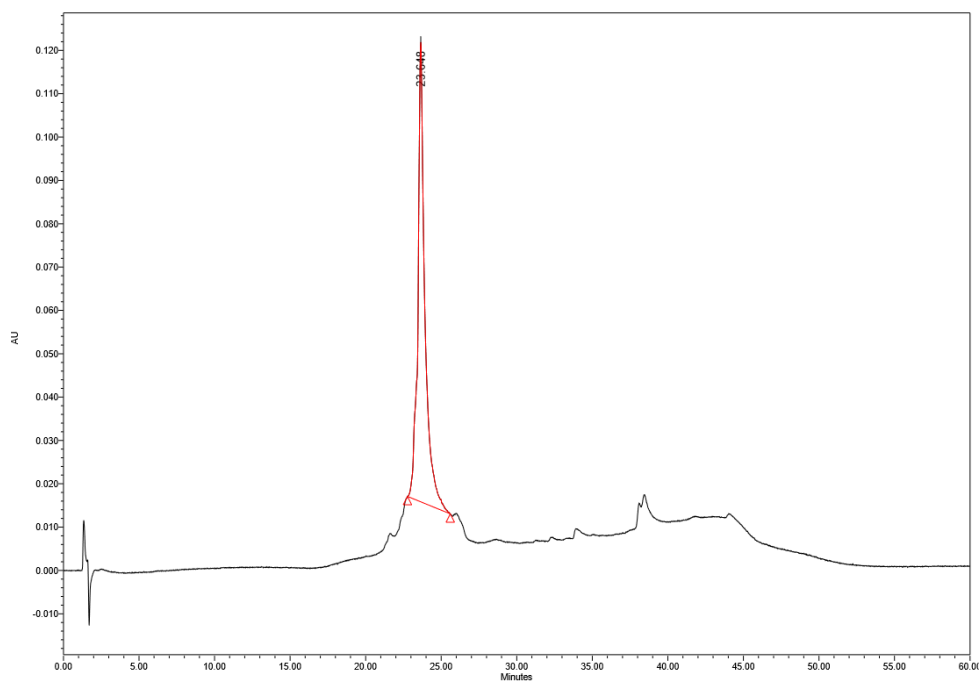


Figure A45. Analytical HPLC chromatogram of T4U^{2BF}T4

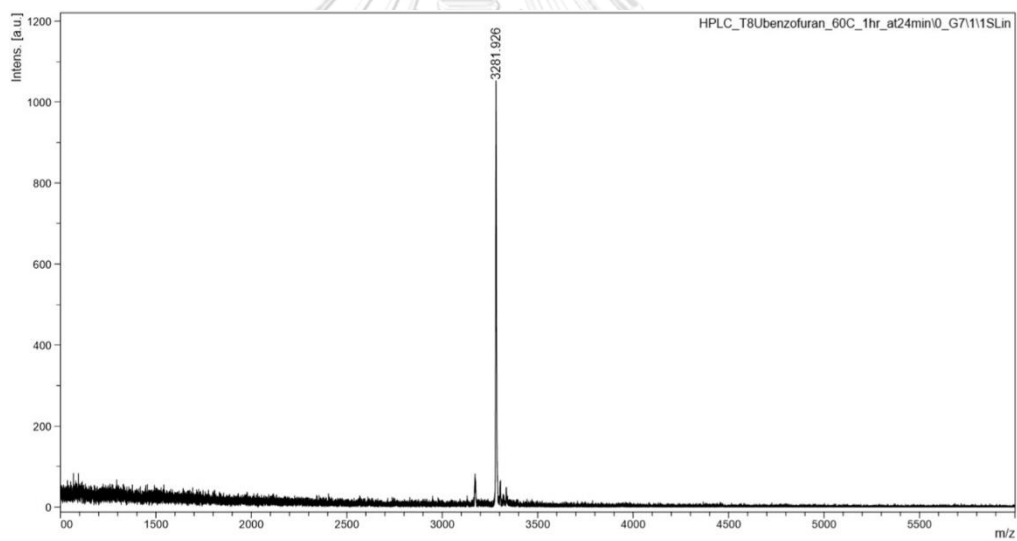


Figure A46. MALDI-TOF mass spectrum of T4U^{2BF}T4 (calcd for $[M \cdot H]^+ = 3281.4$)

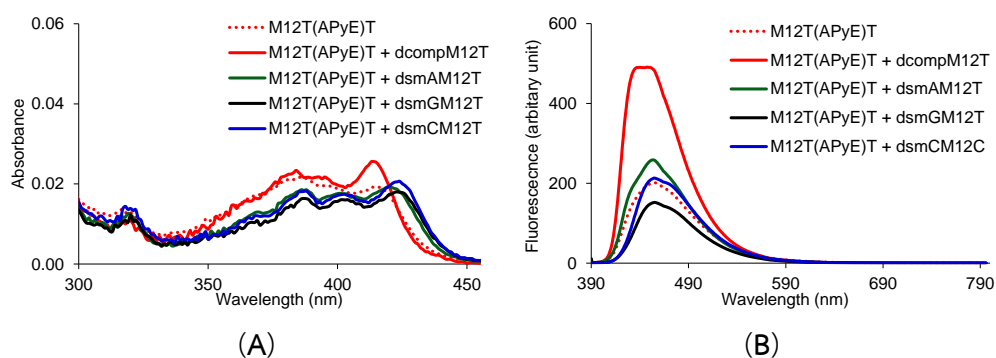


Figure A47. (A) UV-vis spectra, (B) fluorescence spectra of $M12T(A^{PyE})T$ and its DNA hybrids; Conditions: $1.0 \mu\text{M}$ PNA, $1.2 \mu\text{M}$ DNA, 10 mM phosphate buffer pH 7.0, λ_{ex} 376 nm

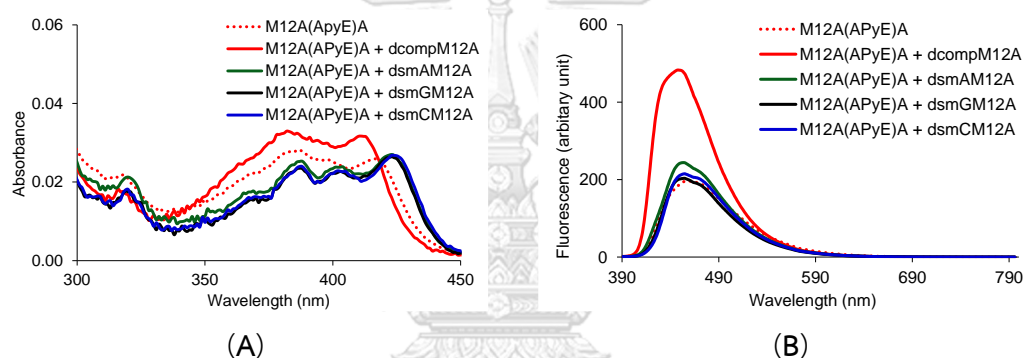


Figure A48. (A) UV-vis spectra, (B) fluorescence spectra of $M12A(A^{PyE})A$ and its DNA hybrids; Conditions: $1.0 \mu\text{M}$ PNA, $1.2 \mu\text{M}$ DNA, 10 mM phosphate buffer pH 7.0, λ_{ex} 376 nm

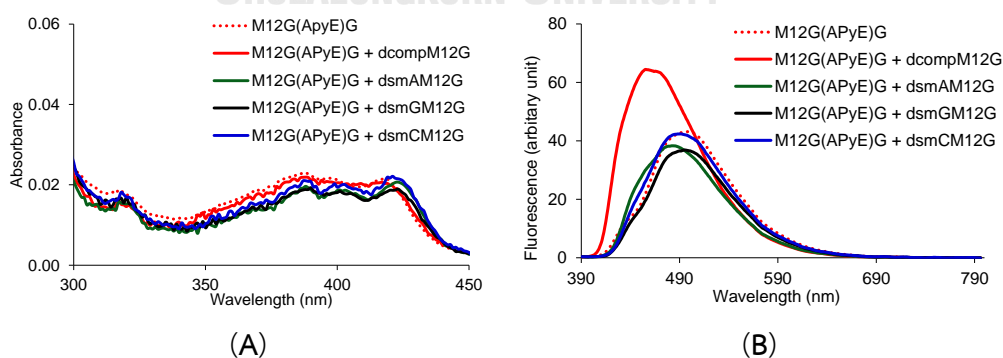


Figure A49. (A) UV-vis spectra, (B) Fluorescence spectra of $M12G(A^{PyE})G$ and its DNA hybrids; Conditions: $1.0 \mu\text{M}$ PNA, $1.2 \mu\text{M}$ DNA, 10 mM phosphate buffer pH 7.0, λ_{ex} 376 nm

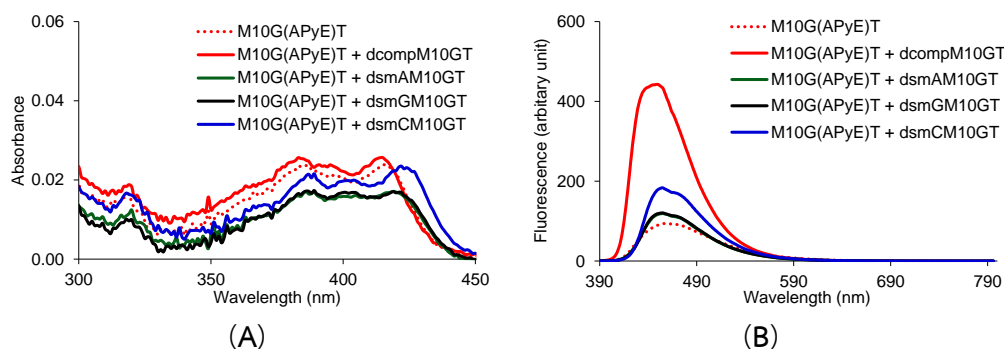


Figure A50. (A) UV-vis spectra, (B) Fluorescence spectra of $M10G(A^{PyE})T$ and its DNA hybrids; Conditions: $1.0 \mu\text{M}$ PNA, $1.2 \mu\text{M}$ DNA, 10 mM phosphate buffer pH 7.0, λ_{ex} 376 nm

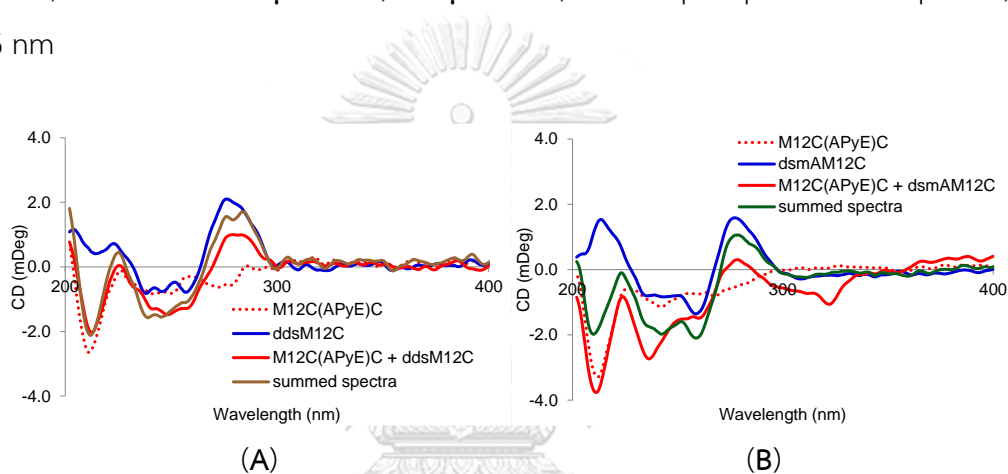


Figure A51. CD spectra of $M12C(A^{PyE})C$ (A: double mismatched hybrid with dCAGTITITG ACT, B: single mismatched hybrid with dCAGTGAGTGACT); Conditions: $1.0 \mu\text{M}$ PNA, $1.2 \mu\text{M}$ DNA (A) or $2.0 \mu\text{M}$ PNA, $2.4 \mu\text{M}$ DNA (B) in 10 mM phosphate buffer pH 7.0

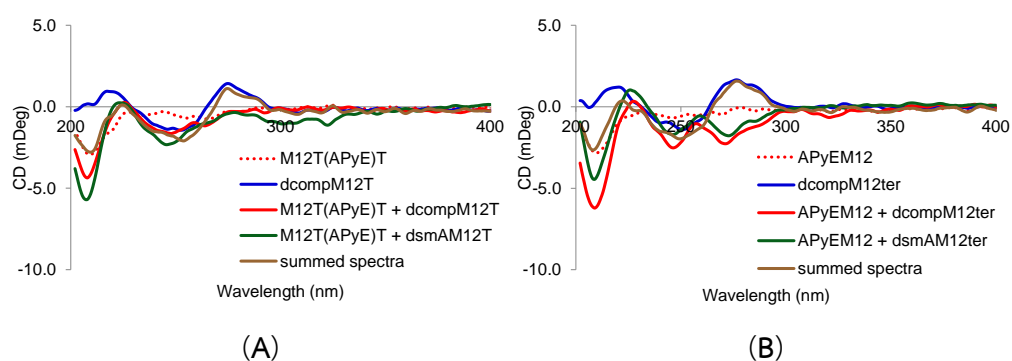


Figure A52. CD spectra of (A) $M12T(A^{PyE})T$ (complementary hybrid with $dCAGTAIATGACT$, single mismatched hybrid with $dCAGTAAATGACT$) and (B) $A^{PyE}M12$ (complementary hybrid with $dCAGTATATGACI$, single mismatched hybrid with $dCAGTATATGACA$); Conditions: $1.0 \mu M$ PNA, $1.2 \mu M$ DNA, 10 mM phosphate buffer pH 7.0

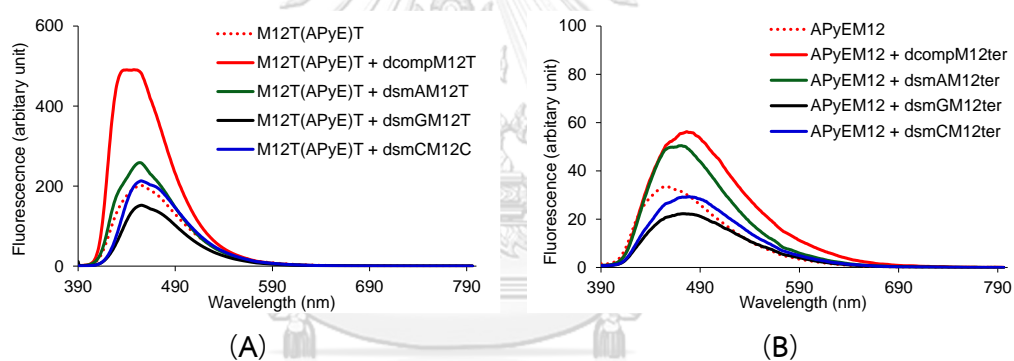


Figure A53. Fluorescence spectra of $M12T(A^{PyE})T$ (A) and $A^{PyE}M12$ (B) and their DNA hybrids; Conditions: $1.0 \mu M$ PNA, $1.2 \mu M$ DNA, 10 mM phosphate buffer pH 7.0, λ_{ex} 376 nm

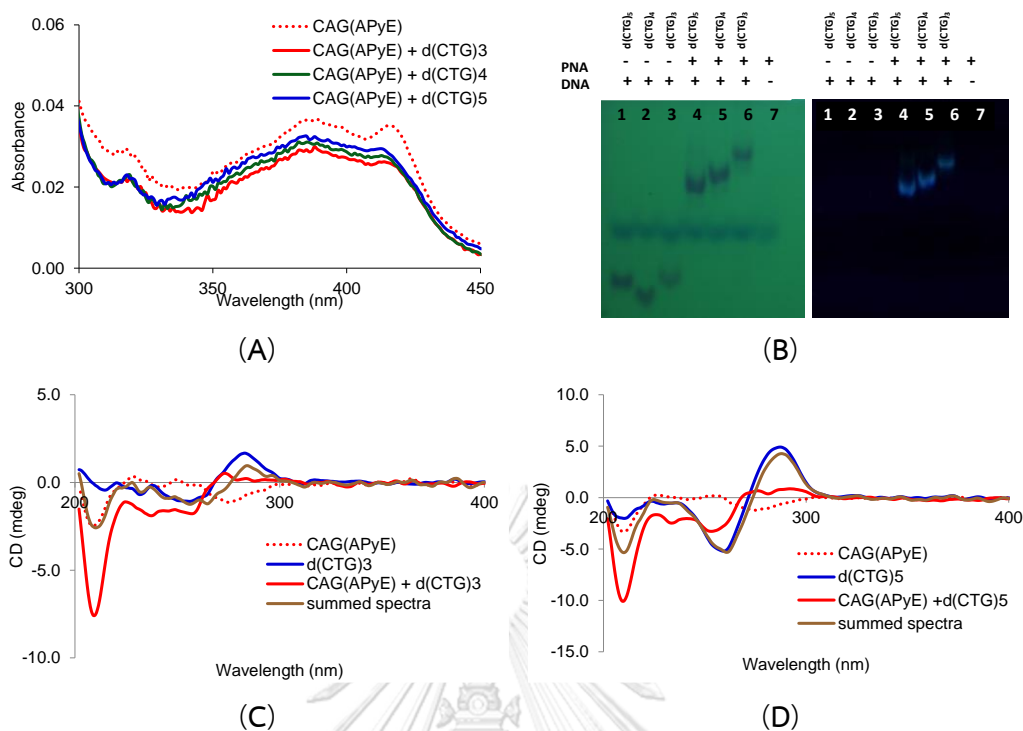


Figure A54. (A) UV-vis spectra, (B) gel electrophoresis (left, UV shadowing at 265 nm; right, viewed under transilluminator at 365 nm), (C) and (D) CD spectra of CAG(APyE) and its DNA hybrids. Conditions: 1.0 μM PNA, 1.2 μM DNA, 10 mM phosphate buffer pH 7.0, λ_{ex} 376 nm

Table A1. UV absorption data of A^{PyE}-modified acpcPNA probes (condition: 1.0 μ M PNA, 1.2 μ M DNA, 10 mM phosphate buffer pH 7.0).

Entry	PNA	DNA ^a (5' to 3')	λ_{\max} (abs), (nm)	Notes
1		-	386*, 394, 416	ss
2	M12T(A ^{PyE})T	CAG TAT ATG ACT	385, 397, 414*	ds, complementary
3		CAG TAA ATG ACT	388, 403, 420*	ds, mismatched A
4		CAG TAG ATG ACT	386, 404, 423*	ds, mismatched G
5		CAG TAC ATG ACT	388,405, 425*	ds, mismatched C
6		-	386*, 398, 417	ss
7	M12A(A ^{PyE})A	CAG TTT TTG ACT	382*, 413	ds, complementary
8		CAG TTA TTG ACT	388, 404,423*	ds, mismatched A
9		CAG TTG TTG ACT	388, 403,423*	ds, mismatched G
10		CAG TTC TTG ACT	388, 405, 423*	ds, mismatched C
11		-	387*, 397, 419	ss
12	M12G(A ^{PyE})G	CAG TCT CTG ACT	388* , 419	ds, complementary
13		CAG TCA CTG ACT	388, 403, 423*	ds, mismatched A
14		CAG TCG CTG ACT	390, 401, 423*	ds, mismatched G
15		CAG TCC CTG ACT	387,399, 421*	ds, mismatched C
16		-	386*, 394, 414	ss
17	M12C(A ^{PyE})C	CAG TGT GTG ACT	389*, 412*	ds, complementary
18		CAG TGA GTG ACT	389*, 405, 425	ds, mismatched A
19		CAG TGG GTG ACT	388, 404*, 421	ds, mismatched G
20		CAG TGC GTG ACT	388, 404, 426*	ds, mismatched C
21		CAG TGT GAG ACT	389*, 412	ds, indirect mismatched A 3'
22		CAG AGT GTG ACT	386*, 396, 417	ds, indirect mismatched A 5'
23		CAG TIT ITG ACT	388*, 396, 417	ds, double mismatched
24		-	386*, 396, 416	ss
25	M10A(A ^{PyE})C	AGT GTT CTA C	385, 412*	ds, complementary
26		AGT GAT CTA C	389, 401, 422*	ds, mismatched A
27		AGT GGT CTA C	386, 399, 421*	ds, mismatched G
28		AGT GCT CTA C	388, 405, 425*	ds, mismatched C
29		AGT G Φ T CTA C	387, 405, 424*	ds, direct abasic site
30		-	383*, 395, 416*	ss
31	M10G(A ^{PyE})T	AGT GAT CTA C	383*, 395, 415*	ds, complementary
32		AGT GAA CTA C	386*, 395, 419*	ds, mismatched A
33		AGT GAG CTA C	386*, 401, 419*	ds, mismatched G
34		AGT GAC CTA C	389, 404, 422*	ds, mismatched C

^aMismatched bases in the DNA sequence are indicated by underlining. ^b λ_{\max} is indicated by *

Table A1. UV absorption data of A^{PyE}-modified acpcPNA probes (condition: 1.0 μ M PNA, 1.2 μ M DNA, 10 mM phosphate buffer pH 7.0). (Continued)

Entry	PNA	DNA ^a (5' to 3')	λ_{\max} (abs), (nm)	Notes
35		-	385*, 414	ss
36		CAG TAT ATG ACT	385*, 413	ds, complementary
37	A ^{PyE} M12	CAG TAT ATG <u>ACA</u>	386*, 415	ds, mismatched A
38		CAG TAT ATG <u>ACG</u>	385*, 415	ds, mismatched G
39		CAG TAT ATG <u>ACC</u>	387*, 414	ds, mismatched C
40		-	385*, 389, 417	ss
41	CAG(A ^{PyE})	CTG CTG CTG	388*, 414	ds, short DNA
42		CTG CTG CTG CTG	382*, 413	ds, full complementary
43		CTG CTG CTG CTG CTG	384*, 413	ds, longer DNA

^aMismatched bases in the DNA sequence are indicated by underlining. ^b λ_{\max} is indicated by *

Table A2. UV absorption data of doubly A^{PyE}-modified acpcPNA probes (condition: 1.0 μ M PNA, 1.2 μ M DNA, 10 mM phosphate buffer pH 7.0)

Entry	PNA	DNA ^a (5' to 3')	λ_{\max} (abs), (nm)	Notes
1		-	385*, 401, 421	ss
2	T8A ^{PyE} 2_0B	AAA ATT AAA A	385*, 399, 421	ds, complementary
3		AAA <u>AAA</u> AAA A	385*, 400, 418	ds, double mismatched
4		AAA <u>ATA</u> AAA A	386*, 399, 422	ds, single mismatched
5		-	386*, 397, 417	ss
6	T8A ^{PyE} 2_3B	AAA <u>IAA</u> <u>ATA</u> A	385*, 398, 417	ds, complementary
7		AAA <u>AAA</u> <u>AAA</u> A	387*, 398, 418	ds, double mismatched
8		AAA TAA <u>AAA</u> A	386*, 399, 417	ds, single mismatched

^aMismatched bases in the DNA sequence are indicated by underlining. ^b λ_{\max} is indicated by *

VITA

Miss Duangrat Nim-anussornkul was born in October 12, 1985 in Bangkok, Thailand. She graduated with Bachelor's Degree of Science (Chemistry) in 2009 and the Master's Degree (Chemistry) from Faculty of Science, Chiang Mai University, Chiang Mai province, Thailand in 2012.

Contact information: duangratnim@gmail.com

Publications

1. Yotapan, N.; Nim-anussornkul, D.; Vilaivan, T. Pyrrolidinyl peptide nucleic acid terminally labeled with fluorophore and end-stacking quencher as a probe for highly specific DNA sequence discrimination. *Tetrahedron* 2016, 72, 7992–7999.

2. Nim-anussornkul, D.; Vilaivan, T. Synthesis and optical properties of pyrrolidinyl peptide nucleic acid bearing a base discriminating fluorescence nucleobase 8-(pyrene-1-yl)-ethynyladenine. *Bioorg. Med. Chem.* 2017, 25, 6388-6397.

3. Park, Y. J.; Nim-anussornkul, D.; Vilaivan, T.; Morii, T.; Kim, B. H. Facile conversion of ATP-binding RNA aptamer to quencher-free molecular aptamer beacon. *Bioorg. Med. Chem. Lett.* 2018, 28, 77-80.